DISSERTATION

# AN INVESTIGATION OF THE MOLECULAR COMPLEXITIES THAT REGULATE MOLTING IN DECAPOD CRUSTACEANS

Submitted by

Natalie Lynn Pitts

Graduate Degree Program in Cell and Molecular Biology

In partial fulfillment of the requirements

For the Degree of Doctor of Philosophy

Colorado State University

Fort Collins, Colorado

Fall 2015

Doctoral Committee:

Advisor: Donald L. Mykles

Deborah M. Garrity
Ronald B. Tjalkens
Susan Tsunoda

ABSTRACT

AN INVESTIGATION OF THE MOLECULAR COMPLEXITIES THAT REGULATE MOLTING IN DECAPOD CRUSTACEANS

Molting in decapod crustaceans is regulated by the interaction of two hormones, molt inhibiting hormone (MIH) and ecdysteroids. Ecdysteroids are steroid hormones secreted from the molting gland or Y-organ (YO) and fluctuations in hemolymph ecdysteroid titers regulate progression through the molt cycle. Secretion of ecdysteroids is controlled by the peptide hormone MIH, which is synthesized and released from the X-organ/sinus gland (XO/SG) complex in the eyestalk ganglia (ESG). The field of crustacean endocrinology has mainly focused on understanding the molecular underpinnings of MIH's action on ecdysteroid production in the YO. The goal of this dissertation was to examine how MIH synthesis and secretion from the XO/SG complex contributes to molt cycle progression.

Blackback land crabs, *Gecarcinus lateralis,* were induced to molt via autotomy of five or more walking legs (multiple limb autotomy or MLA). ESG were collected from intermolt, premolt, and post-molt animals and changes in expression of *Gl-MIH* and mTOR signaling pathway components were investigated. There was a significant effect of molt stage on *Gl-MIH* and mTOR signaling pathway gene expression in the ESG of *G. lateralis*. Continuous elevation of MIH transcript abundance during pre and post molt indicates that MIH titers in the hemolymph are not regulated by changes in transcript abundance. Molting also significantly increased expression of *Gl-Akt, Gl-mTOR, Gl-Rheb*, and *Gl-S6K* in one or more molt stages. Akt inhibits the tuberous sclerosis complex allowing for the activation of Rheb. Rheb is a GTPase that binds and activates the mechanistic target of rapamycin (mTOR). mTOR activates S6 kinase (S6K), increasing protein synthesis. ESG of naturally molting green crabs, *Carcinus maenas*, were also collected from intermolt, early premolt, and post molt animals. Molting had little effect on gene expression in *C. maenas*, confirming previous findings that molt progression is regulated post transcriptionally.

This dissertation identifies a novel nitric oxide (NO) binding protein in the SG of *C. maenas*. The hypothesis is that NO negatively regulates MIH secretion from the SG thereby controlling molt progression. This unidentified endogenous binding protein allows NO to be present in the SG for a

prolonged period and can therefore continually regulate neuropeptide release. Localization of the enzyme that produces NO (nitric oxide synthase; NOS) and MIH in the SG of *C. maenas, G. lateralis*, and *Metacarcinus magister* is consistent with the hypothesis that NO is a regulator of neuropeptide release in the crustacean SG.

The second goal of this dissertation was to explore why some crustacean populations or individuals within a population are refractory to molt induction. The Bodega Bay population of *C. maenas* is refractory to molt induction techniques and a similar phenomenon is observed in *G. lateralis*. Some *G. lateralis* induced to molt via MLA did not enter premolt 90 days post induction and were classified as "blocked." These animals underwent a second molt induction technique, eyestalk ablation (ESA), and YO, brain (Br), and thoracic ganglia (TG) were collected at 1, 3, and 7 days post ESA. Gene expression of MIH and mTOR signaling pathway genes was examined in all three tissues (see Figure 3 for MIH signaling pathway components and there interactions). Results from this experiment suggested that a similar mechanism of molt resistance exists between *C. maenas* and *G. lateralis*. ESA did not increase hemolymph ecdysteroid titers of blocked animals, whereas ESA significantly increased ecdysteroid titers in control and intermolt animals. *Gl-MIH* expression in the ESG and expression of many *Gl-MIH* signaling components in the YO were upregulated in blocked animals, suggesting that the blocked animals were in a "hyper-repressed" state, and therefore resistant to molt induction by ESA and MLA. In both species, MIH is expressed in the Br and TG. The hypothesis is that MIH secretion from these other central nervous system (CNS) tissues contributes to a resistance to molt induction techniques. Expression of MIH signaling pathway genes is unchanged in the Br and TG in response to ESA. These data suggest that MIH does not activate a signaling pathways in CNS tissues but like the ESG, MIH is synthesized and secreted from these tissues. This experiment also supports the growing body of literature that mTOR inhibition activates downstream transcription factors which are important in maintaining energy homeostasis in times of environmental stress.

ACKNOWLEDGEMENTS

I sincerely thank my advisor Dr. Donald Mykles for his guidance, time, patience, and unwavering support throughout my doctoral degree. I would also like to thank my committee members Dr. Deborah Garrity, Dr. Ronald Tjalkens, and Dr. Susan Tsunoda for their encouragement and advice. My deepest gratitude to past and present crab lab members Dr. Kyle MacLea, Megan Mudron, Hanna Schulz, Dr. Sunetra Das, Dr. Sukkrit Nimitkul and Lindsay Martin.

I would also like to thank my parents, Janice and Malcolm Pitts, without whom none of this would have been possible. I am the person I am today because of your unconditional love and support. I am truly blessed to have you as my parents.

Finally, I would like to thank Ian Marsden for his encouragement, love, and advice throughout this entire journey. I am a better scientist and person because of you.

TABLE OF CONTENTS

# CHAPTER ONE

# INTRODUCTION

## The biology of molting in decapod crustaceans

Arthropod growth is dependent on the degradation and reformation of a rigid exoskeleton in a process known as molting. This delicate process requires the precise coordination and timing of various physiological functions. Nearly every tissue undergoes a biochemical, biophysical, or morphological change prior to molting. The molt cycle is regulated by the secretion of molting hormones (ecdysteroids) from the molting gland or Y-organ (YO) (Skinner, 1985b). Ecdysone is the principle ecdysteroid secreted from the YO (Chang and O'Connor, 1977; Mykles, 2011) and it is the prohormone for 20-hydroxyecdysone (20E) (Horn et al., 1966). Injection of ecdysteroids in animals lacking YO's induces molting, indicating that the YO is the main source of ecdysone (Keller and Willig, 1976). Ecdysone is synthesized from cholesterol in the YO and is converted to 20E by peripheral tissues (Chang and O'Connor, 1977; Mykles, 2011). The rate of synthesis and/or secretion of ecdysone by the YO regulates and defines the four stages of the molt cycle: intermolt, premolt (early, mid, and late), ecdysis, and post molt (Figure 1.1) (Chang and Mykles, 2011; Skinner, 1985a).

The four stages of the molt cycle mark the beginning and/or culmination of the physiological transformations required for ecdysis. When environmental conditions are favorable animals enter early premolt during which limb bud formation begins (Skinner, 1962b), claw muscles begin to atrophy (Mykles and Skinner, 1981; Skinner, 1966), the exoskeleton degrades (Skinner, 1985a), and a new epicuticle and exocuticle begin to form (Chang, 1992). By the end of mid-premolt these physiological processes have completed and limbs are fully regenerated (Skinner, 1962a), 40% of the claw muscle is atrophied (Mykles and Skinner, 1981; Skinner, 1966), 75% of the old exoskeleton is degraded (Skinner, 1985a), and the new epicuticle and exocuticle are formed (Skinner, 1985a). The transition into late premolt is marked by the expansion of the new exoskeleton in preparation for ecdysis. After successful ecdysis the animal enters post molt and the final layer of the exoskeleton, the endocuticle, begins to form beneath the epicuticle and exocuticle (Chang, 1992; Skinner, 1985a). The transition from post molt to intermolt is marked by the completion of exoskeleton synthesis and deposition the membranous layer. During the

post molt period, the exocuticle and endocuticle hardens by sclerotization and calcification and tissues that underwent atrophy in preparation for ecdysis regenerate.

Fluctuations in ecdysteroids titers induce systemic physiological transformations which include changes in the YO (Figure 1.1). During the molt cycle the YO transitions between four physiological states; basal, activated, committed, and repressed (Chang and Mykles, 2011). Transitions between these stages is orchestrated by the interaction between ecdysteroids and a peptide hormone, molt inhibiting hormone (MIH). MIH hemolymph titers are high during intermolt and post molt, repressing ecdysteroid synthesis and keeping the YO in a basal state (Chang and Mykles, 2011). A reduction in MIH hemolymph titers allows the YO to transition into an activated state and ecdysteroidgenesis increases. Ecdysteroid synthesis continues to rise as the animal transitions from early premolt to mid-premolt and the YO enters the committed phase (Chang and Mykles, 2011). Ecdysteroid titers peak at the end of mid-premolt and rapidly decline as the animals enters late premolt (Chang and Mykles, 2011). This drastic decrease in ecdysteroids triggers the transition of the YO from the committed to repressed state as the crab approaches ecdysis (Chang and Mykles, 2011).

**Why study molting?**

Understanding the molecular mechanisms that regulate molting is both ecologically and economically important. Ecologically the more knowledge fishery management groups gain about molting the better they can protect and preserve natural crustacean populations. Regulations set in place by fishery management groups helps to not only sustain populations, but also provides economic stability to human populations that rely on fishing to make a living. Along these lines, understanding molting also has benefits for sustaining and growing the aquaculture industry. Many marine crustacean species are difficult to farm in captivity and a better understanding of molt regulation could potentially help to overcome this problem. Crustaceans are also a good model for studying the effects of endocrine disrupting chemicals. Molting is a hormone dependent process, therefore delays or accelerations in growth in these animals could provide early insight into the effects of endocrine disrupting chemicals on an ecosystem.

**Species of study**

*Blackback land crab, Gecarcinus lateralis*

The blackback land crab, *Gecarcinus lateralis*, is a semi-terrestrial species found throughout the Caribbean (Bliss, 1979). Adult females release their eggs directly into the ocean where they remain for the first larval stages and emerge on land as juvenile crabs (Bliss, 1979). Adult land crabs live in burrows dug in dunes above coral sand beaches (Bliss, 1979). These burrows provide the crabs with a refuge from predators and environmental stress, as well as a place to safely shed their exoskeletons (Bliss, 1979).

*G. lateralis* serves as an excellent model in the study of the molecular regulation of molting because molting is easily induced by multiple limb autotomy (MLA). MLA is the loss of five or more walking legs and mimics a natural molt. Molt cycle progression is tracked using a regeneration index (R-index) (R = limb bud length/carapace width * 100). The R-index increases from 0 to 23 prior to ecdysis (Skinner and Graham, 1972; Yu et al., 2002). Intermolt animals are defined by an R-index of 8-12.9, early premolt, 13-15, mid premolt 16-18, and late premolt 19-22. When the length of the limb bud is approximately 23-24% of the carapace width, the animal is within a few days or hours of ecdysis. Molt stage is confirmed by measuring ecdysteroid titers in the hemolymph using a competitive enzyme-linked immunosorbent assay.

*Green crab, Carcinus maenas*

The green crab is a marine species native to Europe and northern Africa. They are one of the world's most successful aquatic invaders establishing populations in North and South America, Australia, South Africa, and Japan (Darling et al., 2008). This species was originally introduced in the United States on the East coast in 1817 and again on the west coast in 1989 (Cohen et al., 1995). The success of these aquatic invaders can be attributed to their high tolerance of variations in salinity, water temperature, habitat types, and oxidative stress (Klassen and Locke, 2007). Two different morphs exist, the molting green morphs found in the intertidal zone and the reproductive red morphs found in subtidal waters (McGaw et al., 2011). On the West coast of the United States molting occurs twice a year, once during the Spring and again in the Fall. The population of green crabs studied in this dissertation are from Bodega Bay, CA. This population is particularly interesting because they are unresponsive to molt

induction techniques (Abuhagr et al., 2014a). Therefore naturally molting populations are relied upon for studying molt cycle progression in this species.

**Neurobiology and anatomy of the nervous system in decapod crustaceans**

*History*

The crustacean nervous system has contributed substantially to the basic knowledge of synaptic transmission and function. Neurosecretion was demonstrated for the first time in the X-organ/sinus gland (XO/SG) complex of brachyuran crustaceans (Bliss, 1951; Passano, 1951). The electrophysiological properties of these neurosecretory nerve terminals was defined decades later in the SG's of *Cardisoma guanhumi* and *C. carnifex* (Cooke, 1985). The field of electrical synaptic transmission was initially established based on studies in the abdominal nerve cord of the crayfish (Furshpan and Potter, 1957). Additionally, synaptic excitation and inhibition was first studied in the crustacean neuromuscular system (Wiersma, 1961a, 1961b; Wiersma and Hughes, 1961). Shortly following, amino acid neurotransmitters γ-aminobutyric acid and glutamic acid were defined in crustacean neuromuscular junctions (Kravitz et al., 1963; Takeuchi and Takeuchi, 1963). Despite early contributions of the crustacean nervous system to the understanding of synaptic function, the intracellular pathways that regulate neuroendocrine secretion are not fully understood (Chung et al., 2010; Hopkins, 2012; Nakatsuji et al., 2009). The anatomy and neurobiology of three neuroendocrine structures, the thoracic ganglia (TG), the brain (Br), and the eyestalk ganglia (ESG) are discussed here.

*Thoracic ganglia*

In brachyuran decapods the thoracic ganglion (TG) lies posterior to the esophageal ganglion (EG) and ventral to the heart (Figure 1.2 and Chapter 4 Figure 4.3B). The TG is fused with the EG and abdominal ganglia (abn) and is a bilaterally symmetrical (Matsumoto, 1954; Stewart et al., 2013; Wood and Derby, 1996). Five segmental neurons (sn) send projections laterally to the walking legs (Sandeman, 1982; Stewart et al., 2013). The cell clusters that innervate the TG are closely associated with the roots of the sns, which control the movement of the walking legs (Stewart et al., 2013). Each cell cluster is centrally located near the thoracic core (hemocoele), where neuropeptides may be secreted into the hemolymph. The ultrastructure of these nerve clusters are defined by the presence of three types of cells, designated A, B, and C (Matsumoto, 1954). Type A cells, also known as giant neurons (GNs), are

neurosecretory cells (~ 55-140 μm in diameter) with a large, vesiculated nucleus (Matsumoto, 1954; Stewart et al., 2013). Type B cells are smaller (~ 25-30 μm in diameter) and have a granulated cytoplasm (Matsumoto, 1954; Stewart et al., 2013). Type C cells are similar in size to type B cells and also have a granulated cytoplasm. However, type C cells have highly dispersed chromatin and a poorly defined nucleolus (Matsumoto, 1954; Stewart et al., 2013).

*Brain*

The circumesophageal connectives (coc) innervate the brain (Br) from the TG (Figure 1.2 and Chapter 4 Figure 4.3C) (Sandeman, 1982). The coc enter the brain at the level of the tritocerebrum (Krieger et al., 2012; Sandeman, 1982; Sandeman and Scholtz, 1995). The tritocerebrum is principally constructed from two neuropils, the median antenna neuropil (MaN) and a pair of lateral antenna II neuropils (AnN) (Stewart et al., 2013). The MaN is anterior to the posterior-medial protocerebral neuropils (PMPN) and marks the transition from the tritocerebrum to the protocerbrum (Stewart et al., 2013). The PMPN are mirrored across a central body (CB) by another group of neuropils, the anterior-medial protocerebral neuropils (AMPN) (Atwood and Sandeman, 1982). The third region of the Br, the deutocerebrum, contains the most prominent structures in the Br, the olfactory lobes (OL) (Sandeman, 1982). These globular structures are positioned on the lateral sides of the deutocerebrum and link the deutocerebrum to the protocerebrum via the olfactory globular tract neuropils (OGTN) (Sandeman, 1982). The majority of cell clusters in the Br are located in the protocerebrum (Stewart et al., 2013). Three cell types make up these populations: GNs, small or globuli neurons, and glial cells (Stewart et al., 2013). Cell populations can be distinguished based on the homogeneity or heterogeneity of their cell types.

*Eyestalk ganglia*

The eyestalk ganglia (ESG) is the central location for neuropeptide synthesis and secretion (Figure 1.2 and Chapter 4 Figure 4.3A). It is innervated by the Br via the optic nerve at the level of the medulla terminalis (MT) (Sandeman, 1982). The MT is one of three ganglionic neuropils that make up the ESG (Bliss, 1951). The MT houses the XO, a cluster of ~150 neurosecretory cells that produce neuropeptides (Hopkins, 2012; Skinner, 1985b). Neuropeptides are transported distally along axonal tracts to the sinus gland (SG), a neurohemal organ located at the junction of two neuropils, the medulla interna (MI) and the medulla externa (ME) (Bliss and Welsh, 1952; Passano, 1951). The SG is comprised

of axon terminals, axons, and glial cells (Hanstrom 1935, 1937; Azzouna and Rezig, 2001). Projections from the XO contribute to at least 90% of the terminals in the SG (Nagano and Cooke, 1987), the remaining 10% originate from other cell clusters in the ESG, Br, and TG (Sandeman, 1982). Electron microscopy reveals that the neuron terminals are packed with secretory vesicles (Andrew and Shivers, 1976), serving as a storage site for neurosecretory products (Hanström, 1939). Morphological and biochemical studies indicate that the XO/SG complex is purely a peptidergic system (Cooke and Sullivan, 1982; Newcomb et al., 1985; Stuenkel, 1983). Neuropeptides are released into the hemolymph by exocytosis (Weitzman, 1969) and the tight packing of secretory granules in the SG gives this structure a white, iridescent appearance (Stuenkel and Cooke, 1988).

**Regulation of ecdysteroidgenesis in crustaceans and insects: A comparison between molt-inhibiting hormone (MIH) and prothoracicotropic hormone (PTTH)**

*Molt inhibiting hormone*

Molt inhibiting hormone (MIH) was originally stumbled upon by Zeleny (Zeleny, 1905) when he discovered that the molt cycle could be accelerated by removing the eyestalks of the fiddler crab, *Uca pugilator,* and the snapping shrimp, *Alpheus dentipes.* MIH is a unique inhibitory neuropeptide only found in crustaceans (Chang and Mykles, 2011). MIH is synthesized in the eyestalk ganglia (ESG) by the XO. Axons from the XO project distally to the sinus gland (SG) and MIH is secreted from the SG into the hemolymph. MIH is a 113-amino acid preprohormone, which is cleaved to form a 78-amino acid mature peptide. Three intramolecular disulfide bonds and seven cysteine residues are essential for MIH folding and biological activity (Fanjul-Möles, 2006; Keller, 1992; Nakatsuji et al., 2009; Webster et al., 2012).

MIH inhibits ecdysteroidgenosis by binding an unidentified receptor on the YO plasma membrane, activating two cyclic nucleotides that suppress ecdysteroid synthesis (Figure 1.4) (Chang and Mykles, 2011). The MIH receptor is hypothesized to be a G-protein coupled receptor that when bound activates adenylyl cyclase (AC), producing cyclic adenosine monophosphaste (cAMP). cAMP activates protein kinase A (PKA), which causes a transient inhibition of ecdysteroidgenesis (Baghdassarian et al., 1996; Chang and Mykles, 2011; Covi et al., 2009; Nakatsuji et al., 2009). PKA also induces $Ca^{2+}$ influx, activating calmodulin (CaM). CaM activation initiates a NO/cGMP signaling pathway, which through the

activation of protein kinase G (PKG), sustains inhibition of ecdysteroid synthesis (Chang and Mykles, 2011).

*Prothoracicotropic hormone*

Prothoracicotropic hormone (PTTH) was originally discovered in the caterpillar, *Lymantria dispar* (Kopec, 1922). Seven decades later this protein was characterized and purified from the silkworm, *Bombyx mori* (Kataoka and Suzuki, 1991). The 224-amino acid precursor protein is cleaved into 109-amino acid monomer and assembled into a homodimeric structure (Marchal et al., 2010). Folding of the biologically active protein is dependent upon three intramolecular disulfide bonds and a single cysteine-cysteine interaction (Gilbert et al., 2002; Kataoka and Suzuki, 1991; Kawakami et al., 1990).

PTTH is a neuropeptide that is synthesized by a pair of neurosecretory cells in the insect brain (McBrayer et al., 2007; Rybczynski, 2005; Siegmund and Korge, 2001). PTTH stimulates ecdysteroid production in the molting glands (prothoracic gland; PG) of insects (Marchal et al., 2010; Yamanaka et al., 2013). Release of this peptide is regulated by physiological (i.e. - nutrient status) and environmental factors (i.e. - photoperiod) that determine when to progress to the next development stage (Gilbert et al., 2002; Huang et al., 2008; Rybczynski, 2005). The PTTH receptor was originally proposed to be a GPCR (Nagata et al., 2006). However, current data from *M. sexta* indicates that PTTH activates a RTK encoded by the *torso* gene (Rewitz et al., 2009). Binding of PTTH to its receptor on the PG activates a similar signaling cascade in the PG as it does in the YO. PTTH activates cAMP and through an influx of $Ca^{2+}$ and activation of several protein kinases initiates a series of protein phosphorylations (Marchal et al., 2010). The most notable is the phosphorylation of protein S6 which increases translation of several mRNAs necessary for developmental progression and ecdysteroid production (Keightley et al., 1990; Yamanaka et al., 2013).

*Comparison of molt regulation by MIH and PTTH in crustaceans and insects*

Although MIH and PTTH have opposing effects on ecdysteroidogenesis, a remarkable number of similarities exist between these neuropeptides. Both peptides rely on three intramolecular disulfide bonds and cysteine-cysteine interactions for proper folding. Ecdysteroid biosynthesis in the molting glands is similar, both relying on the conversion of cholesterol to 5β-Diketol through a series of enzymes encoded by the *Neverland, Shroud, Spook,* and *Spookiest* genes (Chang and Mykles, 2011; Gilbert and Rewitz,

2009; Hopkins, 2009; Lachaise et al., 1993). This conversion of cholesterol to 5β-Diketol is referred to as the “black box,” since in both insects and crustaceans the exact mechanism is unclear (Chang and Mykles, 2011; Niwa and Niwa, 2014). The remaining signaling cascade converting 5β-Diketol to secreted ecdysteroids is similar in insects and crustaceans, but biosynthesis of ecdysteroids in crustaceans is far more complex. Both insects and crustaceans synthesize ecdysone in the molting gland which is converted to 20E by peripheral tissues (Hopkins, 2009; Marchal et al., 2010; Mykles, 2011; Niwa and Niwa, 2014; Yamanaka et al., 2013). 20E is the primary ecdysteroid in both insects and crustaceans. The YO synthesizes three additional ecdysteroids: 3-Dehhydro-25-deoxyeecdysone, 3-Dehydroecdysonee, and 25-deoxyecdysone, contributing to the increased complexity of ecdysteroidogenesis in crustaceans (Mykles, 2011).

The mechanistic target of rapamycin (mTOR) contributes to the regulation of ecdysteroidgenesis in both the crustacean YO and the PG of insects. In the YO, mTOR upregulates protein synthesis and is inhibited by MIH (Abuhagr et al., 2014b). A similar interaction between PTTH and mTOR signaling plays a role in the nutrition sensing in the PG (Gu et al., 2012; Song and Gilbert, 1994). Production of ecdysteroids in both molting glands is also self-regulating. In insects both positive and negative feedback loops are ecdysone-dependent and have been demonstrated in physiological studies (Beydon and Lafont, 1983; Sakurai and Williams, 1989; Takaki and Sakurai, 2003). The most well-known positive-feedback loop is the transcriptional regulation of EcR by ecdysone (Karim and Thummel, 1992). Negative-feedback mechanisms alter the intracellular concentrations of ecdysone (Guittard et al., 2011; Hock et al., 2000; Rewitz et al., 2010). Positive-feedback loops in crustaceans also act through EcR (Techa and Chung, 2015). During premolt, hemolymph ecdysteroids stimulate MIH synthesis but suppress its secretion from the ESG (Techa and Chung, 2015). The self-regulation of ecdysteroid synthesis in both insect and crustaceans is only in early stages of investigation however, it is clear that similarities exist.

MIH and PTTH are considered to be necessary for ecdysteroid regulation in both insects and crustaceans. However, there are examples from both systems, where molting occurs without input from these neuropeptides. Although MIH in crustaceans is principally found in the eyestalks, in eyestalkless individuals, after the completion of ecdysis, hemolymph ecdysteroids titers decrease to intermolt levels

(Dell et al., 1999; Hopkins, 1992; Nakatsuji and Sonobe, 2004). PTTH loss-of-function studies in *Drosophila melanogaster,* delay but do not inhibit, metamorphosis (McBrayer et al., 2007). Although PTTH is a major regulator of ecdysteroidgenesis in insects, it is not the only regulator (Marchal et al., 2010). Therefore, it is not surprising that insects can successfully undergo metamorphosis in its absence. Initially it was hypothesized that MIH worked much like a light switch, turning molting off when it is released and turning it on when it is absent. However, recent studies have confirmed that MIH's role in the modulation of the molt cycle is not nearly this simplistic (Chung and Webster, 2005; Nakatsuji and Sonobe, 2004).

Recent studies in both crustaceans and insects have revealed a role of both of these proteins in reproduction and development. Studies in the blue crab *Callinectes sapidus* identified MIH binding sites on the hepatopancreas that when bound induce vitellogenesis (Zmora et al., 2009). In female moths, *Manduca sexta*, PTTH is implicated in the function and/or development of reproductive physiology (Rybczynski et al., 2009). The role of PTTH in the regulation of development in insects is well established (Mizoguchi et al., 2015; Mizoguchi et al., 2013; Vafopoulou et al., 2012). However, only recently MIH was discovered to contribute to crustacean development. Fluctuations in MIH expression during embryogenesis in *C. sapidus* suggest that MIH plays a role in development (Techa et al., 2015).

**Molt delay in crustaceans and insects**

Molting in insects and crustaceans is a hormonally regulated process that induces systemic transformations that are critical to growth and development. Given the delicate nature of this process, molting/metamorphosis can be delayed in both insects and crustaceans if environmental factors (i.e. - food availability, overcrowding, etc.) are less than favorable (Highman, 1981; Skinner, 1985b). Nutrient availability is critical for insects prior to entering the non-feeding period that accompanies metamorphosis (Mirth et al., 2009). Consequently, insects will not enter metamorphosis in a nutrient poor environment. As a result of their soft, unhardened exoskeletons, post-ecdysis crustaceans are especially vulnerable to predators. In order for molting to be initiated, animals require isolation and therefore they will not molt in crowded conditions (Skinner, 1985b). In the stage following molt/metamorphosis induction, both insects and crustaceans can suspend molting/metamorphosis in response to changes in physiological or environmental status. In insects this time point is marked by the attainment of a critical weight (Mirth and

Riddiford, 2007; Yamanaka et al., 2013). Once last-instar larvae have obtained a certain body size, metamorphosis begins and a fixed schedule of transition events is activated (Mirth and Riddiford, 2007; Yamanaka et al., 2013). The attainment of critical weight activates ecdysteroidgenesis in the PG, causing the animal to be refractory to any further changes in physiological or environmental status (Caldwell et al., 2005; Colombani et al., 2005; Mirth, 2005; Mirth et al., 2009). A similar refractory period is observed in crustaceans. During the first stage of premolt as ecdysteroid titers begin to rise, molting can be delayed in response to physiological or environmental changes. During this time period, the molting gland is sensitive to MIH and increases in this neuropeptide can suspend molt progression (Chang and Mykles, 2011). As the animal progresses into mid-premolt the molting gland becomes refractory to MIH and molting can no longer be delayed by changes in physiological or environmental status (Chang and Mykles, 2011).

During the time period following molt/metamorphosis induction, molting/metamorphosis can also be delayed to correct a physical abnormality (Highman, 1981; Skinner, 1985b). In *Drosophila*, damage to imaginal discs delays developmental timing (Hackney et al., 2012; Parker and Shingleton, 2011; Stieper et al., 2008). Genetically or physically damaged discs release an insulin-like peptide (Dilp8) that regulates developmental timing (Colombani et al., 2012; Garelli et al., 2012). Dilp8 suspends ecdysteroidgenesis in the PG, allowing for tissue repair as synchronization of growth in damaged and undamaged tissues (Parker and Shingleton, 2011). Another mechanism for metamorphosis delay in animals with damaged imaginal discs is the down regulation of PTTH and therefore a decrease in ecdysteroidgenesis in the PG (Halme et al., 2010). Similarly in *G. lateralis*, molting is suspended if a limb bud regenerate is autotomized during early premolt (Skinner, 1985b). The autotomized limb bud secrets an MIH-like factor, limb autotomy factor-proecdysial ($LAF_{pro}$), that prevents molt progression until a secondary limb bud has regenerated (Skinner, 1985b). This delay in molting allows the animal to molt with a full set of walking legs.

**Project overview**

The primary goal of this dissertation is to provide a novel perspective regarding the molecular regulation of molting in decapod crustaceans by examining changes in gene expression and neurosecretion from the ESG. The secondary goal of the project is to explore why some crustacean

populations are refractory to molt induction techniques. These goals are addressed in the six chapters of this dissertation. Chapter one is an introduction. Chapter two describes changes in ESG mRNA expression of two signaling pathways (mTOR and MIH) throughout the molt cycle. Chapter three identifies an endogenous NO binding protein in the SG of *C. maenas*. Chapter four reports the localization of NOS and MIH in three central nervous system (CNS) tissues of three decapod crustacean species. Chapter five addresses the second goal of this dissertation and examines the impact of molt induction techniques on gene expression in the YO and three CNS tissues. Chapter six summarizes the data sets from chapters two tthrough five.

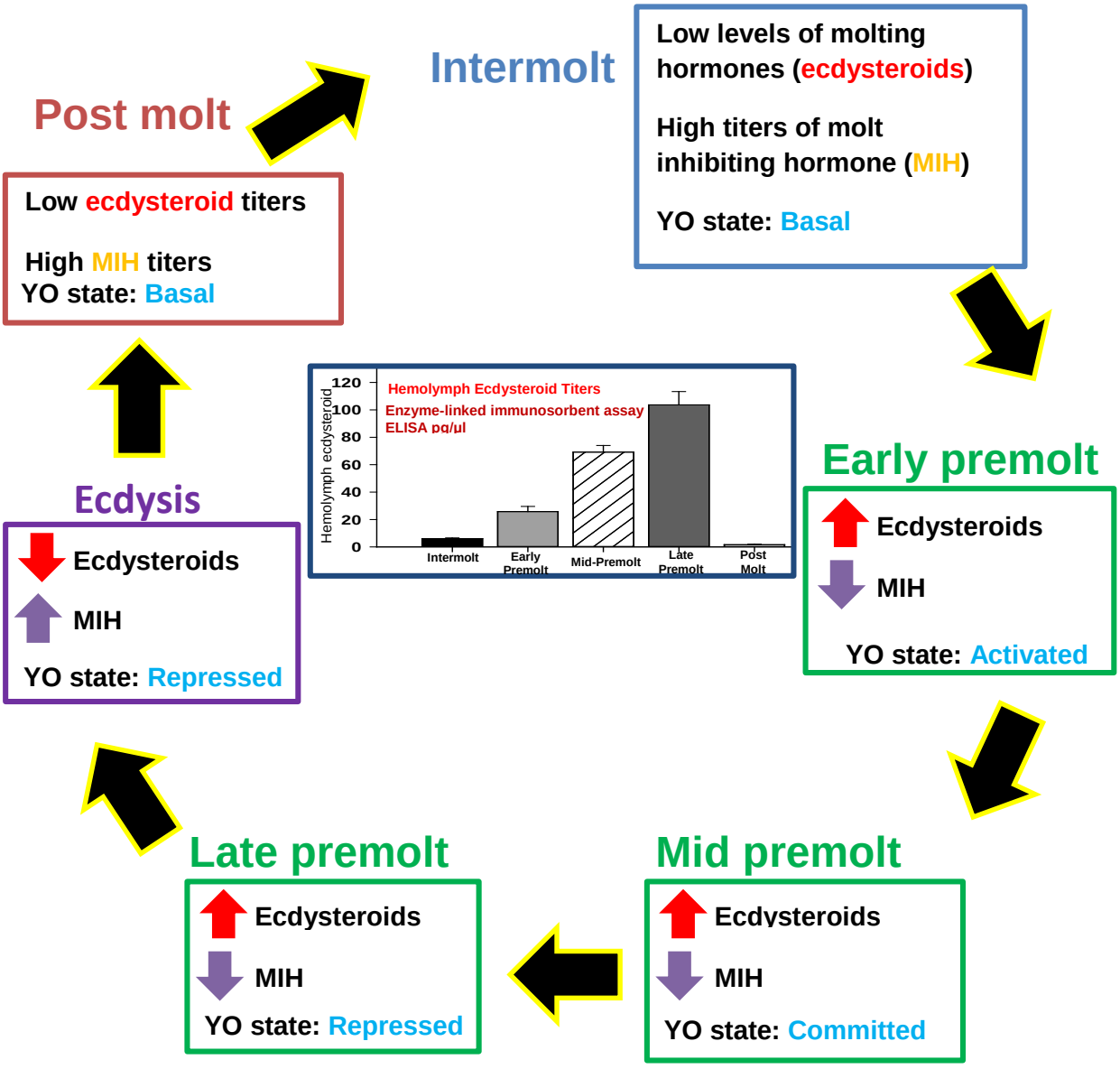


**Figure 1.1 Stages of the crustacean molt cycle.** Diagram illustrating the cyclical nature of the crustacean molt cycle. Levels in ecdysteroid and molt inhibiting hormone (MIH) titers are indicated. Graph displays the increase in ecdysteroid titers as the animal progresses toward molt (ecdysis). YO state at each molt stage is also indicated. Ecdysteroid titers were measured using an enzyme-linked immunosorbent assay (ELISA).

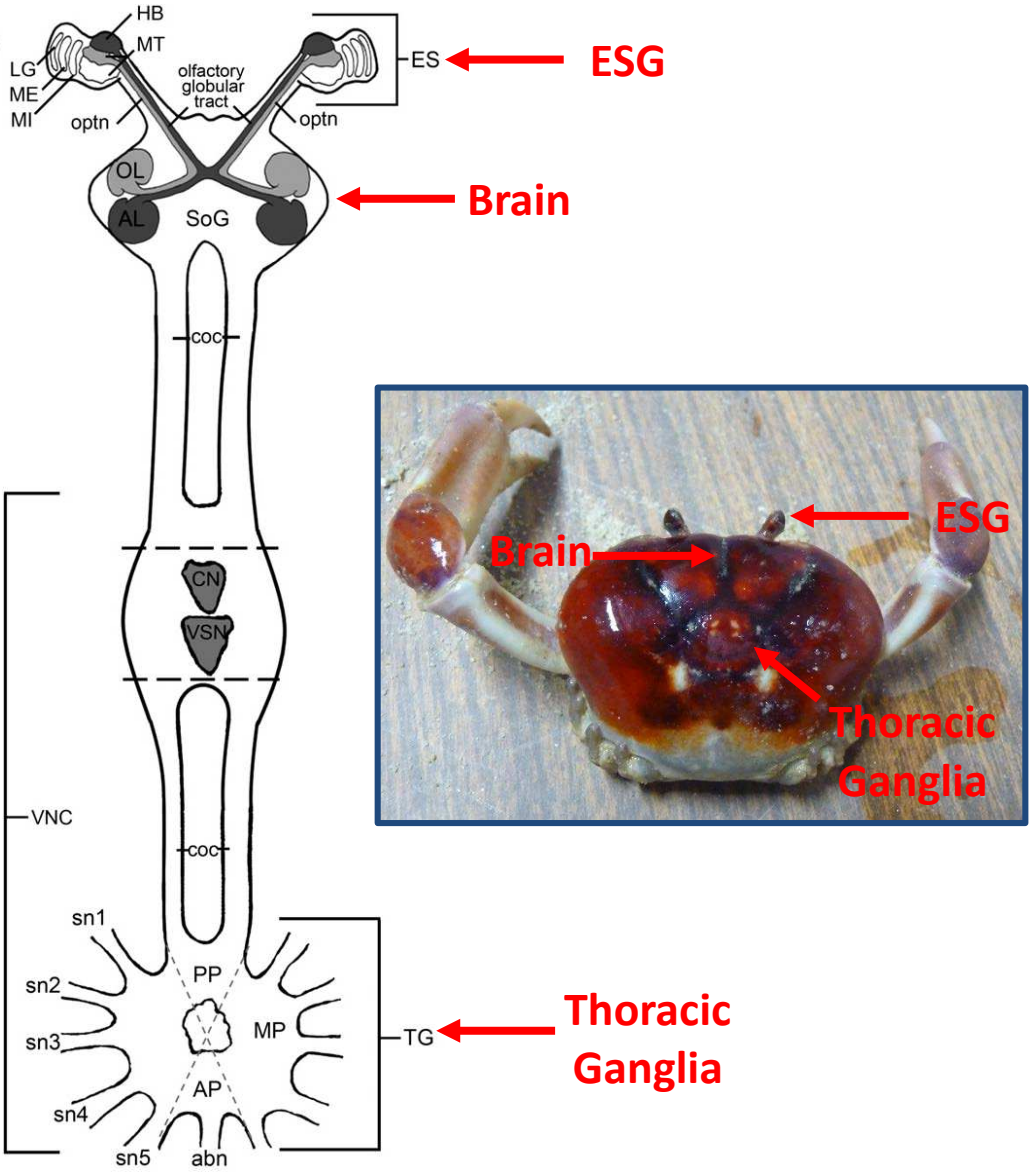


**Figure 1.2 Interconnected crustacean nervous system.** Schematic illustration of the CNS in G. lateralis. Drawing not to scale. Adapted from Stewart *et. al.*, 2013. Abbreviations: abdominal nerve (abn), accessory lobe (AL), anterior part (AP), circumesophageal connectives (coc), commissural neuropil (CN), eyestalk ganglia (ES), hemiellipsoid body (HB), lamina ganglionaris (LG), medial part (MP), medulla externa (ME), medulla interna (MI), medulla terminalis (MT), posterior part (PP), protocerebral tract (PT), optic nerve (optn), olfactory lobe (OL), segmental nerve (sn) superesophageal ganglion (SoG), ventral nerve cord (VNC), ventral sensory neuropil (VSN).

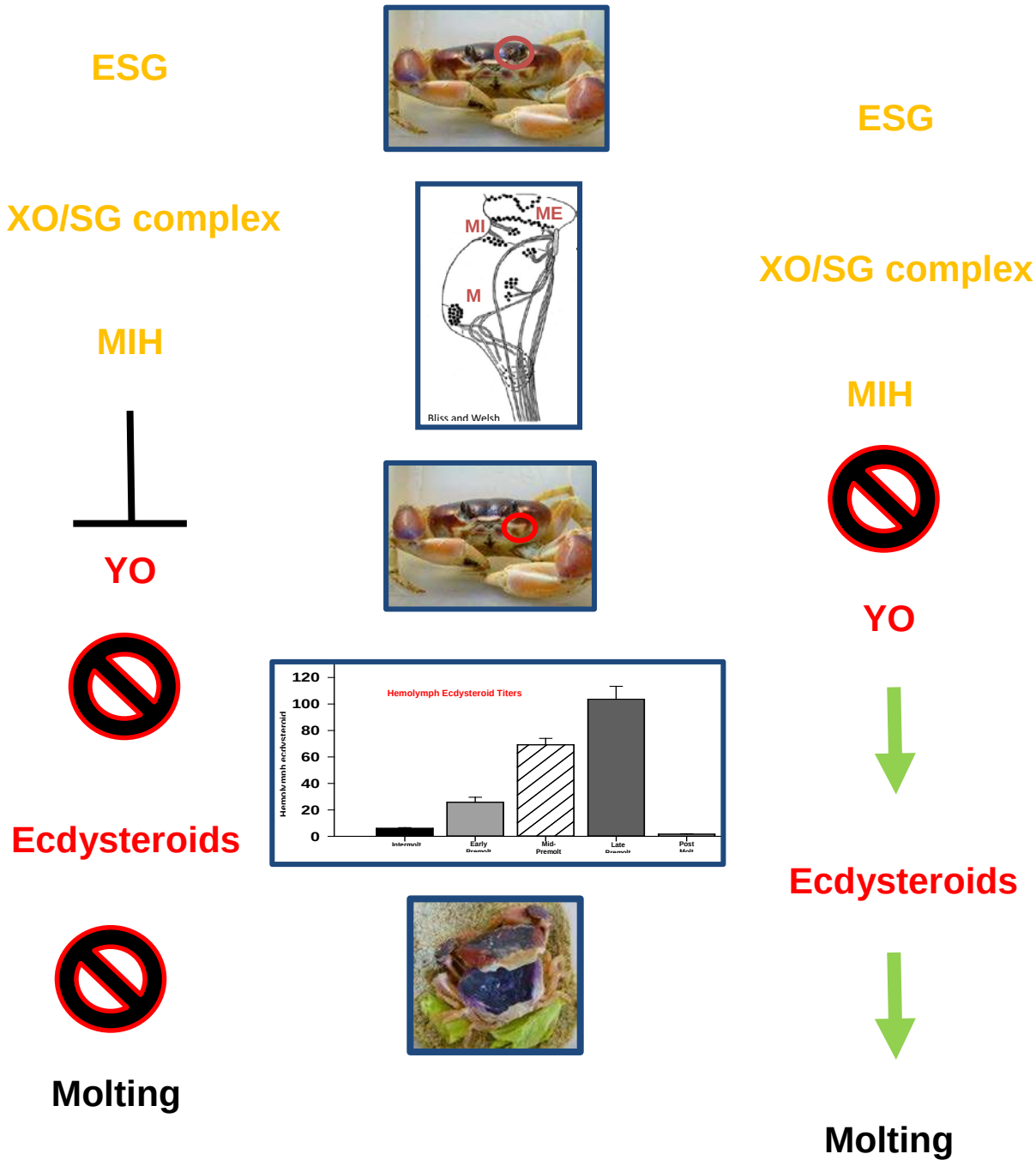


**Figure 1.3 Effects of MIH on ecdysteroid titers and molt progression.** Molt inhibiting hormone (MIH) is synthesized/secreted from the X-organ (XO)/sinus gland (SG) complex in the eyestalk ganglia (ESG). MIH inhibits ecdysteroid production by the molting gland or Y-organ (YO). In the absence of MIH the YO synthesizes ecdysteroids and the animal enters the molt cycle.

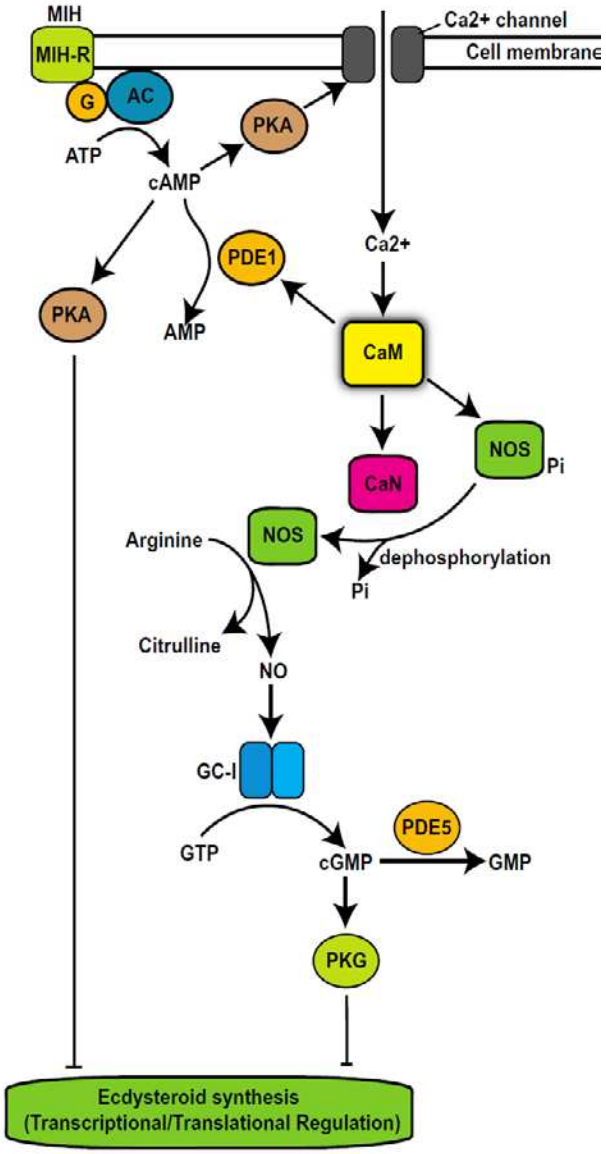


**Figure 1.4 Proposed MIH signaling pathway in the crustacean YO.** MIH is hypothesized to bind a G-protein coupled receptor that activates adenylyl cyclase (AC), producing cyclic adenosine monophosphaste (cAMP). cAMP activates protein kinase A (PKA), which causes a transient inhibition of ecdysteroidgenesis. PKA also induces $Ca^{2+}$ influx, activating calmodulin (CaM). CaM activation initiates a nitric oxide (NO)/cyclic guanosine monophosphate (cGMP) signaling pathway, which through the activation of protein kinase G (PKG), sustains inhibition of ecdysteroid synthesis. Abbreviations: calcineurin (CaN), NO sensitive guanylyl cyclase (GC-I), nitric oxide synthase (NOS), and phosphodiesterase (PDE).

## REFERENCES


Abuhagr, A.M., Blindert, J.L., Nimitkul, S., Zander, I.A., LaBere, S.M., Chang, S.A., MacLea, K.S., Chang, E.S., Mykles, D.L., 2014a. Molt regulation in green and red color morphs of the crab *Carcinus maenas*: Gene expression of molt-inhibiting hormone signaling components. J. Exp. Biol. 217, 796-808.

Abuhagr, A.M., MacLea, K.S., Chang, E.S., Mykles, D.L., 2014b. Mechanistic target of rapamycin (mTOR) signaling genes in decapod crustaceans: Cloning and tissue expression of mTOR, Akt, Rheb, and p70 S6 kinase in the green crab, *Carcinus maenas*, and blackback land crab, *Gecarcinus lateralis*. Comp. Biochem. Physiol. 168, 25-39.

Andrew, R.D., Shivers, R.R., 1976. Ultrastructure of neurosecretory granule exocytosis by crayfish sinus gland induced with ionic manipulations. Journal of Morphology 150, 253-278.

Atwood, H.L., Sandeman, D.C., 1982. The Biology of Crustacea (Vol. 3), Neurobiology: Structure and Function. Academic Press, New York.

Baghdassarian, D., de Besse, N., Saidi, B., Somme, G., Lachaise, F., 1996. Neuropeptide-induced inhibition of steroidogenesis in crab molting glands: Involvement of cGMP-dependent protein kinase. Gen. Comp. Endocrinol. 104, 41-51.

Beydon, P., Lafont, R., 1983. Feedback inhibition of ecdysone production by 20-hydroxyecdysone in *Pieris brassicae* pupae. J. Insect Physiol. 29, 529-533.

Bliss, D.E., 1951. Metabolic effects of sinus gland or eyestalk removal in the land crab, *Gecarcinus laterials*. Anat. Rec. 111, 502-503.

Bliss, D.E., 1979. From sea to tree - saga of a land crab. American Zoologist 19, 385-410.

Bliss, D.E., Welsh, J.H., 1952. The neurosecretroy system of brachyuran crustacea. Biol. Bull. 103, 157-169.

Caldwell, P.E., Walkiewicz, M., Stern, M., 2005. Ras activity in the *Drosophila* prothoracic gland regulates body size and developmental rate via ecdysone release. Curr. Biol. 15, 1785-1795.

Chang, E.S., 1992. Endocrinology, in: A.W. Fast, L.J. Lester (Eds.), Marine Shrimp Culture: Principles and Practices. Developments in Aquaculture and Fisheries Science. Elsevier Science Publisher B.V., Netherlands, 53-93.

Chang, E.S., Mykles, D.L., 2011. Regulation of crustacean molting: A review and our perspectives. Gen. Comp. Endocrinol. 172, 323-330.

Chang, E.S., O'Connor, J.D., 1977. Secretion of alpha ecdysone by crab Y-organs *in vitro*. Proceedings of the National Academy of Sciences of the United States of America 74, 615-618.

Chung, J.S., Webster, S.G., 2005. Dynamics of *in vivo* release of molt-inhibiting hormone and crustacean hyperglycemic hormone in the shore crab, *Carcinus maenas*. Endocrinol. 146, 5545-5551.

Chung, J.S., Zmora, N., Katayama, H., Tsutsui, N., 2010. Crustacean hyperglycemic hormone (CHH) neuropeptides family: Functions, titer, and binding to target tissues. Gen. Comp. Endocrinol. 166, 447-454.

Cohen, A.N., Carlton, J.T., Fountain, M.C., 1995. Introduction, dispersal and potential impacts of the green crab *Carcinus maenas* in San Francisco Bay, California. Marine Biology 122, 225-237.

Colombani, J., Andersen, D.S., Leopold, P., 2012. Secreted peptide Dilp8 coordinates *Drosophila* tissue growth with developmental timing. Science 336, 582-585.

Colombani, J., Bianchini, L., Layalle, S., Pondeville, E., Dauphin-Villemant, C., Antoniewski, C., Carre, C., Noselli, S., Leopold, P., 2005. Antagonistic actions of ecdysone and insulins determine final size in *Drosophila*. Science 310, 667-670.

Cooke, I.M., 1985. Electrophysiological characterization of peptidergic neurosecretory terminals. J. Exp. Biol. 118, 1-35.

Cooke, I.M., Sullivan, R.E., 1982. Hormones and neurosecretion, in: H. Atwood, D. Sanderman (Eds.), The Biology of Crustacea. Academic, New York, 206-290.

Covi, J.A., Chang, E.S., Mykles, D.L., 2009. Conserved role of cyclic nucleotides in the regulation of ecdysteroidogenesis by the crustacean molting gland. Comp. Biochem. Physiol. 152, 470-477.

Darling, J.A., Bagley, M.J., Roman, J., Tepolt, C.K., Geller, J.B., 2008. Genetic patterns across multiple introductions of the globally invasive crab genus *Carcinus*. Mol. Ecol. 17, 4992-5007.

Dell, S., Sedlmeier, D., Böcking, D., Dauphin-Villemant, C., 1999. Ecdysteroid biosynthesis in crayfish Y-organs: Feedback regulation by circulating ecdysteroids. Arch. Insect Biochem. Physiol. 41, 148-155.

Fanjul-Möles, M.L., 2006. Biochemical and functional aspects of crustacean hyperglycemic hormone in decapod crustaceans: Review and update. Comp. Biochem. Physiol. 142C, 390-400.

Furshpan, E.J., Potter, D.D., 1957. Mechanism of nerve-impulse transmission at a crayfish synapse. Nature 180, 342-343.

Garelli, A., Gontijo, A.M., Miguela, V., Caparros, E., Dominguez, M., 2012. Imaginal discs secrete insulin-like peptide 8 to mediate plasticity of growth and maturation. Science 336, 579-582.

Gilbert, L.I., Rewitz, K.F., 2009. The function and evolution of the halloween genes: The pathway to the arthropod molting hormone, in: G. Smagghe (Ed.), Ecdysone: Structures and Function. Springer Netherlands, 231-269.

Gilbert, L.I., Rybczynski, R., Warren, J.T., 2002. Control and biochemical nature of the ecdysteroidogenic pathway. Ann. Rev. Entomol. 47, 883-916.

Gu, S.H., Yeh, W.L., Young, S.C., Lin, P.L., Li, S., 2012. TOR signaling is involved in PTTH-stimulated ecdysteroidogenesis by prothoracic glands in the silkworm, *Bombyx mori*. Insect Biochem. Molec. Biol. 42, 296-303.

Guittard, E., Blais, C., Maria, A., Parvy, J.P., Pasricha, S., Lumb, C., Lafont, R., Daborn, P.J., Dauphin-Villemant, C., 2011. CYP18A1, a key enzyme of *Drosophila* steroid hormone inactivation, is essential for metamorphosis. Dev. Biol. 349, 35-45.

Hackney, J.F., Zolali-Meybodi, O., Cherbas, P., 2012. Tissue damage disrupts developmental progression and ecdysteroid biosynthesis in *Drosophila*. Plos One 7.

Halme, A., Cheng, M., Hariharan, I.K., 2010. Retinoids regulate a developmental checkpoint for tissue regeneration in *Drosophila*. Curr. Biol. 20, 458-463.

Hanström, B., 1939. Hormones in Invertebrates. Oxford University Press, London.

Highman, K.C., 1981. A Survey of Invertebrate Metamorphosis, in: L.I. Gilbert (Ed.), Metamorphosis: A Problem in Developmental Biology. Plenum Press, New York, NY, 68-71.

Hock, T., Cottrill, T., Keegan, J., Garza, D., 2000. The E23 early gene of *Drosophila* encodes an ecdysone-inducible ATP-binding cassette transporter capable of repressing ecdysone-mediated gene activation. Proc. Natl. Acad. Sci. USA 97, 9519-9524.

Hopkins, P.M., 1992. Hormonal control of the molt cycle in the fiddler crab *Uca pugilator*. Am. Zool. 32, 450-458.

Hopkins, P.M., 2009. Crustacean ecdysteroids and their receptors, in: G. Smagghe (Ed.), Ecdysone: Structures and Functions. Springer Netherlands, 73-97.

Hopkins, P.M., 2012. The eyes have it: A brief history of crustacean neuroendocrinology. Gen. Comp. Endocrinol. 175, 357-366.

Horn, D.H.S., Middleton, E.J., Wunderlich, J.A., Hampshire, F., 1966. Identity of the moulting hormones of insects and crustaceans. Chem. Commun., 339-340.

Huang, X., Warren, J.T., Gilbert, L.I., 2008. New players in the regulation of ecdysone biosynthesis. J. Genet. Genom. 35, 1-10.

Karim, F.D., Thummel, C.S., 1992. Temporal coordination of regulatory gene expression by the steroid hormone ecdysone. EMBO J. 11, 4083-4093.

Kataoka, H., Suzuki, A., 1991. Prothoracicotropic hormone of the silkworm, *Bombyx mori*. Abstracts of Papers of the American Chemical Society 202, 10-AGRO.

Kawakami, A., Kataoka, H., Oka, T., Mizoguchi, A., Kimurakawakami, M., Adachi, T., Iwami, M., Nagasawa, H., Suzuki, A., Ishizaki, H., 1990. Molecular cloning of the *Bombyx mori* prothoracicotropic hormone. Science 247, 1333-1335.

Keightley, D.A., Lou, K.J., Smith, W.A., 1990. Involvment of translation and transcription in insect steroidgenesis. Mol. Cell. Endocrinol. 74, 229-237.

Keller, R., 1992. Crustacean neuropeptides: Structures, functions and comparative aspects. Experientia 48, 439-448.

Keller, R., Willig, A., 1976. Experimental evidence of molt controlling function of Y-organ of a macruran decapod, *Orconectes limosus*. J. Comp. Phys. 108, 271-278.

Klassen, G., Locke, A., 2007. A biological synopsis of the European green crab, *Carcinus maenas*. Canadian Manuscript Report of Fisheries and Aquatic Sciences 2818, 1-82.

Kopec, S., 1922. Studies on the necessity of the brain for the inception of insect metamorphosis. Biol. Bull. 42, 323-342.

Kravitz, E.A., Kuffler, S.W., Potter, D.D., 1963. Selective localization of gamma aminobutyric acid (GABA) in isolated inhibitory axons of lobsters. Fed. Proc. 22, 220-230.

Krieger, J., Sombke, A., Seefluth, F., Kenning, M., Hansson, B.S., Harzsch, S., 2012. Comparative brain architecture of the European shore crab *Carcinus maenas* (Brachyura) and the common hermit crab *Pagurus bernhardus* (Anomura) with notes on other marine hermit crabs. Cell Tissue Res. 348, 47-69.

Lachaise, F., Leroux, A., Hubert, M., Lafont, R., 1993. The molting gland of crustaceans; Localization, activity, and endocrine control (a review) J. Crustacean Biol. 13, 198-234.

Marchal, E., Vandersmissen, H.P., Badisco, L., Van de Velde, S., Verlinden, H., Iga, M., Van Wielendaele, P., Huybrechts, R., Simonet, G., Smagghe, G., Vanden Broeck, J., 2010. Control of ecdysteroidogenesis in prothoracic glands of insects: A review. Peptides 31, 506-519.

Matsumoto, K., 1954. Neurosecretion in the thoracic ganglion of the crab, *Eriocheir japonicus*. Biol. Bull. 106, 60-68.

McBrayer, Z., Ono, H., Shimell, M., Parvy, J.P., Beckstead, R.B., Warren, J.T., Thummel, C.S., Dauphin-Villemant, C., Gilbert, L.I., O'Connor, M.B., 2007. Prothoracicotropic hormone regulates developmental timing and body size in *Drosophila*. Dev. Cell 13, 857-871.

McGaw, I.J., Edgell, T.C., Kaiser, M.J., 2011. Population demographics of native and newly invasive populations of the green crab Carcinus maenas. Marine Ecology Progress Series 430, 235-240.

Mirth, C., 2005. Ecdysteroid control of metamorphosis in the differentiating adult leg structures of *Drosophila* melanogaster. Dev. Biol. 278, 163-174.

Mirth, C.K., Riddiford, L.M., 2007. Size assessment and growth control: how adult size is determined in insects. BioEssays 29, 344-355.

Mirth, C.K., Truman, J.W., Riddiford, L.M., 2009. The ecdysone receptor controls the post-critical weight switch to nutrition-independent differentiation in *Drosophila* wing imaginal discs. Development 136, 2345-2353.

Mizoguchi, A., Kamimura, M., Kiuchi, M., Kataoka, H., 2015. Positive feedback regulation of prothoracicotropic hormone secretion by ecdysteroid; A mechanism that determines the timing of metamorphosis. Insect Biochem. Molec. Biol. 58, 39-45.

Mizoguchi, A., Ohsumi, S., Kobayashi, K., Okamoto, N., Yamada, N., Tateishi, K., Fujimoto, Y., Kataoka, H., 2013. Prothoracicotropic hormone acts as a neuroendocrine switch between pupal diapause and adult development. Plos One 8.

Mykles, D.L., 2011. Ecdysteroid metabolism in crustaceans. J. Steroid Biochem. Mol. Biol. 127, 196-203.

Mykles, D.L., Skinner, D.M., 1981. Crustacean muscles: Atrophy and regeneration during molting Journal of General Physiology 78, A6-A7.

Nagano, M., Cooke, I.M., 1987. Comparison of electrical responses of terminals, axons, and somata of a peptidergic neurosecretory system. Journal of Neuroscience 7, 634-648.

Nagata, S., Namiki, T., Ko, R., Kataoka, H., Suzuki, A., 2006. A novel type of receptor cDNA from the prothoracic glands of the silkworm, *Bombyx mori*. Biosci. Biotechnol. Biochem. 70, 554-558.

Nakatsuji, T., Lee, C.Y., Watson, R.D., 2009. Crustacean molt-inhibiting hormone: Structure, function, and cellular mode of action. Comp. Biochem. Physiol. 152A, 139-148.

Nakatsuji, T., Sonobe, H., 2004. Regulation of ecdysteroid secretion from the Y-organ by molt-inhibiting hormone in the American crayfish, *Procambarus clarkii*. Gen. Comp. Endocrinol. 135, 358-364.

Newcomb, R., Stuenkel, E., Cooke, I., 1985. Characterization, biosynthesis, and release of neuropeptides from the X-organ sinus gland system of the crab, *Cardisoma carnifex*. Am. Zool. 25, 157-171.

Niwa, R., Niwa, Y.S., 2014. Enzymes for ecdysteroid biosynthesis: Their biological functions in insects and beyond. Biosci. Biotech. Bioch. 78, 1283-1292.

Parker, N.F., Shingleton, A.W., 2011. The coordination of growth among *Drosophila* organs in response to localized growth-perturbation. Dev. Biol. 357, 318-325.

Passano, L.M., 1951. The X-organ, a neurosectretroy gland controlling molting in crabs. Anat. Rec. 111, 559-559.

Rewitz, K.F., Yamanaka, N., Gilbert, L.I., O'Connor, M.B., 2009. The insect neuropeptide PTTH activates receptor tyrosine kinase torso to initiate metamorphosis. Science 326, 1403-1405.

Rewitz, K.F., Yamanaka, N., O'Connor, M.B., 2010. Steroid hormone inactivation is required during the juvenile-adult transition in *Drosophila*. Dev. Cell 19, 895-902.

Rybczynski, R., 2005. Prothoracicotropic hormone, in: L.I. Gilbert, K. Iatrou, S.S. Gill (Eds.), Comprehensive Molecular Insect Science. Elsevier, Oxford, 61-123.

Rybczynski, R., Snyder, C.A., Hartmann, J., Gilbert, L.I., Sakurai, S., 2009. *Manduca sexta* Prothoracicotropic hormone: Evidence for a role beyond steroidogenesis. Arch. Insect Biochem. Physiol. 70, 217-229.

Sakurai, S., Williams, C.M., 1989. Short-loop negative and positive feedback on ecdysone secretion by prothoracic gland in the tobacco hornworm, *Manduca sexta*. Gen. Comp. Endocrinol. 75, 204-216.

Sandeman, D.C., 1982. Organization of the Central Nervous System, in: H.L. Atwood, D.C. Sandeman (Eds.), The Biology of Crustacea Neurobiology: Structure and Function. Academic Press, New York, NY, 1-54.

Sandeman, D.C., Scholtz, G., 1995. Ground Plans, Evolutionary Changes and Homologies in Decapod Crustacean Brains, in: W. Kutsch, O. Breidbach (Eds.), The Nervous Sytem of Invertebrates: A Comparative Approach. Birkhauser, Basel, 329-348.

Siegmund, T., Korge, G., 2001. Innervation of the ring gland of *Drosophila melanogaster*. J. Comp. Neurol. 431, 481-491.

Skinner, D.M., 1962a. Structure and metabolism of a crustacean integumentary tissue during a molt cycle. Biological Bulletin 123, 635-647.

Skinner, D.M., 1962b. Structure and metabolism of the crustacean integumentary tissue during a molt cycle Biol. Bull. 123, 635-&.

Skinner, D.M., 1966. Breakdown and reformation of somatic muscle during molt cycle of land crab, *Gcarcinus lateralis*. Journal of Experimental Zoology 163, 115-124.

Skinner, D.M., 1985a. Interacting factors in the control of crustacean molt cycle. American Zoologist 25, 275-284.

Skinner, D.M., 1985b. Molting and regeneration, in: D.E. Bliss, L.H. Mantel (Eds.), The Biology of Crustacea. Academic Press, New York, 44-146.

Skinner, D.M., Graham, D.E., 1972. Loss of limbs as a stimulus to ecdysis in Brachyura (true crabs). Biol. Bull. 143, 222-233.

Song, Q.S., Gilbert, L.I., 1994. S6 phosphorylation results from prothoracicotropic hormone stimulation of insect prothoracic glands: A role for S6 kinase. Dev. Genet. 15, 332-338.

Stewart, M.J., Stewart, P., Sroyraya, M., Soonklang, N., Cummins, S.F., Hanna, P.J., Duan, W., Sobhon, P., 2013. Cloning of the crustacean hyperglycemic hormone and evidence for molt-inhibiting hormone within the central nervous system of the blue crab Portunus pelagicus. Comp. Biochem. Physiol. 164A, 276-290.

Stieper, B.C., Kupershtok, M., Driscoll, M.V., Shingleton, A.W., 2008. Imaginal discs regulate developmental timing in *Drosophila* melanogaster. Dev. Biol. 321, 18-26.

Stuenkel, E., Cooke, I.M., 1988. Electrophysiological characteristics of peptidergic nerve terminals correlated with secretion. Current Topics in Neuroendocrinol. 9, 123-150.

Stuenkel, E.L., 1983. Biosynthesis and axonal transport of proteins and identified peptide hormones in the X-organ sinus gland neurosecretory system. Journal of Comparative Physiology 153, 191-205.

Takaki, K., Sakurai, S., 2003. Regulation of prothoracic gland ecdysteroidogenic activity leading to pupal metamorphosis. Insect Biochem. Molec. Biol. 33, 1189-1199.

Takeuchi, A., Takeuchi, N., 1963. Glutamate-induced depolarization in crustaceean muscle. Nature 198, 490-496.

Techa, S., Alvarez, J.V., Chung, J.S., 2015. Changes in ecdysteroid levels and expression patterns of ecdysteroid-responsive factors and neuropeptide hormones during the embryogenesis of the blue crab, *Callinectes sapidus*. Gen. Comp. Endocrinol. 214, 157-166.

Techa, S., Chung, J.S., 2015. Ecdysteroids regulate the levels of molt-inhibiting hormone (MIH) expression in the blue crab, *Callinectes sapidus*. Plos One 10.

Vafopoulou, X., Cardinal-Aucoin, M., Steel, C.G.H., 2012. Rhythmic release of prothoracicotropic hormone from the brain of an adult insect during egg development. Comp. Biochem. Physiol. 161, 193-200.

Webster, S.G., Keller, R., Dircksen, H., 2012. The CHH-superfamily of multifunctional peptide hormones controlling crustacean metabolism, osmoregulation, moulting, and reproduction. Gen. Comp. Endocrinol. 175, 217-233.

Weitzman, M., 1969. Release of neurosecretory material from sinus gland of *Gecarcinus lateralis*. Anat. Rec. 163, 332-340.

Wiersma, C.A., 1961a. The Neuromuscular System, in: T.H. Waterman (Ed.), The Physiology of Crustacea. Academic Press, New York, NY, 191-240.

Wiersma, C.A., 1961b. Reflexes and the Central Nervous System, in: T.H. Waterman (Ed.), The Physiology of Crustacea. Academic Press, New York, NY, 241-279.

Wiersma, C.A., Hughes, G.M., 1961. Functional anatomy of neeuronal units in abdominal cord of crayfish, *Procambarus clarkii* (girard) J. Comp. Neurol. 116, 209-&.

Wood, D.E., Derby, C.D., 1996. Distribution of dopamine-like immunoreactivity suggests a role for dopamine in the courtship display behavior of the blue crab, *Callinectes sapidus*. Cell Tissue Res. 285, 321-330.

Yamanaka, N., Rewitz, K.F., O'Connor, M.B., 2013. Ecdysone Control of Developmental Transitions: Lessons from Drosophila Research, in: M.R. Berenbaum (Ed.), Annual Review of Entomology, Vol 58, 497-516.

Yu, X.L., Chang, E.S., Mykles, D.L., 2002. Characterization of limb autotomy factor-proecdysis ($LAF_{pro}$), isolated from limb regenerates, that suspends molting in the land crab *Gecarcinus lateralis*. Biol. Bull. 202, 204-212.

Zeleny, C., 1905. Compensatory regulation. J. Exp. Zool. 2, 347-369.

Zmora, N., Sagi, A., Zohar, Y., Chung, J.S., 2009. Molt-inhibiting hormone stimulates vitellogenesis at advanced ovarian developmental stages in the female blue crab, *Callinectes sapidus*: Novel specific binding sites in hepatopancreas and cAMP as a second messenger. Saline Systems 5:6, 1-11.

CHAPTER TWO

# EFFECTS OF MOLTING ON GENE EXPRESSION IN THE EYESTALK GANGLIA OF TWO DECAPOD CRUSTACEANS; *GECARCINUS LATERALIS* AND *CARCINUS MAENAS*


## SUMMARY

Molting in decapod crustaceans is regulated by the interaction of two hormones, ecdysteroids and molt-inhibiting hormone (MIH). Ecdysteroids are synthesized and secreted from the molting gland or Y-organ (YO). Ecdysteroid production is inhibited by the peptide hormone MIH, which is produced and released from the eyestalk ganglia (ESG). Most research surrounding molt regulation in decapod crustaceans has focused on understanding the regulation of ecdysteroidogenesis in the YO. The goal of this study was to examine the role of neuropeptides and changes in gene expression in the ESG throughout the molt cycle. ESG were collected from *G. lateralis* induced to molt via multiple limb autotomy (MLA) and naturally molting *C. maenas* during intermolt, premolt, and post molt stages. The effects of molting on gene expression of two neuropeptides (MIH and crustacean hyperglycemic hormone (CHH)), four key mTOR signaling pathway genes (mTOR, Akt, Rheb, and S6K), and NO/cGMP signaling pathway genes (NOS, GC-Iβ, GC-II, and GC-III) were investigated. Expression of *Gl-MIH* was continually elevated throughout the molt cycle. *Cm-MIH* was elevated during post molt. *Gl-GC-Iβ* increased in mid and late premolt, as well as in post molt. Expression of all four mTOR pathway genes increased in one or more molt stages in *G. lateralis*. Molting did not significantly impact gene expression of mTOR or NO/cGMP signaling pathway components in *C. maenas*. These data suggest that regulation of neuropeptide synthesis and secretion is regulated by changes in gene expression in mTOR and NO/cGMP signaling pathway genes in *G. lateralis,* but not *C. maenas*.


## INTRODUCTION

Growth in crustaceans is non-linear process requiring the shedding and regeneration of a hard exoskeleton in a process known as molting. In preparation for molting, crustaceans must undergo a number of precisely timed and coordinated physiological changes. This integrated systemic preparation prior to ecdysis is regulated by the production of molting hormones, or ecdysteroids (Chang and Mykles, 2011; Skinner, 1985). The molt cycle is divided into four stages: intermolt, premolt, ecdysis, and post molt (Skinner, 1985). Premolt is further divided into early, mid, and late stages (Chang and Mykles, 2011)

and is the period during which most of the physiological changes (i.e - skeletal muscle atrophy and degradation of the old exoskeleton) occur in preparation for ecdysis (Skinner, 1985). Ecdysteroids are synthesized and secreted by a pair of molting glands or Y-organs (YOs) and coordinate progression through the molt cycle (Chang and Bruce, 1980; Chang and Mykles, 2011). Hemolymph ecdysteroid titers are low during intermolt, steadily increase during premolt, and then drop just prior to ecdysis (Chang, 1985).

Ecdysteroidgenesis in the YO is regulated by two neuropeptides, molt-inhibiting hormone (MIH) and crustacean hyperglycemic hormone (CHH) (Hopkins, 2012; Webster et al., 2012). Both MIH and CHH are synthesized by a group of ~ 150 cell bodies known as the X-organ (XO), which is located in the medulla terminalis of the eyestalk ganglia (ESG) (Bliss and Welsh, 1952). Neurons from the XO send their axon projections distally to another ESG structure, the sinus gland (SG), a neurohemal organ located at the junction of the medulla interna and medulla externa (Bliss and Welsh, 1952). MIH is expressed in the ESG and throughout the central nervous system (CNS) (Lee et al., 2000; Stewart et al., 2013; Tiu and Chan, 2007; Zhu et al., 2011). The prevailing hypothesis is that MIH controls a single biological function, molt inhibition (Nakatsuji et al., 2009; Webster et al., 2012). In contrast, CHH is a multifunctional peptide that is important in reproduction, energy metabolism, osmoregulation, and molting (Böcking et al., 2002; Chan et al., 2003; Chang et al., 2001; Chung et al., 2010; De Kleijn et al., 1995; Webster et al., 2012). CHH and MIH inhibit ecdysteroid synthesis by binding two distinct receptors on the YO (Covi et al., 2009). CHH binds a membrane receptor guanylyl cyclase, GC-II, activating the intracellular signaling messenger cyclic guanosine monophosphate (cGMP) (Chung and Webster, 2006; Chung et al., 2010; Covi et al., 2009; Goy, 1990). Although the identity of the MIH receptor remains elusive, MIH activates numerous second messengers including cGMP, cAMP, NO, and $Ca^{2+}$, to repress eecdysteroidgenesis (Covi et al., 2009; Covi et al., 2008; Kim et al., 2004; Lee and Mykles, 2006; Mattson, 1986; Mykles et al., 2010; Spaziani et al., 2001; Spaziani et al., 1999). Activation of numerous second and intracellular signaling factors could be explained by MIH binding to a G-protein coupled receptor (Covi et al., 2009). Based on this hypothesis, MIH activation of cGMP would be nitric oxide (NO)-dependent. Expression of the NO producing enzyme, nitric oxide synthase (NOS), and the beta subunit

of a soluble GC-I (NO receptor) supports this hypothesis (Lee et al., 2007b; Lee et al., 2007c; McDonald et al., 2011).

In the ESG, a NO/cGMP signaling pathway is thought to regulate secretion of neuropeptides from the SG. NOS is expressed in the SG of the crayfish *Procambarus clarkii* (Lee et al., 2000), *Gecarcinus lateralis, Carcinus maenas*, and *Metacarcinus magister* (Chapter 4) and NO is produced in the SG of *C. maenas* (Pitts and Mykles, 2015). The half-life of NO is merely seconds in aqueous solutions (Moncada et al., 1991). Therefore, in order for NO to regulate neuropeptide secretion from the SG, NOS and MIH must be in close proximity or NO must be bound by a protein that prevents its degradation. In the SG of *C. maenas*, NO is bound by an unidentified endogenous protein, allowing NO to be released in the SG for prolonged periods (Pitts and Mykles, 2015). Additionally, NOS and MIH are localized in close proximity in the SG of *G. lateralis* and *C. maenas*, supporting the hypothesis that rapid production and degradation also plays a role in the regulation neuropeptide secretion from the SG (see Chapter 4). Evidence supporting both scenarios indicates that both transient and sustained presence of NO is important in the regulation of neuropeptide release from the SG. The present study examined changes in mRNA expression of MIH and CHH, as well as NOS and three GC's in an effort to better understand if peptide secretion from the SG is transcriptionally regulated throughout the molt cycle.

Molt induction techniques have been essential for studying crustacean molting for the last century. Multiple limb autotomy (MLA) is the removal of five or more walking legs and resembles a natural molt induction from predation or injury (MacLea et al., 2012; Skinner and Graham, 1970, 1972; Yu et al., 2002). Most decapod crustaceans, including *G. lateralis*, are responsive to MLA and their progress through the molt cycle can be monitored by measuring limb bud (LB) growth (MacLea et al., 2012; Skinner and Graham, 1970, 1972; Yu et al., 2002). In species responsive to MLA, molting can be suspended by the autotomy of a primary LB (Figure 2.1) (Skinner, 1985; Skinner and Graham, 1972). If LBA occurs during early premolt, molting is paused until a secondary limb bud forms and reaches the same size as the other primary regenerates (Skinner, 1985; Skinner and Graham, 1972). An MIH-like factor, limb autotomy factor - proecdysis ($LAF_{pro}$), is secreted from the secondary regenerate to suspend molting (Skinner, 1985). However, if a primary regenerate is autotomized during mid or late premolt, molting will continue and the crab will molt without a full set of walking legs (Figure 2.1) (Skinner, 1985).

Some species, such as the Bodega Bay population of *C. maenas*, are unresponsive to molt induction techniques (Abuhagr et al., 2014a) and therefore molting must be examined in wild populations.

The mammalian target of rapamycin (mTOR) plays a key role in cellular growth, nutrient signaling, and protein synthesis (Laplante and Sabatini, 2012; Loewith and Hall, 2011; Shaw and Cantley, 2006; Soulard et al., 2009). mTOR is a serine/threonine kinase that integrates mitogenic and nutrient inputs to regulate cell growth (Dobashi et al., 2011; Shaw and Cantley, 2006). mTOR activity is stimulated by amino acids, growth factors, and high energy levels (Dobashi et al., 2011; Laplante and Sabatini, 2012). Upstream of mTOR, protein kinase B (Akt) is activated by insulin and insulin-like peptides and inhibits the tuberous sclerosis complex (TCS) (Dobashi et al., 2011; Laplante and Sabatini, 2012). TCS is an inhibitor of a Ras homolog enriched in brain (Rheb), a GTP binding protein that directly binds and activates mTOR (Dobashi et al., 2011; Laplante and Sabatini, 2012; Shaw and Cantley, 2006). mTOR targets two proteins, p70 S6 kinase (S6K) and 4E (elF4E)-binding protein-1 (4E-BP1), which regulate mRNA translation (Dobashi et al., 2011; Magnuson et al., 2012; Shaw and Cantley, 2006). Understanding of the role of mTOR signaling in crustacean growth and development is still in its early stages. However, there is strong evidence supporting the hypothesis that mTOR performs the same function in crustaceans as it does in other organisms. mTOR signaling pathway components mTOR, Rheb, Akt, and S6K are expressed in the YO of *G. lateralis* and *C. maenas* and are involved in increased ecdysteroidgenesis in the YO (Abuhagr et al., 2014b). Expression of *Gl-mTOR* and *Gl-Akt* is elevated in *G. lateralis* during premolt when ecdysteroid synthesis is at its peak (Abuhagr et al., 2014b). Ecdysteroidgenesis in the molting gland of insects (prothoracic gland, PG) is also mTOR-dependent (Gu et al., 2012; Mirth and Shingleton, 2012). In order to explore if changes in protein synthesis in the ESG could contribute to MIH regulation of molt progression, changes in mRNA expression of four mTOR signaling pathway genes were examined.

In order to gain a better understanding of how peptide production and release in the ESG contributes to molt cycle regulation, the expression of MIH, CHH, NOS, NOSIP, GC-Iβ, GC-II, and GC-III genes were examined in *G. lateralis* induced to molt by MLA and in naturally molting *C. maenas*. Given the importance of mTOR in growth and development in most organisms, four components of the mTOR signaling pathway, mTOR, Akt, Rheb, and S6K, were also examined. Modest changes in gene

expression of all genes examined suggests that neuropeptide secretion from the ESG is regulated post transcriptionally.

## RESULTS

*Effect of molting on hemolymph ecdysteroid titers in G. lateralis*

*G. lateralis* were multiple limb autotomized and entered premolt a few weeks later. Molt stages were monitored using the R-index. Hemolymph ecdysteroid titers were low during intermolt (~ 6 pg/µl; control group), began to rise during early premolt (~ 26 pg/µl; mean R-value ~ 14), continued to increase in mid-premolt (~ 70 pg/µl; mean R-value ~ 17), peaked in late premolt (~ 104 pg/µl; mean R-value ~ 20.8), and dropped below intermolt levels during post molt (~ 1.63 pg/µl) (Figure 2.2). Ecdysteroid titers were lowest during post molt, indicating that the YO's had returned to the basal state.

*Changes in gene expression of neuropeptides and mTOR signaling genes throughout the molt cycle in G. lateralis*

There were significant effects of molting on *Gl-MIH, Gl-CHH, Gl-GC-Iβ, Gl-GC-II*, and *Gl-GC-III* mRNA levels (Figure 2.3A). *Gl-MIH* and *Gl-CHH* increased significantly during mid-premolt compared to intermolt animals (*Gl-MIH* 21.3-fold; *Gl-CHH* 6.7-fold). *Gl-MIH* expression was significantly higher at mid-premolt compared to late premolt (9.6-fold). Increased levels of *Gl-MIH* during mid-premolt caused expression during this molt stage to be significantly higher than late premolt animals (9.6-fold). Additionally, *Gl-MIH* was significantly greater during early premolt (6.1-fold) and post molt (5.4-fold) compared to intermolt animals. There was no significant effect of molt on *Gl-NOS* or *Gl-NOSIP* expression at any time point. *Gl-GC-Iβ* was elevated during mid (12.7-fold) and late (11.4-fold) premolt, as well as during post molt (11.8-fold) compared to intermolt animals. There was an increase in *Gl-GC-II* expression during mid-premolt (14.7-fold) compared to intermolt animals. *Gl-GC-III* expression increased significantly during post molt compared to intermolt (3.6 x $10^3$-fold), mid-premolt (1.5 x $10^3$-fold), and late premolt (1.9 x $10^3$-fold) animals.

Molting significantly affected the expression of all mTOR signaling pathway genes: *Gl-Akt, Gl-mTOR, Gl-S6K*, and *Gl-Rheb*, as well as *Gl-EF2* (Figure 2.3B). Elongation factor 2 (EF2) is a constitutively expressed translation protein and is used as a reference for mTOR independent translation. *Gl-Akt* increased significantly during post molt compared to mid-premolt (46-fold). *Gl-mTOR* expression

was highest during mid-premolt compared to intermolt (57-fold increase), late (7.1-fold increase), and post molt (6-fold increase). Expression of *Gl-S6K, Gl-Rheb*, and *Gl-EF2* all increased in response to molt, having higher expression at all three premolt stages and during post molt compared to intermolt animals. Compared to intermolt, *Gl-S6K* expression increased 14-fold in early premolt, 27-fold at mid-premolt, 13.5-fold during late premolt, and 8.1-fold during post molt. Additionally, there was a significant decrease in *Gl-S6K* expression between mid premolt and post molt (3.4-fold). *Gl-Rheb* expression followed a similar pattern, increasing 53-fold in early premolt, 62-fold in mid and late premolt, and 29-fold during post molt compared to intermolt. Expression of *Gl-EF2* increased by 48-fold during early premolt, 78-fold during mid-premolt, 1.4 x $10^2$-fold during late premolt, and 1.1 x $10^2$-fold during post molt.

*Effects of limb bud autotomy on hemolymph ecdysteroid titers in G. lateralis*

Autotomy of limb buds during early premolt suspends molting while a new limb bud is regenerated, allowing the animal to molt with a full set of walking legs (Skinner, 1985). However, once an animal has entered mid-premolt they are committed to molting and removal of a LB has no effect on molt progression. Limb bud autotomy (LBA) was performed in an attempt to suspend molting in *G. lateralis*. Animals were induced to molt via MLA and regenerating limb buds were autotomized during early, mid, and late premolt. Following LBA molt progression was monitored using an R-index and animals were harvested during early, mid, and late premolt. Hemolymph was taken from LBA animals on the day of harvest. Hemolymph ecdysteroid titers in LBA animals followed a similar pattern as MLA animals, indicating that molt suspension was not successful in this experiment. Titers were low during early premolt (~ 23 pg/µl; R-value ~ 14), increased during mid-premolt (~ 61 pg/µl; R-value ~ 17), and reached a peak in late premolt (~160 pg/µl; R-value ~ 20.8) (Figure 2.4).

*Effects of molt suspension by LBA on gene expression of MIH and mTOR signaling genes in G. lateralis*

LBA had a moderate effect on MIH signaling pathway peptides and components (Figure 2.5A). LBA significantly affected *Gl-MIH* expression during mid-premolt, increasing by 3.6-fold compared to intermolt animals. LBA had no effect on *Gl-CHH* expression. *Gl-NOS* expression was significantly lower in LBA animals during mid (14.4-fold) and late (13.6-fold) premolt compared to mid and late premolt MLA animals. Expression of *Gl-GC-Iβ* was significantly higher in mid (5.6-fold) and late (5.6-fold) premolt LBA

animals compared to intermolt. *Gl-GC-Iβ* expression was lower in LBA animals during early premolt (3.8-fold) compared to early MLA animals.

LBA had a significant effect on *Gl-EF2* and all mTOR signaling pathway genes *Gl-Akt, Gl-mTOR, Gl-S6K*, and *Gl-Rheb* (Figure 2.5B). Expression of *Gl-Akt* decreased significantly compared to intermolt during early ($1.5 \times 10^3$-fold) and late ($2.7 \times 10^2$-fold) premolt. Early LBA ($1.5 \times 10^3$-fold) and late LBA ($3.6 \times 10^2$-fold) expression was also significantly lower compared to MLA at the same time points. *Gl-mTOR* was modestly effected by LBA, expression being higher in late LBA compared to late MLA (9-fold). Similar to MLA, LBA significantly increased expression of *Gl-S6K, Gl-Rheb*, and *Gl-EF2* at all three premolt stages compared to intermolt. *Gl-S6K* increased by 22-fold during early premolt, 13.9-fold during mid-premolt, and 9-fold during late premolt. LBA caused a significant increase in *Gl-Rheb* expression compared to intermolt animals during early (21-fold), mid (44-fold), and late (15-fold) premolt. *Gl-EF2* expression also increased at all three premolt stages (early 9.7-fold; mid 22-fold; late 18-fold).

*Effects of spontaneous molting on hemolymph ecdysteroid titers in Carcinus maenas*

Naturally molting *C. maenas* were collected from Bodega Harbor in Bodega Bay, CA. Molt stage was determined by ELISA and the state of the integumentary tissue. Ecdysteroid titers followed an expected pattern having low concentration during intermolt (~ 6.5 pg/μL), increasing during early premolt (~ 43 pg/μL), and being lowest during post molt (~ 2 pg/μL) (Figure 2.6). Animals at mid and late premolt were not available.

*Changes in gene expression of MIH and mTOR signaling genes in spontaneous molting C.maenas*

In addition to examining the effects of molting on transcription in the ESG of the semi-terrestrial land crab, a marine species, *Carcinus maenas* was also examined for comparison. There was minimal effect of molt stage on gene expression on MIH signaling pathway genes (Figure 2.7A). Molt increased *Cm-MIH* expression in post molt animals by 8.5-fold compared to intermolt. *Cm-GC-II* was the only other MIH signaling pathway gene affected by molt, decreasing in post molt animals by 2.5-fold compared to intermolt and 2.9-fold compared to premolt. There was no effect of molt on *Cm-CHH, Cm-NOS, Cm-GC-Iβ*, or *Cm-GC-III*.

There was also no effect of molt stage on any mTOR signaling pathway genes: *Cm-Akt, Cm-mTOR, Cm-S6K*, and *Cm-Rheb*. There was a significant effect of molt on *Cm-EF2* expression,

decreasing in postmolt by 8.5-fold compared to intermolt (Figure 2.6B). These results suggest that the molecular effects of molting in the Bodega Bay population of *C. maenas* occur post transcriptionally.

## DISCUSSION

Molt progression in decapod crustaceans is principally regulated by two hormones, ecdysteroids (e.g., 20E) and MIH. Ecdysteroids are a class of steroid molting hormones synthesized and secreted by the molting gland or Y-organ (YO) (Chang and Mykles, 2011). MIH is a peptide hormone produced in the XO and is released from the SG in the ESG (Hopkins, 2012). MIH is proposed to inhibit molting by binding an unidentified receptor on the YO membrane, activating a signaling cascade that inhibits the synthesis of ecdysteroids (Chang and Mykles, 2011). MIH isolated from ESG extracts and recombinant MIH inhibits ecdysteroidgenesis *in vitro* and *in vivo* (Chung et al., 2010; Okumura et al., 2005; Soumoff and O' Connor, 1982; Webster and Keller, 1986). The hypothesis is that MIH works as an on on/off switch to regulate molting and therefore MIH concentrations in the hemolymph should be inversely proportional to hemolymph ecdysteroid titers. However, MIH titers in crayfish and crustaceans do not reflect this hypothesis (Chung and Webster, 2005; Nakatsuji and Sonobe, 2004). The effects of MIH on the YO has been widely investigated. However, a limited amount of research examined the regulation of MIH in the ESG. In order to extend the current understanding of MIH regulation in the ESG, the present study compared changes in gene expression in ESG during the molt cycle of two decapod crustacean species, *G. lateralis* and *C. maenas*.

*Effects of molting on neuropeptide expression in the ESG of G. lateralis and C. maenas*

Previous studies found that mRNA levels of MIH and CHH in SG of *C. maenas* are unchanged during the molt cycle (Chung and Webster, 2003). Results from the current study showed a significant increase in MIH transcript levels in post molt *C. maenas* (Figure 2.7A). During post molt the YO re-enters its basal state and again becomes sensitive to MIH (Chang and Mykles, 2011). An increase in MIH expression during post molt would prevent the animal from re-entering the molt cycle until the exoskeleton is fully resynthesized and the YO resumes basal activity. Similar to an increase in MIH hemolymph titers during mid and late premolt in *Procambarus clarkii*, MIH mRNA expression in the ESG increases during mid-premolt in *G. lateralis* (Figure 2.3A). Increased MIH expression in the ESG could contribute to an increase in MIH hemolymph titers in *G. lateralis*. The increase in hemolymph MIH during

mid-premolt would contribute to YO repression following ecdysis (Chang and Mykles, 2011). CHH expression is unchanged throughout the molt cycle in *C. maenas* (Figure 2.7A), which is in agreement with previous findings (Chung and Webster, 2003, 2005). Given that CHH is a multifunctional protein, it is not surprising that it is consistently expressed throughout the molt cycle. In contrast, *Gl-CHH* is significantly greater during mid-premolt compared to intermolt and early premolt (Figure 2.3A). This up-regulation mat be a response to the physiological stress the animal undergoes in preparation for ecdysis.

*Changes in expression of NOS and GC's in response to molting in G. lateralis and C. maenas*

MIH is released in pulses at 5 min intervals from the XO/SG complex (Chung and Webster, 2003; Covi et al., 2012). MIH synthesis in the XO does not occur rapidly enough to keep up with this consistent release (Chung and Webster, 2003). It has long been known that the SG is not only a site for neuropeptide release, but is also a storage site for neuropeptides (Hanström, 1939). Therefore a potential mechanism for the regulation of the pulsatile release of MIH is the control of neuropeptide secretion from the SG. It is hypothesized that the gaseous signaling molecule nitric oxide (NO) negatively regulates neuropeptide release from the SG (Pitts and Mykles, 2015). NO is synthesized by the enzyme NOS in a reaction that requires L-arginine, $O_2$, and NADPH (Colasanti and Venturini, 1998). NO is produced rapidly and diffuses across cell membranes, making it an ideal candidate for controlling the pulsatile release of MIH. In the mammalian adrenal gland, NO negatively regulates hormone release through the activation of a NO/cGMP signaling pathway (Schwarz et al., 1998). NO is produced in the SG of intermolt *C. maenas* (Pitts and Mykles, 2015) and NOS is expressed in close proximity to MIH filled synaptic vesicles (see Chapter 4), which is consistent with the hypothesis that NO regulates neuropeptide secretion from the SG.

In the present study changes in transcript abundance of components of the NO/cGMP signaling pathway were examined. There was no effect of molt stage on the expression of NOS or the NO receptor GC-Iβ in either species (Figure 2.3A and 2.7A). This result indicates that if NO/cGMP contributes to MIH secretion, then its effects are post transcriptional (i.e. the activity of the NOS enzyme). However, expression of the two other GC's were significantly changed in response to molting. In *G. lateralis*, *Gl-GC-III* expression increased in post molt animals (Figure 2.2A). GC-III is a class of GC's that is only expressed in invertebrates (Morton, 2004). Originally discovered in the hawk moth, *Manduca sexta*, GC-

III is a soluble NO-insensitive GC (Morton, 2004; Nighorn et al., 1999). GC-III is thought to regulate hormones during pupal ecdysis in *M. sexta* (Morton and Simpson, 2002) and may play a similar role in hormone regulation during molting in *G. lateralis*. Changes in *Gl-GC-III* expression are not indicative of effects of molting on NO/cGMP signaling, but rather are examined as a baseline for monitoring the overall transcriptional changes in the ESG in response to molting. In post molt *C. maenas*, expression of a membrane bound GC, *Cm-GC-II,* decreased (Figure 2.6A). This decrease in expression may be contribute to a decrease in signaling from extracellular ligands or intracellular activating proteins that bind to this receptor (Padayatti et al., 2004).

*Identification of a nitric oxide synthase inhibitory protein in G. lateralis*

This study identified and examined changes in expression of a nitric oxide synthase inhibitory protein (NOSIP). The sequence for this inhibitory protein was obtained from analysis of the *G. lateralis* YO transcriptome (Das et al., in preparation). NOSIP is an inhibitor of insulin activated nitric oxide production in mammalian blood (Ray et al., 2012). Additionally, NOSIP plays a role in trafficking endothelial NOS in endothelial cells (Su, 2014). There was no effect of molting on *Gl-NOSIP* expression in the SG of *G. lateralis* (Figure 2A). However, given the conserved nature of nitric oxide signaling across animal taxa (Palumbo, 2005), it is likely that the function of NOSIP in crustaceans is similar to mammals and the effects of molting will be observed in the hemolymph or blood vessels.

*Effects of molting on gene expression of mTOR signaling pathway components in G. lateralis and C. maenas.*

mTOR is a kinase that is important in the regulation of growth and metabolism (Laplante and Sabatini, 2012). Four key components of the mTOR signaling pathway were examined in the present study. Akt provides a line of communication between extracellular signals (i.e. environmental cues) and the translational machinery (Roux and Topisirovic, 2012). Ras homolog enriched in brain (Rheb), a member of the Ras super family of GTP binding proteins, directly regulates mTOR activity via the hydrolysis of GTP to GDP (Laplante and Sabatini, 2012; Teleman, 2010). mTOR regulates translation by phosphorylating a downstream target, S6K (Magnuson et al., 2012; Zoncu et al., 2011). mTOR is an important regulator of protein synthesis that is necessary for the activation of the molting glands in both insects and crustaceans (Abuhagr et al., 2014b; Morita et al., 2013; Rewitz et al., 2013; Teleman, 2010;

Thoreen et al., 2012). Given the importance of mTOR signaling in hormone production in the YO, changes in expression of mTOR signaling pathway components were examined in the ESG of both *G. lateralis* and *C. maenas*. *Gl-EF2* was included as a reference for mTOR independent translation.

Molting had a significant effect on the expression of *Gl-EF2* and all mTOR signaling pathway components in *G. lateralis*. An increase in *Gl-Akt* during post molt suggests that an increase in translational regulation occurs during this molt stage (Figure 2.3B). As the exoskeleton beings to harden and reform during post molt, ecdysteroid synthesis must be repressed and an increase in Akt could be a mechanism for signaling the inhibition of further ecdysteroidogenesis. mTOR expression increases during mid-premolt, which could contribute to increased protein synthesis necessary for exoskeleton reformation (Figure 2.3A). *Gl-S6K, Gl-Rheb* and *Gl-EF2* all follow the same pattern of expression, increasing during early premolt and remaining elevated throughout the molt cycle (Figure 2.3B). This suggests that the mTOR pathway may be self-regulating or that another transcription factor regulates transcription of mTOR signaling pathway genes. Recently the transcription factor REPTOR was identified as a regulator of transcription when mTOR signaling is inactivated (Tiebe et al., 2015). During the stressful and taxing process of molting, mTOR may be inactivated for short periods of time and another transcription factor may activate in order continue molt progression and allow for nutrient recovery and mTOR reactivation.

Expression of mTOR signaling genes is unaffected by molt in *C. maenas*, indicating that the effects of molt are regulated post transcriptionally in this species. This is consistent with results from previous studies conducted in this population of *C. maenas* (Abuhagr et al., 2014a). A decrease in *Cm-EF2* during post molt suggests that translation decreases after ecdysis allowing the YO to return to a basal state.

*Effects of molt suspension on MIH and mTOR signaling pathway genes in G. lateralis*

In *G. lateralis*, when a primary limb regenerate is autotomized during early premolt, molting is suspended until a secondary regenerate is formed, allowing the animal to molt with a full set of walking legs (Figure 2.1) (Holland and Skinner, 1976; Skinner and Graham, 1972). However, if a primary limb bud is removed in mid-premolt or later, molting continues and the animal molts without a full set of walking legs (Figure 2.1) (Skinner, 1985). In the present study the effects of molt suspension by LBA on

the expression of MIH and mTOR signaling pathway components was compared to uninterrupted molt induction (MLA).

*Gl-MIH* expression was minimally effected by molt suspension, only increasing significantly during mid-premolt compared to intermolt (Figure 2.4A). This supports the hypothesis that ESG MIH does not contribute to molt suspension but rather a limb autotomy factor-proecdysial ($LAF_{pro}$) secreted from the regenerating secondary LB is responsible for regulating molt suspension (Skinner, 1985). There was a modest but insignificant effect of molt suspension on *Gl-CHH* expression during early premolt (Figure 2.5B). Unlike expression in MLA animals, *Gl-CHH* decreases in LBA animals during early premolt. This suggests that the primary role of $LAF_{pro}$ is to regulate physiological homeostasis during molt suspension. Expression of *Gl-NOS* and *Gl-GC-Iβ* were downregulated in molting suspended animals compared to MLA animals (Figure 2.5A). Decreased expression of *Gl-GC-Iβ* during early premolt in LBA animals was followed by decreased expression of *Gl-NOS* during mid and late premolt. This could impact the release of neuropeptides from the SG which may be necessary in maintaining homeostasis during molt suspension.

The effects of molt suspension were more pronounced in mTOR signaling pathway genes (Figure 2.5B). *Gl-Akt* was downregulated at all three premolt stages compared to intermolt and MLA animals from that same molt stage. This suggests that in order to prevent molt progression, signal transduction regulating translation is decreased in order to maintain the physiological state of the animal. Similar to MLA animals, expression of *Gl-S6K, Gl-Rheb*, and *Gl-EF2* are upregulated during all three premolt stages. The data suggests that LBA was unsuccessful at suspending molting in these animals. Therefore it is not surprising that changes in gene transcript levels in LBA animals is similar to MLA animals.

*Conclusions*

This study contributes to the limited knowledge regarding the regulation of ESG neuropeptides throughout the molt cycle. There was a significant effect of molt stage on MIH and mTOR signaling pathway gene expression in the ESG of *G. lateralis*. Continuous elevation of MIH transcript abundance during pre and post molt indicates that MIH secretion from the SG into the hemolymph is not regulated by changes in transcript abundance. An increase in *Gl-GC-Iβ* expression during mid to late premolt supports

the hypothesis that NO/cGMP signaling may be the mechanism for regulating hemolymph MIH titers throughout the molt cycle. Molting significantly increased expression of *Gl-Akt, Gl-mTOR, Gl-Rheb*, and *Gl-S6K* in one or more molt stages. This is not surprising given that protein synthesis increases systemically in order to accommodate the physiological changes required for successful ecdysis. Molt suspension via LBA does not induce a remarkable change in gene expression and changes in transcript abundance are comparable to MLA animals. There was only a modest effect of molting on gene expression in *C. maenas*. This is in line with previously reported results in this species and supports the hypothesis that molt regulation occurs post transcriptionally.

## MATERIALS AND METHODS

*Animals*

Adult male *Gecarcinus lateralils* were collected in the Dominican Republic and shipped to Denver, CO, USA. Animals were housed at 27℃ ± 2℃ in 85 -95% relative humidity on a 12 h: 12 h light:dark cycle (Covi et al., 2010). Animals were kept in group cages (10-15 animals per cage) with aspen bedding moistened with 10 ppt Instant Ocean and fed a diet of carrots, lettuce, and raisins biweekly. Molting was induced by multiple leg autotomy (MLA), a technique that resembles a “natural” molt. Animals induced to molt by MLA were maintained in individual cages with a quartz sand substrate moistened with 10 ppt Instant Ocean. Prior to entering the molt cycle, animals form basal regenerates which turn into regenerating limbs as the animals enters premolt. These regenerating limbs provide an external measure of molt progression defined as a R-index (regenerate length x 100/carapace width) (Covi et al., 2010; Yu et al., 2002). The R-index increases from 0 to 23 prior to ecdysis (Skinner and Graham, 1972; Yu et al., 2002). Intermolt animals were defined by an R value of 8-12.9, early premolt, 13-15, mid premolt 16-18, and late premolt 19-22. Molting was suspended in *G. lateralis* by limb bud autotomy (LBA). Post MLA, regenerating limb buds were autotomized during early, mid, and late premolt.

*C. maenas* were collected from Bodega Harbor in Bodega Bay, California. They were maintained under ambient conditions in a flow-through sea water system (12-15 ℃) at Bodega Marine Laboratory (Abuhagr et al., 2014a). Molt stage was determined by hemolymph ecdysteroid concentrations and integumentary structure (Abuhagr et al., 2014). Ecdysteroids were quantified in both *G. lateralis* and *C. maenas* using a competitive enzyme-linked immunoassay (ELISA) (Abuhagr et al., 2014a; Kingan, 1989).

*Effects of molting on gene expression in the ESG*

ESG from *G. lateralis* were dissected for qPCR at five difference molt stages (intermolt, early premolt, mid premolt, late premolt, and 10 days post molt) and from naturally molting *C. maenas* at three different molt stages (intermolt, early premolt, and post molt). For both species, hemolymph samples were taken prior to each dissection for ecdysteroid ELISA. RNA was isolated from homogenized tissue using TRIzol reagent (Life Technologies, Carlsbad, CA USA) according to the manufacture's protocol (see (Pitts and Mykles, 2015) for detailed protocol). cDNA was synthesized with Transcriptor Reverse Transcriptase (Roche Diagnostics, Indianapolis, IN USA) and an oligo-dT primer (50 µmol).

A Light Cycler 480 thermal cycler (Roche) was used to quantify levels of *EF2* (Gl - AY552550; Cm – GU808334)*, mTOR* (Gl – HM989973; Cm – JQ864248)*, Rheb* (Gl – HM989971; Cm – HM989970)*, Akt* (Gl – HM989974; Cm – JQ864249)*, S6K* (Gl – HM989975; Cm – JQ86425)*, GC-Iβ* (Gl - DQ355434; Cm – JQ911525)*, GC-II* (Gl - DQ355437; Cm – JQ911527) *, GC-III* (Gl – DQ355438; Cm – JQ911526) *, NOS* (Gl – AY552549; Cm – GQ862349)*, NOSIP* (c141319_g1_i1)*, MIH* (Gl – DQ473354; Cm – X75995)*,* and *CHH* (Gl – DQ473354; Cm – AF88680) mRNA's from both *G. lateralis* and *C. maenas*. For all genes except *NOS* and *MIH*, SYBR green was used to quantify mRNA in both species. 10 µL reactions consisted of 5 µL 2x SYBR Green I Master mix (Roche), 0.5 µL each of 10 mM forward and reverse primers [*mTOR, Rheb, S6K, Akt*, and *EF2* for both species (Abuhagr et al., 2014b)*; Cm-NOS, Cm-MIH, Cm-GC-Iβ, Cm-GC-II* and *Cm-GC-III* (Abuhagr et al., 2014a); *Gl-GC-Iβ, Gl-GC-II* and *Gl-GC-III (Lee et al., 2007b)*; *Gl-CHH* (Lee et al., 2007a); *Gl-NOSIP* and *Cm-CHH* (Table 2.1)], 3 µL nuclease-free water, and 1 µL cDNA or standard. *NOS* and *MIH* were was quantified using universal Probe #17 and #13, respectively (Roche). 10 µL reactions for *Gl-NOS* and *Gl-MIH* were set up with 5 µL LightCycler 480 Probes Master (Roche) 0.2 µL each of 20 mM forward and reverse primers (Table 1), 0.2 µL universal Probe #17 or #13, 1.9 µL nuclease free water, and 2.5 µL of cDNA. PCR conditions were as follows: initial denaturation at 95℃ for 5 min, 50 cycles of denaturation at 95℃ for 10 s, annealin g at 57 ℃ for 30 s and extension at 72℃ for 1 min. For each gene, a series of dsDNA standards were produced by 10-fold serial dilutions and transcript concentrations calculated with the LightCycler 480 software (Roche, version 1.5). Absolute amount of transcript copy numbers per µg of total RNA in the cDNA synthesis reaction were calculated based on the standard curve and the molecular weight of the dsDNA products.

*Analysis and Software*

Statistical analysis was performed using JMP version 12.0 (SAS Institute, Inc., Cary, NC USA) and graphs were generated with SigmaPlot version 12.0 (Systat Software Inc., San Jose CA, USA). All qPCR data was log transformed to reduce variances from the mean. A Brown-Forsythe test ($p < 0.05$) confirmed the variances among log-transformed data were equivalent. Means for transcript abundance were compared using an analysis of variance (ANOVA) and post-hoc multiple comparisons were made using Tukey-Kramer HSD tests. A paired t-test was used to compare the means for transcript abundance between intermolt and other molt stages. Data are represented as mean ± 1 S.E. and the level of significance was set at $\alpha = 0.05$. Fold changes indicated in the text were calculated based on raw expression levels of each gene.

**Table 2.1 qPCR Primer Sequences.** Previously unpublished primer sequences.

| Primer | Sequence (5' – 3') | Product size (bp) |
|---|---|---|
| Gl-NOS F1 | CATCACCCACCCTGAGTACA | 60 |
| Gl-NOS R1 | GGGAGGCCATACCATTGAA | |
| Gl-MIH F1 | AACATTGACTTCCTGTGGTGTG | 71 |
| Gl-MIH R1 | ACGAGCTCACACCGATACGT | |
| Gl-NOSIP F1 | GCAGCCTCTCCCTTCACCC | 178 |
| Gl-NOSIP R1 | GCCTCACCCAACTCCTCCAAC | |
| Cm-CHH F2 | GTGACGATTGTTACAACCTCTACAG | 166 |
| Cm-CHH R2 | GTTTACTTCTTCCTGCCAACCATC | |

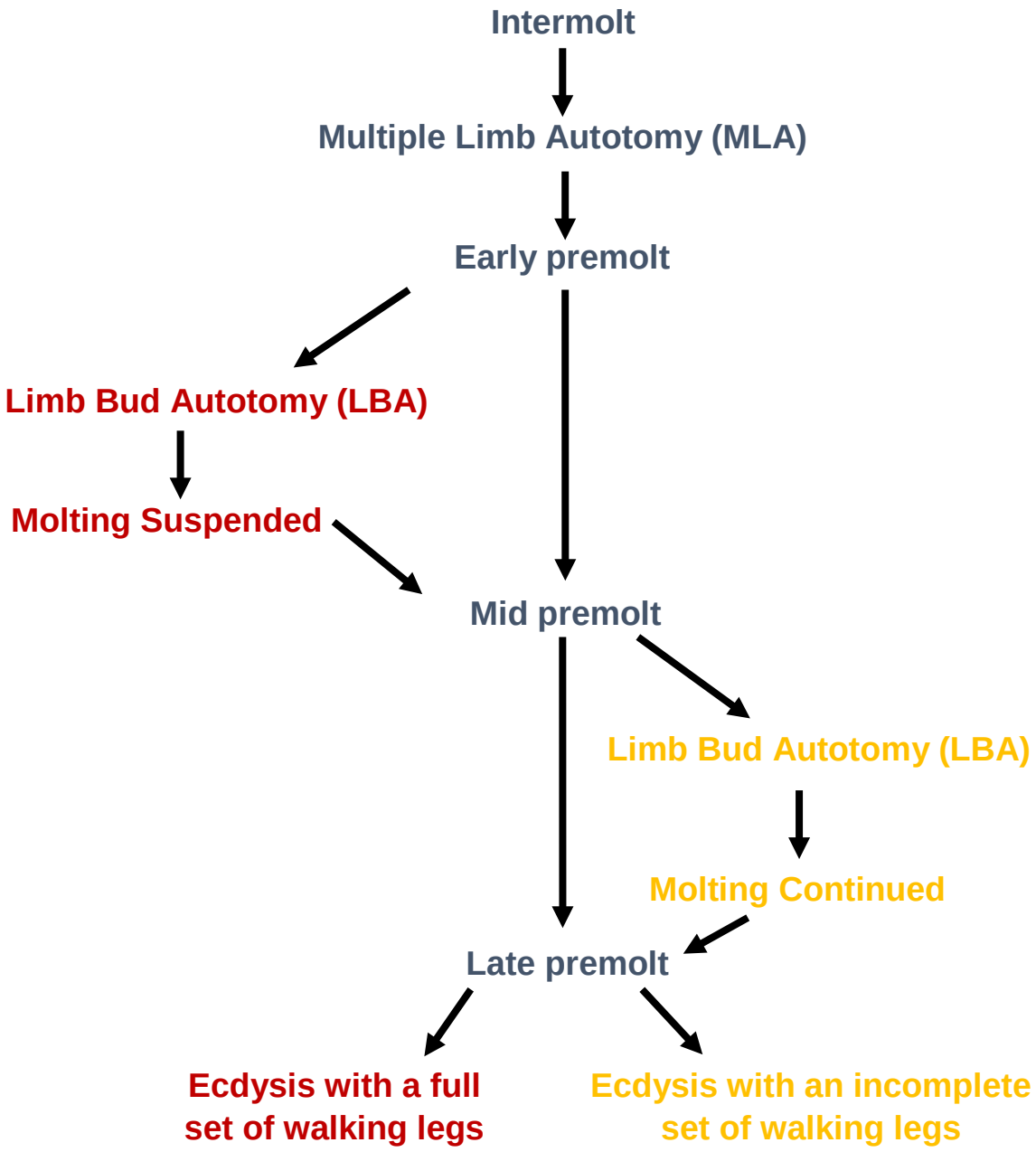


F**igure 2.1 Effects of limb bud autotomy (LBA) during the molt cycle.** Animals induced to molt via multiple limb autotomy (MLA) will suspend molting if a limb bud regenerate is autotomized during early premolt. The animal will suspend molting until a new LB is formed and has grown to the same size as the existing LB's, thus allowing the animal to molt with a full set of walking legs. If a limb bud is autotomized after early premolt molting will continue and the animal will molt with an incomplete set of walking legs.

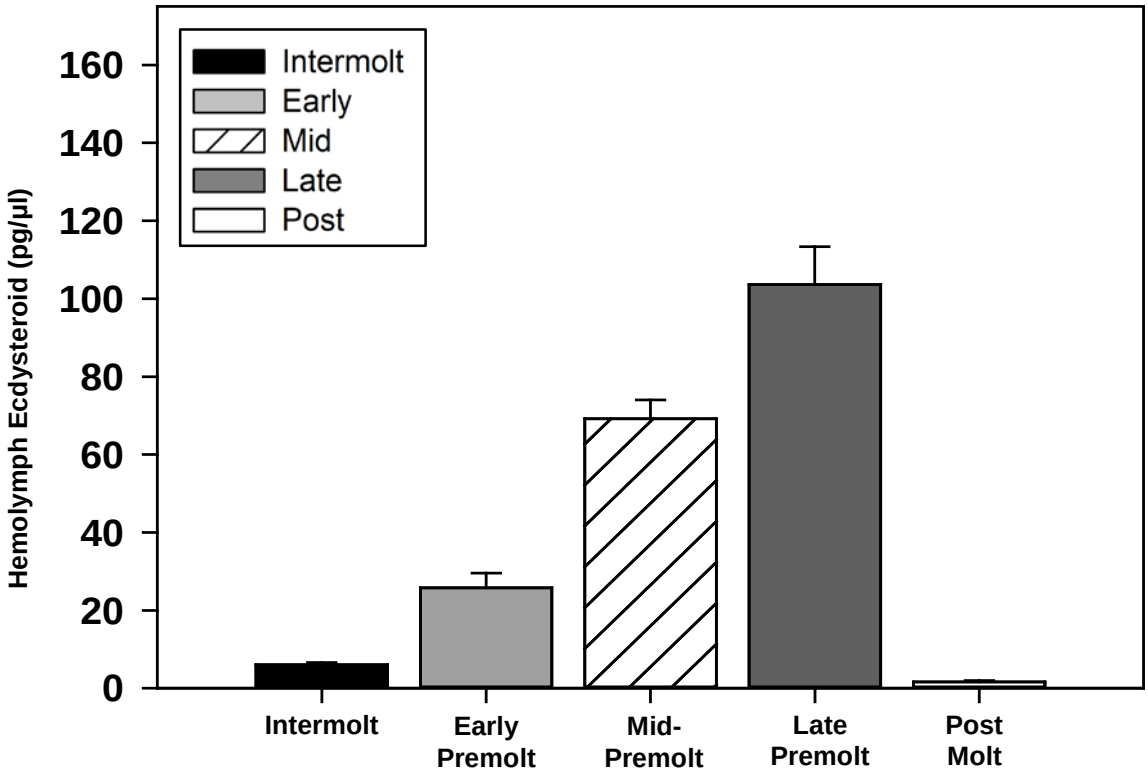


**Figure 2.2 Effects of molting on hemolymph ecdysteroid titers in *G. lateralis*.** Hemolymph was collected from *G. lateralis* induced to molt via MLA. Samples were collected from intermolt, early premolt, mid-premolt, late premolt, and post molt stages determined using an R-index. Ecdysteroid titers were quantified by ELISA. Data are presented as mean $\pm$ S.E. (intermolt n = 12; early premolt n = 40; mid premolt n = 46; late premolt n = 48; post molt n = 17). All means are significantly different ($P < 0.05$) with the exception of intermolt vs. early premolt and intermolt vs. post molt.

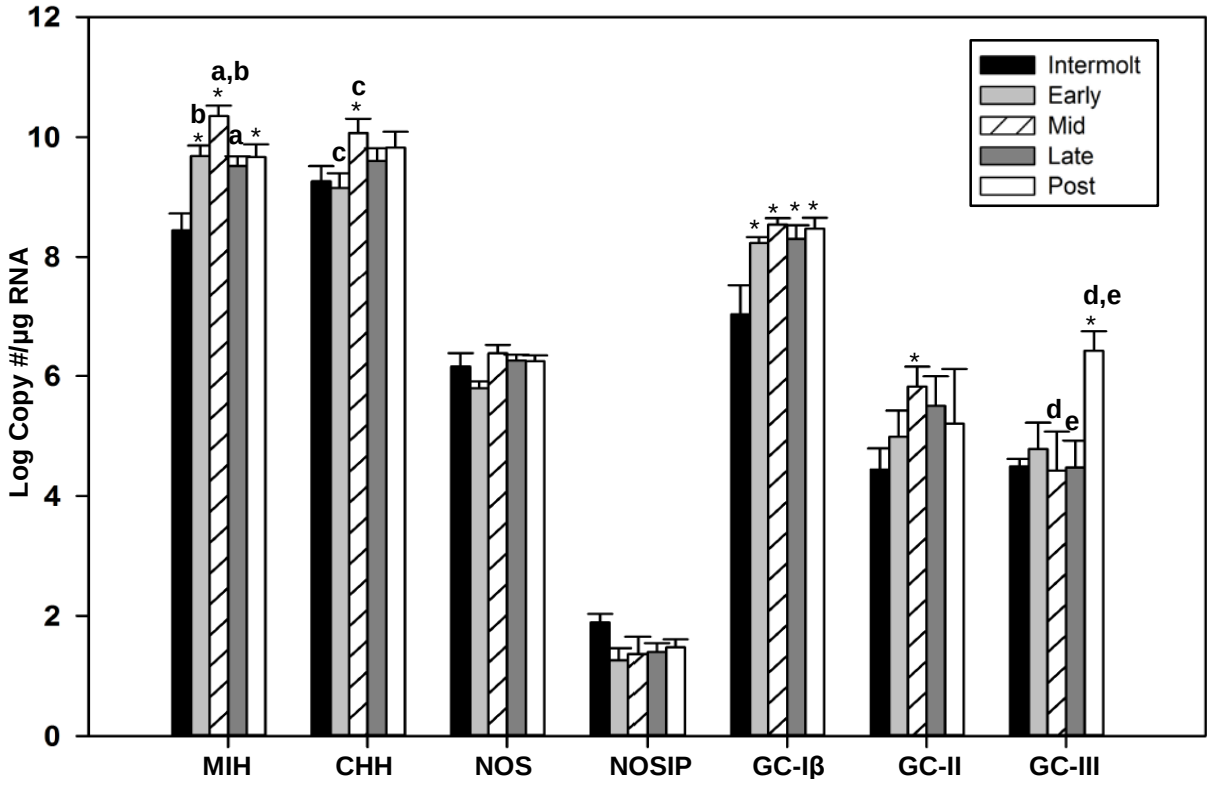


**Figure 2.3A Effects of molting on expression of MIH signaling pathway genes in the ESG of *G. lateralis*.** qPCR quantification of changes in mRNA expression between molt stages in the ESG. ESG were collected from *G. lateralis* induced to molt via MLA. Samples were collected from intermolt, early premolt, mid-premolt, late premolt, and post molt stages determined using an R-index. Time points with means that are significantly different from intermolt are indicated with a "*" and means that share a letter are significantly different. Only 3-fold or greater changes in expression are indicated on the graphs. A. Changes in expression of MIH signaling pathway components and related genes; *Gl-MIH, Gl-CHH, Gl-NOS, Gl-NOSIP, Gl-GC-Iβ, Gl-GC-II*, and *Gl-GC-III*.

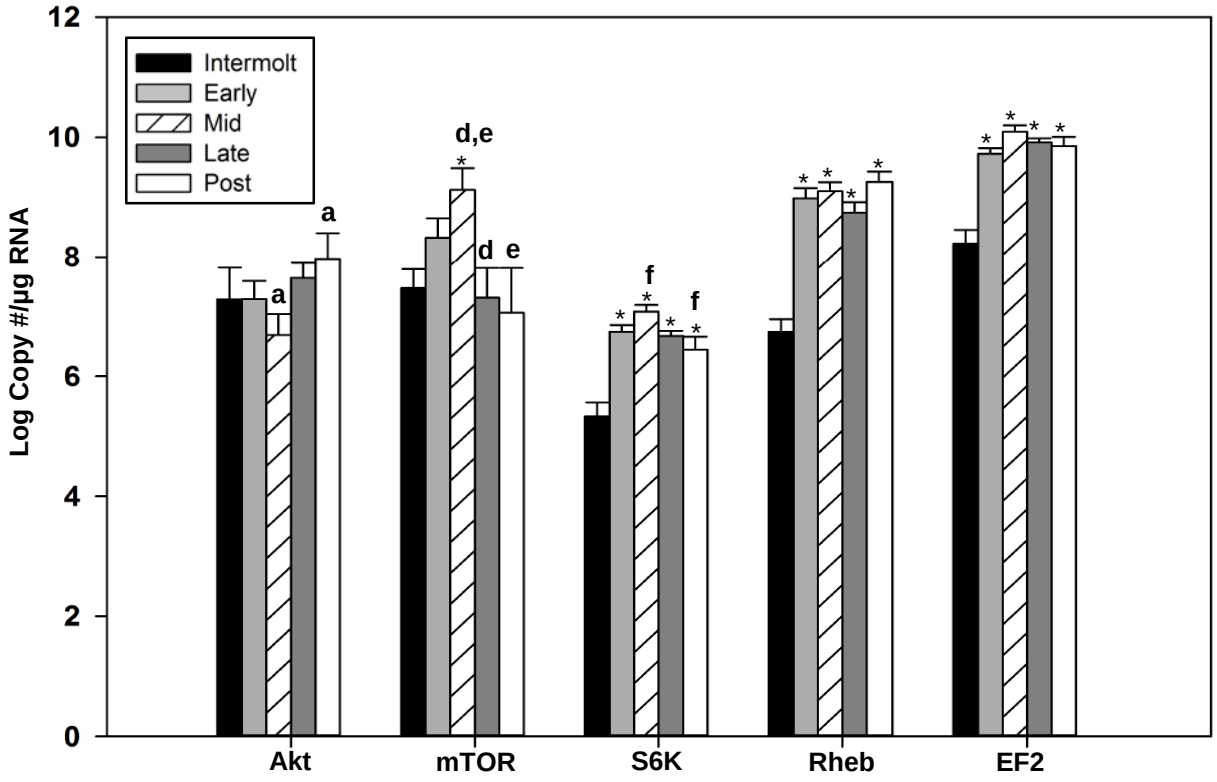


**Figure 2.3B Effects of molting on expression of mTOR signaling pathway genes in the ESG of *G. lateralis*.** qPCR quantification of changes in mRNA expression between molt stages in the ESG. ESG were collected from *G. lateralis* induced to molt via MLA. Samples were collected from intermolt, early premolt, mid-premolt, late premolt, and post molt stages determined using an R-index. Time points with means that are significantly different from intermolt are indicated with a "*" and means that share a letter are significantly different. Only 3-fold or greater changes in expression are indicated on the graphs. Changes in expression of *Gl-EF2* and mTOR signaling pathway genes *Gl-mTOR, Gl-S6K, Gl-Rheb*, and *Gl-Akt*.

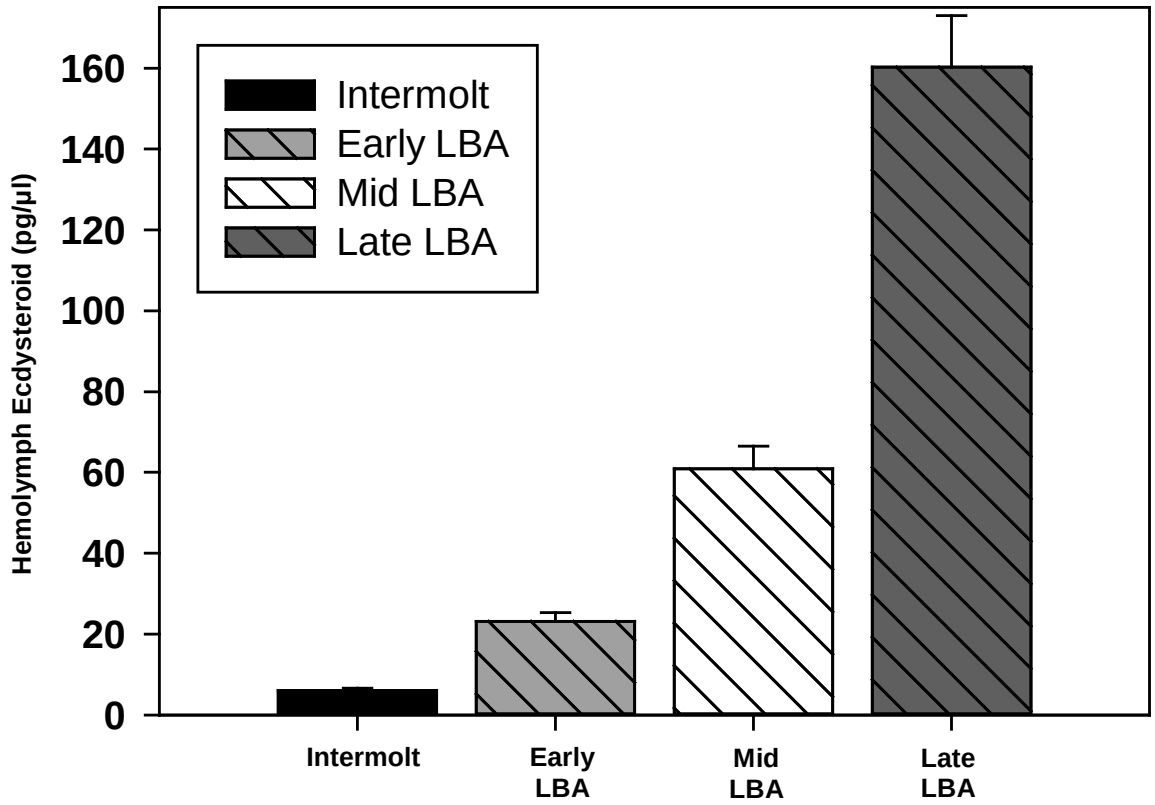


**Figure 2.4 Effects of LBA on hemolymph ecdysteroid titers in *G. lateralis*.** Limb buds (LB) were autotomized at early, mid, and late premolt stages determined based on the R-index. Hemolymph was collected from LBA animals no the day of tissue harvest at all three premolt stages. Ecdysteroid titers were quantified by ELISA. Data are presented as mean ± S.E. (early premolt n = 14; mid premolt n = 11; late premolt n = 13). Intermolt data is the same as in Figure 2.1 and is included as a reference. All means are significantly ($P < 0.05$) different from each one another.

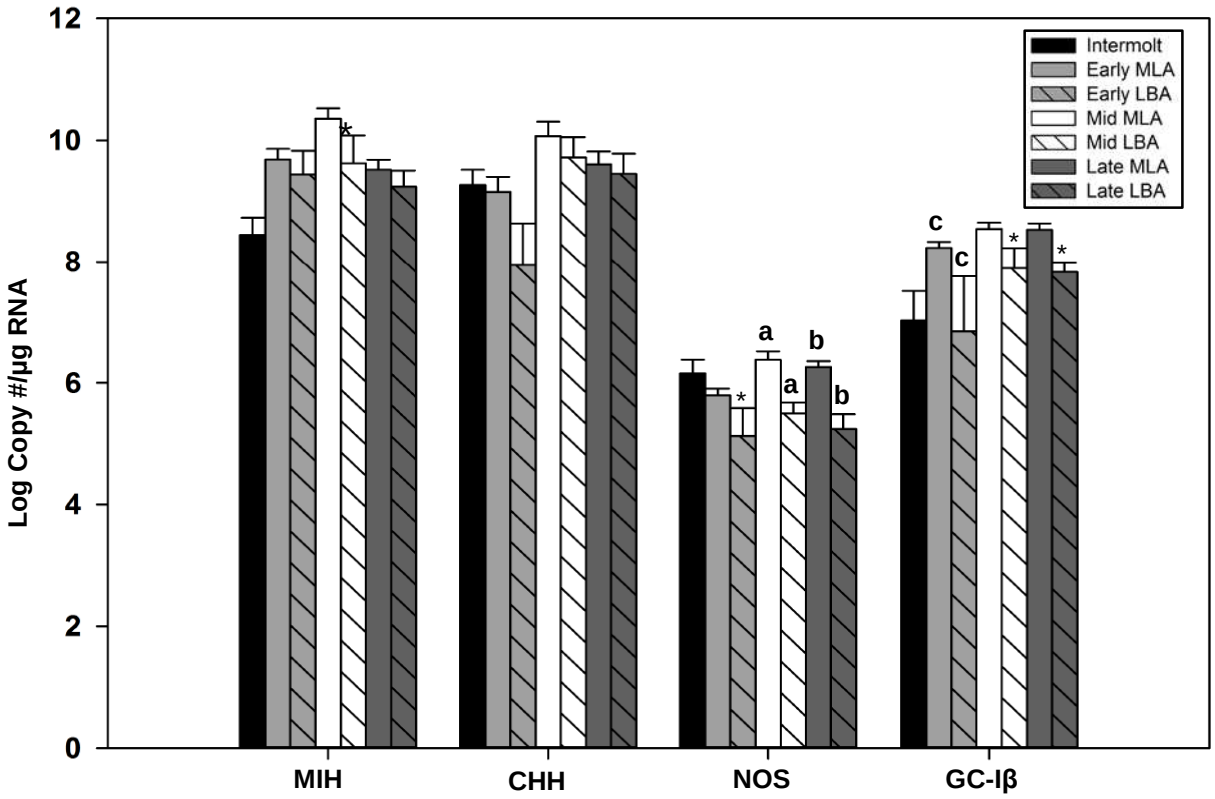


**Figure 2.5A Effects of LBA on gene expression of MIH a signaling pathways in the ESG of *G. lateralis*.** Quantification of changes in mRNA expression levels were detected with qPCR. Limb buds (LB) were autotomized at early, mid, and late premolt stages determined based on the R-index. ESG were collected from LBA animals at all three premolt stages. Data are presented as mean ± S.E. (early premolt n = 14; mid premolt n = 11; late premolt n = 13). MLA data from intermolt and all three premolt time points is the same as in Figure 2.1 and is included as a reference. Time points with means that are significantly different from intermolt are indicated with an asterisk (*) and means that share a letter are significantly different. Only 3-fold or greater changes in expression between intermolt and LBA or MLA and LBA at the same time point are indicated on the graph. Differences in MIH signaling pathway gene expression *Gl-MIH, Gl-CHH, Gl-NOS,* and *Gl-GC-Iβ* at intermolt, early premolt, mid premolt, and late premolt between MLA and LBA animals. There was insufficient cDNA to measure mRNA levels of *Gl-NOSIP*, *Gl-GC-II*, and *Gl-GC-III*.

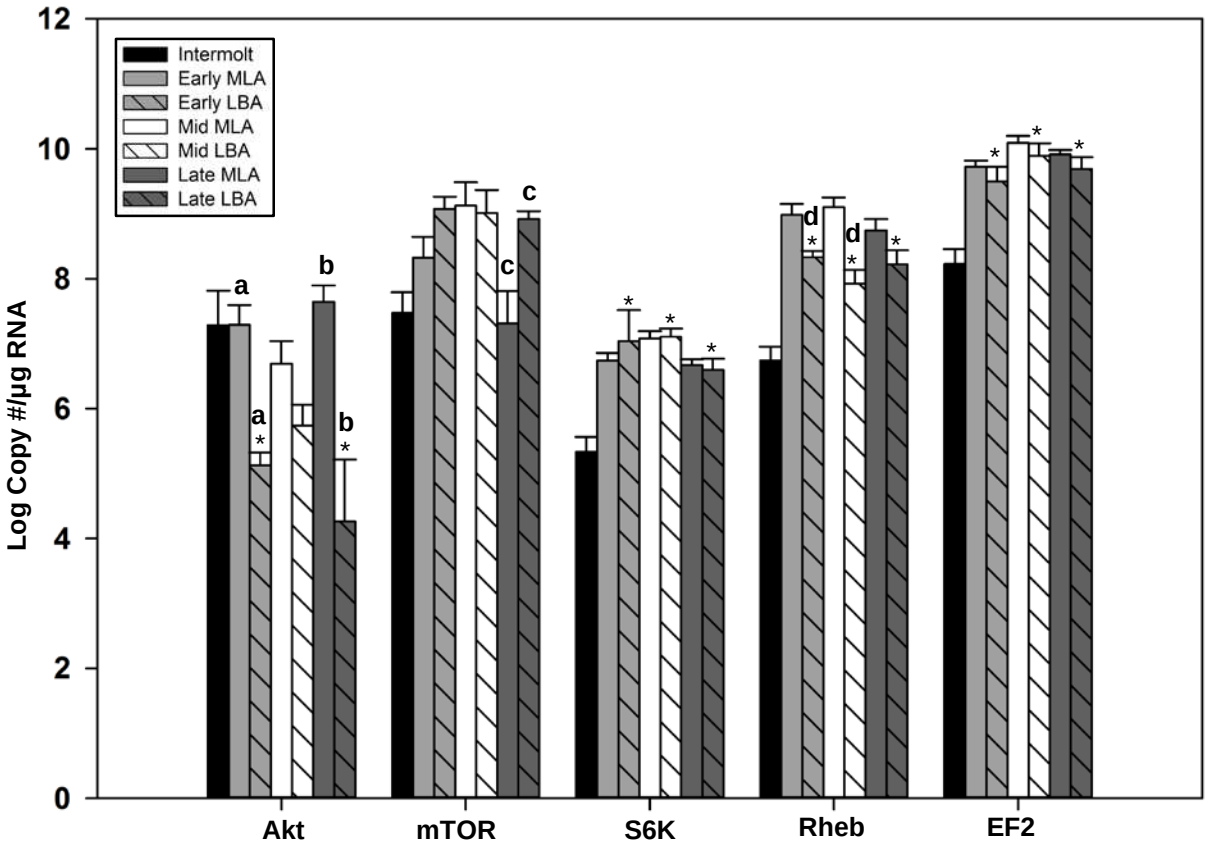


**Figure 2.5B Effects of LBA on gene expression of mTOR signaling pathways in the ESG of *G. lateralis*.** Quantification of changes in mRNA expression levels were detected with qPCR. Limb buds (LB) were autotomized at early, mid, and late premolt stages determined based on the R-index. ESG were collected from LBA animals at all three premolt stages. Data are presented as mean ± S.E. (early premolt n = 14; mid premolt n = 11; late premolt n = 13). MLA data from intermolt and all three premolt time points is the same as in Figure 2.1 and is included as a reference. Time points with means that are significantly different from intermolt are indicated with an asterisk (*) and means that share a letter are significantly different. Only 3-fold or greater changes in expression between intermolt and LBA or MLA and LBA at the same time point are indicated on the graph. Differences in gene expression of *Gl-EF2* and mTOR signaling genes *Gl-mTOR, Gl-S6K, Gl-Rheb*, and *Gl-Akt* mRNA levels at intermolt, early premolt, mid premolt and late premolt between MLA and LBA animals.

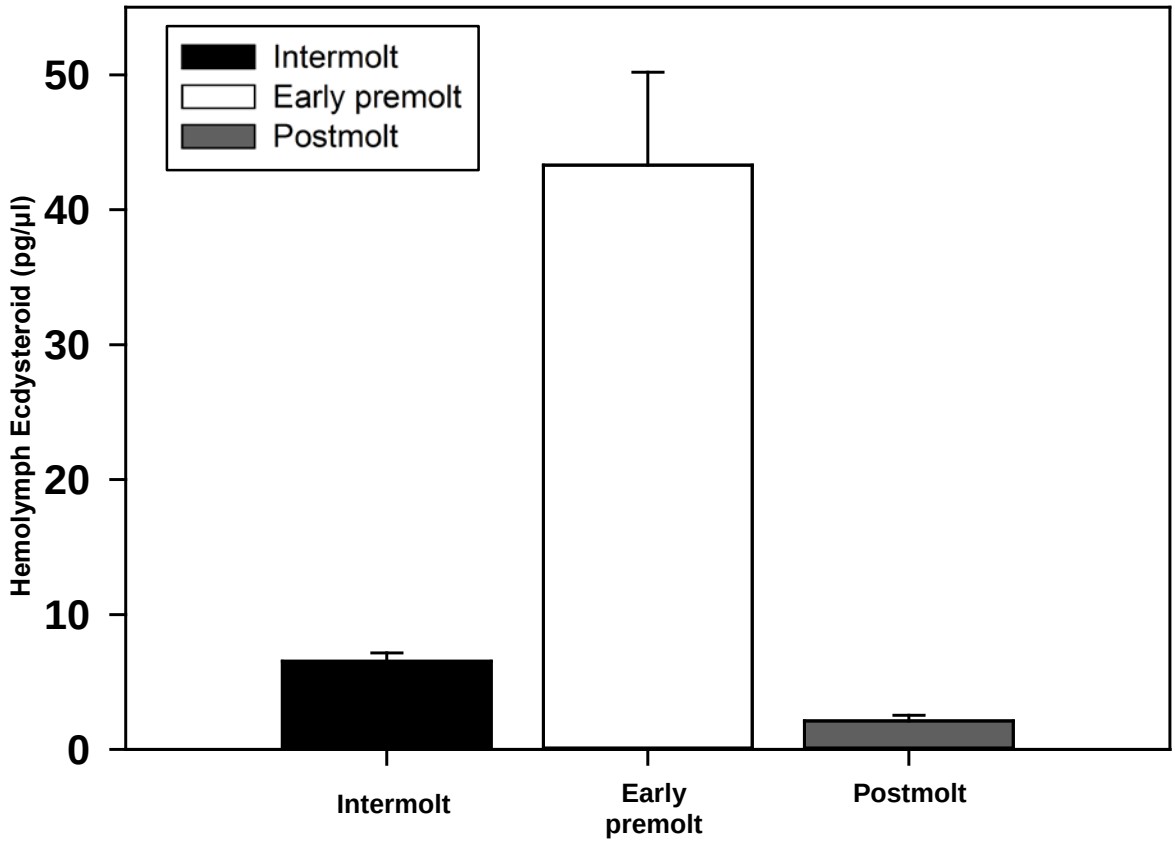


**Figure 2.6 Effects of molting on hemolymph ecdysteroid titers in *C. maenas***. Hemolymph was collected from spontaneously molting green crabs grouped into intermolt, early premolt, and postmolt stages. Ecdysteroid titers were quantified by ELISA. Data are presented as mean ± S.E. (intermolt n = 23; premolt n = 13; post molt n = 31). All means are significantly ($P < 0.05$) different from each one another.

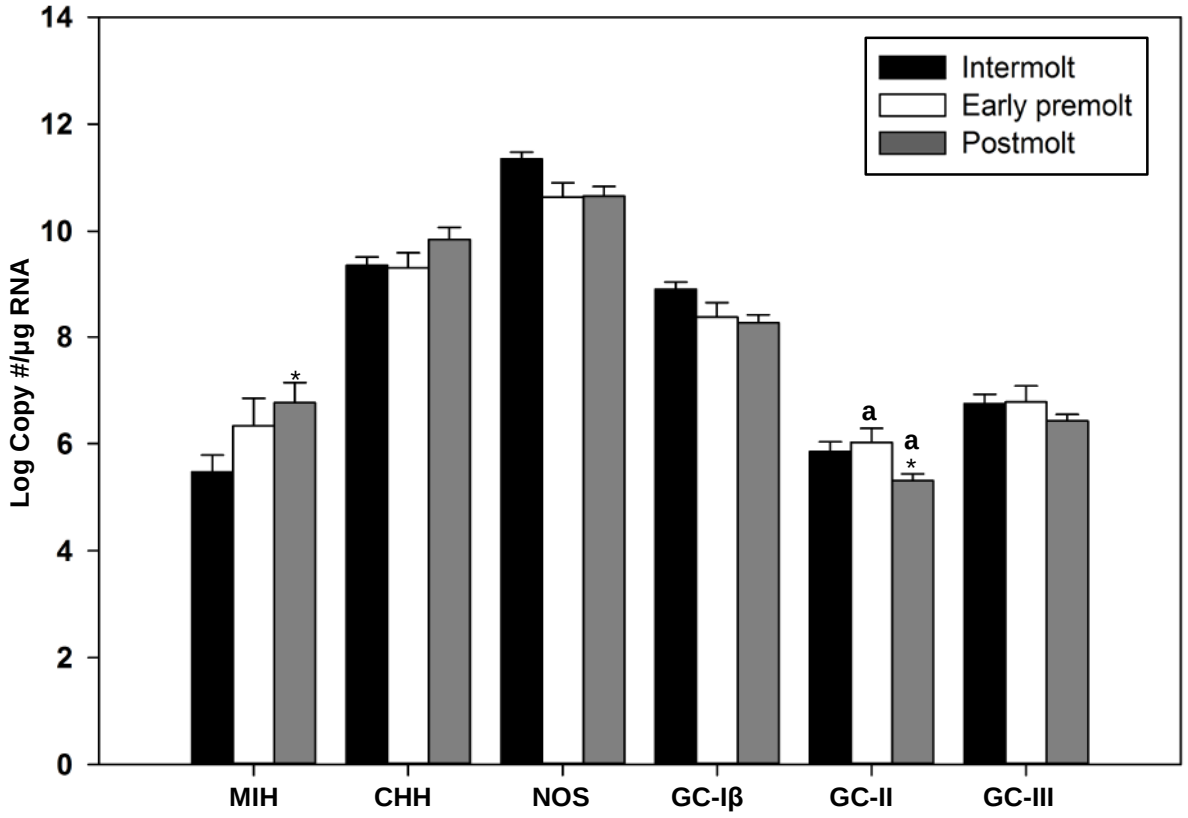


**Figure 2.7A Effect of molting on gene expression of MIH signaling pathway genes in the ESG of *C. maenas*.** Changes in mRNA expression quantified with qPCR. ESG were collected from spontaneously molting green crabs grouped into intermolt, premolt, and postmolt stages. Time points with means that are significantly different from intermolt are indicated with an asterisk (*) and means that share a letter are significantly different. Only 3-fold or greater changes in expression are indicated on the graph. Changes in MIH signaling pathway gene expression *Cm-MIH, Cm-CHH, Cm-NOS, Cm-GC-Iβ Cm-GC-II*, and *Cm-GC-III* between intermolt, premolt, and postmolt animals.

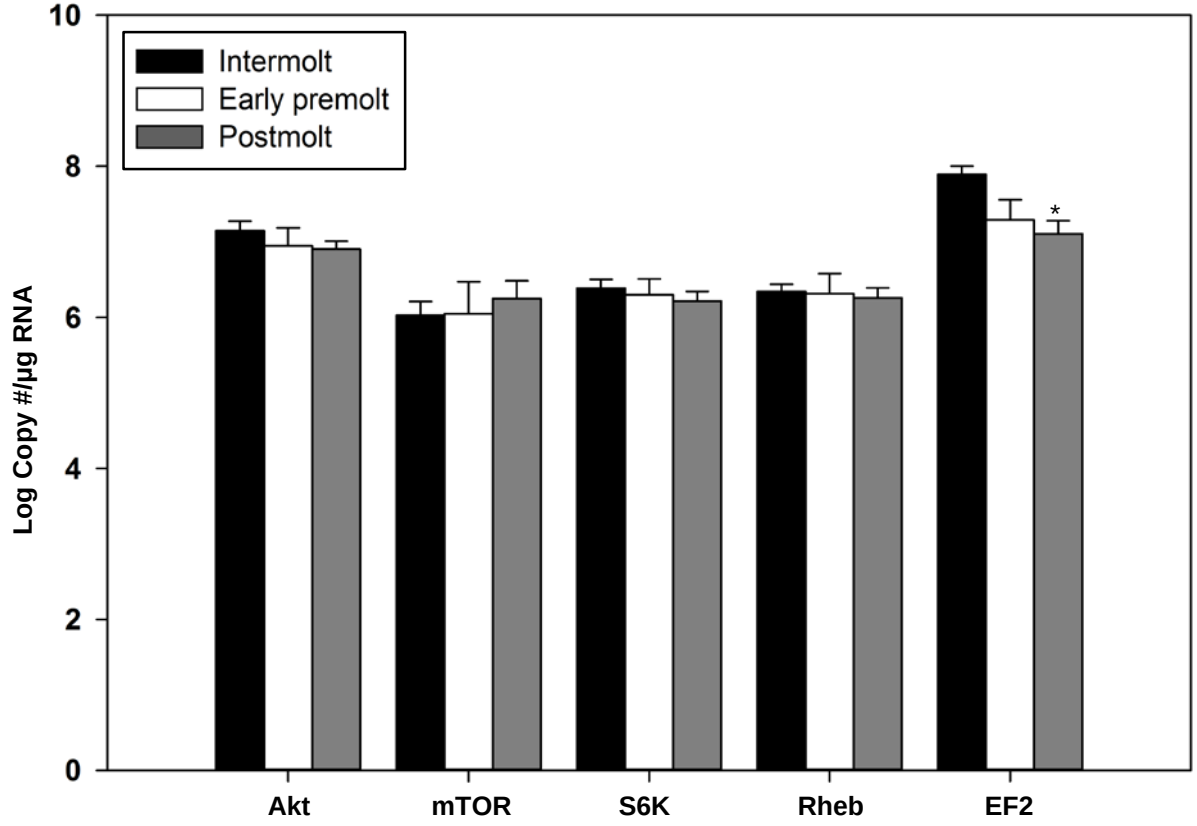


**Figure 2.7B Effect of molting on gene expression of mTOR signaling pathway genes in the ESG of *C. maenas*.** Changes in mRNA expression quantified with qPCR. ESG were collected from spontaneously molting green crabs grouped into intermolt, premolt, and postmolt stages. Time points with means that are significantly different from intermolt are indicated with an asterisk (*) and means that share a letter are significantly different. Only 3-fold or greater changes in expression are indicated on the graph. Changes in *Cm-EF2* and mTOR signaling pathway genes *Cm-mTOR, Cm-S6K, Cm-Rheb*, and *Cm-Akt* between intermolt, premolt, and postmolt animals.

# REFERENCES


Abuhagr, A.M., Blindert, J.L., Nimitkul, S., Zander, I.A., LaBere, S.M., Chang, S.A., MacLea, K.S., Chang, E.S., Mykles, D.L., 2014a. Molt regulation in green and red color morphs of the crab *Carcinus maenas*: Gene expression of molt-inhibiting hormone signaling components. J. Exp. Biol. 217, 796-808.

Abuhagr, A.M., MacLea, K.S., Chang, E.S., Mykles, D.L., 2014b. Mechanistic target of rapamycin (mTOR) signaling genes in decapod crustaceans: Cloning and tissue expression of mTOR, Akt, Rheb, and p70 S6 kinase in the green crab, *Carcinus maenas*, and blackback land crab, *Gecarcinus lateralis*. Comp. Biochem. Physiol. 168, 25-39.

Bliss, D.E., Welsh, J.H., 1952. The neurosecretroy system of brachyuran crustacea. Biol. Bull. 103, 157-169.

Böcking, D., Dircksen, H., Keller, R., 2002. The crustacean neuropeptides of the CHH/MIH/GIH family: Structures and biological activities, in: K. Weise (Ed.), The Crustacean Nervous System, Berlin, 84-97.

Chan, S.M., Gu, P.L., Chu, K.H., Tobe, S.S., 2003. Crustacean neuropeptide genes of the CHH/MIH/GIH family: Implications from molecular studies. Gen. Comp. Endocrinol. 134, 214-219.

Chang, E.S., 1985. Hormonal control of molting in decapod Crustacea. Am. Zool. 25, 179-185.

Chang, E.S., Bruce, M.J., 1980. Ecdysteroid titers of juvenile lobsters following molt induction. J. Exp. Zool. 214, 157-160.

Chang, E.S., Chang, S.A., Mulder, E.P., 2001. Hormones in the lives of crustaceans: An overview. Am. Zool. 41, 1090-1097.

Chang, E.S., Mykles, D.L., 2011. Regulation of crustacean molting: A review and our perspectives. Gen. Comp. Endocrinol. 172, 323-330.

Chung, J.S., Webster, S.G., 2003. Moult cycle-related changes in biological activity of moult-inhibiting hormone (MIH) and crustacean hyperglycaemic hormone (CHH) in the crab, *Carcinus maenas* - From target to transcript. Eur. J. Biochem. 270, 3280-3288.

Chung, J.S., Webster, S.G., 2005. Dynamics of *in vivo* release of molt-inhibiting hormone and crustacean hyperglycemic hormone in the shore crab, *Carcinus maenas*. Endocrinol. 146, 5545-5551.

Chung, J.S., Webster, S.G., 2006. Binding sites of crustacean hyperglycemic hormone and its second messengers on gills and hindgut of the green shore crab, *Carcinus maenas*: A possible osmoregulatory role. Gen. Comp. Endocrinol. 147, 206-213.

Chung, J.S., Zmora, N., Katayama, H., Tsutsui, N., 2010. Crustacean hyperglycemic hormone (CHH) neuropeptides family: Functions, titer, and binding to target tissues. Gen. Comp. Endocrinol. 166, 447-454.

Colasanti, M., Venturini, G., 1998. Nitric oxide in invertebrates. Molec. Neurobiol. 17, 157-174.

Covi, J.A., Bader, B.D., Chang, E.S., Mykles, D.L., 2010. Molt cycle regulation of protein synthesis in skeletal muscle of the blackback land crab, *Gecarcinus lateralis*, and the differential expression of a myostatin-like factor during atrophy induced by molting or unweighting. J. Exp. Biol. 213, 172-183.

Covi, J.A., Chang, E.S., Mykles, D.L., 2009. Conserved role of cyclic nucleotides in the regulation of ecdysteroidogenesis by the crustacean molting gland. Comp. Biochem. Physiol. 152, 470-477.

Covi, J.A., Chang, E.S., Mykles, D.L., 2012. Neuropeptide signaling mechanisms in crustacean and insect molting glands. Invert. Reprod. Dev. 56, 33-49.

Covi, J.A., Kim, H.W., Mykles, D.L., 2008. Expression of alternatively spliced transcripts for a myostatin-like protein in the blackback land crab, *Gecarcinus lateralis*. Comp. Biochem. Physiol. 150A, 423-430.

Das, S., Pitts, N.L., Mudron, M.R., Durica, D.S., Mykles, D.L., in preparation. Transcriptome analysis of the molting gland (Y-organ) from the blackback land crab, *Gecarcinus lateralis*.

De Kleijn, D.P.V., De Leeuw, E.P.H., Van den Berg, M.C., Martens, G.J.M., Van Herp, F., 1995. Cloning and expression of two mRNAs encoding structurally different crustacean hyperglycemic hormone precursors in the lobster *Homarus americanus*. Biochem. Biophys. Acta. Gene Struct. Exp. 1260, 62-66.

Dobashi, Y., Watanabe, Y., Miwa, C., Suzuki, S., Koyama, S., 2011. Mammalian target of rapamycin: A central node of complex signaling cascades. Int. J. of Clin. Exp. Path. 4, 476-495.

Goy, M.F., 1990. Activation of membrane guanylate cyclase by an invertebrate peptide hormone. J. Biol. Chem. 265, 20220-20227.

Gu, S.H., Yeh, W.L., Young, S.C., Lin, P.L., Li, S., 2012. TOR signaling is involved in PTTH-stimulated ecdysteroidogenesis by prothoracic glands in the silkworm, *Bombyx mori*. Insect Biochem. Molec. Biol. 42, 296-303.

Hanström, B., 1939. Hormones in Invertebrates. Oxford University Press, London.

Holland, C.A., Skinner, D.M., 1976. Interactions between molting and regeneration in the land crab. Biol. Bull. 150, 222-240.

Hopkins, P.M., 2012. The eyes have it: A brief history of crustacean neuroendocrinology. Gen. Comp. Endocrinol. 175, 357-366.

Kim, H.W., Batista, L.A., Hoppes, J.L., Lee, K.J., Mykles, D.L., 2004. A crustacean nitric oxide synthase expressed in nerve ganglia, Y-organ, gill and gonad of the tropical land crab, *Gecarcinus lateralis*. J. Exp. Biol. 207, 2845-2857.

Kingan, T.G., 1989. A competitive enzyme-linked immunosorbent assay: application in the assasy of peptides, steroids, and cyclic nucleotides. Anal. Biochem. 183, 283-289.

Laplante, M., Sabatini, D.M., 2012. mTOR signaling in growth control and disease. Cell 149, 274-293.

Lee, C.Y., Zou, H.S., Yau, S.M., Ju, Y.R., Liau, C.S., 2000. Nitric oxide synthase activity and immunoreactivity in the crayfish *Procambarus clarkii*. Neuroreport 11, 1273-1276.

Lee, K.J., Kim, H.W., Gomez, A.M., Chang, E.S., Covi, J.A., Mykles, D.L., 2007a. Molt-inhibiting hormone from the tropical land crab, *Gecarcinus lateralis*: Cloning, tissue expression, and expression of biologically active recombinant peptide in yeast. Gen. Comp. Endocrinol. 150, 505-513.

Lee, S.G., Bader, B.D., Chang, E.S., Mykles, D.L., 2007b. Effects of elevated ecdysteroid on tissue expression of three guanylyl cyclases in the tropical land crab Gecarcinus lateralis: possible roles of neuropeptide signaling in the molting gland. J. Exp. Biol. 210, 3245-3254.

Lee, S.G., Kim, H.W., Mykles, D.L., 2007c. Guanylyl cyclases in the tropical land crab, *Gecarcinus lateralis*: Cloning of soluble (NO-sensitive and -insensitive) and membrane receptor forms. Comp. Biochem. Physiol. 2D, 332-344.

Lee, S.G., Mykles, D.L., 2006. Proteomics and signal transduction in the crustacean molting gland. Integr. Comp. Biol. 46, 965-977.

Loewith, R., Hall, M.N., 2011. Target of Rapamycin (TOR) in nutrient signaling and growth control. Genetics 189, 1177-1201.

MacLea, K.S., Abuhagr, A.M., Pitts, N.L., Covi, J.A., Bader, B.D., Chang, E.S., Mykles, D.L., 2012. Rheb, an activator of target of rapamycin, in the blackback land crab, *Gecarcinus lateralis*: cloning and effects of molting and unweighting on expression in skeletal muscle. J. Exp. Biol. 215, 590-604.

Magnuson, B., Ekim, B., Fingar, D.C., 2012. Regulation and function of ribosomal protein S6 kinase (S6K) within mTOR signalling networks. Biochem. J. 441, 1-21.

Mattson, M.P., 1986. New insights into neuroendocrine regulation of the crustacean molt cycle. Zoological Science 3, 733-744.

McDonald, A.A., Chang, E.S., Mykles, D.L., 2011. Cloning of a nitric oxide synthase from green shore crab, *Carcinus maenas*: A comparative study of the effects of eyestalk ablation on expression in the

molting glands (Y-organs) of *C. maenas*, and blackback land crab, *Gecarcinus lateralis*. Comp. Biochem. Physiol. 158A, 150-162.

Mirth, C.K., Shingleton, A.W., 2012. Integrating body and organ size in *Drosophila*: Recent advances and outstanding problems. Front. Endocrinol. 3, Article 49.

Moncada, S., Palmer, R.M.J., Higgs, E.A., 1991. Nitric oxide; Physiology, pathophysiology, and pharmacology. Pharmacol. Rev. 43, 109-142.

Morita, M., Gravel, S.P., Chenard, V., Sikstrom, K., Zheng, L., Alain, T., Gandin, V., Avizonis, D., Arguello, M., Zakaria, C., McLaughlan, S., Nouet, Y., Pause, A., Pollak, M., Gottlieb, E., Larsson, O., St-Pierre, J., Topisirovic, I., Sonenberg, N., 2013. mTORC1 controls mitochondrial activity and biogenesis through 4E-BP-dependent translational regulation. Cell Metab. 18, 698-711.

Morton, D.B., 2004. Invertebrates yield a plethora of atypical guanylyl cyclases. Molec. Neurobiol. 29, 97-115.

Morton, D.B., Simpson, P.J., 2002. Cellular signaling in eclosion hormone action. J. Insect Physiol. 48, 1-13.

Mykles, D.L., Adams, M.E., Gade, G., Lange, A.B., Marco, H.G., Orchard, I., 2010. Neuropeptide action in insects and crustaceans. Physiol. Biochem. Zool. 83, 836-846.

Nakatsuji, T., Lee, C.Y., Watson, R.D., 2009. Crustacean molt-inhibiting hormone: Structure, function, and cellular mode of action. Comp. Biochem. Physiol. 152A, 139-148.

Nakatsuji, T., Sonobe, H., 2004. Regulation of ecdysteroid secretion from the Y-organ by molt-inhibiting hormone in the American crayfish, *Procambarus clarkii*. Gen. Comp. Endocrinol. 135, 358-364.

Nighorn, A., Byrnes, K.A., Morton, D.B., 1999. Identification and characterization of a novel beta subunit of soluble guanylyl cyclase that is active in the absence of a second subunit and is relatively insensitive to nitric oxide. J. Biol. Chem. 274, 2525-2531.

Okumura, T., Ohira, T., Katayama, H., Nagasawa, H., 2005. *In vivo* effects of a recombinant molt-inhibiting hormone on molt interval and hemolymph ecdysteroid level in the kuruma prawn, *Marsupenaeus japonicus*. Zool. Sci. 22, 317-320.

Padayatti, P.S., Pattanaik, P., Ma, X.L., van den Akker, F., 2004. Structural insights into the regulation and the activation mechanism of mammalian guanylyl cyclases. Pharmacology & Therapeutics 104, 83-99.

Palumbo, A., 2005. Nitric oxide in marine invertebrates: A comparative perspective. Comp. Biochem. Physiol. 142A, 241-248.

Pitts, N.L., Mykles, D.L., 2015. Nitric oxide production and sequestration in the sinus gland of the green shore crab *Carcinus maenas*. J. Exp. Biol. 218, 353-362.

Ray, U., Khan, G.A., Chakraborty, K., Basuroy, S., Patra, S.C., Girish, G., Bhattacharya, G., Sinha, A.K., 2012. Isolation and study of insulin activated nitric oxide synthase inhibitory protein in acute myocardial infarction subjects. J. Thromb. & Thromboly. 33, 218-229.

Rewitz, K.F., Yamanaka, N., O'Connor, M.B., 2013. Developmental checkpoints and feedback circuits time insect maturation, in: Y.B. Shi (Ed.), Animal Metamorphosis, 1-33.

Roux, P.P., Topisirovic, I., 2012. Regulation of mRNA translation by signaling pathways. Cold Spring Harb. Perspect. Biol. 4.

Schwarz, P.M., Rodriguez-Pascual, F., Koesling, D., Torres, M., Forstermann, U., 1998. Functional coupling of nitric oxide synthase and soluble guanylyl cyclase in controlling catecholamine secretion from bovine chromaffin cells. Neurosci. 82, 255-265.

Shaw, R.J., Cantley, L.C., 2006. Ras, PI(3)K and mTOR signalling controls tumour cell growth. Nature 441, 424-430.

Skinner, D.M., 1985. Molting and regeneration, in: D.E. Bliss, L.H. Mantel (Eds.), The Biology of Crustacea. Academic Press, New York, 44-146.

Skinner, D.M., Graham, D.E., 1970. Molting in land crabs: Stimulation by leg removal. Science 169, 383-385.

Skinner, D.M., Graham, D.E., 1972. Loss of limbs as a stimulus to ecdysis in Brachyura (true crabs). Biol. Bull. 143, 222-233.

Soulard, A., Cohen, A., Hall, M.N., 2009. TOR signaling in invertebrates. Curr. Opinion Cell Biol. 21, 825-836.

Soumoff, C., O' Connor, J.D., 1982. Repression of Y-organ secretory activity by molt inhibiting hormone in the crab *Pachygrapsus crassipes*. Gen. Comp. Endocrinol. 48, 432-439.

Spaziani, E., Jegla, T.C., Wang, W.L., Booth, J.A., Connolly, S.M., Conrad, C.C., Dewall, M.J., Sarno, C.M., Stone, D.K., Montgomery, R., 2001. Further studies on signaling pathways for ecdysteroidogenesis in crustacean Y-organs. Am. Zool. 41, 418-429.

Spaziani, E., Mattson, M.P., Wang, W.N.L., McDougall, H.E., 1999. Signaling pathways for ecdysteroid hormone synthesis in crustacean Y-organs. Am. Zool. 39, 496-512.

Stewart, M.J., Stewart, P., Sroyraya, M., Soonklang, N., Cummins, S.F., Hanna, P.J., Duan, W., Sobhon, P., 2013. Cloning of the crustacean hyperglycemic hormone and evidence for molt-inhibiting hormone within the central nervous system of the blue crab *Portunus pelagicus*. Comp. Biochem. Physiol. 164A, 276-290.

Su, Y.C., 2014. Regulation of endothelial nitric oxide synthase activity by protein-protein interaction. Curr. Pharm. Design 20, 3514-3520.

Teleman, A.A., 2010. Molecular mechanisms of metabolic regulation by insulin in *Drosophila*. Biochem. J. 425, 13-26.

Thoreen, C.C., Chantranupong, L., Keys, H.R., Wang, T., Gray, N.S., Sabatini, D.M., 2012. A unifying model for mTORC1-mediated regulation of mRNA translation. Nature 485, 109-U142.

Tiebe, M., Lutz, M., De La Garza, A., Buechling, T., Boutros, M., Teleman, A.A., 2015. REPTOR and REPTOR-BP regulate organismal metabolism and transcription downstream of TORC1. Dev. Cell 33, 272-284.

Tiu, S.H.K., Chan, S.M., 2007. The use of recombinant protein and RNA interference approaches to study the reproductive functions of a gonad-stimulating hormone from the shrimp *Metapenaeus ensis*. FEBS J. 274, 4385-4395.

Webster, S.G., Keller, R., 1986. Purification, characterisation and amino acid composition of the putative moult-inhibiting hormone (MIH) of *Carcinus maenas* (Crustacea, Decapoda). J. Comp. Physiol. 156, 617-624.

Webster, S.G., Keller, R., Dircksen, H., 2012. The CHH-superfamily of multifunctional peptide hormones controlling crustacean metabolism, osmoregulation, moulting, and reproduction. Gen. Comp. Endocrinol. 175, 217-233.

Yu, X.L., Chang, E.S., Mykles, D.L., 2002. Characterization of limb autotomy factor-proecdysis ($LAF_{pro}$), isolated from limb regenerates, that suspends molting in the land crab *Gecarcinus lateralis*. Biol. Bull. 202, 204-212.

Zhu, D.F., Hu, Z.H., Shen, J.M., 2011. Moult-inhibiting hormone from the swimming crab, *Portunus trituberulatus* (Miers, 1876); PCR cloning, tissue distribution, and expression of recombinant protein in *Escherichia coli* (Migula, 1895). Crustaceana 84, 1481-1496.

Zoncu, R., Efeyan, A., Sabatini, D.M., 2011. mTOR: From growth signal integration to cancer, diabetes and ageing. Nature Rev. Molec. Cell Biol. 12, 21-35.

CHAPTER THREE

# NITRIC OXIDE PRODUCTION AND SEQUESTRATION IN THE SINUS GLAND OF THE GREEN SHORE CRAB, *CARCINUS MAENAS*

This chapter was published in the Journal of Experimental Biology in February 2015: Pitts, N.L. and Mykles D.L. (2015). Nitric oxide production and sequestration in the sinus gland of the green shore crab, *Carcinus maenas* *J. Exp. Biol.* (218), 353-362.

## SUMMARY

Molting in decapod crustaceans is regulated by molt-inhibiting hormone (MIH), a neuropeptide produced in the X-organ (XO)/sinus gland (SG) complex of the eyestalk ganglia (ESG). Pulsatile release of MIH from the SG suppresses ecdysteroidogenesis by the molting gland or Y-organ (YO). The hypothesis is that nitric oxide (NO), a neuromodulator that controls neurotransmitter release at presynaptic membranes, depresses the frequency and/or amount of MIH pulses to induce molting. NO synthase (NOS) mRNA was present in *Carcinus maneas* ESG and other tissues and NOS protein was present in the SG. A copper based ligand (CuFL), which reacts with NO to form a highly fluorescent product (NO-FL), was used to image NO in the ESG and SG and quantify the effects of NO scavenger (cPTIO), NOS inhibitor (L-NAME), and sodium azide ($NaN_3$) on NO production in the SG. Preincubation with cPTIO prior to CuFL loading decreased NO-FL fluorescence ~30%; including L-NAME had no additional effect. Incubating SG with L-NAME during preincubation and loading decreased NO-FL fluorescence ~40%, indicating that over half of the NO release was not directly dependent on NOS activity. Azide, which reacts with NO-binding metal groups in proteins, reduced NO-FL fluorescence to near background levels without extensive cell death. Spectral shift analysis showed that azide displaced NO from a soluble protein in SG extract. These data suggest that the SG contains NO-binding protein(s) that sequester NO and releases it over a prolonged period. This NO release may modulate neuropeptide secretion from the axon termini in the SG.

## INTRODUCTION

Nitric oxide (NO) is a signaling molecule that is evolutionarily and functionally conserved across animal taxa (Palumbo, 2005). NO is produced by nitric oxide synthase (NOS) from L-arginine, $O_2$, and NADPH (Colasanti and Venturini, 1998). Three NOS isoforms occur in mammalian cells: endothelial

(eNOS), neuronal NOS (nNOS), and inducible NOS (iNOS) (Nathan and Xie, 1994; Bogdan, 2001; Mungrue et al., 2003). eNOS and nNOS are constitutively expressed and require $Ca^{2+}$ and calmodulin for activation (Roman et al., 2002). iNOS is a $Ca^{2+}$ independent isoform that is up regulated during immunological responses (Colasanti and Venturini, 1998). Decapod crustacean tissues express a single NOS that resembles the $Ca^{2+}$/calmodulin-dependent isoforms in functional domains and biochemical properties (Johansson and Carlberg, 1994; Lee et al., 2000; Scholz et al., 2002; Zou et al., 2002; Kim et al., 2004; McDonald et al., 2011). The crustacean NOS gene is expressed in many tissues, which is consistent with its role as a regulator of diverse physiological functions (Lee et al., 2000; Kim et al., 2004; Inada et al., 2010; Yao et al., 2010; McDonald et al., 2011; Li et al., 2012; Wu et al., 2013).

In the central nervous systems (CNS) of vertebrates and invertebrates, NO functions as a neuromodulator. In vertebrates, NO regulates learning, memory, feeding, sleeping, sensory, and motor functions by acting as an inhibitor or enhancer of neurotransmitter release (Calabrese et al., 2007; Garthwaite, 2008; Virarkar et al., 2013). For example, NO enhances acetylcholine release in the basal forebrain and ventral striatum and inhibits histamine release in the anterior hypothalamus (Philippu and Prast, 2001). In the vertebrate hippocampus and cerebral cortex, NO plays a dual role in the regulation of glutamate release, acting as an inhibitor at low concentrations and a stimulator at high concentrations (Sequeira et al., 1997). In addition, NO has neurotoxic effects that are associated with neurodegenerative disorders, such as Alzheimer's, Parkinson's, and Huntington's diseases (Calabrese et al., 2007; Lorenc-Koci and Czarnecka, 2013; Virarkar et al., 2013;.see Hirst and Robson, 2011 and Russwurm et al., 2013 for comprehensive reviews of NO actions in vertebrates). In decapod crustaceans, NO acts as an enhancer or inhibitor by increasing neurotransmitter release in the stomatogastric ganglion and depressing release in neuromuscular junctions, respectively (Scholz, 1999; Aonuma et al., 2000, 2002).

NO signaling regulates molting and developmental timing in arthropods. In insects, prothoracicotropic hormone (PTTH)-induced stimulation of the molting gland (prothoracic gland or PG) requires NOS activation (Caceres et al., 2011; Rewitz et al., 2013). In the molting gland or Y-organ (YO) of the blackback land crab *Gecarcinus lateralis*, NO donors and YC-1, an agonist of NO-dependent guanylyl cyclase (GC-I), inhibit ecdysteroidogenesis in YO and NOS becomes phosphorylated in the activated YO, which suggests that NOS and GC-I are components of a signaling pathway activated by

molt-inhibiting hormone [MIH (Mykles et al., 2010; Chang and Mykles, 2011; Covi et al., 2012)]. MIH is a neuropeptide that represses the YO to maintain the animal in the intermolt stage; a reduction in MIH release is believed to result in the de-repression of steroidogenesis by the YO (Skinner, 1985; Lachaise et al., 1993; Chang and Mykles, 2011). MIH is synthesized in the X-organ (XO), which consists of a cluster of ~150 neurosecretory cells located in the medulla terminalis (MT) of the eyestalk ganglia (Skinner, 1985; Hopkins, 2012). Axons from the XO terminate in the sinus gland (SG), a neurohemal organ where MIH and other XO neuropeptides are released into the hemolymph (Skinner, 1985; Stuenkel, 1985; Hopkins, 2012). The SG consists of glial cells, axons, and axon terminals (Azzouna and Rezig, 2001). NOS protein is localized to the SG of the crayfish, *Procambarus clarkii*, which is suggestive of a role in neuroendocrine regulation (Lee et al., 2000).

The regulation of neuropeptide synthesis and release by the XO/SG complex is poorly understood. mRNA levels of MIH and crustacean hyperglycemic hormone (CHH) in the ESG remain unchanged throughout the molt cycle in *Carcinus maenas*, indicating that MIH and CHH are regulated post-transcriptionally [(Chung and Webster, 2003); N. L. Pitts and D. L. Mykles, unpublished]. The MIH neurons in the XO/SG complex are under serotonergic control (Rudolph and Spaziani, 1991) and neuropeptide release is triggered by entry of $Ca^{2+}$ (Cooke, 1985). The purpose of this study was to examine the potential role of NO signaling in the XO/SG complex of the green shore crab, *C. maenas*. Endpoint RT-PCR was used to determine the expression of *Cm-NOS* and *Cm-Elongation Factor-2 (EF2)* in the eyestalk ganglia and other tissues. The presence of NOS protein in the SG was determined by Western blot analysis. CuFL, a copper (II) fluorescein-based ligand (Lim et al., 2006), was used to localize NO and quantify the effects of NOS inhibitor (L-NAME), NO scavenger (cPTIO), or both compounds on NO production in the SG. The effect of sodium azide ($NaN_3$), which reacts with heme and other metal groups, on NO-FL fluorescence was quantified. An azide-dependent spectral shift analysis characterized NO-binding protein(s) in SG soluble extract. The results indicate that NO produced by NOS binds to an endogenous store, allowing for prolonged release of the gas to the axon terminals of the SG. To our knowledge, this is the first study using CuFL to quantify and image NO in crustacean tissues and to characterize NO-binding protein(s) in the SG.

## RESULTS

*Tissue expression of Cm-NOS*

The tissue distribution of *Cm-NOS* was assessed by end point PCR in tissues from a single red color morph intermolt male. *Cm-NOS* mRNA was detected in all tissues examined, except the heart and hepatopancreas (Figure 3.1). *Cm-EF2* was expressed in all tissues (Figure 3.1).

*Detection of NOS protein by Western blotting*

NOS protein was present in the SG, as shown by Western blotting with a universal NOS antibody (Figure 3.2). An immunoreactive protein of the predicted molecular weight (~132 kDa) was detected with the primary antibody (Figure 3.2, lane a). A second protein with an estimated mass of 94 kDa may represent a truncated NOS isoform (see Discussion). Based on scanning densitometry, the level of the ~94-kDa protein was about 2-fold greater than the level of the ~132-kDa protein.

*Imaging and quantification of NO-FL fluorescence*

NO was quantified with CuFL. NO reacts with CuFL to form NO-FL, a highly fluorescent product that becomes trapped in the cells (Lim et al., 2006). The CuFL concentration used in the experiments was optimized by loading SG with 10-fold serial dilutions between 0.5 mM and 0.05 µM CuFL in the presence or absence of the NO scavenger cPTIO or the NOS inhibitor L-NAME. Loading time was 1 h. NO-FL was highly fluorescent at higher concentrations (> 5 µM), which saturated the tissue and obscured imaging tissue structure with confocal microscopy. A concentration of 0.05 µM was selected, as at that concentration background fluorescence was minimized, while the effects of cPTIO and/or L-NAME on fluorescent intensity could be quantified with Metamorph imaging software.

Confocal microscopy of the NO-FL fluorescence confirmed that NO was produced in the SG *in situ*. ESG was preincubated in crab saline for 30 min and then loaded with 0.05 µM CuFL for 1 h in the dark. NO-FL fluorescence intensity was greater in the SG compared to the surrounding medulla interna [MI (Figure 3.3, left panel)]. In bright field images, the SG appeared dark due to the accumulation of neuropeptide secretory vesicles in axon termini (Figure 3.3, middle panel). NO-FL fluorescence in the isolated SG was comparable to that of the *in situ* SG (see Figure 3.4B), indicating that the fluorescence in the isolated SG was not an artifact of dissection. The pattern of NO-FL fluorescence indicated that NO was produced in glial and other supporting cells and not in axon termini.

The effects of reagents on NO-FL fluorescence were determined on the isolated SG. Initial experiments examined the effects of pretreatment conditions and also confirmed that NO was produced in the SG. Although the relative NO-FL fluorescence varied between individuals, there was no difference in fluorescence between the two SG from the same individual (data not shown). SG were preincubated in the dark for 30 min in crab saline, 1 mM cPTIO, or 1 mM cPTIO + 1 mM L-NAME, followed by loading for 1 h in the dark with or without 0.05 µM CuFL. SG loaded without CuFL had less than 5% of the fluorescence ($p = 0.002$) compared to SG loaded with CuFL after preincubation in crab saline, showing that the fluorescence was specific for NO-FL and not due to tissue autofluorescence (Figure 3.4A). Representative confocal images show the absence of fluorescence in a SG without CuFL (Figure 3.4B, panel 1), compared with high fluorescence in a SG with CuFL (Figure 3.4B, panel 2). Preincubation with cPTIO alone or in combination with L-NAME reduced NO-FL fluorescence 35% and 26%, respectively, compared to the saline pretreatment control (Figure 3.4A). Corresponding confocal images showed a general overall reduction in fluorescence in SG preincubated with cPTIO or with cPTIO + L-NAME (Figure 3.4B, compare panels 3 & 4 with panel 2). The reduction in fluorescence appeared to be solely the result of cPTIO, as the addition of L-NAME during preincubation did not decrease fluorescence further. This unexpected result suggested that there was significant NO production and/or release during the 1-h loading period. These results showed that the NO concentrations in the SG were within the linear response range at the concentration of CuFL used, and that CuFL was a highly sensitive and specific reagent for localizing and quantifying NO in crustacean tissues.

A second set of experiments examined the effects of cPTIO and L-NAME when in direct competition with CuFL during the loading period. The experiments followed a similar protocol: isolated SG were preincubated in the dark for 30 min in crab saline, 1 mM cPTIO and/or 1 mM L-NAME, followed by loading for 1 h in the dark with 0.05 µM CuFL in crab saline with or without 1 mM cPTIO or 1 mM L-NAME. SG preincubated in saline and then incubated with cPTIO and CuFL during loading had a 23% increase ($p = 0.047$) in fluorescence intensity than the control SG without cPTIO (Figure 3.5A). A similar trend was also observed when SG were preincubated with cPTIO, but the difference was not significant (Figure 3.5A). This suggested that CuFL had a higher NO binding affinity and thus was a better scavenger of free NO than cPTIO. This is particularly striking, considering the 20,000-fold difference in concentration between

cPTIO (1 mM) and CuFL (0.05 µM). As shown in the first set of experiments, the NO-FL fluorescence was similar in SG preincubated with cPTIO alone and SG preincubated with cPTIO + L-NAME (Figure 3.5A, compare columns #2 and #3). Representative confocal images showed similar reductions in NO-FL fluorescence (Figure 3.5B, compare panels #2 and #3 with panel #1). Preincubation with cPTIO and L-NAME followed by L-NAME during the CuFL loading period decreased NO-FL fluorescence 40% ($p < 0.001$) compared to the fluorescence without L-NAME in the loading solution (Figure 3.5A and 3.5B, compare panel #4 with panel #3). However, the fluorescence in the continuous presence of L-NAME in the preincubation and loading periods was well above the baseline level (Figure 3.5A and Figure 3.5B, panel #4), which suggested that more than half of NO-FL fluorescence was not directly dependent on NOS activity.

*Effects of azide on NO-FL fluorescence and spectral shift analysis*

The failure of an NOS inhibitor and an NO scavenger to completely knock down NO-FL fluorescence suggested that a proportion of the NO was bound by an endogenous protein(s), thus preventing its rapid degradation. A variety of metalloproteins, including heme- and copper-centered proteins, bind NO (Cooper, 1999; Wilson and Torres, 2004). During loading, the CuFL would react with the NO as it was released from the metal group(s). In order to test this hypothesis, SG were preincubated with 1 mM $NaN_3$; azide binds nearly irreversibly with metal groups and dislodges bound gases, such as $O_2$, $CO_2$, $H_2S$, and NO (Martin et al., 1990). $NaN_3$ was restricted to the preincubation period, as it would react with CuFL during the loading period and quench fluorescence. Isolated SGs were preincubated in saline containing cPTIO and L-NAME with and without $NaN_3$, followed by L-NAME during the loading period to minimize *de novo* NO production by NOS. $NaN_3$ reduced NO-FL fluorescence 57% ($p = 0.033$) compared to the control without $NaN_3$ (Figure 5A; compare columns #4 and #5). This reduction was in addition to the decreased NO-FL fluorescence with L-NAME, resulting in a fluorescent intensity approaching that without CuFL (Figure 3.4A, column #1). A representative confocal image shows low NO-FL fluorescence, comparable to the images of SG not loaded with CuFL (compare Figure 3.5B, panel #5, with Figure 3.4B, panel #1). These data suggest that an endogenous protein(s) binds NO, which was dissociated from the protein with azide.

The reduction of NO-FL fluorescence by azide was not associated with massive cell death. Azide disrupts aerobic respiration; the reduced ATP production could affect cell viability. Thus, the decrease in NO-FL fluorescence could be caused by the loss of NO-FL from dead cells and not from the release of NO from an endogenous store. A cell viability stain was used to image live and dead cells in SG incubated in crab saline (negative control), 1 mM $NaN_3$, or 70% methanol (positive control) for 30 min. The SG was stained with propidium iodide (PI), which preferentially stained nuclei of dead cells, followed by Hoechst stain, which stained nuclei of all cells. In false-color images with PI in green and Hoechst in red, the nuclei of dead cells appeared orange to yellow when the images were overlayed (Figure 3.6). The numbers of dead and live cells were counted by seven naïve observers and the dead:live ratio was calculated for each treatment. All seven observers counted cells from the same images. There was no significance difference in the ratios between observers ($p = 0.666$). The SG incubated in crab saline had the lowest number of dead cells, with a 1.44 ± 0.42 dead:live ratio (Figure 3.6, left panels). By contrast, in the SG incubated in 70% methanol (MeOH), the PI and Hoechst staining almost completely overlapped, resulting in an 11.38 ± 1.83 dead:live cell ratio; this is equivalent to 89% of all nuclei stained with PI and Hoechst (Figure 3.6, central panels). Azide increased the dead:live cell ratio to 2.66 ± 0.73 (Figure 3.6, right panels). The dead:live cell ratio was significantly different among all three treatments: control *vs.* azide ($p = 0.038$), control *vs.* MeOH ($p < 0.001$), and azide *vs.* MeOH ($p = 0.002$).

In order to characterize the NO binding protein(s), a spectral shift analysis was conducted on SG soluble extract. Spectra from 190 nm to 1100 nm at 1-nm resolution were recorded of SG extract prior to and immediately after the addition of 1 mM $NaN_3$ (Figure 3.7; top panel), and at 5-min intervals following the addition of $NaN_3$ over 1 h (Figure 3.7; bottom panel). Differences in spectral peaks were calculated by subtracting the spectra at each 5 min time interval from the spectrum prior to the addition of $NaN_3$. No spectral shifts were observed in the ranges expected for heme binding (400 nm - 450 nm) or copper binding (600 nm - 700 nm) proteins. In the long UV range (210 to 450 nm), there was an increase in absorption centered broadly at ~234 nm and a reduction in absorption centered broadly at ~272 nm, relative to the untreated sample (Figure 3.7). The absorption changes in these specific regions were completed within the first 5 minutes after the addition of $NaN_3$, although there was a general drift in absorption as the protein precipitated from solution.

## DISCUSSION

NO is an important signaling molecule that mediates numerous physiological processes, such as neuromodulation, endocrine regulation, olfaction, and muscle contraction/relaxation (Radomski et al., 1991; Martinez et al., 1994; Hurst et al., 1999; Bishop and Brandhorst, 2001). The distribution of NOS in nervous and other tissues is consistent with diverse roles of NO in decapod crustaceans [Figure 3.1; (Kim et al., 2004; McDonald et al., 2011)]. The *C. maenas* SG expressed a full-length NOS protein with a mass predicted from the cDNA sequence [~132 kDa; Figure 3.2 (McDonald et al., 2011)]. The observed ~94-kDa protein on the Western blot may represent an uncharacterized truncated NOS isoform in the SG of *C. maenas* (Figure 3.2). In *Drosophila melanogaster*, for example, NOS isoforms ranging in mass between 22 kDa and 151 kDa are generated by alternative splicing and alternative start sites and some truncated isoforms act as dominant negative regulators (Regulski and Tully, 1995; Stasiv et al., 2001). In arthropods, NO production has largely been inferred from NOS localization using immunohistochemistry or NADPH diaphorase histochemistry on fixed tissues (Scholz et al., 1998; Scholz et al., 2002; Zou et al., 2002; Kim et al., 2004; Mahadevan et al., 2004; Yeh et al., 2006; Ott et al., 2007; McDonald et al., 2011). 4,5-Diaminofluorescein-2 (DAF-2) was used to detect NO in the terminal abdominal ganglion of the crayfish, *Pacifastacus leniusculus* and hemocytes in the tiger shrimp, *Penaeus monodon* (Schuppe et al., 2002; Wu et al., 2013). The present study used CuFL to localize and quantify NO production in the eyestalk ganglia and SG. The major findings are: (1) CuFL is a highly specific and sensitive probe for NO in crustacean tissue; (2) NO production in the *C. maenas* SG requires NOS activity; and (3) endogenous protein(s) sequesters NO and releases NO over a prolonged period.

CuFL is a highly specific cell-permeable probe for NO in living cells (Lim et al., 2006; McQuade et al., 2010; Gusarov et al., 2013). In order to establish that the fluorescence observed after CuFL loading was NO-dependent, NOS inhibitor (L-NAME) and NO scavenger (cPTIO) were used to reduce NO-FL fluorescence in the SG. Preincubation with cPTIO or cPTIO + L-NAME decreased NO-FL fluorescence by ~30% (Figure 3.4). Including L-NAME during CuFL loading decreased fluorescence by 40% (Figure 3.5), indicating that more than half of the NO-FL fluorescence was not directly dependent on NOS activity. As NO has a half-life on the order of seconds in aerated aqueous solutions (Moncada et al., 1991), the gas was apparently bound by an endogenous protein, which released NO over the 1 h loading period. In the

salivary glands of several blood sucking insects, such as *Rhodnius prolixus* (Ribeiro et al., 1993), *Cimex lectularius* (Weichsel et al., 2005), and *Triatoma infestans* (Assumpcao et al., 2008), NO is sequestered by heme proteins. NO is reversibly bound to an Fe(III) heme protein that releases NO when exposed to a neutral pH at the site of the wound. We hypothesized that NO was sequestered in a similar manner in the SG of *C. maenas*. In order to test this hypothesis, 1 mM $NaN_3$ was added during preincubation to drive the dissociation of NO from a protein to which it was bound. This resulted in a further 57% reduction in fluorescence compared to SGs preincubated with cPTIO + L-NAME without $NaN_3$ (Figure 3.5), supporting the hypothesis that NO was bound by an endogenous protein. To determine that the large reduction in NO-FL fluorescence by $NaN_3$ was not the result of large-scale cell death, we used a propidium iodide cell viability stain to quantify the dead:live cell ratio in SG incubated in saline, 1 mM $NaN_3$ in saline, or 70% MeOH for 30 min. SG treated with azide had a 1.8-fold increase in dead cells compared to SG treated with crab saline (Figure 3.6). This compares with a 7.2-fold difference in NO-FL fluorescence between SG incubated with or without azide (Figure 3.5A, compare column #1 to #5). Thus, the increased cell death with azide accounts for no more than 13% of the decrease in NO-FL fluorescence with azide.

To further characterize this protein, a spectral shift analysis was performed on a soluble extract of isolated SGs in the presence of $NaN_3$. An azide-dependent dissociation of NO from a heme group would cause a negative spectral shift in the Soret peak [400 nm- 450 nm; see (Ribeiro et al., 1993)]. No spectral shift was observed in this range, indicating the NO-binding moiety was not a heme group (Figure 3.7). Alternatively, if an NO bound to a copper-containing protein is displaced by $NaN_3$, we would expect a negative spectral shift in the 600 nm – 700 nm range (Wilson and Torres, 2004). By contrast, azide caused a positive spectral shift in the 225 nm – 245 nm range and a negative shift in the 245 nm – 290 nm range. Further analysis is needed to identify the NO-binding protein(s) involved. Nevertheless, the spectral shift analysis showed that the SG contains an endogenous NO storage protein, but the moiety that bound NO was not a heme or copper group. Absorption at ~272 nm is typical of phenylalanine, tyrosine, and tryptophan side chains, which may suggest the formation of azidoadducts of aromatic amino acids. p-Azidophenylalanine adducts of dihydrofolate reductase show an increased absorption at ~250 nm (Carrico, 2004) compared to the unmodified enzyme, while 6-azidotryptophan shows an absorption at 248 nm that is not present in unmodified tryptophan (Miles and Phillips, 1985). The data indicate that

azide displaces NO from a metal-containing protein(s), which is associated with the reaction of azide with aromatic side chains.

CuFL was a better scavenger of NO than cPTIO. When cPTIO and CuFL were in direct competition during the loading period, there was no decrease in NO-FL fluorescence in the SG by cPTIO. Surprisingly, the fluorescent intensity was increased moderately (Figure 3.5A), compared to loading with CuFL alone. The concentration of cPTIO was 20,000 times greater than CuFL (1 mM *vs.* 0.5 µM, respectively), suggesting that the increase in fluorescence observed when cPTIO and CuFL were loaded together was a result of the CuFL being a more efficient NO scavenger than cPTIO. This is consistent with results from experiments that included cPTIO during preincubation and loading. cPTIO alone during preincubation could effectively scavenge NO and reduce NO-FL fluorescence (Figure 3.4). However, when CuFL was added to the cPTIO solution during loading, fluorescence increased or did not change (Figure 3.5), indicating that CuFL outcompeted cPTIO for binding to free NO. Similar results were found when DAF-2 was used to quantify NO in plant tissues; at high NO levels cPTIO increased DAF-2 NO fluorescence (Vitecek et al., 2008). This effect was attributed to DAF-2 binding to $N_2O_3$, a byproduct of the reaction of cPTIO and NO. However, CuFL does not react with $N_2O_3$. An alternative explanation is that cPTIO reacts with cellular substrates, such as reductases, which prevents it from scavenging NO (Haseloff et al., 1997). The high affinity of CuFL for NO makes it an excellent NO probe for use in living tissues, even in the presence of NO scavengers.

Figure 8 is a schematic diagram that summarizes the reactions and the effects of reagents during the preincubation and loading conditions. It is assumed that all the NO in the SG is produced by NOS. Some of the NO binds reversibly to endogenous protein (XX-NO), while some binds reversibly to GC-I and other NO-dependent enzymes (not included in the diagram). cPTIO acts as an NO scavenger by converting NO to $NO_2$, which can react with NO to form $N_2O_3$. CuFL reacts with NO to form NO-FL and Cu(I). As CuFL has a higher affinity for NO than cPTIO, the formation of NO-FL is favored over the formation of $NO_2$ when both reagents are present during loading. Azide reacts with the protein ($N_3XX$) and the released NO reacts with water to form nitrite and nitrate. As preincubation with cPTIO or with cPTIO + L-NAME does not affect NO release from endogenous proteins during CuFL loading, NO-FL fluorescence is reduced but not completely eliminated. The largest reduction in NO-FL fluorescence is

achieved when the SG is preincubated with $NaN_3$, cPTIO, and L-NAME. $NaN_3$ drives the release of NO from endogenous stores and the NO reacts with cPTIO. L-NAME inhibits NOS and prevents NO production during the preincubation period, as well as during the CuFL loading period.

Confocal microscopy revealed that NO-FL distribution was not uniform. Images of the SG *in situ* (Figure 3.3), as well as of the isolated SG (Figures 3.4, 3.5), showed that NO-FL fluorescence was preferentially located in cells that surrounded and penetrated the SG. The variation in NO-FL fluorescence was not due to variations in the size and thickness of the tissue. As areas of strong fluorescence occurred throughout the optical sections of the z-stack, the 1 h loading period was sufficient time for the CuFL to penetrate to the interior of the SG. The SG is structured as a network of groups of swollen axon termini separated by glial cell projections (Fu et al., 2005). This is apparent in the cell viability images, in which the nuclei of glial and other supporting cells surround axon termini that lack nuclei (Figure 3.6). The distribution of NO-FL is consistent with the production of NO by supportive tissues containing glial cells (Figures 3.3, 3.4B, and 3.5B). We conclude that the site of NO production, storage, and release is confined to supportive structures and areas within the SG lacking NO-FL fluorescence are axon termini. Additionally, several terminal types are present in the SG (Fu et al., 2005), therefore areas of NO-FL fluorescence may identify supportive cells near terminals from which neuropeptide release is NO dependent and terminals adjacent to areas lacking NO-FL rely on another mechanism for peptide release.

As MIH transcript levels remain constant over the molt cycle, MIH synthesis and secretion are regulated by post-transcriptional mechanisms [(Chung and Webster, 2003); N.L. Pitts and D.L. Mykles, unpublished]. NO inhibits neuropeptide release in the hippocampus, bovine chromaffin cells, basal forebrain, and nucleus accumbens in the mammalian brain (Sequeira et al., 1997; Schwarz et al., 1998; Philippu and Prast, 2001). As NO is produced rapidly and quickly diffuses across cell membranes, we propose that variations in NO release provide a mechanism for regulating the pulsatile release of MIH. If NO inhibits MIH secretion from the SG, then it follows that NO synthesis and release should vary with molt stage: it should be highest during premolt and postmolt stages and lowest during intermolt. There is measureable NO production in SG of intermolt animals, but other molt stages were not examined (Figure 3.3, 3.4, 3.5). The amount of NO released is determined by NOS activity and/or NO sequestration. The

experiments with cPTIO and L-NAME showed that about 60% of the NO-FL fluorescence during the loading period was from the release of NO from an endogenous storage protein (Figures 3.4, 3.5). Sequestration of NO during intermolt would reduce NO release, resulting in elevated MIH secretion from the SG. The higher frequency and amount of MIH release would keep the YO in the basal state (Chung and Webster, 2003; Mykles et al., 2010; Chang and Mykles, 2011; Covi et al., 2012). The hypothesis predicts that NO release increases during premolt, resulting from increased NOS activity, decreased NO sequestration, or a combination of the two. Future work will address this question by measuring total NO-FL fluorescence, as well as the contribution of the NO storage protein to total NO-FL fluorescence, in the SG from intermolt, premolt, and postmolt animals.

In summary, the SG is a site of higher NO production in the ESG of intermolt *C. maenas*. As a highly specific and sensitive indicator of NO, CuFL is an effective probe for NO production in living cells. CuFL readily penetrates tissues and reacts with NO to form NO-FL, making it a more effective NO scavenger than cPTIO. NO-FL is highly fluorescent, requiring very low concentrations (0.05 µM) of CuFL, which minimizes non-specific and possible toxic effects. NO-FL is stable at neutral pH, which allows for the quantification and localization of NO over a period of several hours. To our knowledge, this is the first report using CuFL to image and measure NO in crustacean tissues. The effects of azide, cPTIO, and L-NAME on NO-FL fluorescence indicate that greater than half of the NO synthesized by NOS was sequestered by an endogenous storage protein. Azide-dependent spectral shift analysis of SG soluble extract indicated that NO was bound to a metal-containing protein, but the metal is not iron or copper. The localization of NOS and NO-FL to supportive tissues suggests that NO produced and released by glial cells modulates neuropeptide secretion from axon terminals. The episodic release of MIH may be regulated by a NO/cGMP-dependent feedback mechanism. NO sequestration during intermolt may dampen the feedback mechanism, thus increasing MIH pulses to maintain the YO in the basal state during intermolt (Mykles et al., 2010; Chang and Mykles, 2011; Covi et al., 2012). Increased NO release due to increased NOS activity and/or decreased NO sequestration enhances the negative feedback loop. Consequently, the reduction in MIH pulses drives the transition of YO from the basal to activated state and the animal enters premolt.

## MATERIALS AND METHODS

*Animals*

Green shore crabs were collected from Bodega Harbor in Bodega Bay, California. They were maintained under ambient conditions in a flow-through sea water system (12-15 ℃) at Bodega Marine Laboratory (Abuhagr et al., 2014). Only intermolt (stage $C_4$) adult male crabs were used. Molt stage was determined by hemolymph ecdysteroid concentrations and the presence or absence of the membranous layer in the exoskeleton (Abuhagr et al., 2014). Ecdysteroids were quantified using a competitive enzyme-linked immunoassay (Kingan, 1989; Abuhagr et al., 2014).

*End-point PCR*

Tissue expression of *Cm-NOS* (GenBank accession #GQ862349) was determined using end-point RT-PCR. *Cm-EF2* (GenBank accession #GU808334) is a constitutively expressed gene and served as a control to assess the quality of RNA isolations and cDNA synthesis. RNA was isolated from tissues of an intermolt male *C. maenas* using TRIzol reagent (Life Technologies, Carlsbad, CA USA) according to the manufacture's protocol. Total RNA was treated with DNase I (New England Biolabs, Ipswich, MA USA) followed by a phenol:chloroform extraction. RNA was precipitated overnight in a 3:1 mixture of isoamyl alcohol:sodium acetate (pH 5.2) and re-suspended in 20 µL nuclease free water. RNA was reverse transcribed with Transcriptor Reverse Transcriptase (Roche Diagnostics, Indianapolis, IN USA) and an oligo-dT primer (50 µmol). PCR reactions contained 1 µL template cDNA, 0.5 µL 10 µM forward primer (*Cm-NOS*, 5'-GTG TGG AAG AAG AAC AAG GAC C-3'; *Cm-EF2*, 5'-CCA TCA AGA GCT CCG ACA ATG AGC G-3'), 0.5 µL 10 µM reverse primer (*Cm-NOS*, 5'-TCT GTG GCA TAG AGG ATG GTG G-3'; *Cm-EF2*, 5'-CAT TTC GGC ACG GTA CTT CTG AGC G-3'), 5 µL 2x PCR master mix (Thermo Scientific, Rockford, IL USA), and 3 µL sterile deionized water. Primers were synthesized by Integrative DNA Technologies (Coralville, IA USA). PCR conditions were as follows: 5 min denaturation at 95 ℃, 35 cycles of 30 sec denaturation at 95 ℃, 30 sec annealing at 58 ℃ ( *Cm-NOS*) or 61 ℃ ( *Cm-EF2*), 30 sec extension at 72 ℃, and final extension at 72 ℃ for 7 min. Products were separated on a 1.5% agarose gel and stained with ethidium bromide.

*Western Blot Analysis*

Twelve SG were homogenized in 150 µL buffer containing 20 mM Tris-HCl (pH 7.4), 1 mM EDTA, 20 mM KCl, and 10% protease inhibitor cocktail (Sigma Aldrich, St. Louis, MO USA) for 5 min and centrifuged at 30,000 g for 15 min. A sample of the supernatant fraction (24 µL; 50 µg protein) was combined with 8 µL sodium dodecyl sulfate-polyacrylamide gel electrophoresis (SDS-PAGE) sample buffer (Bio-Rad Laboratories, Inc., Hercules, CA USA) and incubated at 95 ℃ for 10 min. SG protein samples and SeeBlue Plus 2 pre-stained standard (Invitrogen, Carlsbad, CA USA) were separated by SDS-PAGE (200V, 30 min) on a Mini-Protean TGX 4-15% Tris-glycine gel (Bio-Rad Laboratories, Hercules, CA USA) using a Tris-glycine buffer system. Proteins were transferred to a polyvinylidene difluoride (PVDF) membrane (100 V, 1 h) and incubated in Tris-buffered saline + Tween-20 (TTBS) plus 2% goat serum (Vector Laboratories, Inc., Burlingame, CA USA) for 45 min at room temperature (RT), followed by an overnight incubation in a 1:100 dilution of the anti-universal NOS antibody (PA1-38835; Pierce Antibodies, Thermo Scientific, Rockford, IL USA) or 2% goat serum (control without primary antibody). The anti-universal NOS antibody recognized a highly conserved peptide sequence (QKRYHEDIFG) in NOS proteins from various species, including *C. maenas* (McDonald et al., 2011). Proteins were incubated with a goat anti-rabbit biotinylated secondary antibody in TTBS for 1 h at RT, followed by 30 min at RT in Vectastain ABC reagent (both from Vector Laboratories, Burlingame, CA USA). The membrane was developed with WesternBright Sirius chemiluminescent HRP substrate (Advansta, Menlo Park, CA USA) according to kit instructions. Images were obtained using a ChemiDoc XRS+ Molecular Imager (Bio-Rad Laboratories, Hercules, CA USA). Band intensities from the Western Blot analysis were measured with Image Lab software (Bio-Rad Laboratories, Hercules, CA, USA).

*Imaging and quantification of NO-FL fluorescence*

NO was imaged in live cells using Cu-FL, a cell-permeable Cu (II) fluorescein-based ligand, which was made by combining $CuCL_2$ and FL (2-{2-chloro-6-hydroxy-5-[2-methylquinolin-8-ylaminomethyl]-3-oxo3H-xanthen-9}); Strem Chemicals, Newburyport, MA USA) in a 1:1 molar ratio (Lim et al., 2006). ESG and SG were dissected in crab saline, preincubated with crab saline or with 1 mM cPTIO (Cayman Chemical, Ann Arbor, MI, USA), and/or 1 mM L-NAME (Cayman Chemical, Ann Arbor, MI, USA), and/or 1 mM $NaN_3$ in crab saline for 30 min in the dark; and loaded for 1 h with 0.05 µM CuFL in crab saline with

or without 1 mM cPTIO or 1 mM L-NAME in the dark. As SG size and fluorescence intensity varied between individuals, one SG of a pair received the control treatment and the other SG received the experimental treatment. The treatments are detailed in the Results. After CuFL loading, tissues were transferred to crab saline and fluorescence intensity (arbitrary units) was quantified on an Olympus BX50WI microscope (excitation 494 nm, emission 519 nm, exposure time 1 sec, 10x) using Metamorph Image Analysis software (Molecular Devices LLC, Sunnyvale, CA USA). A SG was optically divided into 4 quadrants and the average intensity of each image was summed to calculate the total fluorescence intensity for the entire SG. After quantification, SG were imaged with an Olympus Fluoroview FV 500 confocal laser scanning biological microscope (488 nm excitation, 519 nm emission, 10x objective). Images were composites of 20 stacked optical sections. Quantification and imaging of SG pairs was completed less than 2 h after the end of the loading period.

*Cell viability imaging*

A LIVE/DEAD Sperm Viability Kit (L-7011; Molecular Probes, Eugene, OR, USA) was used to identify live and dead cells in isolated SG. SG were incubated 30 min in crab saline, 70% methanol, or 1 mM $NaN_3$ in crab saline and stained 5 min with 12 µM propidium iodide in crab saline followed by 10 µM Hoechst 33342 stain (H211492; Molecular Probes, Eugene, OR, USA) in crab saline. SG were imaged with an Olympus Fluoroview FV 500 confocal laser scanning biological microscope (358 nm excitation, 461 nm emission for Hoechst and excitation 494 nm, emission 519 nm for PI with 20x objective) as described above. In false-color images, PI staining was set as green and Hoechst staining was set as red. The ratio of dead to live cells was obtained by counting the number of yellow/orange and red nuclei, respectively, for each treatment by 7 naïve observers. The observers were given the 3 unlabeled overlay images (Figure 3.6), as well as a legend showing examples of red, orange, and yellow nuclei. Observers were instructed to count the number of red and yellow/orange cells in each image. The ratio of dead to live cells for each observer was calculated and averaged.

*Spectral shift analysis*

Thirty SG were homogenized in 2 mL of phosphate buffered saline (137 mM NaCl; 10 mM sodium phosphate, pH, 7.4; and 2.7 mM KCl). Homogenate samples (0.5 mL aliquotes) were flash frozen in liquid nitrogen. On the day of the experiment, samples were thawed on ice and centrifuged at 30,000 g for 15 min at 4˚C to remove cellular debris. Samples were kept in the dark whenever possible. Spectra at 1 nm intervals were recorded with 5 sec integration using an Agilent 8453 diode array spectrophotometer (Agilent Technologies, Inc. Santa Clara, CA USA) from 190 nm to 1100 nm and analyzed using UV-Visible Chemstation Version B.01.01 software (Agilent Technologies, Inc. Santa Clara, CA USA). The cuvette path length was 1 cm and spectra ranged from 0.5 to 1.0 absorbance units across the entire spectral range. Following a baseline measurement, 10 µL 1 M $NaN_3$ was added directly to the sample and a reading was taken every 5 min for 1 h. Differences in spectra were calculated by subtracting each 5 min time interval after the addition of azide from the baseline measurement before azide.

*Statistical analyses and software*

Statistical analysis used Sigma Plot 12.0 software (Systat Software Inc., San Jose CA, USA). Differences in mean fluorescent intensities between control and experimental SG used a paired t-test analysis. Differences in dead to live cell ratios between treatment groups and observers used a Kruskal-Wallis analysis (variance on ranks). Data are presented as mean ± 1 s.e. and the level of significance was set at $\alpha = 0.05$. Graphs were constructed in Sigma Plot. All other Figures were created using Illustrator and Photoshop 10 (Adobe Systems, San Jose, CA, USA).

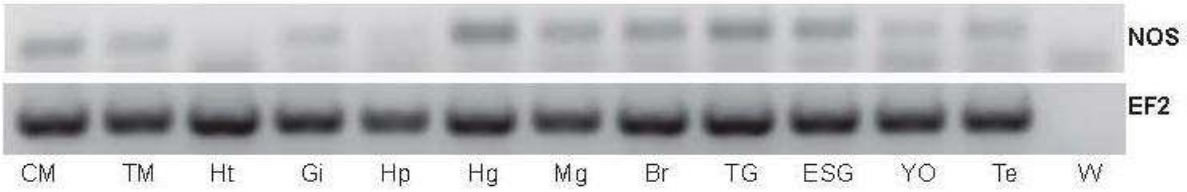


**Figure 3.1 Tissue expression of *Cm-NOS* and *Cm-EF2* using end-point RT-PCR.** PCR products (158 bp for *Cm-NOS* and 278 bp for *Cm-EF2*) were separated on a 1.5% agarose gel and stained with ethidium bromide (inverted images). *Cm-EF2* was expressed in all tissues. *Cm-NOS* was expressed in all tissues except heart (Ht) and hepatopancreas (Hp). Other abbreviations: CM, claw muscle; TM, thoracic muscle; Gi, gill; Hg, hindgut; Mg, midgut; Br, brain; TG, thoracic ganglion; ESG, eyestalk ganglia; Te; testes; W, water (no template control).

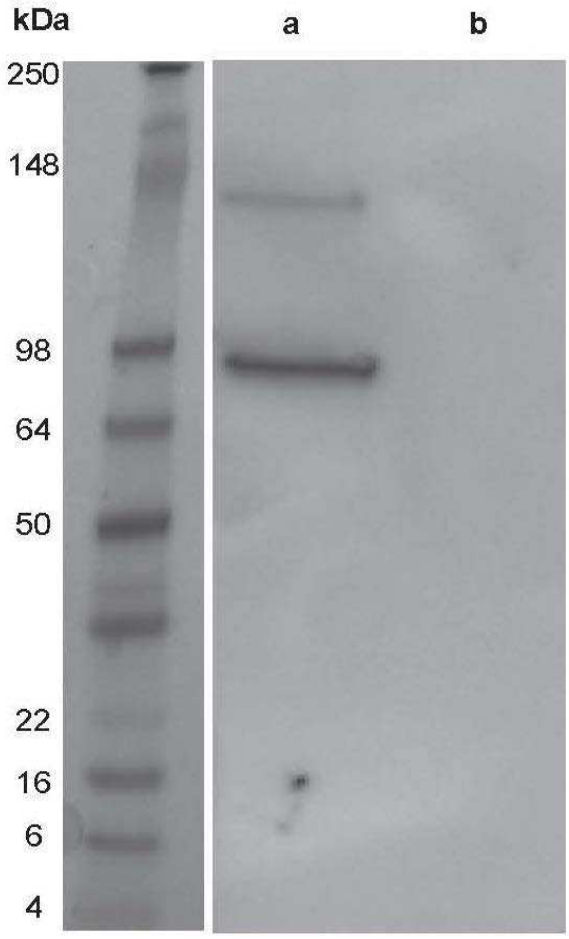


**Figure 3.2 Western blot analysis of Cm-NOS protein in the sinus gland.** SG soluble protein was separated by SDS-PAGE, transferred to PVDF membrane, and probed with (Lane a) or without (Lane b) universal NOS antibody. Detection of primary antibody used a goat anti-rabbit IgG plus ABC reagent and chemiluminescence (see Materials and Methods). The primary antibody recognized a protein of the predicted mass ~132-kDa for Cm-NOS and a second protein (~94 kDa), which may represent an uncharacterized truncated NOS isoform. Protein standards, with approximate masses, are shown in the left panel.

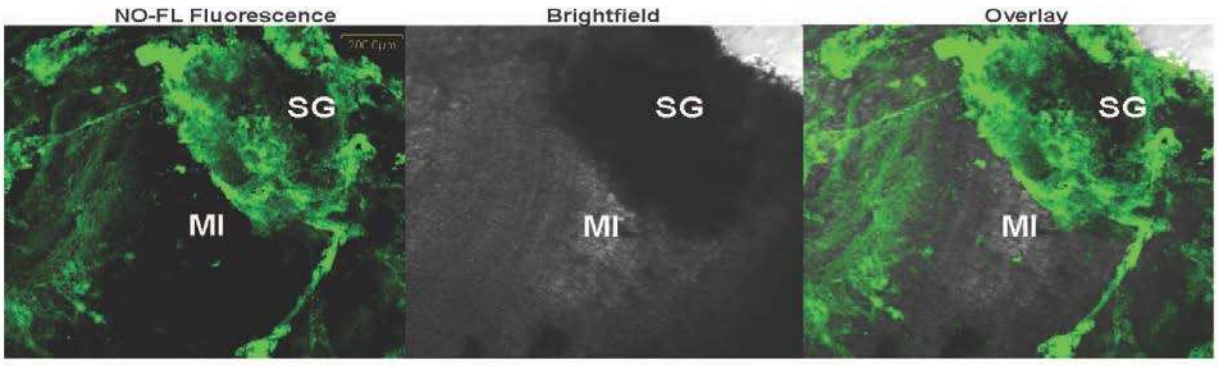


**Figure 3.3 Localization of NO-FL in the sinus gland *in situ*.** (A) Whole ESG was preincubated with crab saline for 30 min and loaded with 0.05 µM CuFL for 1 h in the dark. Stacked images were obtained with a scanning laser confocal microscope at 10x magnification (scale bar = 200 µM). SG; sinus gland MI: medulla interna.

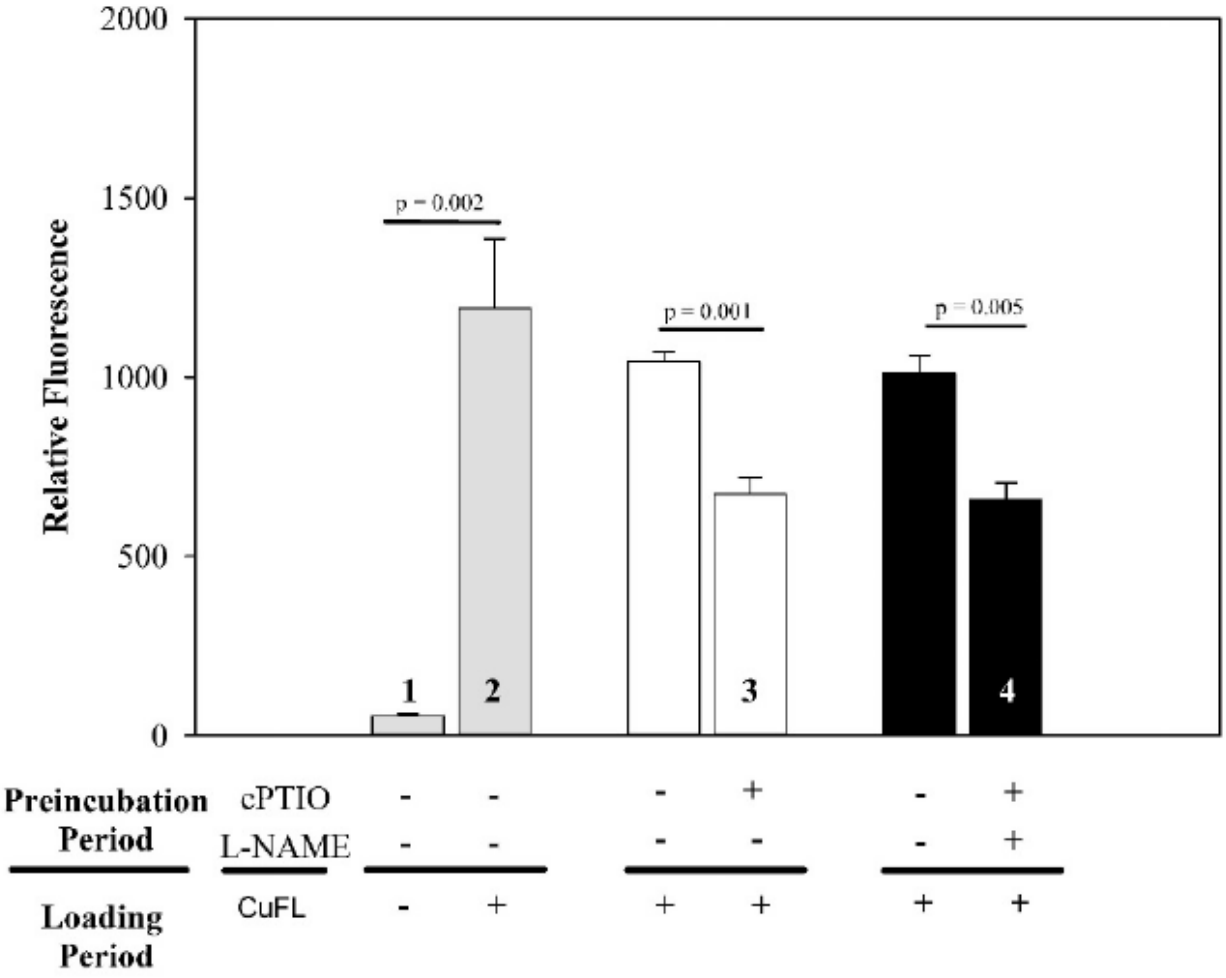


**Figure 3.4A Effects of cPTIO and L-NAME on NO-FL fluorescence in the sinus gland during the preincubation period.** SGs were preincubated with saline, 1 mM cPTIO alone, or cPTIO in combination with 1 mM L-NAME for 30 min and loaded without or with 0.05 µM CuFL for 1 h in the dark. Total NO-FL fluorescence (mean ± 1. s.e., n = 6). Gray-shaded columns compare relative fluorescence intensity between SG pairs preincubated in crab saline and loaded with or without CuFL. Open columns compare fluorescence between SG pairs preincubated with or without cPTIO and loaded with CuFL. Black-filled columns compare fluorescence between SG pairs preincubated with or without cPTIO and L-NAME. Significant differences, with p value, between SG pairs are indicated by horizontal lines. Numbers on the columns correspond to the confocal microscope images in 4B.

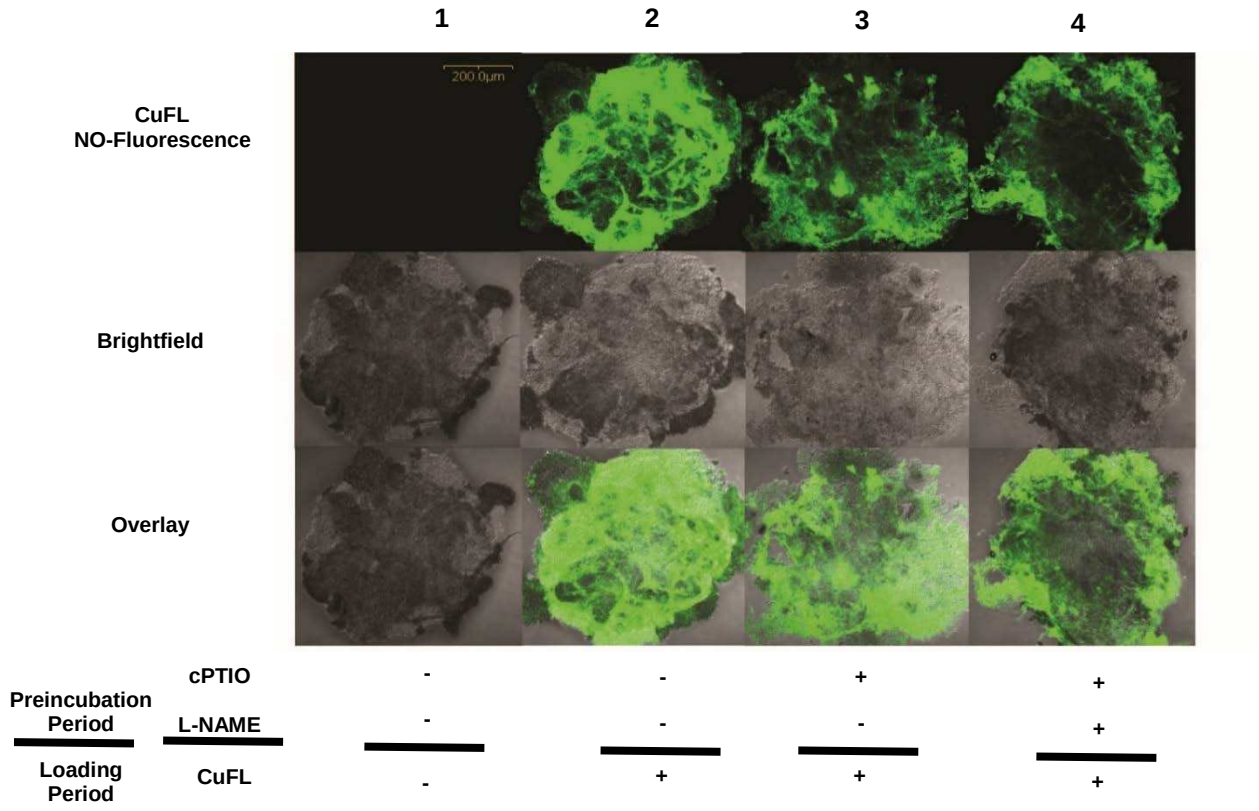


**Figure 3.4B Representative confocal images of SGs from 4A**. Panels 1, 2, 3, and 4 correspond to the column numbers in (A). All images were taken on a scanning laser confocal microscope at 10x (scale bar = 200 µM).

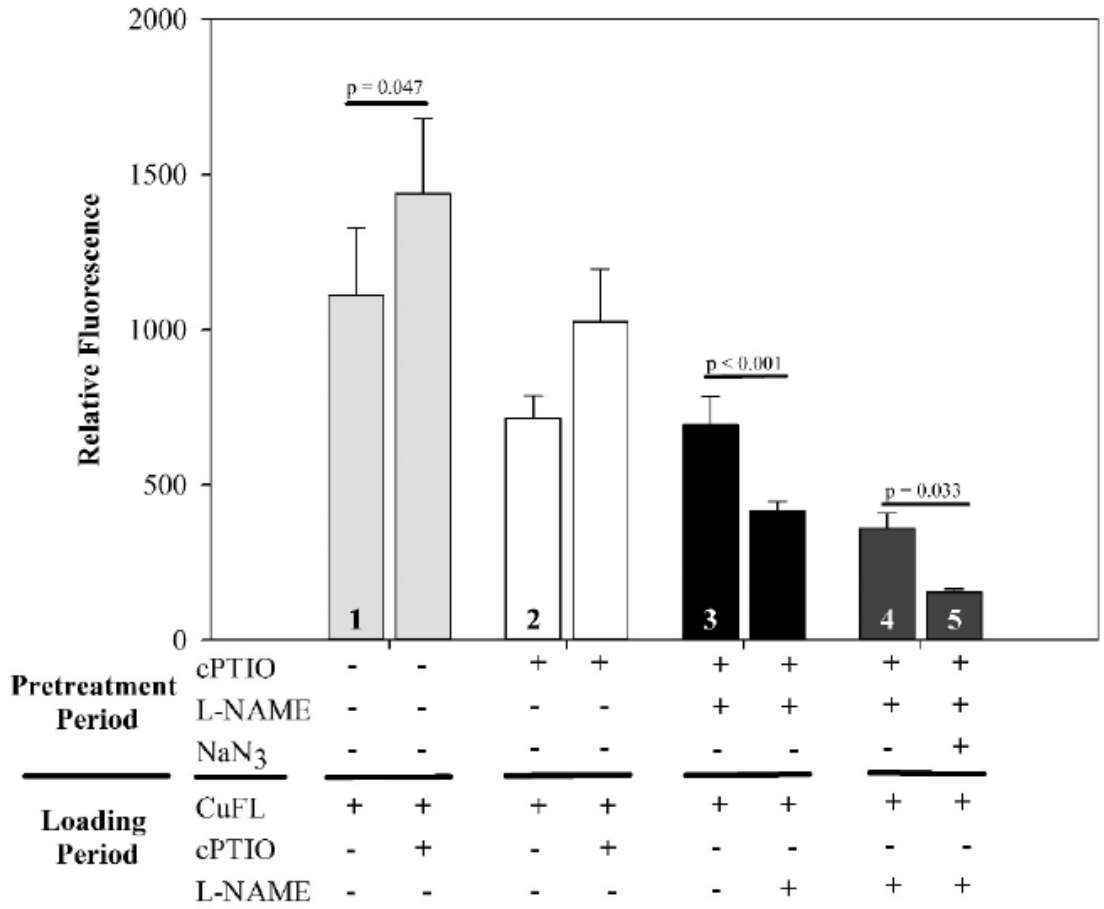


**Figure 3.5A Effects of L-NAME, cPTIO, and $NaN_3$ on NO-FL fluorescence in the sinus gland.** SGs were preincubated with saline or the indicated compound(s) for 30 min and loaded with 0.05 µM CuFL plus the indicated compound(s). The concentration of cPTIO, L-NAME, and $NaN_3$ was 1 mM. (A) Total NO-FL fluorescence (mean ± 1. s.e.). Light gray-shaded columns compare fluorescence between SG pairs preincubated with saline and loaded with CuFL without or with cPTIO (n = 9). Open columns compare fluorescence between SG pairs preincubated with cPTIO and loaded with CuFL without or with cPTIO (n = 12). Black-filled columns compare fluorescence between SG pairs preincubated with cPTIO and L-NAME and loaded with CuFL without or with L-NAME (n = 10). Dark gray-shaded columns compare fluorescence between SG pairs preincubated with cPTIO + L-NAME without or with $NaN_3$ and loaded with CuFL with L-NAME (n = 6). Significant differences, with p value, between SG pairs are indicated by horizontal lines. Numbers in the columns correspond to the confocal images in (B).

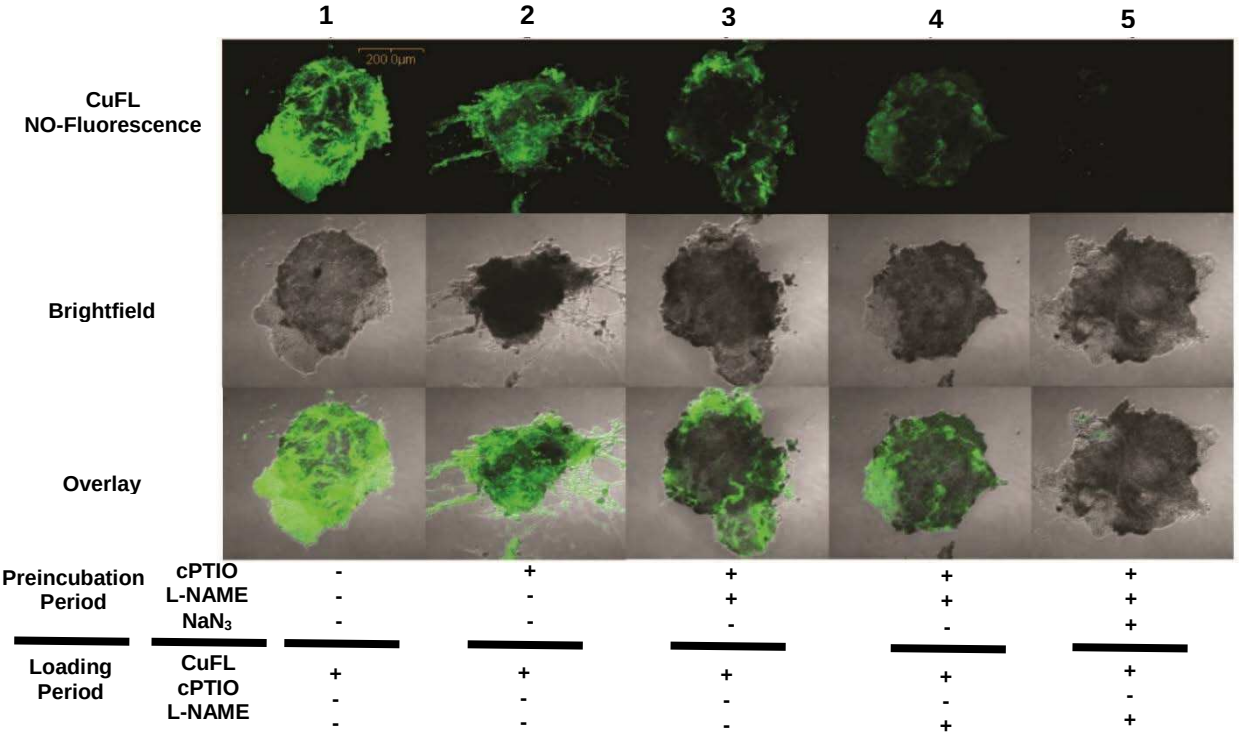


**Figure 3.5B Representative confocal images of SGs from 5A.** Panels 1, 2, 3, and 4 correspond to the column numbers in (A). All images were taken on a scanning laser confocal microscope at 10x (scale bar = 200 µM).

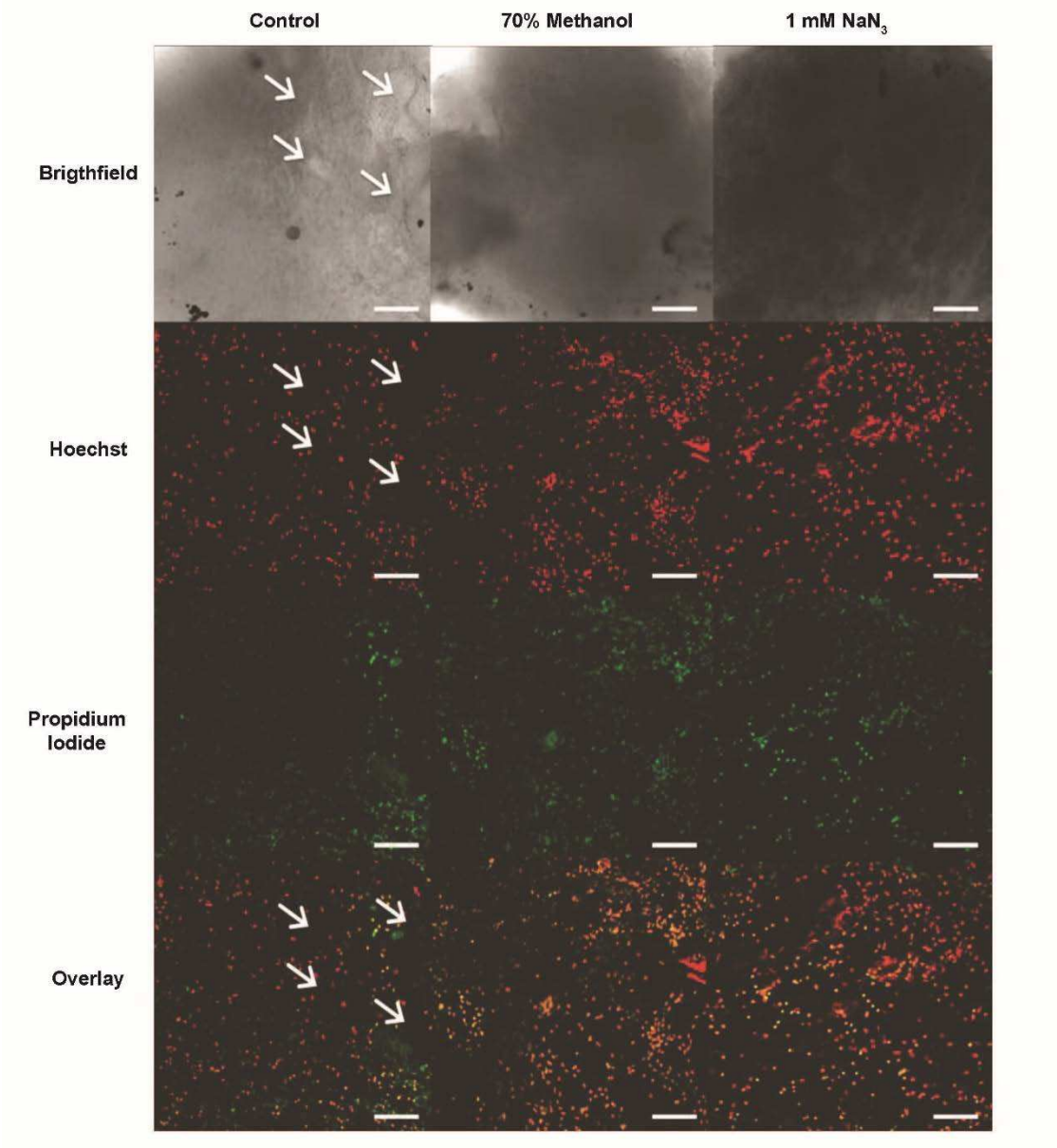


**Figure 3.6 Effects of sodium azide and 70% methanol on SG cell viability.** SG were incubated with crab saline, 1 mM $NaN_3$, or 70% methanol for 30 min, stained with propidium iodide (indicated with green) and Hoechst (indicated with red) stains, and imaged by confocal microscopy (see Materials and Methods). The nuclei of glial and other supportive cells were stained. Groups of axon termini were located in regions lacking nuclei (arrows). Dead cells were identified by nuclei stained with both propidium and Hoechst (orange to yellow) in overlay images. Scale bar = 100 µM.

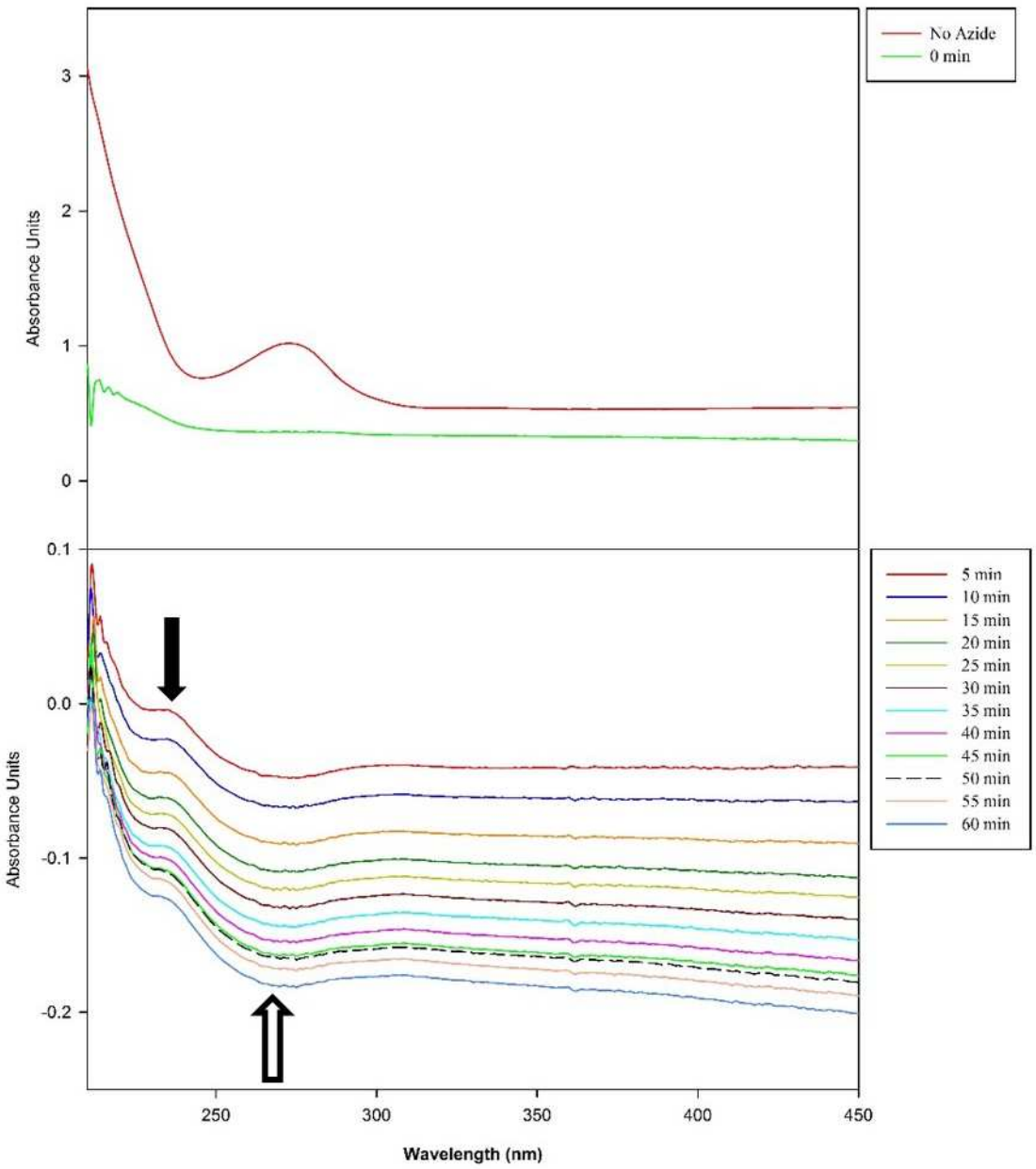


**Figure 3.7 Effect of sodium azide on absorption spectra of soluble proteins from the sinus gland.** Top panel shows the spectra of the SG extract prior to the addition of $NaN_3$ (red line – no azide) and immediately after the addition of 1 mM $NaN_3$ (green line – 0 min). Bottom panel shows spectral shifts at 5-min intervals after the addition of $NaN_3$. Spectra at 0 to 60 min are the differences between the baseline spectrum (no azide) and the spectrum at a specific time point. A positive spectral shift occurred at ~225 nm (black arrow) and a negative spectral shift occurred at ~255 nm (white arrow).

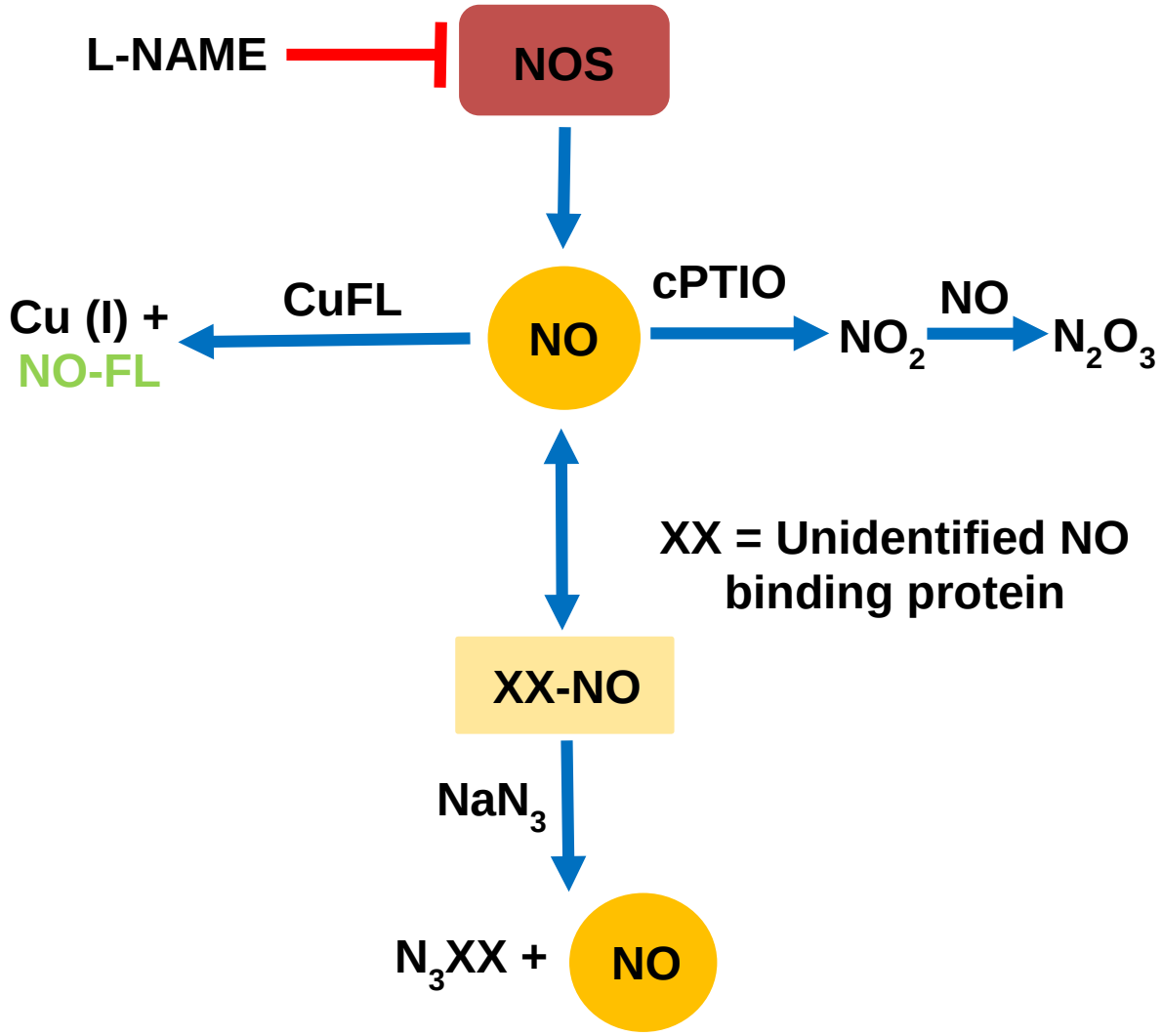


**Figure 3.8 Schematic diagram summarizing the effects of L-NAME, cPTIO, and $NaN_3$ on NO production, sequestration, and degradation in the sinus gland.** NOS produces NO, which binds NO-dependent proteins (not shown) or is sequestered by NO-binding protein (XX-NO). NO scavenger cPTIO converts NO to $NO_2$. CuFL reacts with NO, reducing Cu (II) to Cu (I), to produce highly fluorescent NO-FL. L-NAME decreases NO-FL fluorescence by inhibiting NOS. cPTIO decreases NO-FL fluorescence during preincubation, but is out-competed by CuFL during the loading period. Preincubation of SGs with $NaN_3$ displaces NO from the NO-binding protein ($N_3XX$) and the NO combines with water to form nitrite and nitrate. Maximum reduction of NO-FL fluorescence is achieved when the SG is preincubated with L-NAME, cPTIO, and $NaN_3$ and when L-NAME is included during CuFL loading.

REFERENCES

Abuhagr, A. M., Blindert, J. L., Nimitkul, S., Zander, I. A., LaBere, S. M., Chang, S. A., MacLea, K. S., Chang, E. S. and Mykles, D. L. (2014). Molt regulation in green and red color morphs of the crab *Carcinus maenas*: gene expression of molt-inhibiting hormone signaling components. *J. Exp. Biol.* 217, 796-808.

Aonuma, H., Nagayama, T. and Takahata, M. (2000). Modulatory effects of nitric oxide on synaptic depression in the crayfish neuromuscular system. *J. Exp. Biol.* 203, 3595-3602.

Aonuma, H., Nagayama, T. and Takahata, M. (2002). Nitric oxide and cyclic GMP modulate synaptic transmission in the local circuits of the crayfish. In *The Crustacean Nervous System*, (ed. K. Wiese), pp. 305-312. Berlin: Springer.

Assumpcao, T. C. F., Francischetti, I. M. B., Andersen, J. F., Schwarz, A., Santana, J. M. and Ribeiro, J. M. C. (2008). An insight into the sialome of the blood-sucking bug *Triatoma infestans*, a vector of Chagas' disease. *Insect Biochem. Molec. Biol.* 38, 213-232.

Azzouna, A. and Rezig, M. (2001). Ultrastructural study of the sinus gland of the shrimp *Palaemonetes mesogenitor* Sollaud, 1912. *B. Soc. Zool. Fr.* 126, 217-219.

Bishop, C. D. and Brandhorst, B. P. (2001). The role of NO/cGMP and HSP90 in regulating metamorphosis of the sea urchin *Lytechinus pictus*. *Dev. Biol.* 235, 251-251.

Bogdan, C. (2001). Nitric oxide and the regulation of gene expression. *Trends Cell Biol.* 11, 66-75.

Caceres, L., Necakov, A. S., Schwartz, C., Kimber, S., Roberts, I. J. H. and Krause, H. M. (2011). Nitric oxide coordinates metabolism, growth, and development via the nuclear receptor E75. *Genes Dev.* 25, 1476-1485.

Calabrese, V., Mancuso, C., Calvani, M., Rizzarelli, E., Butterfield, D. A. and Stella, A. M. G. (2007). Nitric oxide in the central nervous system: neuroprotection versus neurotoxicity. *Nat. Rev. Neurosci.* 8, 766-775.

Carrico, I. S. (2004). Protein Engineering Through *in vivo* Incorporation of Phenylalanine Analogs. Doctor of Philosophy. Pasadena, CA: California Institute of Technology.

Chang, E. S. and Mykles, D. L. (2011). Regulation of crustacean molting: A review and our perspectives. *Gen. Comp. Endocrinol.* 172, 323-330.

Chung, J. S. and Webster, S. G. (2003). Moult cycle-related changes in biological activity of moult-inhibiting hormone (MIH) and crustacean hyperglycaemic hormone (CHH) in the crab, *Carcinus maenas* - From target to transcript. *Eur. J. Biochem.* 270, 3280-3288.

Colasanti, M. and Venturini, G. (1998). Nitric oxide in invertebrates. *Molec. Neurobiol.* 17, 157-174.

Cooke, I. M. (1985). Electrophysiological characterization of peptidergic neurosecretory terminals. *J. Exp. Biol.* 118, 1-35.

Cooper, C. E. (1999). Biochemistry of nitric oxide. *Biochim. Biophys. Acta* 1411, 215-216.

Covi, J. A., Chang, E. S. and Mykles, D. L. (2012). Neuropeptide signaling mechanisms in crustacean and insect molting glands. *Invert. Reprod. Dev.* 56, 33-49.

Fu, Q., Kutz, K. K., Schmidt, J. J., Hsu, Y. W. A., Messinger, D. I., Cain, S. D., De la Iglesia, H. O., Christie, A. E. and Li, L. J. (2005). Hormone complement of the *Cancer productus* sinus gland and pericardial organ: An anatomical and mass spectrometric investigation. *J. Comp. Neurol.* 493, 607-626.

Garthwaite, J. (2008). Concepts of neural nitric oxide-mediated transmission. *Eur. J. Neurosci.* 27, 2783-2802.

Gusarov, I., Gautier, L., Smolentseva, O., Shamovsky, I., Eremina, S., Mironov, A. and Nudler, E. (2013). Bacterial nitric oxide extends the lifespan of *C. elegans*. *Cell* 152, 818-830.

Haseloff, R. F., Zollner, S., Kirilyuk, I. A., Grigorev, I. A., Reszka, R., Bernhardt, R., Mertsch, K., Roloff, B. and Blasig, I. E. (1997). Superoxide-mediated reduction of the nitroxide group can prevent detection of nitric oxide by nitronyl nitroxides. *Free Radical Res.* 26, 7-17.

Hirst, D.G. and Robson T. (2011). Nitric oxide physiology and pathology. *Methods in Molec. Biol.* 704, 1-13.

Hopkins, P. M. (2012). The eyes have it: A brief history of crustacean neuroendocrinology. *Gen. Comp. Endocrinol.* 175, 357-366.

Hurst, W. J., Moroz, L. L., Gillette, M. U. and Gillette, R. (1999). Nitric oxide synthase immunolabeling in the molluscan CNS and peripheral tissues. *Biochem. Biophys. Res. Commun.* 262, 545-548.

Inada, M., Mekata, T., Sudhakaran, R., Okugawa, S., Kono, T., El Asely, A. M., Linh, N. T. H., Yoshida, T., Sakai, M., Yui, T. et al. (2010). Molecular cloning and characterization of the nitric oxide synthase gene from kuruma shrimp, *Marsupenaeus japonicus*. *Fish Shellfish Immunol.* 28, 701-711.

Johansson, K. U. I. and Carlberg, M. (1994). NADPH-diaphorse histrochemistry and nitric oxide synthase activity in deutocerebrun of the crayfish, *Pacifastacus leiusculus* (Crustacea, Decapoda). *Brain Res.* 649, 36-42.

Kim, H. W., Batista, L. A., Hoppes, J. L., Lee, K. J. and Mykles, D. L. (2004). A crustacean nitric oxide synthase expressed in nerve ganglia, Y-organ, gill and gonad of the tropical land crab, *Gecarcinus lateralis*. *J. Exp. Biol.* 207, 2845-2857.

Kingan, T. G. (1989). A competitive enzyme-linked immunosorbent assay: application in the assasy of peptides, steroids, and cyclic nucleotides. *Anal. Biochem.* 183, 283-289.

Lachaise, F., Leroux, A., Hubert, M. and Lafont, R. (1993). The molting gland of crustaceans: localization, activity, and endocrine control (a review). *J. Crustacean Biol.* 13, 198-234.

Lee, C. Y., Zou, H. S., Yau, S. M., Ju, Y. R. and Liau, C. S. (2000). Nitric oxide synthase activity and immunoreactivity in the crayfish *Procambarus clarkii*. *Neuroreport* 11, 1273-1276.

Li, S. K., Zhang, Z., Li, C. B., Zhou, L. Z., Liu, W. H., Li, Y. Y., Zhang, Y. L., Zheng, H. P. and Wen, X. B. (2012). Molecular cloning and expression profiles of nitric oxide synthase (NOS) in mud crab *Scylla paramamosain*. *Fish Shellfish Immunol.* 32, 945-946.

Lim, M. H., Xu, D. and Lippard, S. J. (2006). Visualization of nitric oxide in living cells by a copper-based fluorescent probe. *Nat. Chem. Biol.* 2, 375-380.

Lorenc-Koci, E. and Czarnecka, A. (2013). Role of nitric oxide in the regulation of motor function. An overview of behavioral, biochemical and histological studies in animal models. *Pharmacol. Rep.* 65, 1043-1055.

Mahadevan, A., Lappe, J., Rhyne, R. T., Cruz-Bermudez, N. D., Marder, E. and Goy, M. F. (2004). Nitric oxide inhibits the rate and strength of cardiac contractions in the lobster *Homarus americanus* by acting on the cardiac ganglion. *J. Neurosci.* 24, 2813-2824.

Martin, K. D., Saari, L., Wang, G. X., Wang, T., Parkhurst, L. J. and Klucas, R. V. (1990). Kinetics and thermodynamics of oxygen, CO, and azide binding by the subcomponents of soybean leghemoglobin. *J. Biol. Chem.* 265, 19588-19593.

Martinez, A., Riverosmoreno, V., Polak, J. M., Moncada, S. and Sesma, P. (1994). Nitric oxide (NO) synthase immunoreactivity in the starfish *Marthasterias glacialis*. *Cell Tiss. Res.* 275, 599-603.

McDonald, A. A., Chang, E. S. and Mykles, D. L. (2011). Cloning of a nitric oxide synthase from green shore crab, *Carcinus maenas*: A comparative study of the effects of eyestalk ablation on expression in the molting glands (Y-organs) of *C. maenas*, and blackback land crab, *Gecarcinus lateralis*. *Comp. Biochem. Physiol.* 158A, 150-162.

McQuade, L. E., Ma, J., Lowe, G., Ghatpande, A., Gelperin, A. and Lippard, S. J. (2010). Visualization of nitric oxide production in the mouse main olfactory bulb by a cell-trappable copper(II) fluorescent probe. *Proc. Natl. Acad. Sci. USA* 107, 8525-8530.

Miles, E. W. and Phillips, R. S. (1985). Photoinactivation and photoaffinity labeling of tryptophan synthase alpha-2 beta-2 complex by the product analog 6-azido-L-tryptophan. *Biochem.* 24, 4694-4703.

Moncada, S., Palmer, R. M. J. and Higgs, E. A. (1991). Nitric oxide; physiology, pathophysiology, and pharmacology. *Pharmacol. Rev.* 43, 109-142.

Mungrue, I. N., Bredt, D. S., Stewart, D. J. and Husain, M. (2003). From molecules to mammals: what's NOS got to do with it? *Acta Physiol. Scand.* 179, 123-135.

Mykles, D. L., Adams, M. E., Gade, G., Lange, A. B., Marco, H. G. and Orchard, I. (2010). Neuropeptide action in insects and crustaceans. *Physiol. Biochem. Zool.* 83, 836-846.

Nathan, C. and Xie, Q. W. (1994). Nitric oxide synthases: roles, tolls, and controls. *Cell* 78, 915-918.

Ott, S. R., Aonuma, H., Newland, P. L. and Elphick, M. R. (2007). Nitric oxide synthase in crayfish walking leg ganglia: Segmental differences in chemo-tactile centers argue against a generic role in sensory integration. *J. Comp. Neurol.* 501, 381-399.

Palumbo, A. (2005). Nitric oxide in marine invertebrates: A comparative perspective. *Comp. Biochem. Physiol.* 142A, 241-248.

Philippu, A. and Prast, H. (2001). Role of histaminergic and cholinergic transmission in cognitive processes. *Drug News Perspect.* 14, 523-529.

Prast, H. and Philippu, A. (1992). Nitric oxide releases acetylcholine in the basal forebrain. *Eur. J. Pharmacol.* 216, 139-140.

Prast, H., Tran, M. H., Fischer, H. and Philippu, A. (1998). Nitric oxide-induced release of acetylcholine in the nucleus accumbens, role of cyclic GMP, glutamate, and GABA. *J. Neurochem.* 71, 266-273.

Prast, H., Fischer, H., Werner, E., Wernerfelmayer, G. and Philippu, A. (1995). Nitric oxide modulates the release of acetylcholine in the ventral striatum of the freely moving rat. *Naunyn Schmiedebergs Arch. Pharmacol.* 352, 67-73.

Radomski, M. W., Martin, J. F. and Moncada, S. (1991). Synthesis of nitric oxide by the hemocytes of the American horseshoe crab (*Limulus polyphemus*) *Phil. Trans. R. Soc. Lond. B.* 334, 129-133.

Regulski, M. and Tully, T. (1995). Molecular and biochemical characterization of dNOS: a *Drosophila* $Ca^{2+}$/calmodulin-dependent nitric oxide synthase. *Proc. Natl. Acad. Sci. USA* 92, 9072-9076.

Rewitz, K. F., Yamanaka, N. and O'Connor, M. B. (2013). Developmental checkpoints and feedback circuits time insect maturation. In *Animal Metamorphosis*, vol. 103 (ed. Y. B. Shi), pp. 1-33.

Ribeiro, J. M. C., Hazzard, J. M. H., Nussenzveig, R. H., Champagne, D. E. and Walker, F. A. (1993). Reversible binding of nitric oxide by a salivary heme protien from a bloodsucking insect. *Science* 260, 539-541.

Roman, L. J., Martasek, P. and Masters, B. S. S. (2002). Intrinsic and extrinsic modulation of nitric oxide synthase activity. *Chem. Rev.* 102, 1179-1189.

Rudolph, P. H. and Spaziani, E. (1991). Neurons demonstrable by nickel lysine backfilling of the optic peduncle in the crab *Cancer antennarius*. *Comp. Biochem. Physol.* 99C, 179-184.

Russwurm M., Russwurm C., Koesling D., Evanthia M. (2013). NO/cGMP: The past, present, and the future. *Methods in Molec. Biol.* 1020, 1-16.

Scholz, N. L. (1999). NO/cGMP signaling and the specification of motor networks in the crab stomatogastric ganglion. *Am. Zool.* 39, 46A-46A.

Scholz, N. L., Chang, E. S., Graubard, K. and Truman, J. W. (1998). The NO/cGMP pathway and the development of neural networks in postembryonic lobsters. *J. Neurobiol.* 34, 208-226.

Scholz, N. L., Labenia, J. S., De Vente, J., Graubard, K. and Goy, M. F. (2002). Expression of nitric oxide synthase and nitric oxide-sensitive guanylate cyclase in the crustacean cardiac ganglion. *J. Comp. Neurol.* 454, 158-167.

Schuppe, H., Cuttle, M., Chad, J. E. and Newland, P. L. (2002). 4,5-Diaminofluoroscein imaging of nitric oxide synthesis in crayfish terminal ganglia. *J. Neurobiol.* 53, 361-369.

Schwarz, P. M., Rodriguez-Pascual, F., Koesling, D., Torres, M. and Forstermann, U. (1998). Functional coupling of nitric oxide synthase and soluble guanylyl cyclase in controlling catecholamine secretion from bovine chromaffin cells. *Neurosci.* 82, 255-265.

Sequeira, S. M., Ambrosio, A. F., Malva, J. O., Carvalho, A. P. and Carvalho, C. M. (1997). Modulation of glutamate release from rat hippocampal synaptosomes by nitric oxide. *Nitric Oxide-Biol. Ch.* 1, 315-329.

Skinner, D. M. (1985). Molting and regeneration. In *The Biology of Crustacea*, vol. 9 eds. D. E. Bliss and L. H. Mantel), pp. 44-146. New York: Academic Press.

Stasiv, Y., Regulski, M., Kuzin, B., Tully, T. and Enikolopov, G. (2001). The *Drosophila* nitric oxide synthase gene (dNOS) encodes a family of proteins that can modulate NOS activity by acting as dominant negative regulators. *J. Biol. Chem.* 276, 42241-42251.

Stuenkel, E. L. (1985). Simultaneous monitoring of electrical and secretory activity in peptidergic neurosecretory terminals of the crab. *J. Physiol. Lond.* 359, 163-187.

Virarkar, M., Alappat, L., Bradford, P. G. and Awad, A. B. (2013). L-arginine and nitric oxide in CNS function and neurodegenerative diseases. *Crit. Rev. Food Sci. Nutr.* 53, 1157-1167.

Vitecek, J., Reinohl, V. and Jones, R. L. (2008). Measuring NO production by plant tissues and suspension cultured cells. *Molec. Plant* 1, 270-284.

Weichsel, A., Maes, E. M., Andersen, J. F., Valenzuela, J. G., Shokhireva, T. K., Walker, F. A. and Montfort, W. R. (2005). Heme-assisted S-nitrosation of a proximal thiolate in a nitric oxide transport protein. *Proc. Natl. Acad. Sci. USA* 102, 594-599.

Wilson, M. T. and Torres, J. (2004). Reactions of nitric oxide with copper containing oxidases; Cytochrome c oxidase and laccase. *Iubmb Life* 56, 7-11.

Wu, C. H., Siva, V. S. and Song, Y. L. (2013). An evolutionarily ancient NO synthase (NOS) in shrimp. *Fish Shellfish Immunol.* 35, 1483-1500.

Yao, C. L., Ji, P. F., Wang, Z. Y., Li, F. H. and Xiang, J. H. (2010). Molecular cloning and expression of NOS in shrimp, *Litopenaeus vannamei*. *Fish Shellfish Immunol.* 28, 453-460.

Yeh, F. C., Wu, S. H., Lai, C. Y. and Lee, C. Y. (2006). Demonstration of nitric oxide synthase activity in crustacean hemocytes and anti-microbial activity of hemocyte-derived nitric oxide. *Comp. Biochem. Physol.* 144B, 11-17.

Zou, H. S., Chang, Y. Z., Chen, S. C., Yau, S. M., Shen, Y. L. and Lee, C. Y. (2002). Localization of NADPH-diaphorase and nitric oxide synthase activity in the eyestalk of the crayfish, *Procambarus clarkii*. *Zool. Stud.* 41, 244-250.

CHAPTER FOUR

# INSIGHTS INTO NEUROSECRETION IN THE CENTRAL NERVOUS SYSTEM OF DECAPOD CRUSTACEANS; LOCALIZATION OF MOLT-INHIBITING HORMONE (MIH) AND NITRIC OXIDE SYNTHASE (NOS)


## SUMMARY

Molt inhibiting hormone (MIH) is an important regulator of crustacean molting. MIH is produced and secreted from the eyestalk ganglia (ESG). MIH production occurs in the X-organ (XO) where it is packaged into synaptic vesicles and transported to the sinus gland (SG). MIH secreted from the SG into the hemolymph negatively regulates the production of molting hormones (ecdysteroids) by the molting gland or Y-organ (YO). The mechanism that regulates MIH release from the SG is unknown, however recent studies indicate that it may be dependent on the gaseous signaling molecule nitric oxide (NO). To test this hypothesis an anti-MIH antibody was developed and used in double immunofluorescence assay to determine the proximity of nitric oxide synthase (NOS; the enzyme that produces NO) and MIH filled synaptic vesicles. It was originally hypothesized that the ESG was only source of MIH. However, recent studies identified MIH positive cells throughout the central nervous system (CNS). Therefore, NOS/MIH immunofluorescence was assessed in three CNS tissues: brain (Br), thoracic ganglion (TG), and eyestalk ganglion (ESG), from three decapod crustacean species; *Gecarcinus lateralis, Carcinus maenas*, and *Metacarcinus magister*. The MIH antibody binds MIH in all three CNS tissues from all three species. MIH and NOS are localized in close proximity in the ESG and TG of *G. lateralis* and *C. maenas*, supporting the hypothesis that MIH secretion is regulated by NO. Expression of *Gl-MIH, Gl-CHH, Gl-NOS*, and *Gl-EF2* was detected in all three CNS tissues. *Gl-MIH* and *Gl-CHH* expression was $10^5$ higher in the ESG compared to both the Br and the TG. *Gl-NOS* and *Gl-EF2* expression in the ESG was two to three orders of magnitude greater compared to the Br or TG. Expression of all four genes was also higher in the Br than in the TG by one to two orders of magnitude.


## INTRODUCTION

Growth in decapod crustaceans is characterized by the shedding and regeneration of exoskeleton in a process known as molting. The cellular events that lead to the physiological changes required for molting rely heavily on the endocrine system's production and secretion of two hormones.

Steroid hormones (ecdysteroids) are synthesized by a pair of Y-organs (YO) and trigger the cellular events required for molt induction (Chang and Mykles, 2011; Lachaise et al., 1993; Skinner, 1985). Ecdysteroid synthesis is negatively regulated by a peptide hormone, molt inhibiting hormone (MIH) that is produced and secreted from the X-organ/sinus gland complex (XO/SG) in the eyestalk ganglia (ESG) (Hopkins, 2012; Skinner, 1985). MIH is a member of the crustacean hyperglycemic hormone (CHH) superfamily of proteins (Chan, 1998; Chen et al., 2007) and its sequence is highly conserved among brachyuran crabs (Nakatsuji et al., 2009; Webster et al., 2012). MIH is expressed as a preprohormone of 113 amino acids (Webster et al., 2012). MIH is cleaved into two smaller peptides a 35 amino acid signal peptide and a 78 amino acid mature peptide that acts on the YO to inhibit ecdysteroid synthesis (Webster et al., 2012). The 9 kDa mature peptide contains six spatially conserved cysteine residues and three disulfide bridges that are key for stability and folding of the peptide (Fanjul-Möles, 2006; Nakatsuji et al., 2009; Webster et al., 2012). Early models of molt regulation hypothesize that MIH is restricted to the ESG and its sole function is molt regulation (Chung et al., 1998; Echalier, 1954; Webster and Keller, 1986). More recent studies find that MIH is expressed throughout the central nervous system (CNS), suggesting that MIH may serve multiple physiological functions (Abuhagr et al., 2014a; Stewart et al., 2013; Tiu and Chan, 2007; Zhu et al., 2011).

The crustacean nervous system consists of three major structures, the thoracic ganglion (TG), the brain (Br), and the eyestalk ganglia (ESG). The TG is a bilaterally symmetrical structure consisting of a single abdominal ganglion (abn) located posteriorly to five segmental neurons (sn) that send projections laterally to the walking legs (Sandeman, 1982; Stewart et al., 2013). The anterior TG connects to the Br via the circumesophageal connectives (coc) (Sandeman, 1982). The coc innervate the posterior region of the Br, the tritocerebrum (Krieger et al., 2012; Sandeman, 1982; Sandeman and Scholtz, 1995). The deutocerebrum lies between the tritocerebrum and the protocerebrum (Sandeman, 1982). The protocrebrum projects to the ESG via the optic nerve, which innervates the medulla terminalis (Sandeman, 1982). The MT is one of three ganglionic neuropils that make up the ESG (Bliss and Welsh, 1952). The MT houses the XO, a cluster of ~150 neurosecretory cells that produce MIH and other neuropeptides (Hopkins, 2012; Skinner, 1985). Synaptic vesicles filled with MIH are transported distally along axonal tracts to the SG, a neurohemal organ located at the junction of two neuropils, the medulla

interna (MI) and the medulla externa (ME) (Bliss and Welsh, 1952; Passano, 1951). MIH was originally proposed to be confined to the ESG (Hopkins, 2012; Webster et al., 2012). However, MIH is expressed in the Br and TG as well (Abuhagr et al., 2014a; Gu and Chan, 1998; Stewart et al., 2013; Tiu and Chan, 2007; Webster and Dircksen, 1991; Zhu et al., 2011).

MIH expression in tissues outside of the ESG does not conform to the classical understanding of MIH synthesis and secretion from the XO/SG complex. However, it is a reoccurring topic in the field of crustacean endocrinology (Abuhagr et al., 2014a; Chan, 1998; Sun, 1995; Tiu and Chan, 2007; Webster and Dircksen, 1991; Zhu et al., 2011). Alternative sources of MIH provide a plausible explanation for why, in some species, the removal of the eyestalks (the principle source of MIH) does not induce molting (Abuhagr et al., 2014a). In the TG of *Portunus pelagicus* MIH is localized to cell clusters that are adjacent to the sternal artery and the hemocoele (Hec), suggesting that MIH synthesized in the TG is directly released into the hemolymph, similar to MIH secretion from the SG (Stewart et al., 2013).

Despite early contributions of the XO-SG to understanding how electric and ionic stimulation induces synaptic vesicle release (Andrew and Saleuddin, 1978; Keller et al., 1994), the molecular components that regulate the release of neuropeptides from the SG is poorly characterized. The SG is a storage site for neuropeptides and is comprised of axon terminals, axons, and glial cells (Azzouna and Rezig, 2001; Hanström, 1939). Neuropeptides in the presynaptic terminals of the SG are stored in synaptic vesicles (Bunt and Ashby, 1967, 1968) and release their contents into the hemolymph by exocytosis (Weitzman, 1969). At the mammalian presynaptic membrane synaptic vesicle binding requires the assembly of the SNARE complex and $Ca^{2+}$ influx for exocytosis (Chen et al., 1999). Injection of antibodies against two mammalian SNARE complex proteins α-SNAP and synaptogamin, increases transmitter release from the crayfish SG, suggesting that a complex similar to the mammalian SNARE complex is present in crustaceans (He et al., 1999; Huang et al., 2008). Additionally, electrophysiological experiments in the SG of several crustacean species provide evidence that neuropeptide secretion from the SG is $Ca^{2+}$-dependent (Cooke, 1985).

In the mammalian adrenal gland, $Ca^{2+}$ influx is negatively regulated by a nitric oxdie (NO)/cyclic guanosine monophosphate (cGMP) pathway (Schwarz et al., 1998). In this negative feedback loop, $Ca^{2+}$ activates nitric oxide synthase (NOS) which produces NO. NO binds a guanylyl cyclase receptor (GC-Iβ),

producing cGMP and thus preventing $Ca^{2+}$ influx (Schwarz et al., 1998). Electrophysiological data from the SG of *Cardisoma carnifex* provides evidence that $Ca^{2+}$ influx regulates voltage-gated $Ca^{2+}$ channels in a negative feedback loop that would inhibit synaptic vesicle binding (Richmond et al., 1996). NOS is expressed in the SG of the crayfish *P. clarkki* and NO is produced in the SG of the green shore crab *C. maenas* (Lee et al., 2000; Pitts and Mykles, 2015), suggesting that this $Ca^{2+}$ dependent negative feedback loop in crustaceans may also be NO/cGMP dependent.

In an effort to expand upon the current body of knowledge regarding the expression and molecular regulation of MIH secretion, we developed an antibody against MIH from *G. lateralis.* The specificity of the antibody was verified against three MIH peptides from *G. lateralis, C. maenas*, and *Metacarcinus magister* via western blot. ESG from all three species were double labeled with the MIH antibody and a universal NOS antibody to determine the proximity of these two proteins. We show that in the ESG of *G. lateralis* and *C. maenas* MIH and NOS are closely localized, supporting the hypothesis that NO negatively regulates MIH secretion from the SG. MIH and NOS show similar localization in the TG of these species, indicating that the mechanism of secretion for this peptide is conserved throughout the CNS. MIH is localized in the Br of all three species but no NOS staining was detected. This study contributes to the limited data concerning the molecular regulation of neurosecretion in decapod crustaceans and expands on upon the basic understanding of MIH expression throughout the crustacean CNS.

## RESULTS

### *Peptide Selection and Specificity*

An antipeptide antibody was raised against a 15-mer synthetic peptide (CPNVIGNRDIFKKVD) corresponding to amino acids 7-21 of the *G. lateralis* mature MIH peptide. MIH peptide selection was made based on the location of a previously developed MIH antibody in *Callinectes sapidus* (Lee and Watson, 2002), the antigenicity of this peptide region (Tang et al., 1999; Trier et al., 2012), uniqueness of this region within the peptide, and the conservation of the peptide sequence across several decapod crustacean species (Figure 4.1). The peptide sequence was nearly 100% conserved among the three species in this paper having only a single amino acid difference at the C-terminus in *C. maenas* and *M. magister*.

To assess the specificity of the antibody, a Western blot (Figure 4.2) was performed with SG extracts from three decapod crustacean species, *C. maenas* (lane a)*, G. lateralis* (lane b), and *M. magister* (lane c). An immunoreactive band at ~7 kDa was detected in all three species and is consistent with previously published results (Lee and Watson, 2002; Watson et al., 2001a). No band was detected in the extract from *G. lateralis* walking leg muscle (lane d).

*Neuroanatomy of CNS tissues*

*ESG*

The ESG (Figure 4.3A) is comprised of three distinct regions, the medulla terminalis (MT), medulla interna (MI), and the medulla externa (ME) (Bliss and Welsh, 1952; Stewart et al., 2013). These regions are stacked on top of one another, the ME is distal to the MI, and the MT is proximal to MI. Arguably the most important cell cluster in the ESG is the X-organ (XO), which is located in the MT. Nerve fibers from the XO terminate in the sinus gland (SG), located at the MI/ME junction. The SG is a neurohemal organ, releasing neuropeptides synthesized in the XO into the circulating hemolymph.

*TG*

The TG (Figure 4.3B) is located ventral to the heart (Sandeman, 1982; Stewart et al., 2013). It is bilaterally symmetrical, having 5 segmental nerves (sn 1-5) on each side which radiate out to and control the movement of the walking legs. Cell clusters located near the hemocoele (Hec) extend laterally along the root of each sn (clusters 10-15). A single abdominal ganglion (abn) located posteriorly innervates the abdomen. Anteriorly, the thoracic ganglion (cell cluster 8) is fused with the subesophagael ganglion (cell cluster 7). The inset shows a pair of giant neurons (GN) (Matsumoto, 1954) in cell cluster 7.

*Brain*

The Br (Figure 4.3C) is divided into three regions: protocerebrum, deutocerebrum, and the tritocerebrum (Krieger et al., 2012). The tritrocerebrum is the most posterior and connects to the TG via the coc (not shown). Nerve clusters 4 and 6 are located within this region and are comprised of giant neurons (GN), small neurons (SN), and globular glial cells (Stewart et al., 2013). Caudo-laterally to the olfactory (OL) and accessory lobes (AL) is the antenna II neuropil (AnN), which is at the anterior most portion of the tritocerebrum (Sandeman, 1982). Posterior to the accessory lobe is neuronal cell cluster 5. Cell cluster 2 is anterior to the olfactory globular tract neuropil (OGTN). Cell cluster 3, posterior to the OL

and anterior to the optic nerve (optn), is distinguishable from the other cell clusters as it was made principally of SN (Stewart et al., 2013). The median antenna I neuropil (MAN) is part of the deutocerebrum located posterior to the protocerebrum. The main components of the protocerebrum are the posterior-medial protocerebral neuropils (PMPN) and the anterior-medial protocerebral neuropils (AMPN) which are separated by a central body (CB). Cell cluster 1 has a diverse cell population comparable to clusters 4 and 6 and is the most posterior structure of the protocerebrum (Stewart et al., 2013).

*Immunofluorescence Microscopy*

The binding properties of the antibody were further evaluated with immunofluorescence microscopy. In all three species, the antibody specifically labeled axon terminals in the SG (Figure 4.4). Expression of MIH was restricted to the SG. Previous studies (Pitts and Mykles, 2015) show that NO is localized to the SG of *C. maenas* and is predicted to be a regulator of neuropeptide release. Given this, sections were also labeled with a universal nitric oxide synthase (NOS; enzyme that produces NO) antibody. In *G. lateralis* and *C. maenas,* NOS immunoreactivity was detected in the SG and in some areas co-localized with MIH (Figures 4.4A and 4.4B). NOS was not detected in the SG of *M. magister* (Figure 4.4C).

Detection of MIH mRNA transcripts in the Br and TG of *C. maenas* (Abuhagr et al., 2014a) prompted immunohistochemical analysis of both tissues with the MIH antibody. In all three species MIH was localized to the TG (Figure 4.5). Localization of MIH in the TG in all three species was found in the cell clusters that extend laterally along sn 1-5. MIH was detected near the GN (arrows) in *G. lateralis* and *C. maenas* (Figures 4.5A and 4.5B) and within the GN in *M. magister* (Figure 4.5C). MIH expression was robust in *M. magister* compared to *G. lateralis* and *C. maenas*. NOS was localized adjacent to MIH in the TG of both *G. lateralis* and *C. maenas* (arrowheads). NOS was strongly expressed in *G. lateralis* and *C. maenas* but is only faintly present in *M. magister.*

MIH was also localized to the Br of all three species (Figure 4.6). MIH was detected in the OL in both *G. lateralis* and *C. maenas* but only a few cells are MIH positive (Figures 4.6A and 4.6B). In *M. magister*, MIH was confined to cell cluster 3, posterior to the OL (Figure 4. 6C). *M. magister* had a larger

population of MIH positive cells in the Br compared to the other two species. NOS was not detected in the Br of any species (Figure 4.6).

*mRNA expression of NOS, MIH, CHH, and EF2 in CNS tissues*

qPCR from intermolt animals was quantified for *Gl-MIH, Gl-CHH, Gl-NOS*, and *Gl-EF2* (Figure 4.7). As expected, expression of both neuropeptides was higher in the ESG compared to the Br and TG (MIH 1.52 x $10^5$-fold greater compared to Br, 7.82 x $10^5$-fold greater compared to TG; CHH 7 x$10^5$-fold greater compared to Br, 8.5 x $10^5$-fold greater compared to TG). Expression of both neuropeptides was also significantly higher in the Br compared to the TG (MIH 5-fold; CHH 12.2-fold). *Gl-NOS* expression was 11.3-fold greater in the ESG compared to the Br and 133-fold greater compared to the TG. *Gl-NOS* was 11.8-fold greater in the Br compared to the TG. *Gl-EF2* was included as a reference and expression was greatest in the ESG (4.8 x $10^2$-fold greater than the Br, 3.3 x$10^3$-fold greater than the TG). Expression was 6.9-fold higher in the Br compared to the TG.

## DISCUSSION

Despite early contributions of the crustacean nervous system to understanding synaptic transmission (Hoyle and Wiersma, 1958a, b; Wiersma, 1961a, 1961b), the molecular characterization of crustacean presynaptic terminals is relatively poor. *Drosophila* antibodies against synaptic proteins, synaptotagmin, synapsin, dynamin, and frequenin recognize homologus proteins in crustaceans (Cooper et al., 1995; Jeromin et al., 1999), suggesting that synaptic vesicle binding and transmitter release in crustaceans is similar to *Drosophila*. One of the goals of this study was to extend upon current knowledge of the molecular make-up of crustacean presynaptic terminals. As neurotransmitter release in the mammalian adrenal gland is negatively regulated by NO (Schwarz et al., 1998) and NO is localized to the SG of *C. maenas* (Pitts and Mykles, 2015), it is hypothesized that NO negatively regulates neuropeptide release from the SG in decapod crustaceans. To test this hypothesis, an antibody against the neuropeptide MIH was developed (Figure 4.1) and ESG from three decapod crustacean species were double labeled with MIH and NOS. To prevent any cross reactivity of the MIH antibody with other members of the CHH-superfamily of proteins, an area of the MIH peptide that is highly conserved among several decapod species (Figure 4.1), but is not homologous to other CHH-superfamily proteins, was selected. This resulted in the detection of a ~7 kDa band in the SG extract of *C. maenas*, *G. lateralis*, and

*M. magister* via western blot (Figure 4.2). The observed mass was less than the estimated mass of the translated mature peptide [Gl ~ 8.5 kDa (Lee et al., 2007); Cm ~ 9.2 kDa (Webster and Dircksen, 1991); Mm ~ 9.23 kDa (Umphrey et al., 1998)]. This discrepancy is accounted for by the negative charge of the MIH mature peptide ($^{-}$1), causing it to migrate through the gel at a faster rate. MIH in the SG of these species is in agreement with findings in other crab and shrimp species (Bliss et al., 1954; Dircksen and Soyez, 1998; Gu et al., 2001; Gu et al., 2002; Lee and Watson, 2002; Skinner, 1985; Watson et al., 2001a; Watson et al., 2001b).

In the SG of *C. maenas*, NO is produced by the enzyme NOS and sequestered by an unidentified NO binding protein proposed to modulate neuropeptide secretion over a prolonged period (Pitts and Mykles, 2015). NO is a gaseous neurotransmitter with a half-life of seconds and therefore can only diffuse a short distance before degradation (Moncada et al., 1991). If NO regulates the release of neuropeptides from the SG it must be synthesized in the SG to directly inhibit synaptic vesicle release at presynaptic terminals, or be bound by an endogenous storage protein. NOS and MIH were closely associated in the SG of *G. lateralis* and *C. maenas* (Figures 4.4A and 4.4B), supporting the hypothesis that NO regulates neuropeptide secretion from the SG in these species. NOS staining in the SG of *M. magister* is minimal (Figure 4.4C). However, since this is the case in all three *M. magister* tissues, it is likely that the NOS antibody does not strongly recognize NOS in this species. The NOS sequence in *M. magister* has yet to be determined. Therefore, it is uncertain whether the uNOS peptide sequence is conserved in this species. Further studies quantifying MIH release from the SG in the presence of NOS antagonists, NO donors, and NO scavengers will provide stronger evidence to establish the exact relationship between NO and neurosecretion of peptides from the SG.

MIH in the TG of all three species in this study further demonstrates the wide distribution of MIH in the CNS and suggests that MIH function extends beyond molt regulation. MIH is found in cell clusters between all five segmental nerves in the TG (Figure 4.5). MIH is also present in cells cluster 7, 8, and 9 (data not shown). In all three species MIH is localized to GN cells, which is in agreement with previous findings (Stewart et al., 2013). In both *G. lateralis* and *C. maenas*, MIH is restricted to the periphery of GN cells (Figures 4.5A and 4.5B). Similar to the SG, MIH and NOS are closely localized, suggesting that the mechanism regulating neuropeptide release in these species is conserved throughout the CNS. MIH

in *M. magister* is also localized to GN cells but is not confined to periphery, which is in accordance with findings in other species (Stewart et al., 2013). Limited NOS immunoreactivity is detected in the TG of *M. magister,* suggesting that neurosecretion in the CNS of this species is not regulated by NO, or that the uNOS antibody does not bind NOS in *M. magister.*

MIH is localized to the Br in all three species (Figure 4.6). In *G. lateralis* and *C. maenas,* MIH is detected in the OL (Figures 4.6A and 4.6B). Only a few MIH cells are present and are not found in any other regions of the Br. Significantly more cells are MIH positive in the Br of *M. magister*. However these cells are localized to cell cluster 3, posterior to the OL (Figure 4.6C). MIH production in and near the OL was an unexpected result. Previous studies reporting MIH localization in the Br report MIH positive cells in the optn, MaN, and the AnN (Stewart et al., 2013). It is hypothesized that adjacent nerve fibers and connective tissue surrounding these structures act as carriers of MIH from the CNS to the esophageal ganglion (Stewart et al., 2013). Given the proximity of the OL to the optn, it is possible that MIH is transported from the OL to nerve fibers in the optn that project up to the ESG. NOS immunoreactivity is not detected in the Br of any species. This is surprising given that nitric oxide is widely expressed in the Br of *Homarus americanus* (Benton et al., 2007) and mRNA expression of NOS is detected in the Br of *G. lateralis* (Figure 4.7). These results introduce the possibility that as in mammalian species, another isoform of NOS may be expressed in the crustacean Br. Previous work in this species reported expression of a truncated NOS isoform is present in the YO (Kim et al., 2004). Additionally, in *Drosophila* multiple NOS isoforms are expressed during development as a result of alternative mRNA splicing (Regulski and Tully, 1995; Stasiv et al., 2001). The uNOS antibody sequence is fully or partially conserved in most of these *Drosophila* isoforms. Between eighteen and twenty two alternative NOS transcripts are expressed in the mosquito *Anopheles stephensi* (Luckhart and Li, 2001). This data suggests that the NOS isoform in the Br of decapod crustaceans is alternatively spliced and not recognized by the uNOS antibody.

mRNA expression of the neuropeptides MIH and CHH in all three CNS tissues and supports the hypothesis that peptide production is not confined the ESG (Figure 4.7). CHH has numerous functions in decapod crustaceans, including carbohydrate metabolism, molting, reproduction, and osmoregulatory functions (Fanjul-Möles, 2006). The prevailing understanding of MIH function is that it acts to inhibit

synthesis of molting hormones (ecdysteroids) by the YO's (Chang and Bruce, 1980; Keller and Schmidt, 1979; Soumoff and O' Connor, 1982). Studies in the blue crab *Callinectes sapidus* identify MIH binding sites on the hepatopancreas that when bound induce vitellogenesis (Zmora et al., 2009). More recently, Techa et al. (2015) found that MIH expression in *C. sapidus* fluctuates during embryogenesis, suggesting that MIH may play an important role in development. Based data from *C. sapidus* and the expression of MIH throughout the CNS in *G. lateralis*, *C. maenas*, and *M. magister*, it seems likely that like CHH, MIH is a multifunctional protein and the current hypothesis regarding MIH function needs to be reevaluated.

In summary, a 15-mer anti-MIH antibody was developed against the mature peptide sequence from *G. lateralis*. The antibody recognizes MIH in the ESG, Br, and TG from three decapod crustacean species. Localization of MIH and NOS in the SG in close proximity supports the hypothesis that NO is a negative regulator of neuropeptide release. Further studies examining how NOS inhibitors, NO donors and NO scavengers affect neuropeptide release from the SG will reveal if NO inhibits synaptic vesicle binding in crustaceans in a manner similar to the mammalian mechanism. Alternative sources of MIH in the Br and TG provide an explanation for how animals who have undergone molt induction by ESA do not enter premolt. MIH expression throughout the CNS also indicates that this neuropeptide may serve more physiological functions than molt inhibition and that this long-standing hypothesis needs reconsideration.

## MATERIALS AND METHODS

*Antibody production*

The 15-mer peptide was commercially synthesized by Pacific Immunology Corp. (Ramona, CA USA) and was coupled to the carrier protein, keyhole limpet hemocyanin (KLH), through the cysteine residue at the N-terminus of the peptide using gluteraldehyde as a cross linking reagent. The immunization of two New Zealand White rabbits was performed at Pacific Immunology Crop. Five ml of pre-immune serum was collected from each rabbit prior to immunization. The rabbits were initially immunized with the MIH peptide conjugated to KLH in Freund's complete adjuvant and were boosted with antigen in Freud's incomplete adjuvant in weeks 3, 6, and 10. The antiserum was collected in two week intervals from week 7 to week 13 after the first immunization. The final exsanguination bleed was collected at week 14. Anti-*G. lateralis* MIH antisera were used for immunodetection in both Western and Immunohistochemistry applications.

*Western blot analysis*

Sinus glands from *G. lateralis*, *C. maenas,* and *M. magister* were homogenized in 20 mM Tris-HCl buffer (pH 7.4) containing 1 mM EDTA, 20 mM KCl, and 10% protease inhibitor cocktail (Sigma Aldrich, St. Louis, MO USA). The extracts were centrifuged at 30,000 g for 15 min. Protein concentration for each sample was determined using a Bradford assay. Twenty µg of sinus gland protein from each species and 20 µg of *G. lateralis* walking leg muscle (control) were combined with NuPAGE LDS sample buffer (2.5 µL), NuPAGE reducing reagent (1 µL), and dd$H_2O$ (10 µL reaction volume) and heated at 70℃ for 10 min. Denatured protein samples and See Blue Plus 2 prestained protein standards (ThermoFisher Scientific, Waltman, MA USA) were separated (200 V, 35 min) on a 12% NuPAGE Bis-Tris SDS precast polyacrylamide gel (ThermoFisher Scientific) using a 2-(N-morpholino) ethane sulfonic acid (MES) buffer system. Proteins were transferred to 0.2 µm PVDF membrane (30 V, 1 h) and membranes subsequently incubated in 2% goat serum (Vector Laboratories, Inc., Burlingame, CA USA) for 45 min at room temperature (RT). Membranes were washed in 0.05 mM Tris-buffered saline plus 0.05% tween-20 (TBST) then incubated in the primary antibody (anti-*G. lateralis* MIH, 1:100) overnight at 4℃ . Following this overnight incubation, membranes were washed in TBST and incubated in the secondary antibody (biotinylated goat anti-rabbit; Vector Laboratories) for 1 h at RT. This was followed by washes in 0.05 mM Tris-buffered saline (TBS) and incubation in the ABC reagent (prepared according to kit instructions; Vector Laboratories) for 30 min at RT. Membranes were developed with Amersham ECL Western blotting detection reagents (GE Healthcare UK Limited, Little Chalfont, Buckinghamshire UK). Bands were visualized with chemiluminescence using a ChemiDoc XRS+ Molecular Imager (Bio-Rad Laboratories, Hercules, CA USA).

*Immunofluorescence microscopy*

ESG, TG, and Br from three decapod species (*G. lateralis*, *C. maenas*, and *M. magister*) were fixed in 4% paraformaldehyde for ~24 h at RT, dehydrated in an ethanol and xylene series and embedded in paraffin. *C. maenas* and *M. magister* were collected from Bodega Harbor in Bodega Bay, California; *G. lateralis* were shipped from the Dominican Republic. Sections (12 µm) were affixed to OptiPlus™ Positive-Charged Microscope Barrier Slides (BioGenex, Fremont, CA USA) by heating overnight at 45 ℃, deparaffinized in xylenes, and rehydrated in an ethanol series. Slides were placed in pre-boiled 0.01 M

sodium citrate (pH 6) buffer, heated in a pressure cooker for 3 min, and blocked in 2% goat serum at 4 ℃ for 1 h. Sections were incubated overnight at 4 ℃ in the first primary antib ody (anti-*G. lateralis* MIH at 1:100), washed in TBST then incubated 1 hr at RT in the first secondary antibody, [1:100 Alexa Fluor488 (496 nm excitation, 519 nm emission conjugated to the $F(ab')_2$ fragment; ThermoFisher Scientific)]. This was followed by overnight incubation at 4 ℃ in the second primary [1:50 anti-universal NOS (ThermoFisher Scientific)], washed in TBST, and incubated 1 hr at RT in the second secondary antibody [1:5000 Alexa Fluor555 (555 nm excitation, 565 nm emission; ThermoFisher Scientific)] (Lewis Carl et al., 1993). Slides were mounted with Vectasheild 4'6'-diamindino-2-phenylindole DAPI mounting medium (360 nm excitation, 460 nm emission; Vector Laboratories) and sealed with nail polish. Every third section was stained with hematoxylin/eosin (H&E) to image tissue structure.

H&E images at 5x and 40x were collected with a Leica CTR 5500 microscope equipped with a Leica DFC 450 camera. Low (10x) and high (40x) fluorescent images were taken with a Zeiss Axiovert 200M microscope equipped with a Hammatsu ORCA-ER cooled charge-coupled device camera (Olympus America, Inc. Melville, NY, USA) at 350 nm excitation, 460 nm emission for DAPI (500 ms); 570 nm excitation, 590 nm emission for Rhodamine Red (Alexa555, 1500 ms); and 494 nm excitation, 518 nm emission for FITC (Alexa488, 500 ms).

*Quantitative PCR*

ESG, Br, and TG were dissected from intermolt *G. lateralis* and stored in RNA later (ThermoFisher Scientific) at -20℃ until RNA isolation. RNA was isolated from homogenized tissue using TRIzol reagent (Life Technologies, Carlsbad, CA USA) according to the manufacture's protocol (see Pitts and Mykles 2015 for detailed protocol). cDNA was synthesized with Transcriptor Reverse Transcriptase (Roche, Indianapolis, IN USA) and an oligo-dT primer (50 µmol).

A Light Cycler 480 thermal cycler (Roche) was used to quantify levels of *Gl-EF2* (AY552550.1), *Gl-NOS* (AY552549.1), *Gl-MIH* (DQ473354.1), *and Gl-CHH* (DQ492296.2) mRNAs. *Gl-EF2* and *Gl-CHH* were quantified using SYBR green. 10 µL reactions consisted of 5 µL 2x SYBR Green I Master mix (Roche), 0.5 µL each of 10 mM forward and reverse primers [EF2 (Abuhagr et al., 2014b); CHH (Lee et al., 2007)], 3 µL nuclease-free water, and 1 µL cDNA or standard. *NOS* and *MIH* were quantified using universal Probe #17 and #13, respectively (Roche). 10 µL reactions for *NOS* and *MIH* were set up with 5

µL LightCycler 480 Probes Master (Roche Applied Sciences, Indianapolis, IN, USA), 0.2 µL each of 20 mM forward and reverse primers (Table 1), 0.2 µL universal Probe #17 or #13, 1.9 µL nuclease free water, and 2.5 µL cDNA. PCR conditions were as follows: initial denaturation at 95℃ for 5 min, 50 c ycles of denaturation at 95℃ for 10 s, annealing at 57 ℃ for 30 s and extension at 72℃ for 1 min. For each gene, a series of dsDNA standards were produced by serial dilutions and transcript concentrations calculated with the LightCycler 480 software (Roche, version 1.5). Absolute amount of transcript copy numbers per µg of total RNA in the cDNA synthesis reaction were calculated based on the standard curve and the molecular weight of the dsDNA products.

**Table 4.1 qPCR Primer Sequences for Gl-NOS and Gl-MIH**

| Primer | Sequence (5' – 3') | Product size (bp) |
|---|---|---|
| Gl-NOS F1 | CATCACCCACCCTGAGTACA | 60 |
| Gl-NOS R1 | GGGAGGCCATACCATTGAA | |
| Gl-MIH F1 | AACATTGACTTCCTGTGGTGTG | 71 |
| Gl-MIH R1 | ACGAGCTCACACCGATACGT | |

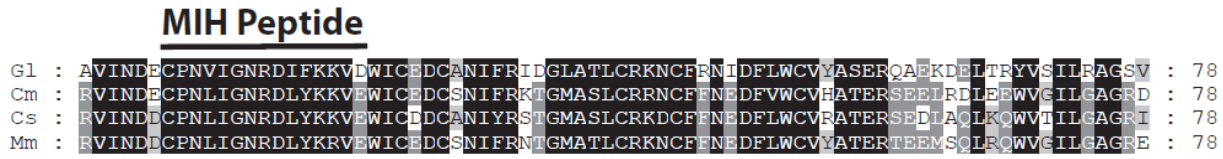


**Figure 4.1 Sequence of anti-*Gl-MIH* antibody.** Mature MIH peptide sequence alignment from four decapod crustacean species; Gl *Gecarcinus lateralis* (DQ473354.1), Cm *Carcinus maenas* (X75995.1), Cs *Callinectes sapidus* (U19764.1), and Mm *Metacarcinus magister* (AF031493.1). The location of the MIH peptide sequence used to make the anti-MIH antibody is indicated.

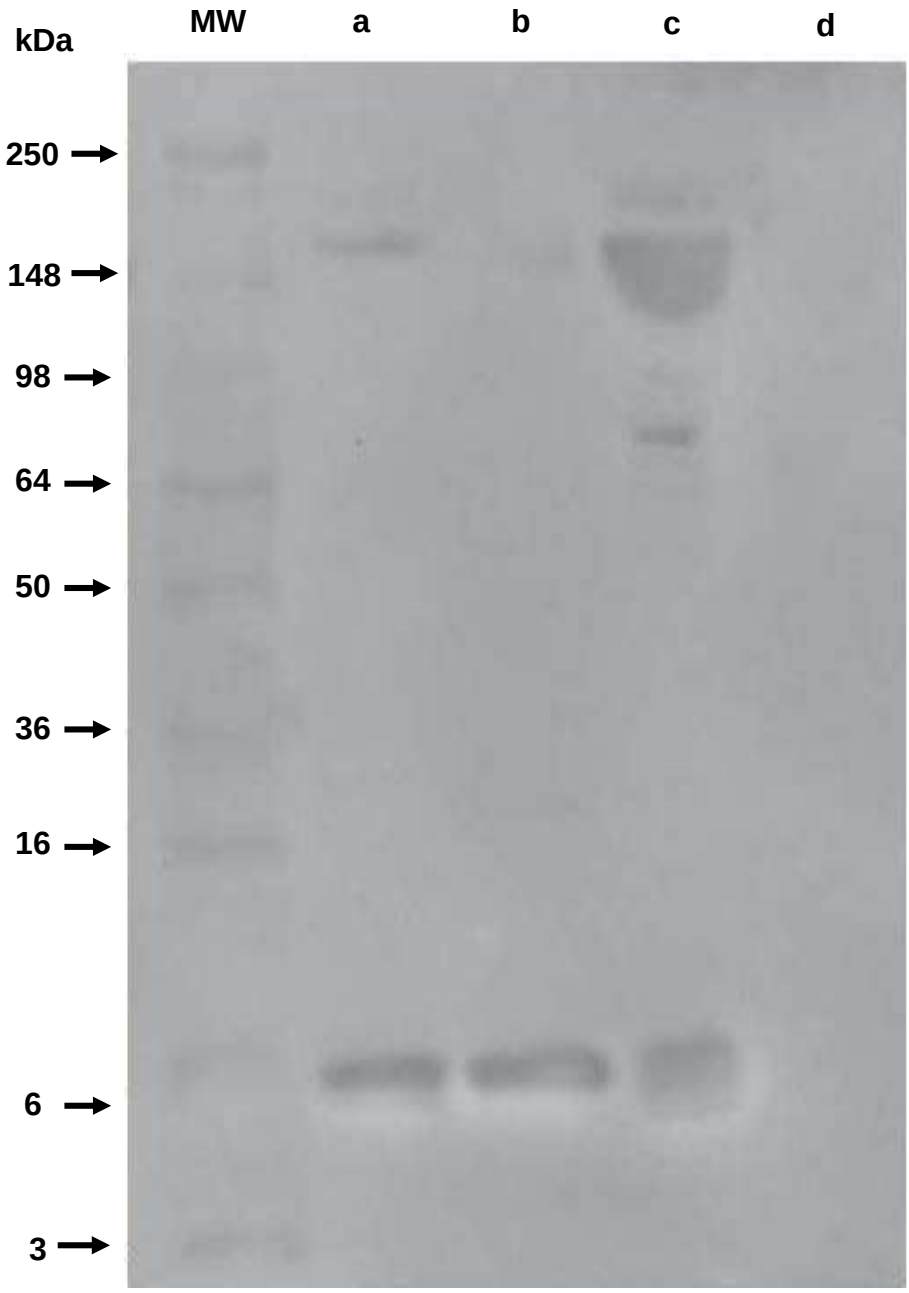


**Figure 4.2 Western blot analysis comparing the binding properties of the MIH antibody in the SG of three decapod crustacean species.** SG extract from *Cm* (lane a), *Gl* (lane b), and *Mm* (lane c) were separated on a NuPAGE gel and blotted to PVDF. An MIH positive band at ~7 kDa was detected in all three species. Walking leg muscle from *Gl* was used as a control (lane d) and no immunoreactive band is present. Approximate molecular weights based on a See Blue Plus 2 ladder are indicated on the left.


**Figure 4.3A H&E staining and neuroanatomy of *C.maenas* ESG**. Longitudinal 5x section of the ESG stained with H&E. The X-organ (XO) is located on the periphery of the medulla terminalis (MT) and sends axonal projections dorsally to the sinus gland (SG). The medulla externa (ME) is distal to the medulla interna (MI) and MT. The SG is located laterally to the ME/MI junction.

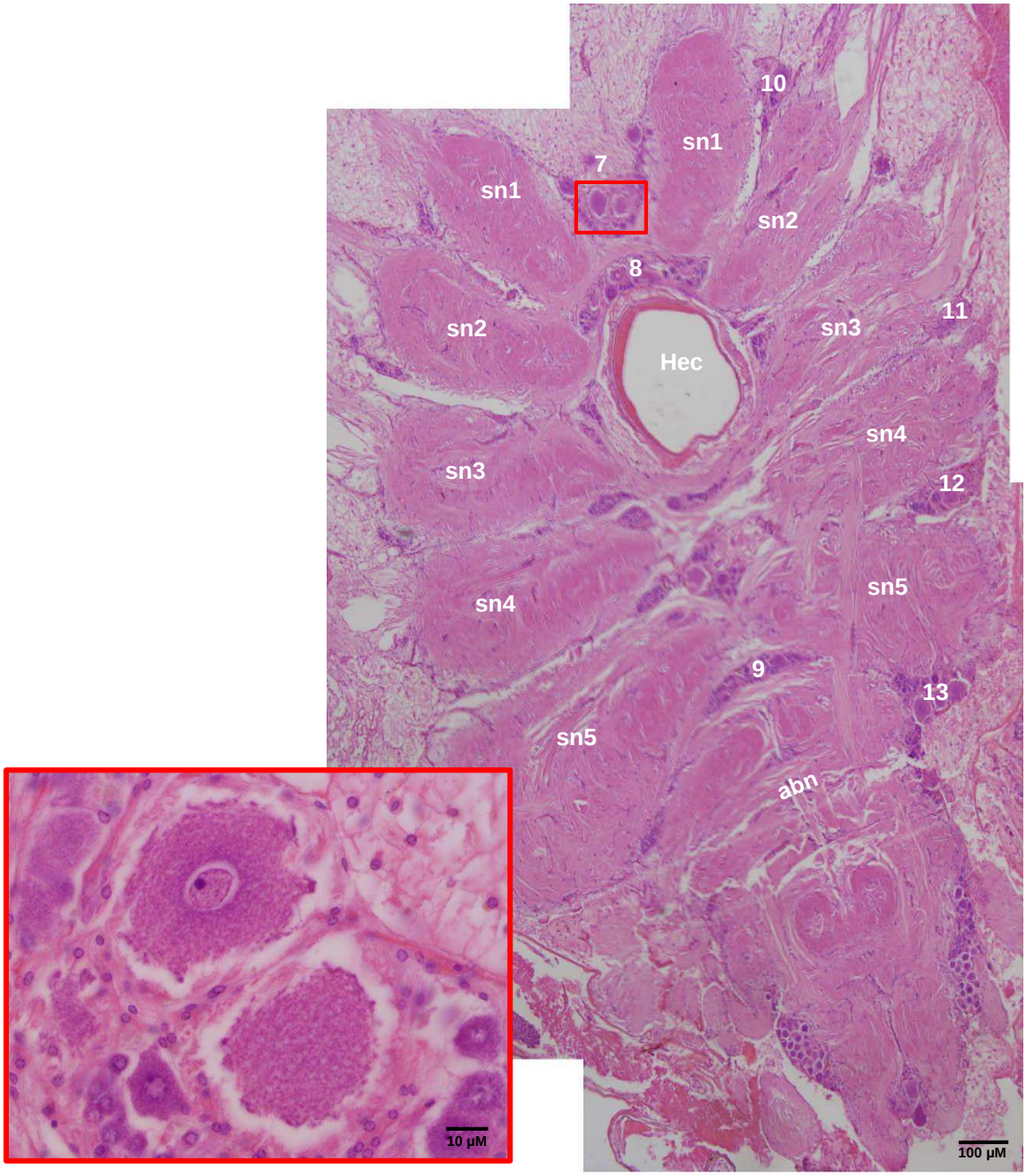


**Figure 4.3B H&E staining and neuroanatomy of *C.maenas* TG**. 5x horizontal section of the TG stained with H&E. Five paired segmental nerves (sn 1-5) that project to the thoracic appendages create a bilaterally symmetrical TG. A single abdominal nerve (abn) is located posterior to the hemocoele (Hec). Among the thoracic and abdominal nerves are numerous neuronal cell clusters (7-13). Inset shows giant neurons (GN) in cell cluster 7 at 40x.

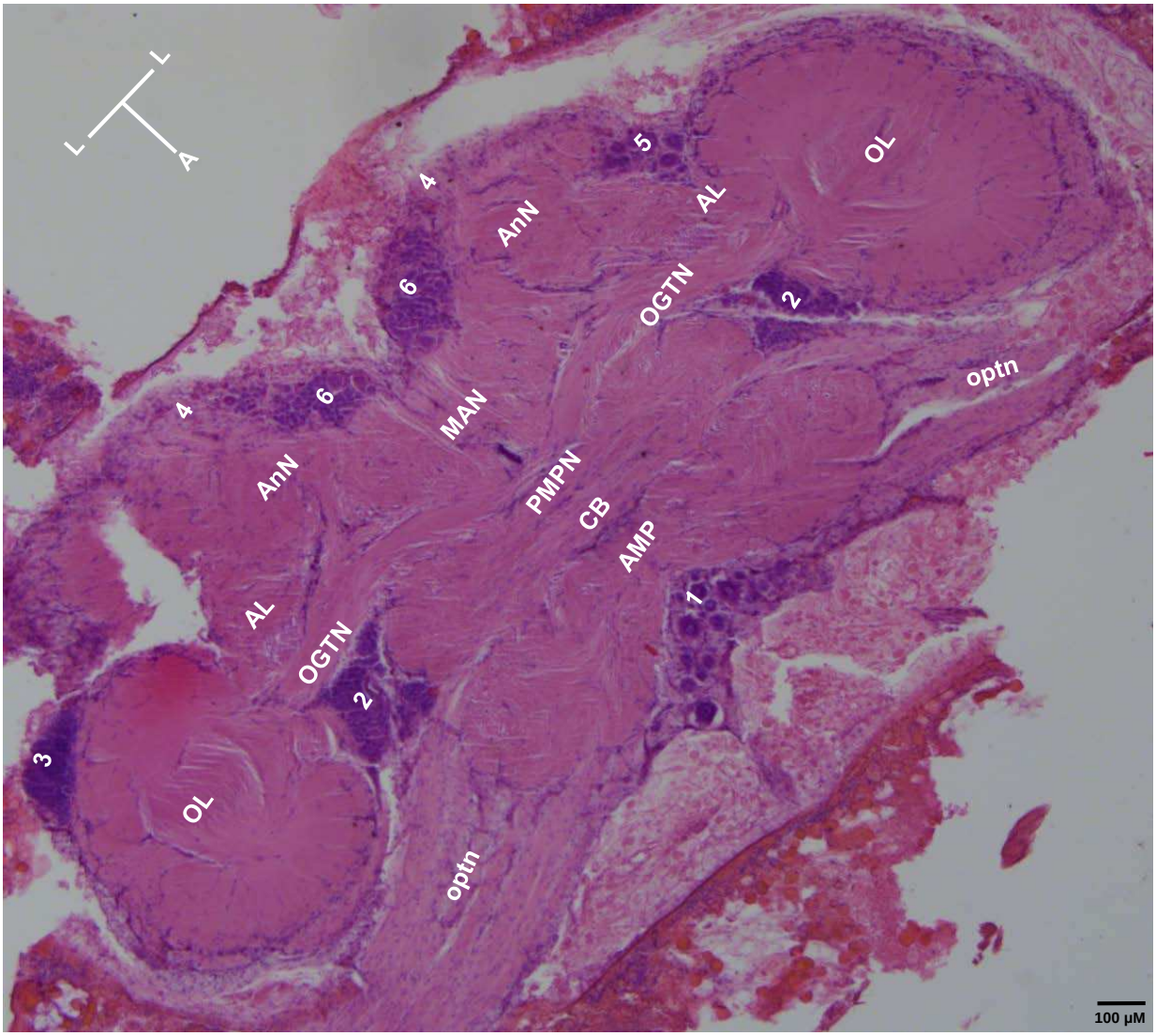


**Figure 4.3C H&E staining and neuroanatomy of *C.maenas* Br**. 5x horizontal H&E of the Br. Neuronal cluster 1 (anterior medial cells) lies anterior to the large pair of anterior-medial protocerebral neuropils (AMPN) and posterior-medial protocerebral neuropils (PMPN) which are separated by a central body (CB). Neuronal cell clusters 4 (ventral lateral cells) and 6 (posterior medial cells) are located lateral to the median antenna neuropil (MAN) which lies posterior to the PMPN. The olfactory lobe (OL) is lateral to structures of the protocerebrum. Neuronal cluster 3 (olfactory lobe cells) is located posterior to the OL. The optic nerve (optn) runs anterior to the OL; neuronal cluster 2 (dorsal lateral cells) lies between the optn and the OL. Neuronal cluster 5 (posterior lateral cells) is posterior to the accessary lobe (AL) and the antenna II neuropils (AnN) is posterior to the olfactory globular tract neuropil (OGTN).

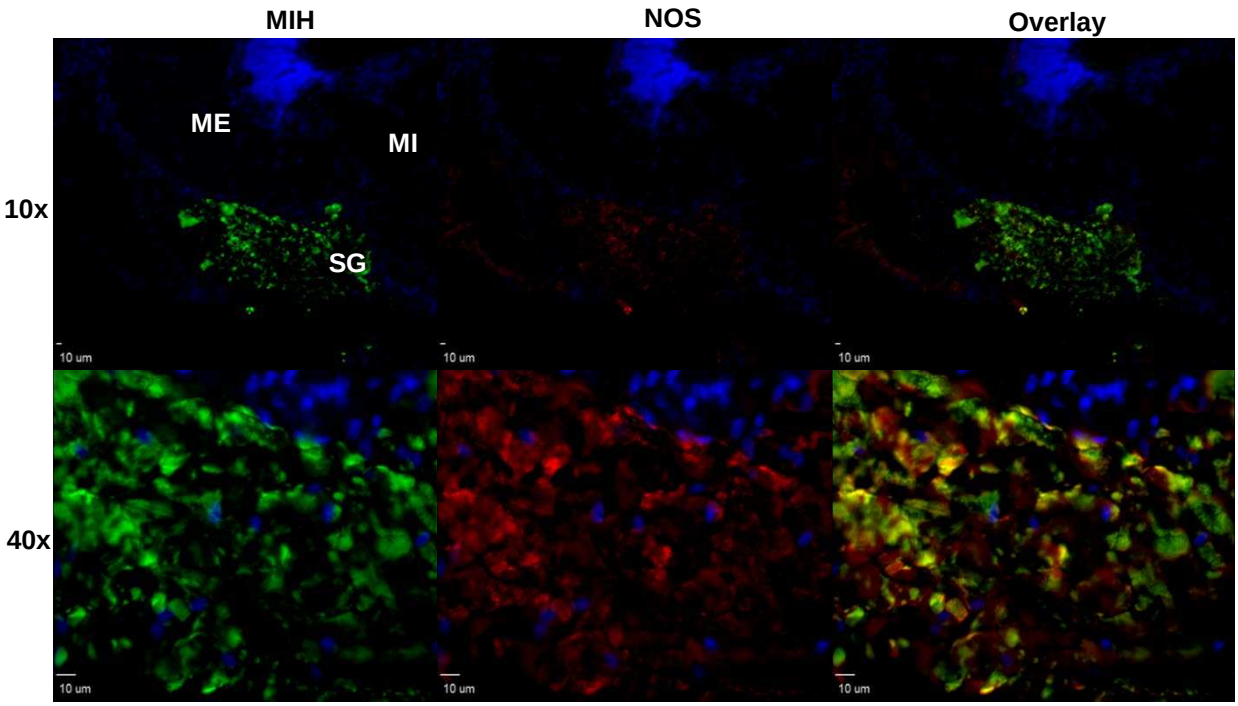


**Figure 4.4A Double immunofluorescence of MIH and NOS in the ESG of *G. lateralis.*** MIH localization is green, NOS is red. Immunofluorescence at low (10x) and high (40x) magnification shows that both MIH and NOS localization within the ESG is specific to the SG in *G. lateralis*. The overlay of NOS and MIH fluorescence staining shows the close proximity of the two proteins. Structure labels are the same as in Figure 3A.

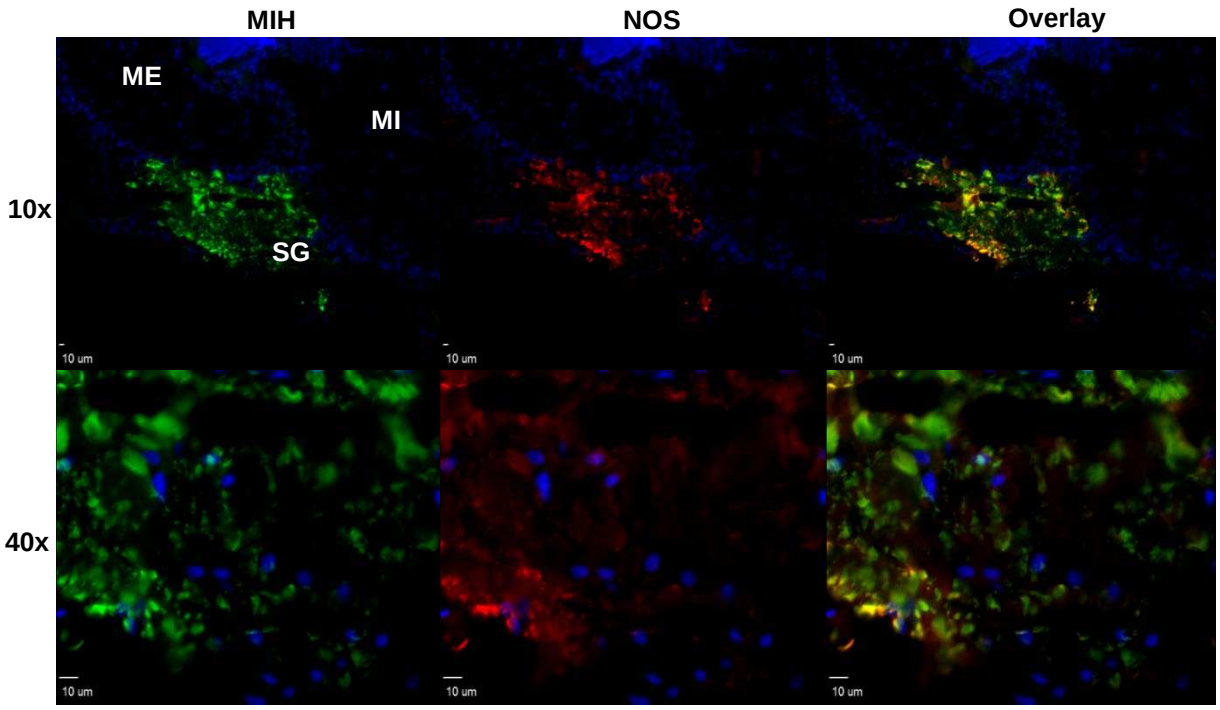


**Figure 4.4B Double immunofluorescence of MIH and NOS in the ESG of *C. maenas*.** MIH localization is green, NOS is red. Immunofluorescence at low (10x) and high (40x) magnification shows that both MIH and NOS localization within the ESG is specific to the SG in *C. maenas.* Structure labels are the same as in Figure 3A.

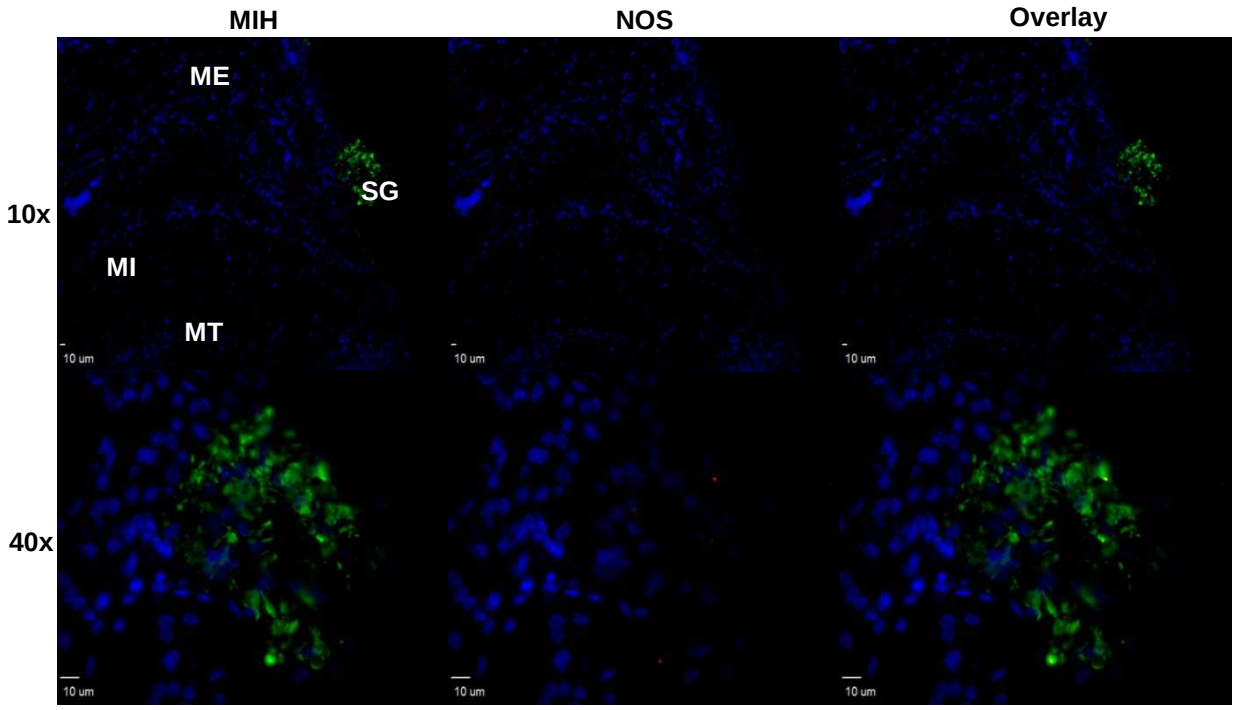


**Figure 4.4C Double immunofluorescence of MIH and NOS in the ESG *M. magister*.** MIH localization is green, NOS is red. MIH is localized to the SG of *M. magister*. However, no NOS staining is visible at low (10x) or high (40x) magnification. Structure labels are the same as in Figure 3A.

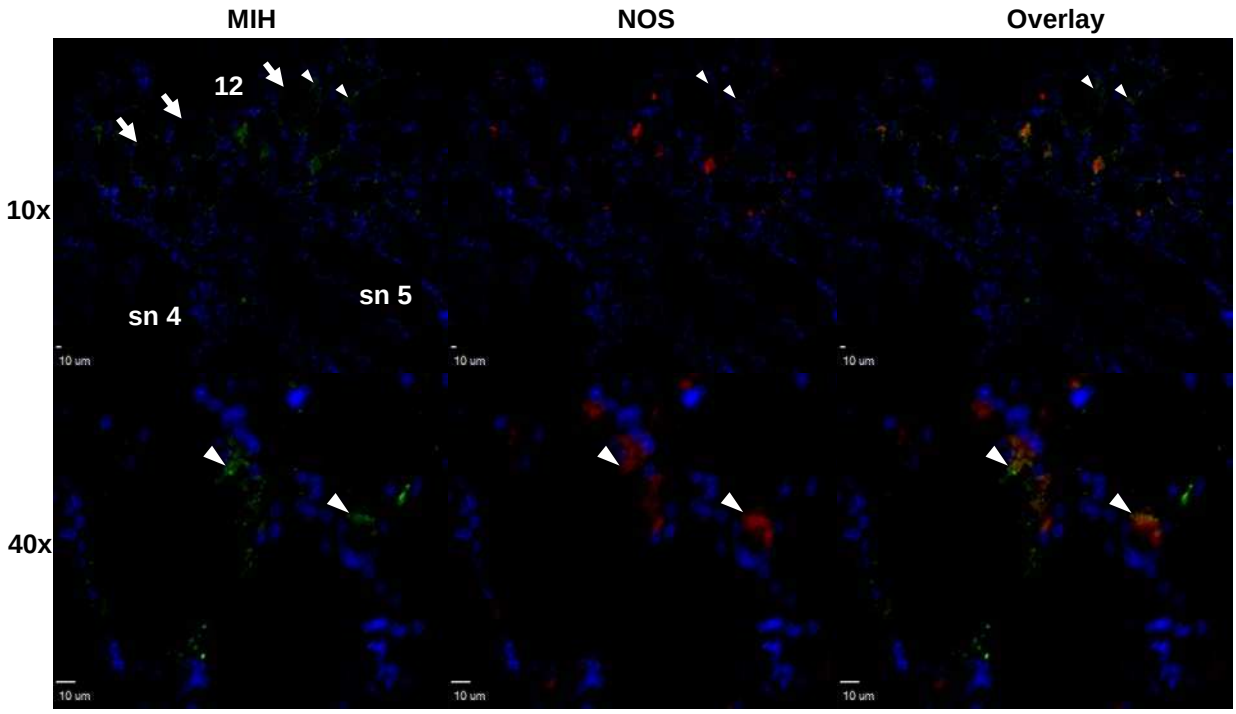


**Figure 4.5A Double immunofluorescence of MIH and NOS in the TG of *G. lateralis*.** MIH localization is green, NOS is red. Immunofluorescence in the TG of *G. lateralis* at low (10x) and high (40x) magnification shows MIH and NOS staining at the periphery of giant neurosecretory cells (GN; arrows) and between segmental nerves (sn) 4 and 5. As in the ESG, the overlay shows NOS and MIH in close proximity (arrowheads). Structure labels are the same as in Figure 3B.

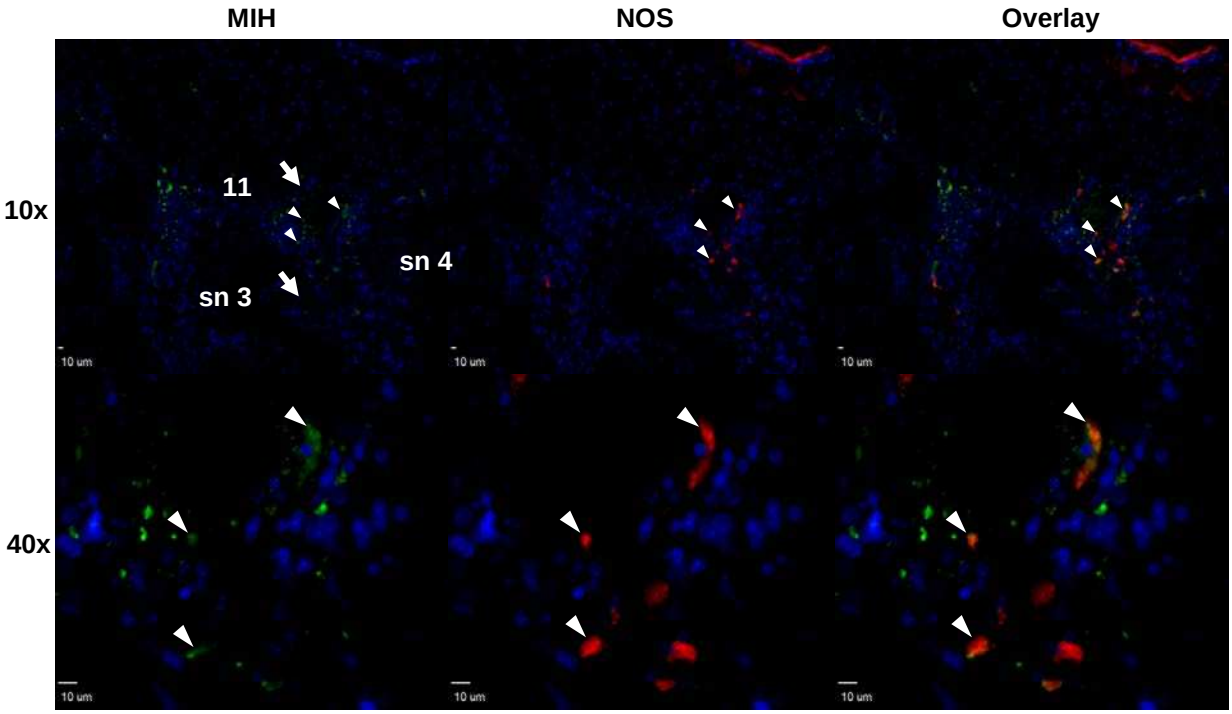


**Figure 4.5B Double immunofluorescence of MIH and NOS in the TG of *C. maenas*.** MIH localization is green, NOS is red. Immunofluorescence in the TG of *G. lateralis* at low (10x) and high (40x) magnification shows MIH and NOS staining at the periphery of giant neurosecretory cells (GN; arrows) and between segmental nerves (sn) 4 and 5. As in the ESG, the overlay shows NOS and MIH in close proximity (arrowheads). Structure labels are the same as in Figure 3B.

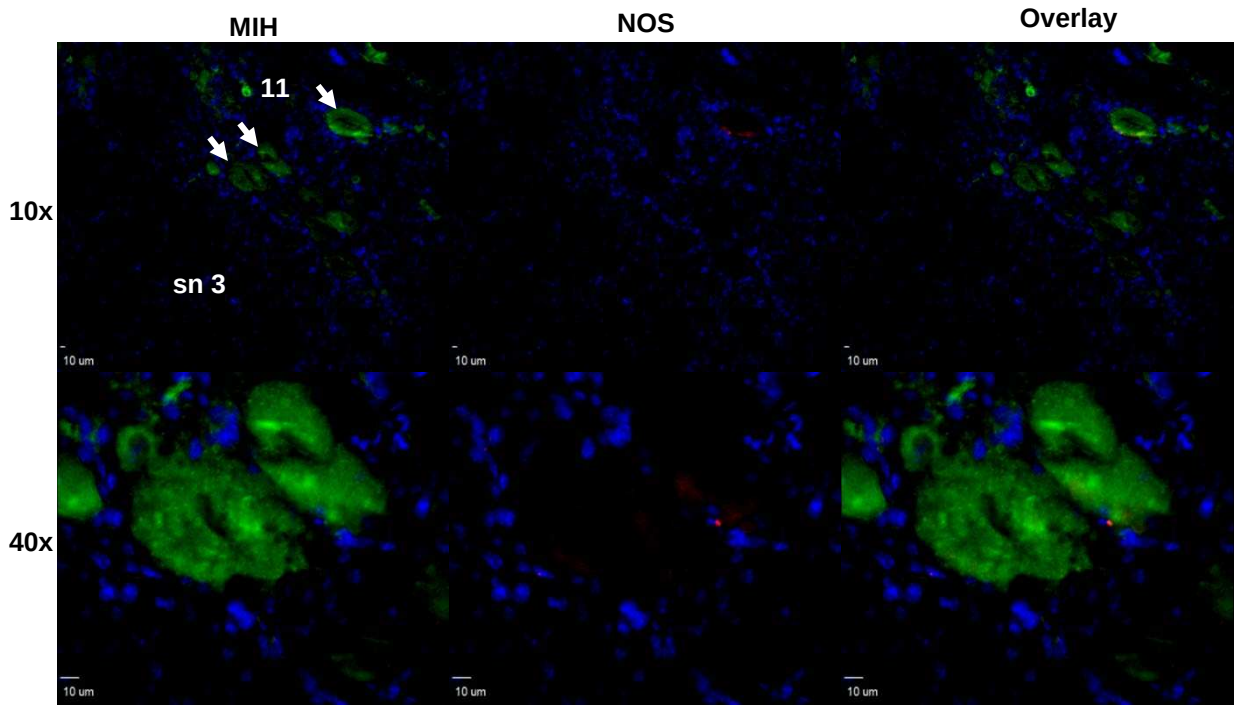


**Figure 4.5C Double immunofluorescence of MIH and NOS in the TG of *M. magister*.** MIH localization is green, NOS is red. Immunofluorescence in the TG of *M. magister* at low (10x) and high (40x) magnification shows MIH localized to the entire region of GN cells (arrows) in a neuronal cluster between two segmental nerves. NOS is minimally localized to the periphery of GN cells. Structure labels are the same as in Figure 3B.

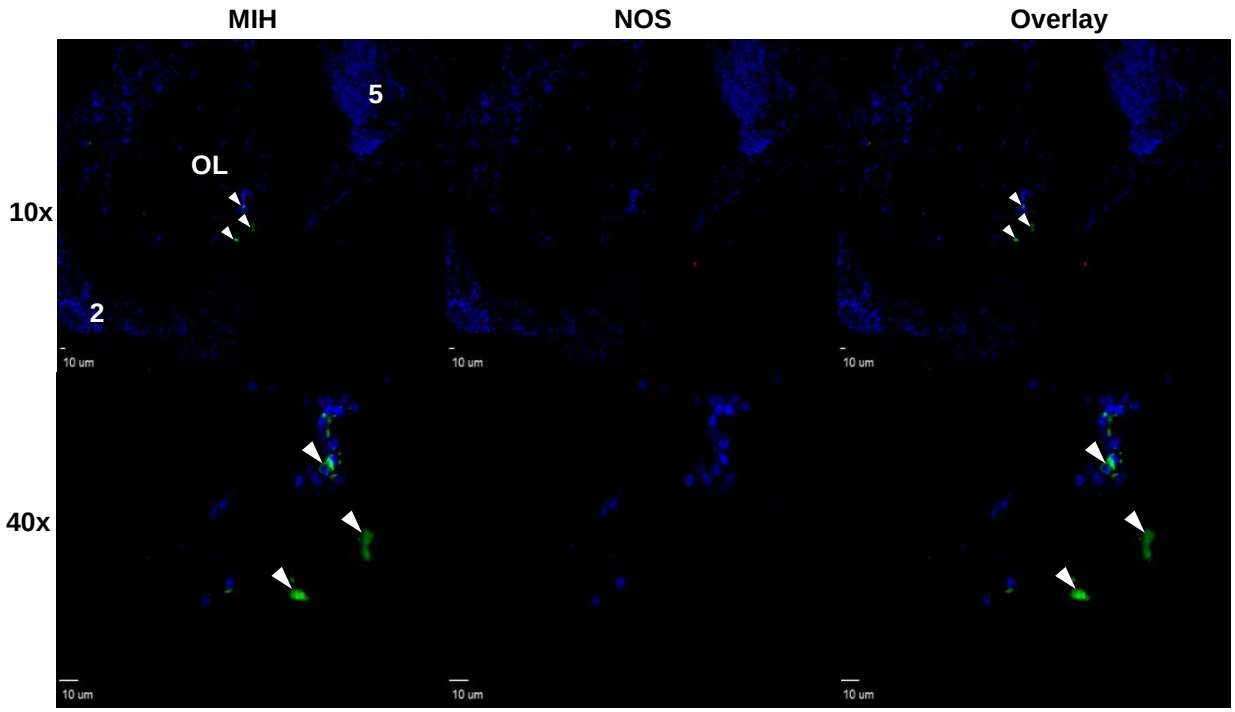


**Figure 4.6A Double immunofluorescence of MIH and NOS in the Br of *G. lateralis*.** MIH localization is green, NOS is red. Immunofluorescence of MIH and NOS at low (10x) and high (40x) magnification in the Br of *G. lateralis*. MIH is localized to a few cells in the OL (arrowheads). No NOS fluorescence is detectable. Structure labels are the same as in Figure 3C.

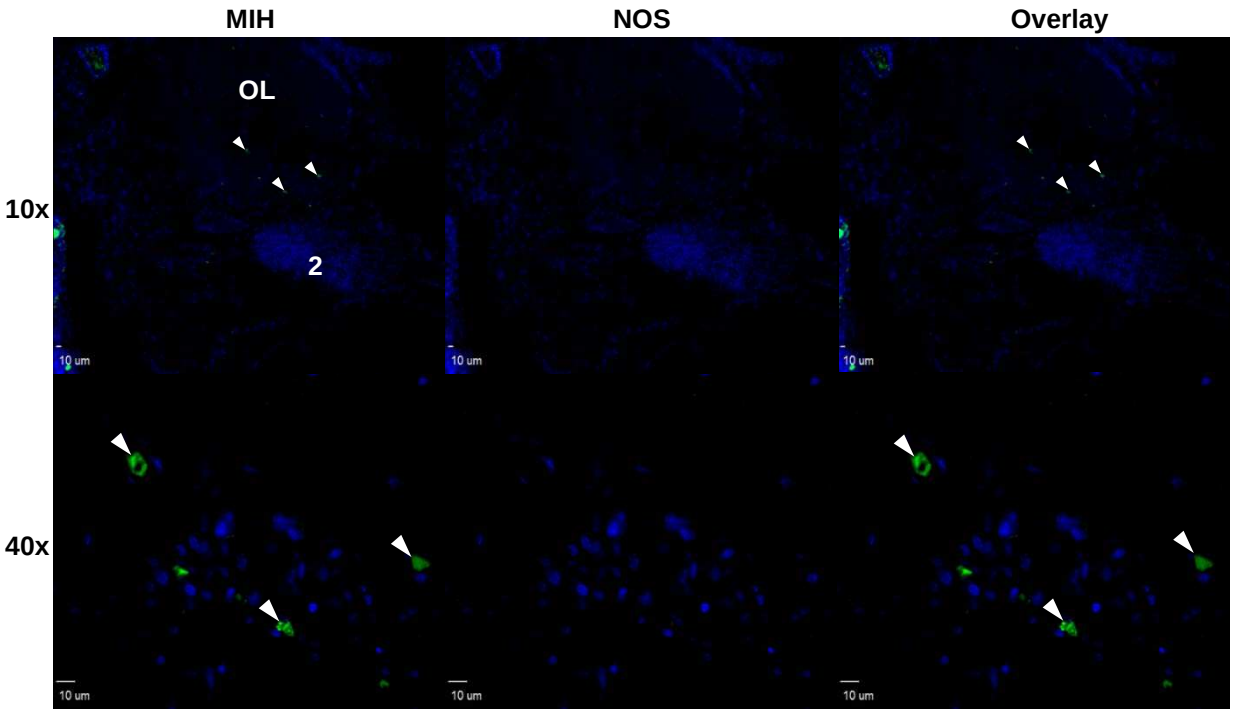


**Figure 4.6B Double immunofluorescence of MIH and NOS in the Br of *C. maenas*.** MIH localization is green, NOS is red. Immunofluorescence of MIH and NOS at low (10x) and high (40x) magnification in the Br of *C. maenas*. MIH is localized to a few cells in the OL (arrowheads). No NOS fluorescence is detectable. Structure labels are the same as in Figure 3C.

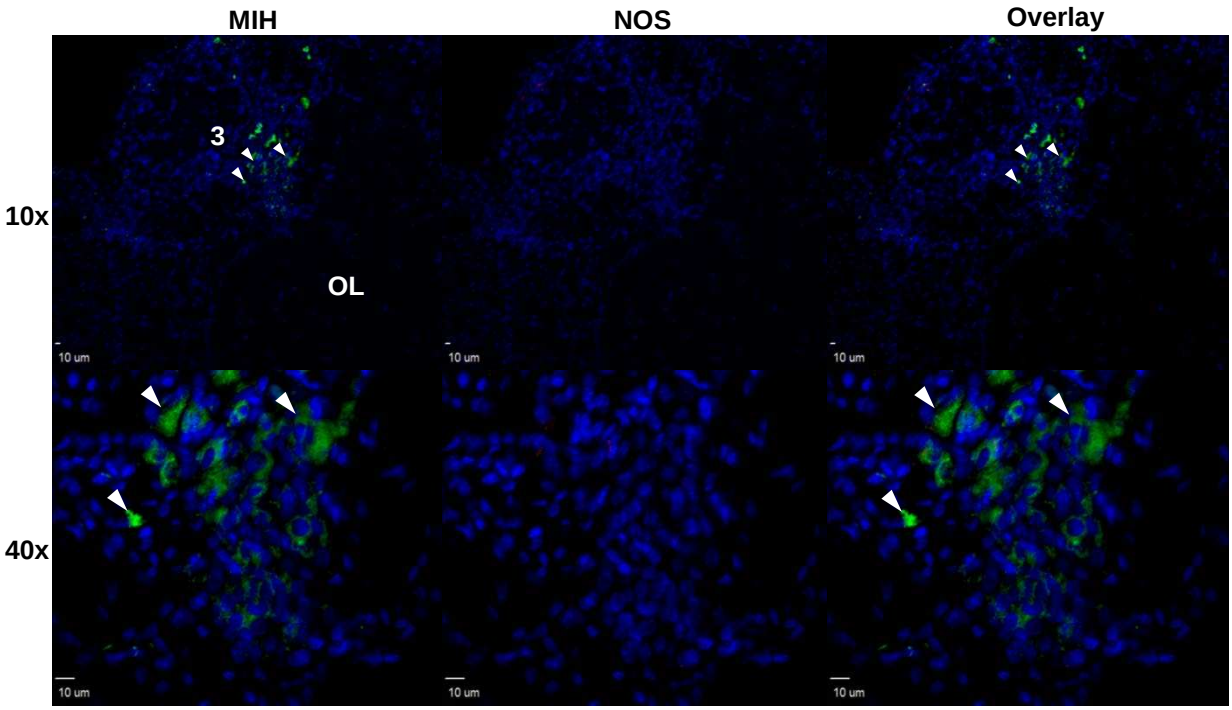


**Figure 4.6C Double immunofluorescence of MIH and NOS in the Br of *M. magister*.** MIH localization is green, NOS is red. There are more MIH immuno-positive cells in the brain of *M. magister* compared to *G. lateralis* and *C. maenas*. Unlike the other species, MIH positive cells are located posterior to the OL in neuronal cell cluster 3 (arrowheads). Similar to *G. lateralis* and *C. maenas* no NOS staining is detectable. Structure labels are the same as in Figure 3**C**.

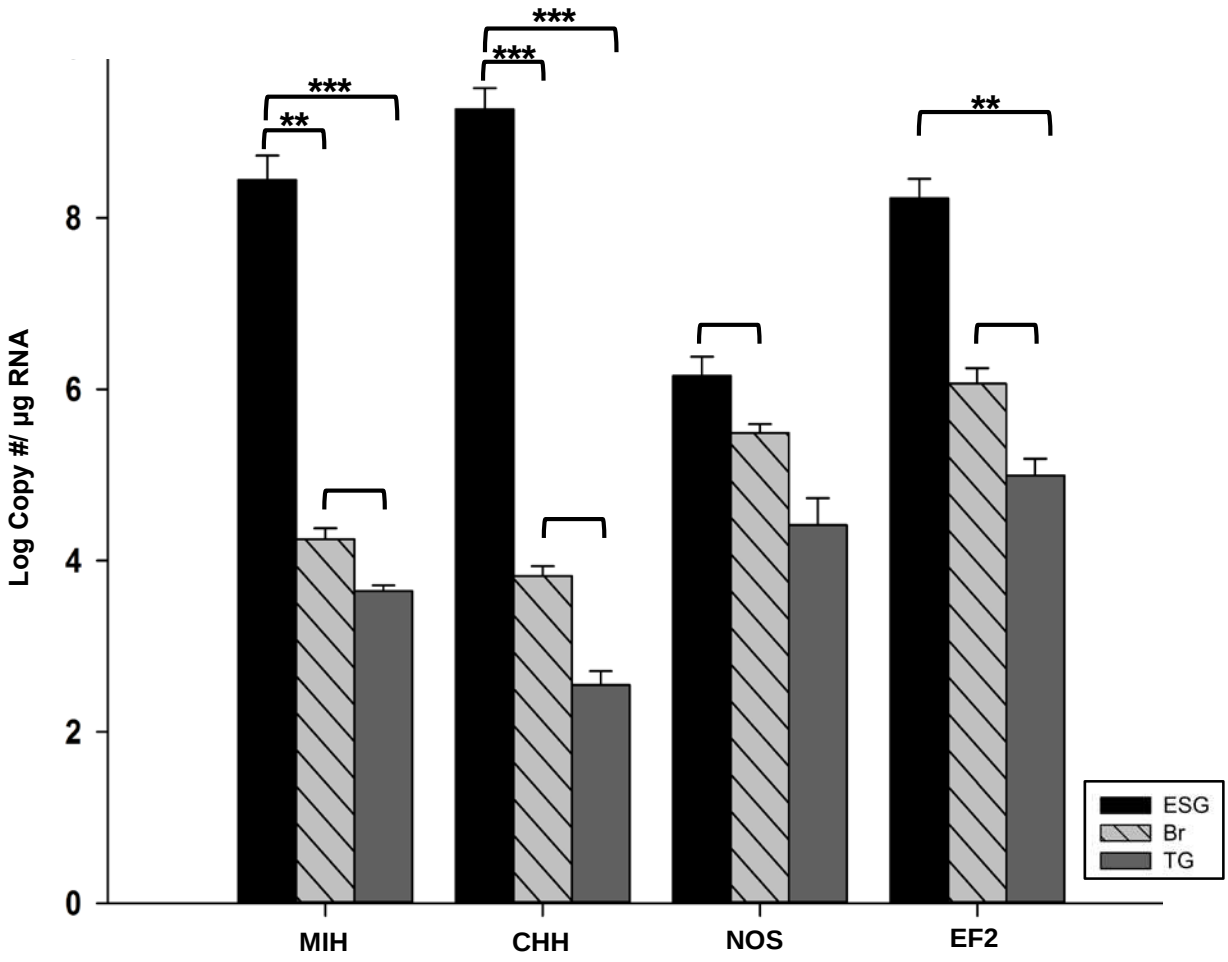


**Figure 4.7 Gene expression of *Gl-MIH, Gl-CHH, Gl-NOS*, and *Gl-EF2* in CNS tissues from intermolt animals**. Data are presented as mean ± S.E. (ESG n= 12; TG n = 20; Br n = 18). *Gl-MIH, Gl-CHH, Gl-NOS,* and *Gl-EF2* mRNA levels were quantified in three CNS tissues from intermolt animals. Brackets indicate s significant difference at $P < 0.01$. Asterisk's indicate range fold differences between the means. **** indicates a fold difference greater than $1.0 \times 10^6$, *** indicates a fold difference between $1.0 \times 10^5$ to $1.0 \times 10^6$, ** indicates a fold difference of $1.0 \times 10^3$ to $1.0 \times 10^4$, * indicates a fold difference of $1.0 \times 10^2$ to $1.0 \times 10^3$. Fold change less than $1.0 \times 10^2$ are indicated by a bracket. P-values are all < 0.01.

# REFERENCES


Abuhagr, A.M., Blindert, J.L., Nimitkul, S., Zander, I.A., LaBere, S.M., Chang, S.A., MacLea, K.S., Chang, E.S., Mykles, D.L., 2014a. Molt regulation in green and red color morphs of the crab *Carcinus maenas*: Gene expression of molt-inhibiting hormone signaling components. J. Exp. Biol. 217, 796-808.

Abuhagr, A.M., MacLea, K.S., Chang, E.S., Mykles, D.L., 2014b. Mechanistic target of rapamycin (mTOR) signaling genes in decapod crustaceans: Cloning and tissue expression of mTOR, Akt, Rheb, and p70 S6 kinase in the green crab, *Carcinus maenas*, and blackback land crab, *Gecarcinus lateralis*. Comp. Biochem. Physiol. 168, 25-39.

Andrew, R.D., Saleuddin, A.S.M., 1978. Structure and innervation of a crustacean neurosecretory cell. Can. J. Zool. 56, 423-430.

Azzouna, A., Rezig, M., 2001. Ultrastructural study of the sinus gland of the shrimp *Palaemonetes mesogenitor* Sollaud, 1912. B. Soc. Zool. Fr. 126, 217-219.

Benton, J.L., Sandeman, D.C., Beltz, B.S., 2007. Nitric oxide in the crustacean brain: Regulation of neurogenesis and morphogenesis in the developing olfactory pathway. Dev. Dyn. 236, 3047-3060.

Bliss, D.E., Durand, J.B., Welsh, J.H., 1954. Neurosecretory systems in decapod Crustacea. Z. Zellforsch. Mikroskop. Anat. 39, 520-536.

Bliss, D.E., Welsh, J.H., 1952. The neurosecretroy system of brachyuran crustacea. Biol. Bull. 103, 157-169.

Bunt, A.H., Ashby, E.A., 1967. Ultrastructural study of sinus gland in crayfish *Procambarus clarkii*. Am. Zool. 7, 200-&.

Bunt, A.H., Ashby, E.A., 1968. Ultrastructural changes in crayfish sinus gland following electrical stimulation. Gen. Comp. Endocrinol. 10, 379-&.

Chan, S.M., 1998. Cloning of a shrimp (*Metapenaeus ensis*) cDNA encoding a nuclear receptor superfamily member: An insect homologue of E75 gene. FEBS Lett. 436, 395-400.

Chang, E.S., Bruce, M.J., 1980. Ecdysteroid titers of juvenile lobsters following molt induction. J. Exp. Zool. 214, 157-160.

Chang, E.S., Mykles, D.L., 2011. Regulation of crustacean molting: A review and our perspectives. Gen. Comp. Endocrinol. 172, 323-330.

Chen, H.Y., Watson, R.D., Chen, J.C., Liu, H.F., Lee, C.Y., 2007. Molecular characterization and gene expression pattern of two putative molt-inhibiting hormones from *Litopenaeus vannamei*. Gen. Comp. Endocrinol. 151, 72-81.

Chen, Y.A., Scales, S.J., Patel, S.M., Doung, Y.C., Scheller, R.H., 1999. SNARE complex formation is triggered by $Ca^{2+}$ and drives membrane fusion. Cell 97, 165-174.

Chung, J.S., Wilkinson, M.C., Webster, S.G., 1998. Amino acid sequences of both isoforms of crustacean hyperglycemic hormone (CHH) and corresponding precursor-related peptide in *Cancer pagurus*. Regul. Pept. 77, 17-24.

Cooke, I.M., 1985. Electrophysiological characterization of peptidergic neurosecretory terminals. J. Exp. Biol. 118, 1-35.

Cooper, R.L., Hampson, D.R., Atwood, H.L., 1995. Synaptotagmin-like expression in the motor nerve terminals of crayfish. Brain Res. 703, 214-216.

Dircksen, H., Soyez, D., 1998. The lobster thoracic ganglia-pericardial organ neurosecretory system: A large source of novel crustacean hyperglycemic hormone-like peptide., in: E.W. Roubos, Wendelaar Bonga, S.E., Vaudry, H., De Loof, A. (Ed.), Recent Developments in Comparative Endocrinology and Neurobiology Proceedings of the 19th Conference for European Comparative Endocrinologists. European Society for Comparative Endocrinology, Univ. of Nijmegen, Nijmegen.

Echalier, G., 1954. Rcherchs expeerimentales sur le role de lorgane Y dans la mue de *Carcinus moenas* crustace decapode. Comptes Rendus Hebdomadaires Des Seances De L Academie Des Sciences 238, 523-525.

Fanjul-Möles, M.L., 2006. Biochemical and functional aspects of crustacean hyperglycemic hormone in decapod crustaceans: Review and update. Comp. Biochem. Physiol. 142C, 390-400.

Gu, P.L., Chan, S.M., 1998. The shrimp hyperglycemic hormone-like neuropeptide is encoded by multiple copies of genes arranged in a cluster. FEBS Lett. 441, 397-403.

Gu, P.L., Chu, K.H., Chan, S.M., 2001. Bacterial expression of the shrimp molt-inhibiting hormone (MIH): Antibody production, immunocytochemical study and biological assay. Cell Tiss. Res. 303, 129-136.

Gu, P.L., Tobe, S.S., Chow, B.K.C., Chu, K.H., He, J.G., Chan, S.M., 2002. Characterization of an additional molt inhibiting hormone-like neuropeptide from the shrimp *Metapenaeus ensis*. Peptides 23, 1875-1883.

Hanström, B., 1939. Hormones in Invertebrates. Oxford University Press, London.

He, P., Southard, R.C., Chen, D., Whiteheart, S.W., Cooper, R.L., 1999. Role of alpha-SNAP in promoting efficient neurotransmission at the crayfish neuromuscular junction. J. Neurophysiol. 82, 3406-3416.

Hopkins, P.M., 2012. The eyes have it: A brief history of crustacean neuroendocrinology. Gen. Comp. Endocrinol. 175, 357-366.

Hoyle, G., Wiersma, C.A.G., 1958a. Excitation at neuromuscular junction in crustacea. J. Physiol. Lond. 143, 403-425.

Hoyle, G., Wiersma, C.A.G., 1958b. Inhibition at neuromuscular junction in crustacea. J. Physiol. Lond. 143, 426-440.

Huang, X., Warren, J.T., Gilbert, L.I., 2008. New players in the regulation of ecdysone biosynthesis. J. Genet. Genom. 35, 1-10.

Jeromin, A., Shayan, A.J., Msghina, M., Roder, J., Atwood, H.L., 1999. Crustacean frequenins: Molecular cloning and differential localization at neuromuscular junctions. J.Neurobiol. 41, 165-175.

Keller, R., Haylett, B., Cooke, I., 1994. Neurosecretion of crustacean hyperglycemic hormone evoked by axonal stimulation or elevation of saline $K^+$ concentration quantified by a sensitive immunoassay method J. Exp. Biol. 188, 293-316.

Keller, R., Schmidt, E., 1979. *In vitro* secretion of ecdysteroids by Y-organs and lack of secretion by mandibular organs of the crayfish following molt induction. J. Comp. Physiol. 130, 347-353.

Kim, H.W., Batista, L.A., Hoppes, J.L., Lee, K.J., Mykles, D.L., 2004. A crustacean nitric oxide synthase expressed in nerve ganglia, Y-organ, gill and gonad of the tropical land crab, *Gecarcinus lateralis*. J. Exp. Biol. 207, 2845-2857.

Krieger, J., Sombke, A., Seefluth, F., Kenning, M., Hansson, B.S., Harzsch, S., 2012. Comparative brain architecture of the European shore crab *Carcinus maenas* (Brachyura) and the common hermit crab *Pagurus bernhardus* (Anomura) with notes on other marine hermit crabs. Cell Tissue Res. 348, 47-69.

Lachaise, F., Leroux, A., Hubert, M., Lafont, R., 1993. The molting gland of crustaceans; Localization, activity, and endocrine control (a review) J. Crustacean Biol. 13, 198-234.

Lee, C.Y., Zou, H.S., Yau, S.M., Ju, Y.R., Liau, C.S., 2000. Nitric oxide synthase activity and immunoreactivity in the crayfish *Procambarus clarkii*. Neuroreport 11, 1273-1276.

Lee, K.J., Kim, H.W., Gomez, A.M., Chang, E.S., Covi, J.A., Mykles, D.L., 2007. Molt-inhibiting hormone from the tropical land crab, *Gecarcinus lateralis*: Cloning, tissue expression, and expression of biologically active recombinant peptide in yeast. Gen. Comp. Endocrinol. 150, 505-513.

Lee, K.J., Watson, R.D., 2002. Antipeptide antibodies for detecting crab (*Callinectes sapidus*) molt-inhibiting hormone. Peptides 23, 853-862.

Lewis Carl, S.A.L., Gilleteferguson, I., Ferguson, D.G., 1993. An indirect immunofluorescence procedure for staining the same cryosection with 2 mouse monoclonal primary antibodies. J. Histochem. Cytochem. 41, 1273-1278.

Luckhart, S., Li, K., 2001. Transcriptional complexity of the *Anopheles stephensi* nitric oxide synthase gene. Insect Biochem. Molec. Biol. 31, 249-256.

Matsumoto, K., 1954. Neurosecretion in the thoracic ganglion of the crab, *Eriocheir japonicus*. Biol. Bull. 106, 60-68.

Moncada, S., Palmer, R.M.J., Higgs, E.A., 1991. Nitric oxide; Physiology, pathophysiology, and pharmacology. Pharmacol. Rev. 43, 109-142.

Nakatsuji, T., Lee, C.Y., Watson, R.D., 2009. Crustacean molt-inhibiting hormone: Structure, function, and cellular mode of action. Comp. Biochem. Physiol. 152A, 139-148.

Passano, L.M., 1951. The X-organ, a neurosectretroy gland controlling molting in crabs. Anat. Rec. 111, 559-559.

Pitts, N.L., Mykles, D.L., 2015. Nitric oxide production and sequestration in the sinus gland of the green shore crab *Carcinus maenas*. J. Exp. Biol. 218, 353-362.

Regulski, M., Tully, T., 1995. Molecular and biochemical characterization of dNOS: A *Drosophila* $Ca^{2+}$/calmodulin-dependent nitric oxide synthase. Proc. Natl. Acad. Sci. USA 92, 9072-9076.

Richmond, J.E., Penner, R., Keller, R., Cooke, I.M., 1996. Characterization of the $Ca^{2+}$ current in isolated terminals of crustacean peptidergic neurons. J. Exp. Biol. 199, 2053-2059.

Sandeman, D.C., 1982. Organization of the Central Nervous System, in: H.L. Atwood, D.C. Sandeman (Eds.), The Biology of Crustacea Neurobiology: Structure and Function. Academic Press, New York, NY, 1-54.

Sandeman, D.C., Scholtz, G., 1995. Ground Plans, Evolutionary Changes and Homologies in Decapod Crustacean Brains, in: W. Kutsch, O. Breidbach (Eds.), The Nervous Sytem of Invertebrates: A Comparative Approach. Birkhauser, Basel, 329-348.

Schwarz, P.M., Rodriguez-Pascual, F., Koesling, D., Torres, M., Forstermann, U., 1998. Functional coupling of nitric oxide synthase and soluble guanylyl cyclase in controlling catecholamine secretion from bovine chromaffin cells. Neurosci. 82, 255-265.

Skinner, D.M., 1985. Molting and regeneration, in: D.E. Bliss, L.H. Mantel (Eds.), The Biology of Crustacea. Academic Press, New York, 44-146.

Soumoff, C., O' Connor, J.D., 1982. Repression of Y-organ secretory activity by molt inhibiting hormone in the crab *Pachygrapsus crassipes*. Gen. Comp. Endocrinol. 48, 432-439.

Stasiv, Y., Regulski, M., Kuzin, B., Tully, T., Enikolopov, G., 2001. The *Drosophila* nitric oxide synthase gene (dNOS) encodes a family of proteins that can modulate NOS activity by acting as dominant negative regulators. J. Biol. Chem. 276, 42241-42251.

Stewart, M.J., Stewart, P., Sroyraya, M., Soonklang, N., Cummins, S.F., Hanna, P.J., Duan, W., Sobhon, P., 2013. Cloning of the crustacean hyperglycemic hormone and evidence for molt-inhibiting hormone within the central nervous system of the blue crab *Portunus pelagicus*. Comp. Biochem. Physiol. 164A, 276-290.

Sun, P.S., 1995. Expression of the molt-inhibiting hormone like gene in the eyestalk and brain of the white shrimp *Penaeus vannamei*. Mol. Mar. Biol. Biotechnol. 4, 262-268.

Tang, Y.M., Chen, G.F., Thompson, P.A., Lin, D.X., Lang, N.P., Kadlubar, F.K., 1999. Development of an antipeptide antibody that binds to the C-terminal region of human CYP1B1. Drug Metab. Dispos. 27, 274-280.

Tiu, S.H.K., Chan, S.M., 2007. The use of recombinant protein and RNA interference approaches to study the reproductive functions of a gonad-stimulating hormone from the shrimp *Metapenaeus ensis*. FEBS J. 274, 4385-4395.

Trier, N.H., Hansen, P.R., Houen, G., 2012. Production and characterization of peptide antibodies. Methods 56, 136-144.

Umphrey, H.R., Lee, K.J., Watson, R.D., Spaziani, E., 1998. Molecular cloning of a cDNA encoding molt-inhibiting hormone of the crab, *Cancer magister*. Molec. Cell. Endocrinol. 136, 145-149.

Watson, R.D., Lee, K.J., Borders, K.J., Dircksen, H., Lilly, K.Y., 2001a. Molt-inhibiting immunoreactive neurons in the eyestalk neuroendocrine system of the blue crab, *Callinectes sapidus*. Arthropod Struct. Dev. 30, 69-76.

Watson, R.D., Lee, K.J., Qiu, S.H., Luo, M., Umphrey, H.R., Roer, R.D., Spaziani, E., 2001b. Molecular cloning, expression, and tissue distribution of crustacean molt-inhibiting hormone. Am. Zool. 41, 407-417.

Webster, S.G., Dircksen, H., 1991. Putative molt-inhibiting hormone in larvae of the shore crab *Carcinus maenas* L.: An immunocytochemical approach. Biol. Bull. 180, 65-71.

Webster, S.G., Keller, R., 1986. Purification, characterisation and amino acid composition of the putative moult-inhibiting hormone (MIH) of *Carcinus maenas* (Crustacea, Decapoda). J. Comp. Physiol. 156, 617-624.

Webster, S.G., Keller, R., Dircksen, H., 2012. The CHH-superfamily of multifunctional peptide hormones controlling crustacean metabolism, osmoregulation, moulting, and reproduction. Gen. Comp. Endocrinol. 175, 217-233.

Weitzman, M., 1969. Release of neurosecretory material from sinus gland of *Gecarcinus lateralis*. Anat. Rec. 163, 332-340.

Wiersma, C.A., 1961a. The Neuromuscular System, in: T.H. Waterman (Ed.), The Physiology of Crustacea. Academic Press, New York, NY, 191-240.

Wiersma, C.A., 1961b. Reflexes and the Central Nervous System, in: T.H. Waterman (Ed.), The Physiology of Crustacea. Academic Press, New York, NY, 241-279.

Zhu, D.F., Hu, Z.H., Shen, J.M., 2011. Moult-inhibiting hormone from the swimming crab, *Portunus trituberulatus* (Miers, 1876); PCR cloning, tissue distribution, and expression of recombinant protein in *Escherichia coli* (Migula, 1895). Crustaceana 84, 1481-1496.

Zmora, N., Sagi, A., Zohar, Y., Chung, J.S., 2009. Molt-inhibiting hormone stimulates vitellogenesis at advanced ovarian developmental stages in the female blue crab, *Callinectes sapidus*: Novel specific binding sites in hepatopancreas and cAMP as a second messenger. Saline Systems 5:6, 1-11.

CHAPTER 5

# WHAT MAKES SOME CRUSTACEAN POPULATIONS REFRACTORY TO MOLT INDUCTION TECHNIQUES? AN EXAMINATION OF HOW GENE REGULATION CONTRIBUTES TO THIS PHENOMENON


## SUMMARY

Molt induction techniques have helped to build the foundation of the field of crustacean endocrinology. Multiple limb autotomy (MLA) and eyestalk ablation (ESA) are commonly used to control molt cycle progression in a laboratory setting. MLA induces the loss of five or more walking legs and mimics a natural molt. ESA is the removal of the eyestalks, the primary source of molt inhibiting hormone (MIH). MIH is a peptide hormone that negatively regulates molting by inhibiting production of molting hormones (ecdysteroids) from the molting gland or Y-organ (YO). Recent work in *Carcinus maneas* found that this population is refractory to molt induction techniques. Similar observations were made in *Gecarcinus lateralis*, therefore this study sought to explore the molecular mechanisms regulating this phenomenon. *G. lateralis* refractory to MLA (blocked) underwent a second molt induction by ESA and the YO, eyestalk ganglia (ESG), thoracic ganglia (TG), and brain (Br) were harvested 1, 3, and 7 days post ESA. Quantitative PCR (qPCR) was used to examine changes in gene expression of MIH and mTOR signaling pathway genes in all four tissues. MIH expression in the TG and Br increased in blocked animals, supporting the hypothesis that molt resistance may be attributed to MIH secretion from these central nervous system tissues. *Gl-Rheb* and *Gl-S6K* increased in the ESG and Br of blocked animals indicating that inhibition of mTOR activates downstream transcription factors which aid in maintaining energy homeostasis in times of environmental stress. A separate study examined the effect of the mTOR inhibitor rapamycin on gene expression in the Br and TG of animals induced to molt via ESA. Changes in transcript abundance of MIH and mTOR signaling pathway genes in rapamycin and dimethyl sulfoxide (DMSO) injected animals was notably different from blocked animals. These results suggest that injection alone (rapamycin or DMSO) has a significant physiological effect on the animal.


## INTRODUCTION

Growth in decapod crustaceans is a nonlinear process that is dependent upon the shedding and regeneration of a rigid exoskeleton to accommodate growth. In this process known as molting,

crustaceans undergo a number of physiological changes that must be precisely coordinated for molting to be successful. This delicate process is orchestrated by the secretion of steroid hormones (ecdysteroids) from the Y-organ (YO) into the hemolymph from (Chang and Mykles, 2011; Lachaise et al., 1993; Skinner, 1985). Fluctuations in hemolymph ecdysteroids titers regulate progression through the four stages of the molt cycle; intermolt, premolt, ecdysis, and post molt (Chang and Mykles, 2011; Skinner, 1985).

Molt induction techniques have been critical in the study of crustacean molting. Originally stumbled upon by Zeleny in 1905, eyestalk ablation (ESA) removes the primary source of a peptide hormone, molt inhibiting hormone (MIH), a negative regulator of ecdysteroid synthesis. A second technique, multiple limb autotomy (MLA), which resembles a natural molt, removes five or more walking legs. Both of these techniques induce successful premolt induction in most adult *G. lateralis* (Abuhagr et al., 2014b; MacLea et al., 2012; Yu et al., 2002). Ecdysteroid titers in *G. lateralis* steadily increase during premolt, peaking (> 600 pg/µL) just prior to ecdysis and then drastically drop off (< 5 pg/µL) during post molt (Abuhagr et al., 2014b). The increase in ecdysteroid titers during premolt is correlated with physiological changes such as degradation of the old exoskeleton, synthesis of a new exoskeleton, and atrophy of the claw muscles (Skinner, 1985). In some cases, *G. lateralis* does not respond to MLA (unpublished observations) and are determined to be "blocked." A similar phenomenon occurs in an adult population of *C. maneas* from Bodega Harbor in Bodega Bay, CA (Abuhagr et al., 2014a). In these animals ESA and MLA are ineffective at inducing molt and ecdysteroid titers never rise above ~60 pg/µL, even 90 days post molt induction (Abuhagr et al., 2014a).

One of the principle goals of this study was to examine whether the blocked phenomenon is a result of increased activity of MIH signaling. In order to explore this possibility, changes in gene expression of signaling components from the proposed MIH signaling pathway in the YO were evaluated by qPCR (Chang and Mykles, 2011). MIH is synthesized by a group of ~150 neurosecretory cells (X-organ; XO) located in the medulla terminalis (MT) of the eyestalk ganglia (ESG) (Hopkins, 2012; Skinner, 1985). Axons from the XO terminate in the sinus gland (SG) a neurohemal organ from which MIH and other neuropeptides are secreted (Hopkins, 2012; Skinner, 1985; Stuenkel, 1985). MIH binds an unidentified receptor on the surface of the YO, activating a signaling pathway that inhibits

ecdysteroidgenesis (Chang and Mykles, 2011). In this proposed signaling pathway, MIH activates cyclic nucleotides cAMP and cGMP that inhibit both inhibit ecdysteroid genesis *in vitro* (Covi et al., 2009). Binding of MIH activates adenylyl cyclase, producing cAMP, and activating of PKA, resulting in an acute inhibition of ecdysteroidgenesis (Chang and Mykles, 2011). In addition to transiently inhibiting ecdysteroidgenesis, PKA is proposed to induce $Ca^{2+}$ influx, which activates a NO/cGMP signaling pathway that prolongs the inhibition of ecdysteroid production (Chang and Mykles, 2011). A reduction in MIH titers is hypothesized to decrease activity of the MIH signaling pathway, activating the YO and increase ecdysteroid production (Chang and Mykles, 2011; Lachaise et al., 1993; Skinner, 1985).

Although the prevailing view is that MIH is produced and secreted exclusively from the XO/SG complex, there are numerous reports of MIH expression in other central nervous system (CNS) tissues (Abuhagr et al., 2014a; Gu and Chan, 1998; Stewart et al., 2013; Tiu and Chan, 2007; Webster and Dircksen, 1991; Zhu et al., 2011). Peripheral sources of MIH could be attributable to how some species are refractory to molt induction even after the removal of the ESG (Abuhagr et al., 2014a). Secretion of MIH from these tissues shares similar properties to release of MIH from the SG. For example, MIH is localized in cell clusters adjacent to the sternal artery and the hemocoele, suggesting that MIH from the TG is directly secreted into the circulating hemolymph (Stewart et al., 2013). Additionally, a sharp decline in ecdysteroids following ecdysis in crustaceans without eyestalks suggests that if MIH does inhibit ecdysteroidgenesis, then alternative sources of MIH are necessary for a successful molt in these species (Dell et al., 1999; Hopkins, 2012; Nakatsuji and Sonobe, 2004).

During premolt, the mechanistic target of rapamycin (mTOR) is required for full activation of the YO, which undergoes changes in size and ecdysteroidogenic capacity during premolt (Covi et al., 2012; Skinner, 1985). Upregulation of *Gl-mTOR* and *Gl-Akt* is correlated with an increase in ecdysteroid titers during premolt in *G. lateralis* (Abuhagr et al., 2014b). The importance of mTOR signaling in ecdysteroid synthesis in both insects and crustaceans is emphasized by experiments utilizing the mTOR inhibitor rapamycin. In insects, rapamycin prevents ecdysteroid production and release in *Bombyx mori* and delays molting and ecdysteroid production in *Manduca sexta* (Gu et al., 2012; Kemirembe et al., 2012). Rapamycin inhibits ecdysteroid production in *G. lateralis* and *C. maneas* YO's *in vitro* (Abuhagr et al.,

2014b). Evidence from these studies supports the hypothesis that activation of the YO and therefore molt progression is mTOR dependent.

The purpose of this study was to investigate potential molecular mechanisms that contribute to the blocked phenomenon in *G. lateralis*. It is hypothesized that this phenomenon is regulated by MIH, therefore changes in the expression of components from the predicted MIH signaling pathway using quantitative PCR was examined. Three tissues were examined the YO, the TG, and the Br. In the YO expression of MIH signaling pathway components was generally greater in blocked animals compared to controls at D0. ESA induced an increase of MIH pathway gene expression in both blocked and control animals. mTOR signaling pathway genes in blocked and control animals were comparable at D0 and mTOR pathway genes did not respond to ESA in either group. The most notable change in gene expression in the TG and Br was a higher level of expression of neuropeptides in blocked animals compared to controls at D0. ESA also increased expression of these peptides in both groups. mRNA transcript levels in the ESG from blocked animals was greater than controls in nearly every gene examined. The effects of ESA on gene expression in rapamycin injected animals was minimal.

## RESULTS

*Effects of ESA on hemolymph ecdysteroid titers in blocked and control animals*

*G. lateralis* were induced to molt via multiple limb autonomy (MLA). Some animals entered premolt a few weeks later, others never initiated premolt (based on the R-index) and were determined to be blocked. Blocked animals were defined as animals that did not enter premolt 12 weeks post MLA. A second molt induction technique, eyestalk ablation (ESA), was performed on these animals. Tissues were harvested from blocked and control animals at Day 0 (D0), 1 d post ESA (D1), or 7 d post ESA (D7). ESG were collected from blocked and control animals at D0; Br and TG were collected at all three time points. The control group underwent molt induction by ESA alone and were used as a baseline for comparison to blocked animals. Hemolymph ecdysteroid titers in blocked animals at D0 was 6.6-fold greater compared to controls. Ecdysteroid titers in blocked animals did not change in response to ESA. However titers in control animals increased ~10-fold by D7 (Figure 5.1A).

*Effects of ESA on gene expression in the YO and three CNS tissues from blocked and control animals*

*Y-organ*

Elevated ecdysteroid titers in blocked animals at D0 compared to controls was matched by increased expression of MIH signaling pathway components *Gl-AC* (3.5 x $10^3$-fold difference), *Gl-PKA* (8.2 x $10^3$-fold difference), *Gl-NOS* (2.7 x $10^4$-fold difference), *Gl-GC-Iβ* (4.6 x$10^2$-fold difference) and *Gl-PKG* (1 x $10^4$-fold difference) in blocked compared to control animals (Figure 5.1A). At D0 there was no significant difference between blocked and control animals in the expression of mTOR signaling pathway genes *Gl-mTOR, Gl-Rheb, Gl-S6K*, and *Gl-Akt* (Figure 5.1B). *Gl-EF2* was used as a reference gene for monitoring mTOR independent transcription and was 2.5 x $10^2$-fold greater in blocked animals compared to controls at D0.

ESA did not affect gene expression in control animals until 7 days post ESA. Expression of four MIH signaling pathway genes was effected by ESA (Figure 5.1A, solid diamonds): *Gl-AC* (35-fold increase), *Gl-PKA* (14-fold increase occurs at D1 and is maintained until D7), *Gl-GC-Iβ* (83-fold increase), and *Gl-PKG* (57-fold decrease). Control animals did not demonstrate any effect of ESA on mTOR signaling pathway genes *Gl-mTOR, Gl-Rheb, Gl-S6K*, and *Gl-Akt* at any time point (Figure 5.1B). There was no effect of ESA on *Gl-EF2* expression in control animals.

ESA had little effect on gene expression in blocked animals. Two MIH signaling pathway genes, *Gl-AC* and *Gl-PKA,* increased by 47 and 89-fold respectively, at 7 days post ESA (Figure 5.1A, open diamonds). ESA did not significantly effect expression of mTOR signaling pathway genes *Gl-mTOR, Gl-Rheb, Gl-S6K*, and *Gl-Akt* or *Gl-EF2* at any time point in blocked animals (Figure 5.1B).

Expression of *Gl-CHH* and *Gl-MIH* was below detection level by qPCR. In summary, blocked animals did not respond to ESA, as there was no significant increase in ecdysteroid titers indicating that these animals were refractory to molt induction similar to *C. maenas* (Abuhagr et al., 2014a). Higher expression of MIH signaling pathway components in blocked animals compared to controls at D0 suggests that their inability to enter premolt may be dependent on MIH or an MIH-like factor. There was no significant difference in mTOR pathway expression between blocked and control animals at D0 nor was there an effect of ESA on either group.

*Eyestalk Ganglia*

Differences in expression of MIH and mTOR signaling pathway genes was quantified in ESG from the animals induced to molt via ESA. ESG were collected from control and blocked animals at D0. Gene expression in the ESG was higher in blocked animals compared to controls for nearly every MIH and mTOR signaling pathway gene examined. Expression of neuropeptide hormones *Gl-MIH* and *Gl-CHH* was greater in the ESG in blocked compared to control animals by 93-fold and 64-fold, respectively (Figure 5.2A). MIH signaling pathway genes *Gl-NOS* (21-fold greater), *Gl-GC-Iβ* (28-fold greater), *Gl-GC-II* (62-fold greater), and *Gl-GC-III* (33-fold greater) has significantly higher expression in blocked compared to control animals (Figure 5.2A). No significant difference in the expression of *Gl-NOSIP* was detected between blocked and control animals (Figure 5.2A). Expression of mTOR signaling pathway genes was also higher in three of the four mTOR signaling pathway genes examined: *Gl-mTOR* (3.7 x$10^2$-fold), *Gl-Rheb* (2.8 x$10^2$-fold), *Gl-S6K* (2.2 x $10^2$-fold) (Figure 5.2B). There was no significant difference in expression of *Gl-Akt* between blocked and control animals. *Gl-EF2* mRNA level was 2.7 x $10^2$-fold greater in blocked animals compared to controls (Figure 5.2B).

*Brain*

Brain tissues were collected at the same time as the YOs to quantify gene expression in the CNS. At D0, expression of both neuropeptides was significantly greater in blocked animals compared to controls: *Gl-CHH* (7.4 x$10^2$-fold) and *Gl-MIH* (13-fold) (Figure 5.3A). With the exception of a 127-fold lower expression in *Gl-GC-III*, there was no significant difference in the expression of MIH signaling pathway genes between blocked and control animals in the Br at D0 (Figure 5.3A). Similarly, the only mTOR signaling pathway gene that was significantly different from controls was *Gl-Rheb* (34-fold greater in blocked animals) at D0. There was also no difference in *Gl-EF2* expression at D0 between these groups (Figure 5.3B).

ESA significantly affectd the expression of both neuropeptides in control animals at D7 compared to D0 (*Gl-CHH* 5.9 x $10^4$-fold increase; *Gl-MIH* 346-fold increase). ESA had a significant effect on *Gl-GC-III* expression, decreasing by 70-fold at D1 compared to D0. ESA did not significantly affect gene expression of any other MIH signaling pathway components (Figure 5.3A). ESA had a significant effect on two mTOR signaling pathway genes in control animals. Expression of *Gl-Rheb* was significantly

higher at both D1 (44-fold) and D7 (482-fold) compared to D0. *Gl-S6K* expression decreased by 881-fold at D1 compared to D0 and increased by 14-fold at D7 compared to D0. There was no significant effect of ESA on *Gl-mTOR*, *Gl-Akt*, or *Gl-EF2* expression in the Br of control animals (Figure 5.3B).

ESA induced an increase in the expression of both neuropeptides in the Br of blocked animals. At D7, expression of *Gl-CHH* was 449-fold greater relative to D0 and *Gl-MIH* expression was 891-fold greater compared to D0. ESA had a similar effect on the expression of MIH signaling pathway genes in blocked animals as it did in controls. Only *Gl-GC-III* expression in blocked animals was significantly impacted by ESA at D1 (48-fold increase) compared to D0. ESA did not have a significant impact on the expression of any other MIH signaling pathway components in the Br of blocked animals (Figure 5.3A). ESA only effected one mTOR signaling pathway gene in blocked animals, increasing the expression of *Gl-Rheb* by 38-fold at D1 and 23-fold at D7 compared to D0. ESA did not significantly impact gene expression of *Gl-mTOR, Gl-S6K, Gl-Akt*, or *Gl-EF2* in blocked animals (Figure 5.3B).

*Thoracic Ganglia*

Neuropeptide expression in the TG was elevated in blocked animals compared to controls at D0, following a similar trend that was observed in the Br. *Gl-CHH* expression was 186-fold higher and *Gl-MIH* was 668-fold higher in blocked animals at D0. With the exception of *Gl-GC-II* and *Gl-GC-III*, expression of MIH signaling pathway genes was the same in blocked and control animals at D0. Expression of *Gl-GC-II* ($7.4 \times 10^3$-fold) and *Gl-GC-III* ($3.4 \times 10^3$-fold) was lower in blocked animals compared to controls at D0 (Figure 5.4A). Gene expression in the TG of three mTOR signaling pathway components, *Gl-mTOR* (142-fold difference), *Gl-Rheb* (293-fold difference), and *Gl-S6K* (110-fold difference) was greater in blocked animals compared to controls. There was no significant difference in *Gl-Akt* and *Gl-EF2* expression in blocked versus control animals at D0 (Figure 5.4B).

ESA had a similar effect on neuropeptide expression in the TG of control animals as it did in the Br, elevating expression of both *Gl-CHH* ($1.3 \times 10^4$-fold) and *Gl-MIH* (104-fold) at 7 days post ESA compared to D0. ESA significantly decreased the expression of both *Gl-GC-II* (342-fold) and *Gl-GC-III* ($1.7 \times 10^3$-fold decrease) 7 days post ESA compared to D0. ESA had no effect on any other MIH signaling pathway components in control animals (Figure 5.4A). ESA significantly increased the expression of three mTOR pathway components, *Gl-mTOR, Gl-Rheb*, and *Gl-S6K*. Expression was

higher at D7 compared to D0 for all three genes (*Gl-mTOR* 4-fold; *Gl-Rheb* 21-fold; *Gl-S6K* 100-fold). Additionally, *Gl-Rheb* was 44-fold greater at 1 day post ESA compared to D0. ESA did not have a significant effect on *Gl-Akt* or *Gl-EF2* in control animals (Figure 5.4B).

ESA significantly increased expression of *Gl-CHH* (78-fold) and *Gl-MIH* (8-fold) at D7 compared to D0 in the TG of blocked animals. *Gl-GC-III* expression decreased in response to ESA at D7 by 18-fold. ESA did not have a significant effect on gene expression of any other MIH signaling pathway genes (Figure 5.4A). Expression of mTOR signaling pathway genes and *Gl-EF2* in the TG of blocked animals was also unaffected by ESA (Figure 5.4B).

*Effects of ESA on hemolymph ecdysteroid titers in rapamycin injected and control animals*

Animals were injected with rapamycin (injected) or DMSO (controls) and induced to molt via ESA. Br and TG were collected 0, 1, 3, and 7 days post ESA/injection. There was a significant effect of ESA on ecdysteroid titers in both injected and control animals. At D3, titers increased by 13.7-fold in control animals, whereas titers in injected animals only increased by 5-fold compared to D0. ESA also had a significant effect on both injected and controls at D7 (control 12.7-fold increase; injected 9.7-fold increase both compared to D0). Titers increased at a slower rate in injected animals which can be attributed to the inhibitory effects of rapamycin on mTOR activity (Figure 5.5A).

*Effects of ESA on gene expression in Br and TG of rapamycin and control animals*

*Brain*

*Gl-CHH* was the only gene effected by ESA in control animals. At D3 *Gl-CHH* had decreased by 141-fold and expression further declined by 484-fold at D7 compared to D0. There was no effect of ESA on any other MIH or mTOR signaling pathway genes in the Br of control animals (Figure 5.5A). ESA significantly impacted expression of both neuropeptides in injected animals. Similar to controls, *Gl-CHH* expression in injected animals decreased at D3 (691-fold) and D7 ($1.7 \times 10^3$-fold) compared to D0. ESA had the opposite effect on *Gl-MIH* and expression at D7 increased by 45-fold compared to D0. ESA had minimal effects on the expression of MIH and mTOR signaling pathway genes in injected animals, effecting expression of only one gene from each pathway. Expression of *Gl-GC-Iβ*, a NO receptor in the MIH signaling pathway, increased in injected animals by $1.1 \times 10^3$-fold at D3 and $1.5 \times 10^3$-fold at D7 compared to D0. *Gl-S6K*, a component of the mTOR signaling pathway, showed a decrease in

expression (9.9-fold) in response to ESA in injected animals. There was no change in expression in any other MIH or mTOR signaling pathway genes in the Br of injected animals in response to ESA (Figure 5.5A).

*Thoracic Ganglia*

There was no effect of ESA on gene expression in the TG of control animals (Figure 5.5B). ESA had a similar effect on neuropeptide expression in the TG of injected animals as it did in the Br. *Gl-CHH* expression decreased by 19-fold at D7 and expression of *Gl-MIH* increased by 28-fold at D7 compared to D0. Expression of two MIH signaling pathway genes in the TG decreased in injected animals in response to ESA. Expression of *Gl-GC-III* and *Gl-GC-II* both had significantly lower expression at D3 (*Gl-GC-III* 84-fold; *Gl-GC-III* 97-fold) and D7 (*Gl-GC-III* 4.5 x $10^3$-fold; *Gl-GC-III* 3.1 x $10^3$-fold) compared to D0. *Gl-S6K* followed the same trend in the TG of injected animals as it did in the Br and expression decreased by 17-fold at D7. ESA did not effect expression of any other mTOR signaling pathway genes in injected animals. Expression of *Gl-EF2* decreased by 24-fold in at D7 compared to D0, suggesting that rapamycin injection may effect protein synthesis in the TG.

## DISCUSSION

Since Zeleny's (Zeleny, 1905) discovery that the removal of the eyestalks (ESG) in crayfish stimulates molting, molt induction techniques have been a cornerstone for advancement in the field of crustacean endocrinology. The ability to induce molting in a laboratory setting is paramount for exploring the molecular mechanisms that regulate molting. Two techniques can be employed to induce molting. As Zeleny discovered, the removal of the ESG accelerates an animal's progression into premolt. At the time Zeleny was unaware that he had inadvertently removed the primary source of the molt inhibiting hormone MIH. In the absence of MIH, the molting gland or Y-organ (YO) becomes active and releases molting hormones or ecdysteroids, initiating the physiological changes required for molt progressoin. MLA mimics a natural molt induction by the loss of five or more walking legs, similar to the animal's response when escaping the clutches of a predator (Skinner, 1985).

This study was sparked by a long standing observation that molt induction via MLA in *G. lateralis* is not always successful at accelerating progression into premolt. Animals that do not enter premolt 12 weeks post MLA are identified as blocked. Although ecdysteroid titers are higher in blocked animals

compared to controls at D0, further molt induction by ESA does not significantly increase ecdysteroid concentrations (Figure 5.1A). This low concentration in response to ESA indicates that blocked animals are refractory to molt induction techniques. A similar phenomenon is observed in a population of *C. maenas* from Bodega Harbor in Bodega Bay, CA. In this population ecdysteroid titers in ESA and/or MLA animals do not exceed 60 pg/µl at 90 days post induction (Abuhagr et al., 2014a). The current study sought to examine whether resistance to molt induction in *G. lateralis* could be linked to changes in gene expression, uncovering the molecular mechanism(s) behind why some animals are refractory to molt induction techniques.

*Effects of ESA on gene expression in the YO of blocked animals*

Data from *G. lateralis* YO's indicates that the proposed MIH signaling pathway (Chang and Mykles, 2011) is upregulated in blocked animals and contributes to molt induction resistance. At D0, five genes in the proposed pathway, *Gl-AC, Gl-PKA, Gl-GC-Iβ*, and *Gl-PKG*, have higher levels of expression compared to controls (Figure 5.1A). Additionally, *Gl-NOS* expression increased but not significantly ($p = 0.088$). An active MIH signaling pathway in the YO would inhibit ecdysteroidgenesis, preventing the physiological changes required for ecdysis. Ecdysteroid synthesis requires translation, therefore it is not surprising that in blocked animals mTOR activity is low (Figure 5.1B). A decrease in mTOR activity may contribute to the increase in expression of MIH signaling pathway genes through the activation of a downstream transcription factor. In *Drosophila*, the transcription factor RECTOR is activated when mTOR is inhibited and is responsible for ~90% of translation induction when mTOR is inactive (Tiebe et al., 2015). A similar mechanism may be at work in blocked *G. lateralis* given that MIH signaling pathway genes are elevated when mTOR is inhibited.

ESA minimally impacts gene expression in the YO of blocked and control animals. Ecdysteroid titers significantly increase at D7 in controls, but are unchanged in blocked animals (Figure 5.1A). Ecdysteroid concentrations in blocked animals reach ~ 60 pg/µl, the same threshold that titers in *C. maenas* remained at 90 days post induction (Abuhagr et al., 2014a). Expression of *Gl-AC* and *Gl-PKA* increases in blocked animals (Figure 5.1A) and is an indication that the MIH signaling pathway remains active. There is no change in the expression of *Gl-GC-Iβ, Gl-GC-II*, and *Gl-GC-III* in response to ESA in blocked animals (Figure 5.1A), which is consistent with results from the Bodega Bay population of *C.*

*maenas* (Abuhagr et al., 2014a). ESA in control animals increased expression of three MIH signaling pathway genes: *Gl-AC, Gl-PKA,* and *Gl-GC-Iβ* 7 days post ESA (Figure 5.1A). In the proposed MIH signaling pathway, activation of PKA and PKG inhibit ecdysteroidgenesis. However the opposite effect is observed here (Mykles, 2011). The significant increase in ecdysteroid titers at D7 suggests that the MIH pathway is inactive, therefore a PKA-dependent pathway in the YO unrelated to molt inhibition could be active. Support for the existence of the proposed MIH signaling pathway is evident in a decrease of *Gl-PKG* expression in control animals at D7 (Figure 5.1A). A decrease in PKG activity would lift the inhibition of ecdysteroid production in the YO allowing for progression into premolt.

*Differences in gene expression in the ESG of blocked and control animals*

Comparison of gene expression between control and blocked animals in the ESG reveals that both signaling peptides are greater in blocked animals (Figure 5.2B). An increase in MIH release from the ESG helps to sustain the animal in intermolt (Covi et al., 2010). Increased CHH production is likely a response to the stress of environmental factors such as living in the dark for 3 months or longer (mimicking the safety of a burrow to encourage molting). A significant increase in the expression of all three GC's may decrease neuropeptide release from the SG by the activation of an NO/cGMP signaling pathway. mTOR signaling pathway genes *Gl-mTOR, Gl-Rheb*, and *Gl-S6K* are all elevated in blocked animals as is *Gl-EF2* (Figure 5.2B). Increased expression of these genes likely contributes to increased peptide synthesis. Heightened production of signaling neuropeptides in the ESG and elevated expression of MIH signaling pathway components in the YO argues that the blocked state of molting is an MIH-dependent phenomenon in *G. lateralis*.

*Effect of ESA on gene expression in CNS tissues of blocked and control animals*

A proposed mechanism for resistance to molt induction is the expression of MIH in CNS tissues outside of the ESG. MIH is expressed in the TG and Br of the Bodega Bay population of *C. maenas,* as well as in several other decapod species (Abuhagr et al., 2014a; Gu and Chan, 1998; Stewart et al., 2013; Tiu and Chan, 2007; Webster and Dircksen, 1991; Zhu et al., 2011). To determine if alternative sources of MIH could contribute to resistance to molt induction in *G. lateralis*, Br and TG were harvested from blocked and control animals at 0, 1, and 7 days post ESA. In both CNS tissues, block had a positive effect on the expression of *Gl-mTOR* (TG only), *Gl-Rheb*, and *Gl-S6K* at D0 (Figure 5.3B and 5.4B).

Elevated mTOR activity likely contributes to increased synthesis of the neuropeptides CHH and MIH (Figure 5.3A and 5.4A). However, despite elevated peptide production there is no change in MIH signaling pathway gene expression in either tissue. This argues that either MIH does not signal through the same pathway in CNS tissues as it does in the YO or that it is being synthesized in CNS tissues and secreted into the hemolymph. Evidence of elevated MIH production in the Br and TG in blocked animals suggests that synthesis of MIH in the CNS contributes to a resistance to molt induction in *G. lateralis*.

With the exception of an increase in *Gl-Rheb* expression in the Br at D7, mTOR pathway components in blocked animals are not effected by ESA (Figure 5.3B). However, in control animals, *Gl-mTOR* (TG only), *Gl-Rheb*, and *Gl-S6K* are all upregulated in response to ESA. Again, this increase in mTOR activity likely contributes to increased peptide synthesis. *Gl-MIH* and *Gl-CHH* expression increases in response to ESA in both the Br and TG (Figure 5.3A and 5.4A). This increase is observed in both blocked and control animals and may be a mechanism to dampen the effects of losing the primary source of neuropeptides during ESA. Increased MIH synthesis in secondary sources of MIH could account for the increase in MIH signaling pathway genes *Gl-AC* and *Gl-PKA* in the YO 7 days post ESA (Figure 5.1A). There is no effect of ESA on the expression of MIH signaling pathway genes in either tissue for either treatment, supporting the hypothesis that MIH signals through a different pathway in CNS tissues, or its actions occur in tissues outside of the CNS.

*Effect of ESA on gene expression in CNS tissue of rapamycin injected and control animals*

To explore whether mTOR activity is required for gene regulation in CNS tissues *G. lateralis* were injected with an mTOR inhibitor rapamycin and induced to molt via ESA. Br and TG were collected at 0, 1, 3, and 7 days post ESA/injection. Ecdysteroid titers increased to ~ 60 pg/µl in both control and injected animals. However, titers in injected animals rose gradually compared to controls indicating that rapamycin had the predicted effect on mTOR activity in the YO (Figure 5.5A). *Gl-CHH* expression in both injected and control animals significantly decreased in both the Br and TG at 3 and 7 days post ESA (Figure 5.5A and 5.5B). This is in direct contrast to what is observed in the blocked experiment and suggests that stress associated with injection has a significant physiological effect. Interestingly, MIH increases at 7 days post injection in the Br and TG of rapamycin injected animals (Figure 5.5A and 5.5B).

This indicates that in the presence of rapamycin, the predicted compensatory effects in response to the loss of the primary source of MIH is sustained.

Rapamycin had a significant impact on the expression of GC's in both CNS tissues. *Gl-GC-Iβ* expression is in the Br of injected animals significantly increases at D3 and D7 (Figure 5.5A). In the TG *Gl-GC-II* expression decreases in response to ESA in injected animals and *Gl-GC-III* expression also decreased in injected animals at D3 and D7 (Figure 5.5B).

Expression of mTOR signaling pathway components is significantly reduced in rapamycin injected animals, *Gl-S6K* decreasing in both tissues and *Gl-mTOR* decreasing in the TG (Figure 5.5A and 5.5B). These results support the hypothesis that mTOR inhibition activates a downstream transcription factor to maintain energy hemostasis in the absence of mTOR signaling (Tiebe et al., 2015). This is in opposition to the effects of ESA in the blocked experiment, further indicating that the stress associated with injection has a powerful physiological impact.

*Conclusions*

Results from the blocked experiment suggest that a similar mechanism of molt resistance exists between *C. maenas* and *G. lateralis*. This mechanism may be attributed to the synthesis and secretion MIH in CNS tissues. Evidence from this study indicates that MIH either does not act through the predicted MIH signaling pathway in CNS tissues or that like the ESG it is only synthesized and secreted from these tissues. The blocked experiment also supports the growing body of literature that mTOR inhibition activates downstream transcription factors which are important in maintaining energy homeostasis in times of environmental stress. It is evident from comparison of the blocked and rapamycin experiments that injection alone has a significant physiological effect on the animal.

## MATERIALS AND METHODS

*Gecarcinus lateralis molt induction in blocked animals*

Adult male *G. lateralis* were collected in the Dominican Republic and shipped to Denver, CO, USA. Animals were housed at 27℃ ± 2℃ in 85 -95% relative humidity on a 12 h: 12 h light:dark cycle (Covi et al., 2010). Animals were kept in group cages (10 – 15 animals per cage) with aspen bedding moistened with 10 ppt Instant Ocean and fed a diet of carrots, lettuce, and raisins biweekly. Molting was induced by multiple leg autonomy (MLA). Animals induced to molt by MLA were maintained in individual

cages with a quartz sand substrate hydrated with 10 ppt Instant Ocean. Premolt progression was tracked using a limb regeneration (R) index (calculated as the length of the regenerate x 100/carapace width) (Covi et al., 2010; Yu et al., 2002). The R-index increases from 0 to 23 prior to ecdysis (Skinner and Graham, 1972; Yu et al., 2002). Intermolt animals were defined by an R value of 8-12.9, early premolt 13-15.9, mid premolt 16-18.9, and late premolt 19-23. Animals that did not enter premolt 12 weeks after MLA induction where considered blocked. 17 ESG, 8 Br, and 8 TG were harvested from blocked animals (D0). Remaining blocked animals were eyestalk ablated (ESA) and Br and TG where harvested at 1 day and 7 days post ESA (D1; Br n = 7, TG n = 7; D7 Br n = 6, TG = 5). As a baseline measurement, all three tissues were collected from intact (D0) animals (ESG n = 12; Br n = 17; TG n = 19) and 8 Br and TG were collected from animals at 1 and 7 days post ESA (D1 and D7). All tissues were stored in RNA later at -20℃ until RNA isolation. An enzyme linked immunoassay (ELISA) was used to quantif y ecdysteroids and verify molt stage (Abuhagr et al., 2014a; Kingan, 1989).

*Rapamycin Injection*

The effects of the mTOR inhibitor rapamycin (Selleck Chemicals, Houston, TX, USA) on the Br and TG were determined *in vivo*. *G. lateralis* were cared for as above. Intermolt animals were eyestalk ablated and injected with DMSO (Sigma Aldrich, St. Louis, MO USA) or 10 mM Rapamycin (Selleckchem, Huston, TX USA) dissolved in DMSO. Injection volume was calculated as 0.3% * body weight (in grams). Br and TG were harvested 0, 1, 3, and 7 days post injection/ESA. For both control and injected n = 11 at each time point for both tissues. All tissues were stored in RNA later at -20℃ until RNA isolation. An enzyme linked immunoassay (ELISA) was used to quantify ecdysteroids and verify molt stage (Abuhagr et al., 2014a; Kingan, 1989).

*Effects of molt induction and rapamycin injection on gene expression in crustacean tissues*

RNA was isolated from homogenized tissue using TRIzol reagent (Life Technologies, Carlsbad, CA USA) according to the manufacture's protocol (see Pitts and Mykles 2015 for a full protocol). cDNA was synthesized with qScript (Quanta Biosciences, Gaithersburg, MD USA). A Light Cycler 480 thermal cycler (Roche Applied Science, Indianapolis IN USA) was used to quantify levels of Gl-*EF2* (AY552550), *Gl-mTOR* (HM989973), *Gl-Rheb (*HM989971), *Gl-Akt* (HM989974), *Gl-S6K* (HM989975), *Gl-GC-Iβ* (DQ355434), *Gl-GC-II* (DQ355437), *Gl-GC-III* (DQ355438), *Gl-NOS* (AY552549), *Gl-NOSIP*

(c141319_g1_i1), *Gl-MIH* (DQ473354), *and Gl-CHH* (DQ473354) mRNA's in the rapamycin injection experiment. These genes plus Gl-*AC* (c141940_g2_i1), *Gl-PKA* (c143855_g2_i2), *Gl-CaM* (c140625_g7_i1), *Gl-CaN* (c143456_g3_i1), and *Gl-PKG* (c131028_g4_i1) were quantified in the blocked experiment. SYBR green was used to quantify all genes except *NOS* and *MIH*. 10 µL reactions consisted of 5 µL 2x SYBR Green I Master mix (Roche), 0.5 µL each of 10 mM forward and reverse primers, 3 µL nuclease-free water, and 1 µL cDNA or standard. Primer sequences for mTOR signaling pathway genes *Gl-mTOR*, *Gl-EF2*, *Gl-Akt*, *Gl-Rheb*, and *Gl-S6K* match previously published sequences (Abuhagr et al., 2014b). Lee et al (Lee et al., 2007b) published the primer sequences for *Gl-GC-Iβ*, *Gl-GC-III*, and *Gl-GC-III* and *Gl-CHH* (Lee et al., 2007a). Unpublished sequences can be found in Table 5.1. *NOS* and *MIH* were quantified using universal Probe #17 and #13 (Roche), respectively. 10 µL reactions for *NOS* and *MIH* were set up with 5 µL LightCycler 480 Probes Master (Roche) 0.2 µL each of 20 mM forward and reverse primers (Table 5.1), 0.2 µL universal Probe #17 or #13, 1.9 µL nuclease free water, and 2.5 µL of cDNA. PCR conditions were as follows: initial denaturation at 95℃ for 10 min, 50 cycles of denaturation at 95℃ for 10 s, annealing at 57 ℃ for 30 s and extension at 72℃ for 1 min. For each gene, a series of dsDNA standards were produced by serial dilutions and transcript concentrations calculated with the LightCycler 480 software (Roche, version 1.5). Absolute amounts of transcript copy numbers per µg of total RNA in the cDNA synthesis reaction were calculated based on the standard curve and the molecular weight of the dsDNA products.

*Analysis and Software*

Statistical analysis was performed using JMP version 12.0 (SAS Institute, Inc., Cary, NC USA) and graphs were generated in SigmaPlot version 12.0 (Systat Software Inc., San Jose CA, USA). All qPCR data was log transformed to reduce variances from the mean. A Brown-Forsythe test ($P<0.05$) confirmed the variances among log-transformed data were equivalent. Means for transcript abundance were compared using an analysis of variance (ANOVA) and post-hoc multiple comparisons were made using Tukey-Kramer HSD tests. A paired t-test was used to compare the means for transcript abundance between controls and blocked at each time point. Data are represented as mean ± 1 S.E. and the level of significance was set at $\alpha = 0.05$. Fold changes in expression were calculated based the raw expression level of genes.

**Table 5.1: qPCR Primer Sequences.** Previously unpublished primer sequences.

| Primer | Sequence (5' – 3') | Product size (bp) |
|---|---|---|
| Gl-NOS F1 | CATCACCCACCCTGAGTACA | 60 |
| Gl-NOS R1 | GGGAGGCCATACCATTGAA | |
| Gl-MIH F1 | AACATTGACTTCCTGTGGTGTG | 71 |
| Gl-MIH R1 | ACGAGCTCACACCGATACGT | |
| Gl-CaM F1 | GCAGATCAACTGACTGAGGAGC | 384 |
| Gl-CaM R2 | GCCGTCAATATCCGCTTCTCG | |
| Gl-CaN F1 | GGTCACGGAGATGCTGGTAAATG | 381 |
| Gl-CaN R1 | GCGACAGGTTGTGGTATGGCTG | |
| Gl-AC F3 | CACACGCCAAGAAGACCTCAAC | 323 |
| Gl-AC R1 | CAGGGTGACCCACGAGTACG | |
| Gl-PKA F1 | GCCAGGGAGGACACACTCATC | 193 |
| Gl-PKA R1 | CGTTGCGGTACTCGTTAGCC | |
| Gl-PKG F1 | GCGTGGAGGTCAGCAAGG | 188 |
| Gl-PKG R1 | CTGGCGGATGAGACAGGTC | |
| Gl-NOSIP F1 | GCAGCCTCTCCCTTCACCC | 178 |
| Gl-NOSIP R1 | GCCTCACCCAACTCCTCCAAC | |

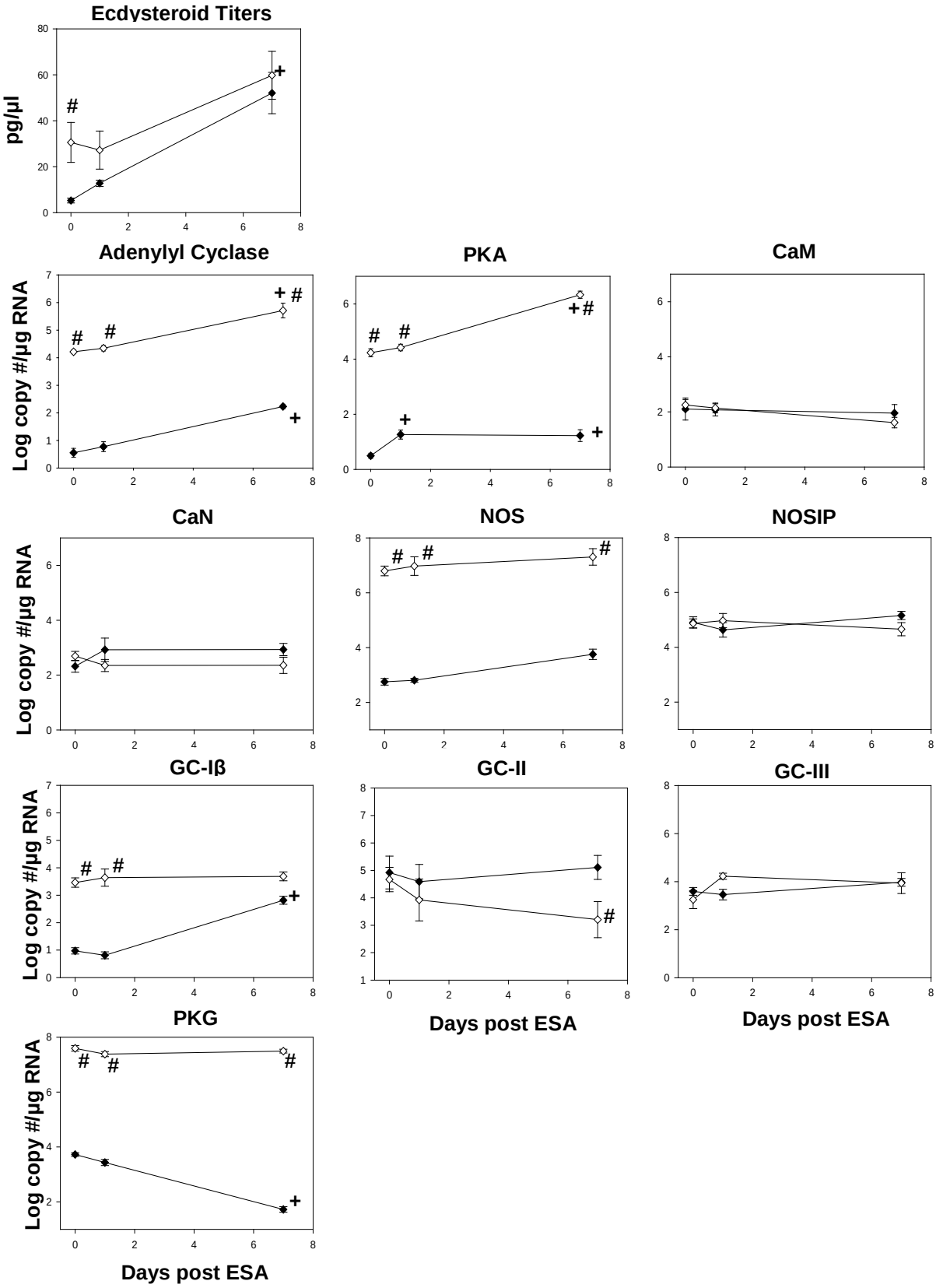
Ecdysteroid Titers
pg/µl
Adenylyl Cyclase
PKA
CaM
CaN
NOS
NOSIP
GC-Iß
GC-II
GC-III
PKG
Log copy #/µg RNA
Days post ESA

**5.1A**

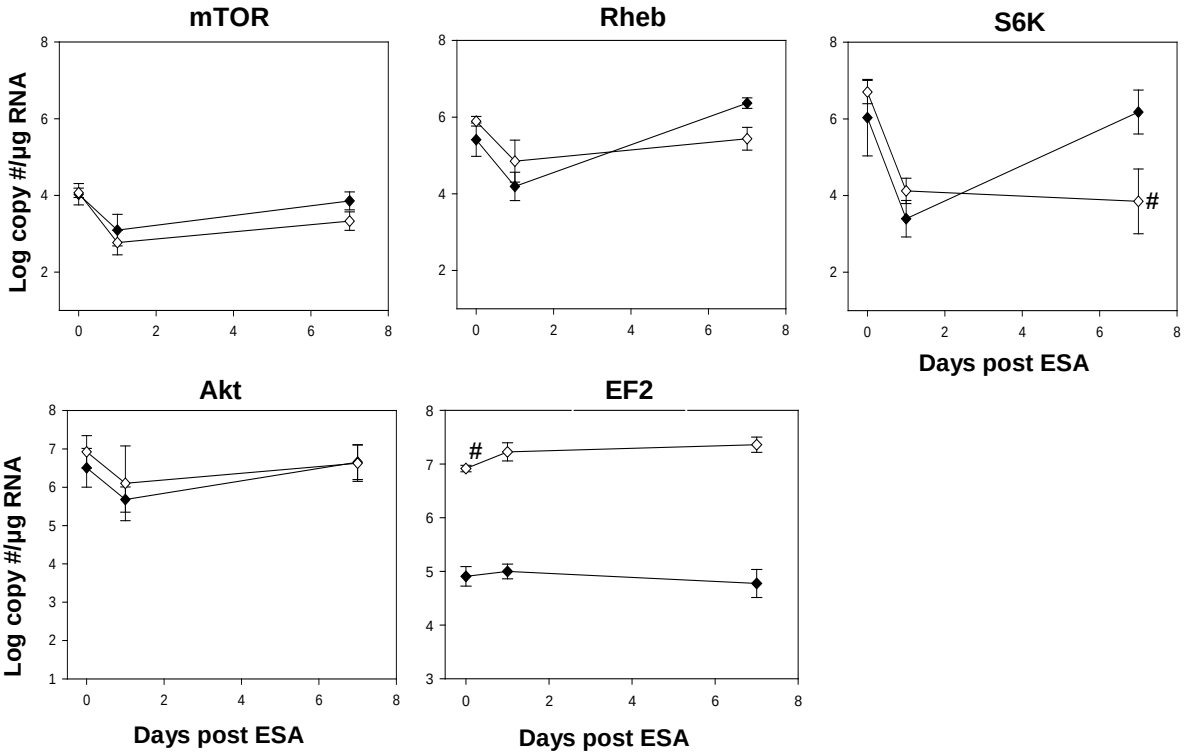


**5.1B**

**Figure 5.1: Changes in YO expression of mTOR and MIH signaling pathway components in control and blocked animals in response to molt induction by ESA.** Data for blocked animals is represented by open diamonds and control by filled diamonds. Significant differences between control and blocked animals at the same time point are indicated with a "#". Significant differences between D0 and D1 or D7 between animals within the same group are indicated by a "+". Only significant differences of $p < 0.01$ are indicated on the graphs. A. Gene expression of *Gl-AC, Gl-PKA, Gl-NOS,* and *Gl-PKG* was greater in blocked an animals at all three time points and at D0 and D1 for *Gl-GC-Iβ.* Expression was lower in blocked animals at D7 for *Gl-GC-II.* At D7 *Gl-AC* and *Gl-PKA* expression was higher in both control and blocked animals. *Gl-PKA* expression was also higher in blocked animals at D1. *Gl-PKG* expression decreased at D7 in controls. B. Expression of *Gl-EF2* was greater in blocked animals at all three time points and significantly increased in controls at 7 days post ESA. *Gl-S6K* was lower in blocked animals compared to controls at D7.

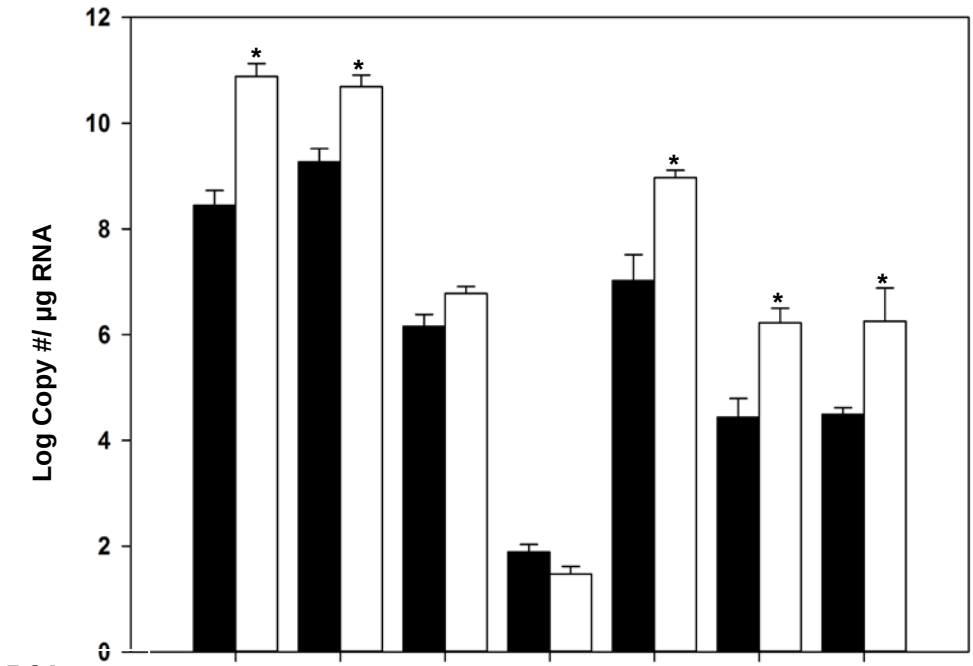


5.2A

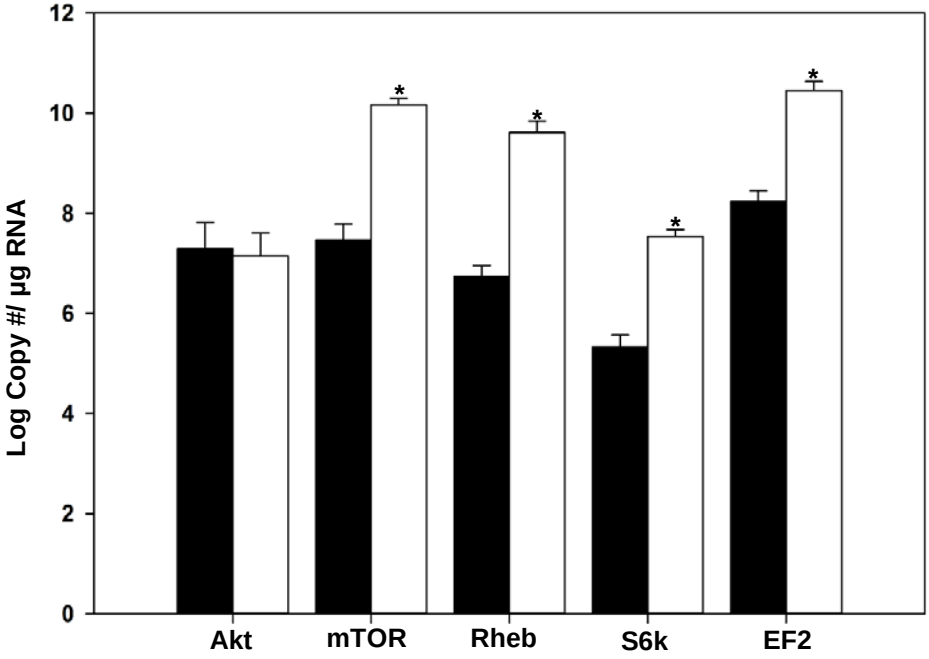


5.2B

**Figure 5.2: Comparison of gene expression between intermolt and blocked animals in the ESG.**

White bars represent data for blocked animals, black for intermolt. Only significant differences of $p < 0.01$ are indicated on the graphs (*). A. Expression of MIH signaling pathway genes *Gl-MIH, Gl-CHH, Gl-GC-Iβ, Gl-GC-II*, and *Gl-GC-III* was greater in blocked compared to control animals. B. Expression of mTOR signaling pathway genes *Gl-mTOR, Gl-Rheb, Gl-S6K*, and *Gl-EF2* was also greater in blocked animals.

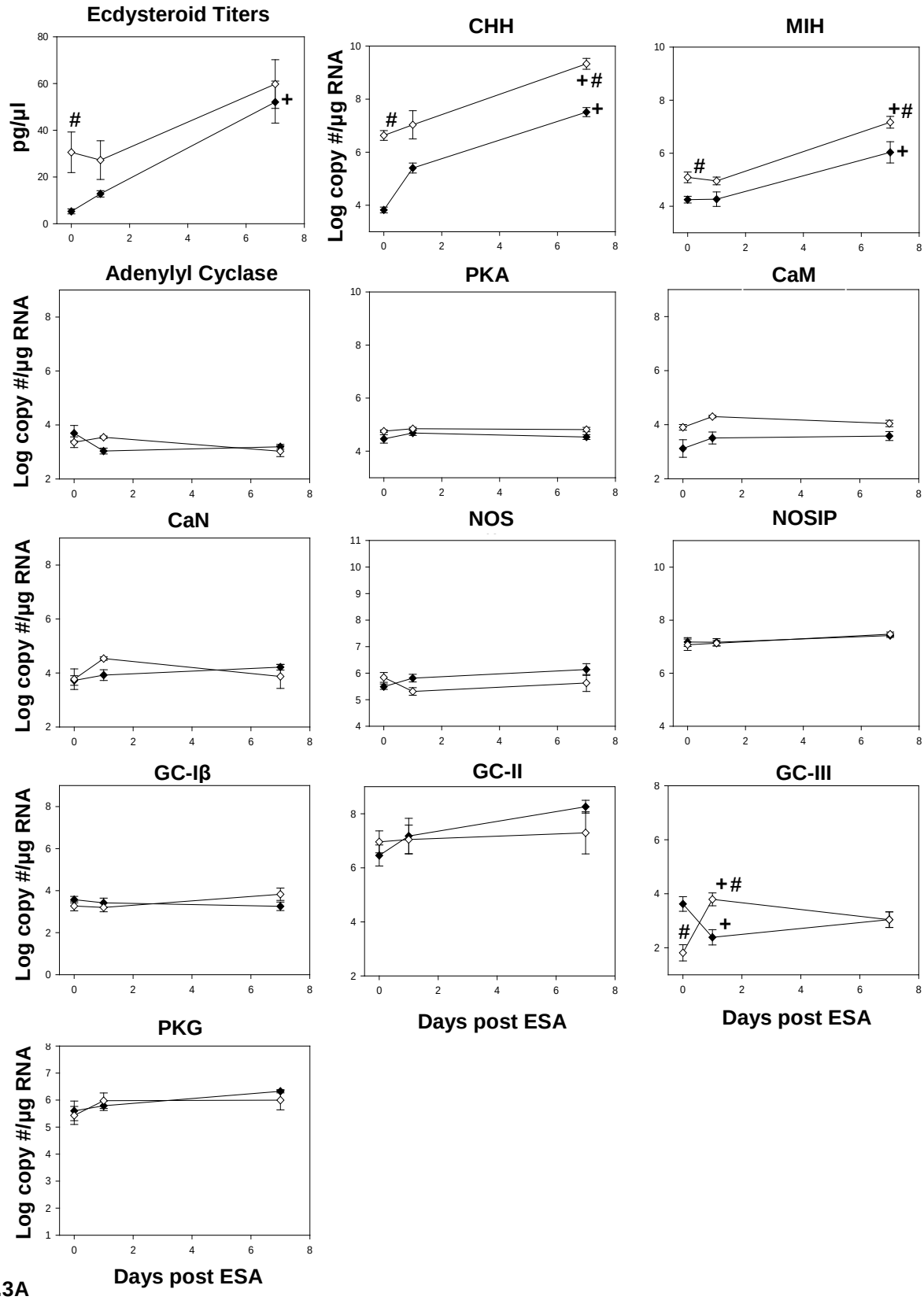
Ecdysteroid Titers
pg/µl
CHH
MIH
Log copy #/µg RNA
Adenylyl Cyclase
PKA
CaM
CaN
NOS
NOSIP
GC-Iβ
GC-II
GC-III
PKG
Days post ESA
Days post ESA
Days post ESA

**5.3A**

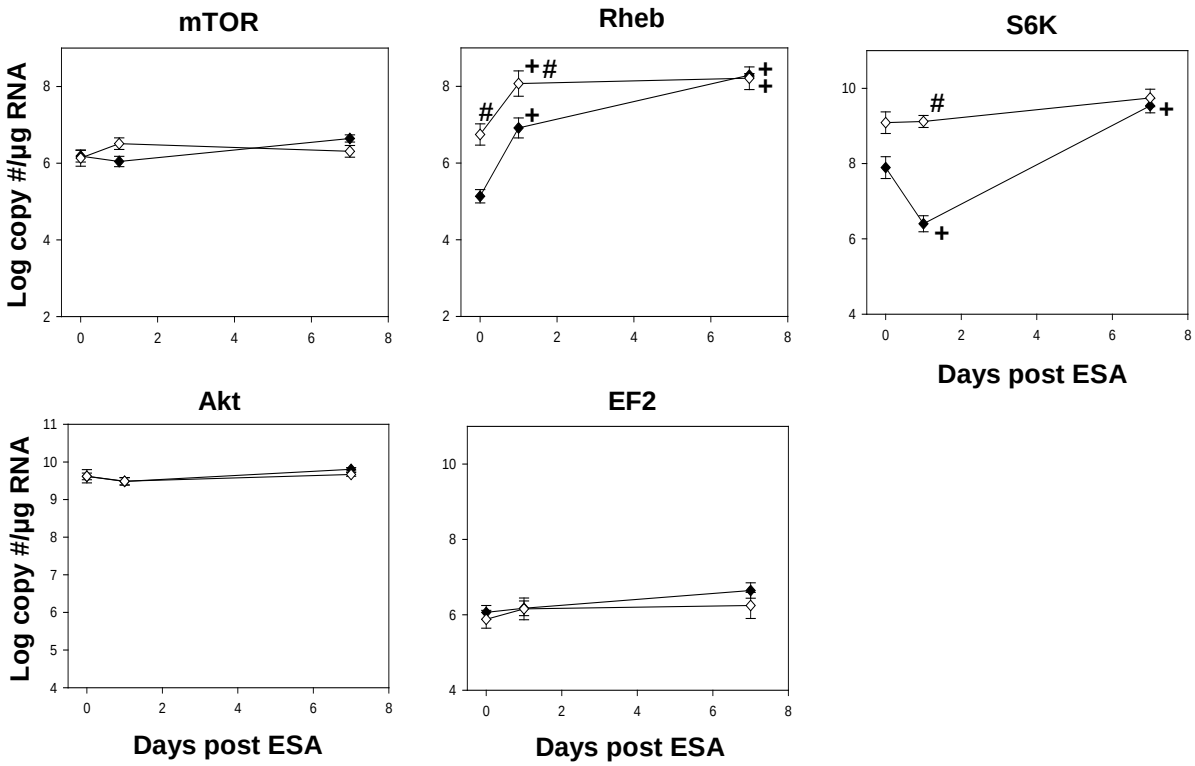


**Figure 5.3: Changes in Br expression of mTOR and MIH signaling pathway components in control and blocked animals in response to molt induction by ESA.** Data for blocked animals is represented by open diamonds and control by filled diamonds. Significant differences between control and blocked animals at the same time point are indicated with a "#". Significant differences between D0 and D1 or D7 within the same group are indicated by a "+". Only significant differences of $p < 0.01$ are indicated on the graphs. A. Gene expression of MIH *Gl-CHH* and *Gl-MIH* increased in both control and blocked animals by D7. Expression of both genes was greater in blocked animals at D0 and D7. *Gl-GC-III* increased at D1 in blocked animals and decreased in controls. B. Expression of *Gl-Rheb* increased at D1 and D7 in both control and blocked animals. Expression was higher in blocked animals at D0 and D1. *Gl-S6K* expression decreased at D1 then increased at D7 in controls. *Gl-S6K* expression in blocked animals is higher at D1.

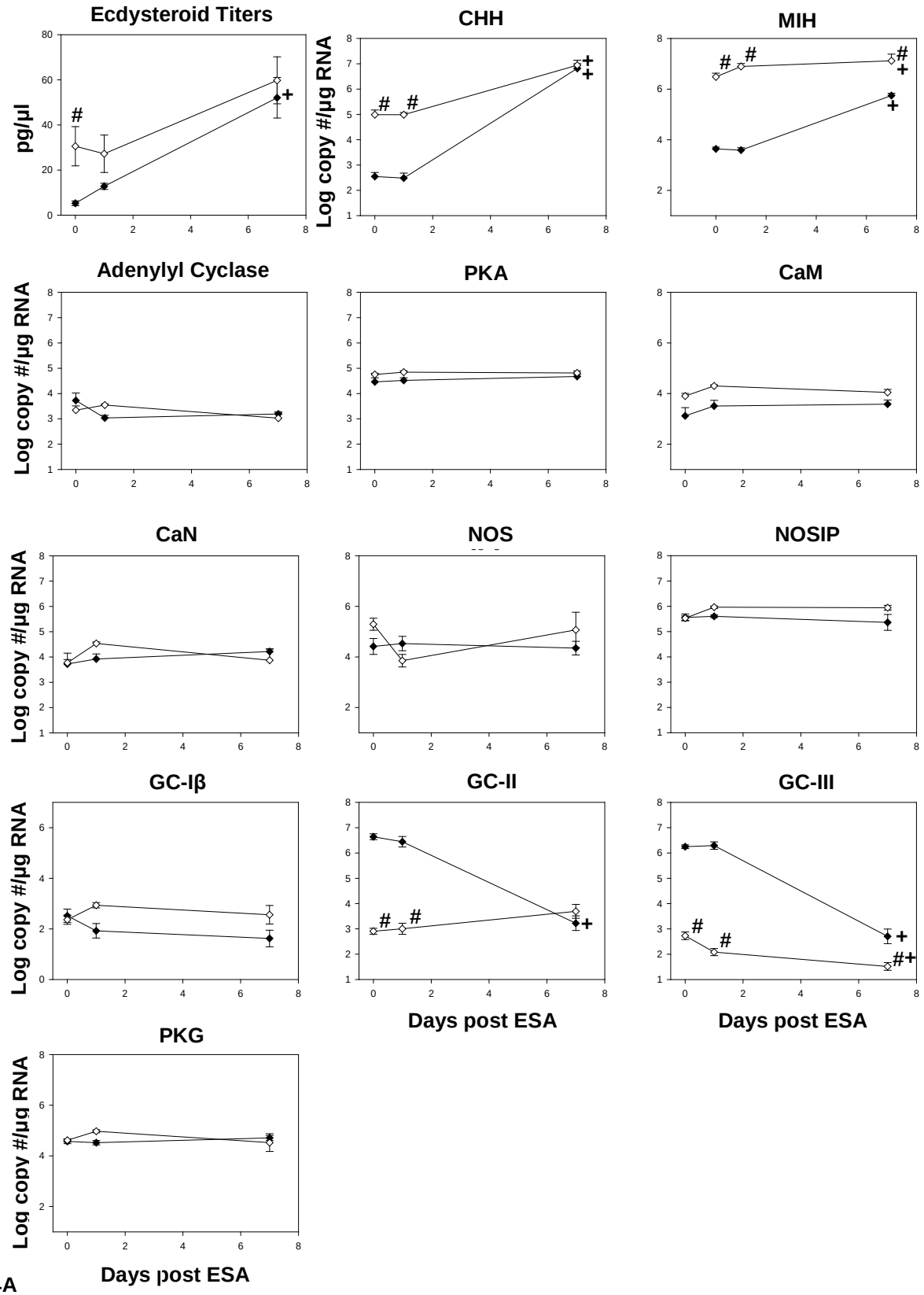
Ecdysteroid Titers
pg/µl
CHH
MIH
Log copy #/µg RNA
Adenylyl Cyclase
PKA
CaM
CaN
NOS
NOSIP
GC-Iβ
GC-II
GC-III
PKG
Days post ESA
Days post ESA
Days post ESA

**5.4A**

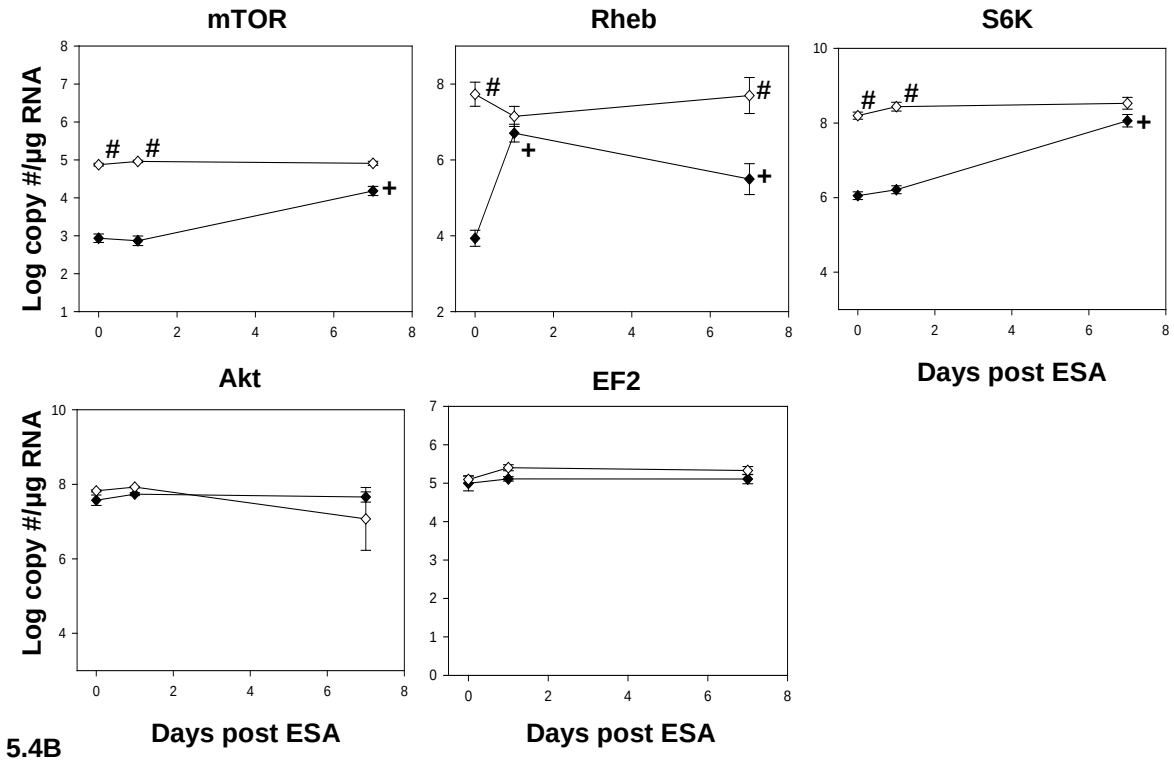


**Figure 5.4: Changes in TG expression of mTOR and MIH signaling pathway components in intact and blocked animals in response to molt induction by ESA.** Data for blocked animals is represented by open diamonds and control by filled diamonds. Significant differences between D0 and blocked animals at the same time point are indicated with a "#". Significant differences between control and D1 or D7 between animals within the same group are indicated by a "+". Only significant differences of $p < 0.01$ are indicated on the graphs. A. Ecdysteroid titers were greater in blocked compared to controls at D0. Titers significantly increased 7 days post ESA in control but not blocked animals. Gene expression of *Gl-CHH* and *Gl-MIH* increased in response to ESA in both control and blocked groups. Gene expression at all three time points (*Gl-MIH*) and at D0 and D1 (*Gl-CHH*) was greater in blocked animals. *GC-II* and *GC-III* expression decreased in response to ESA in controls and *GC-III* decreased in blocked animals. Gene expression at all three time points (*Gl-GC-III*) and at D0 and D1 (*Gl-GC-II*) was greater in controls. B. *Gl-mTOR,* and *Gl-S6K* expression was greater in blocked animals at D0 and D1. *Gl-Rheb* expression was higher at D0 and D7 in blocked animals. Expression of all three genes (mTOR, Rheb and S6K) in controls increased in response to ESA at D7 and *Gl-Rheb* also increased at D1.

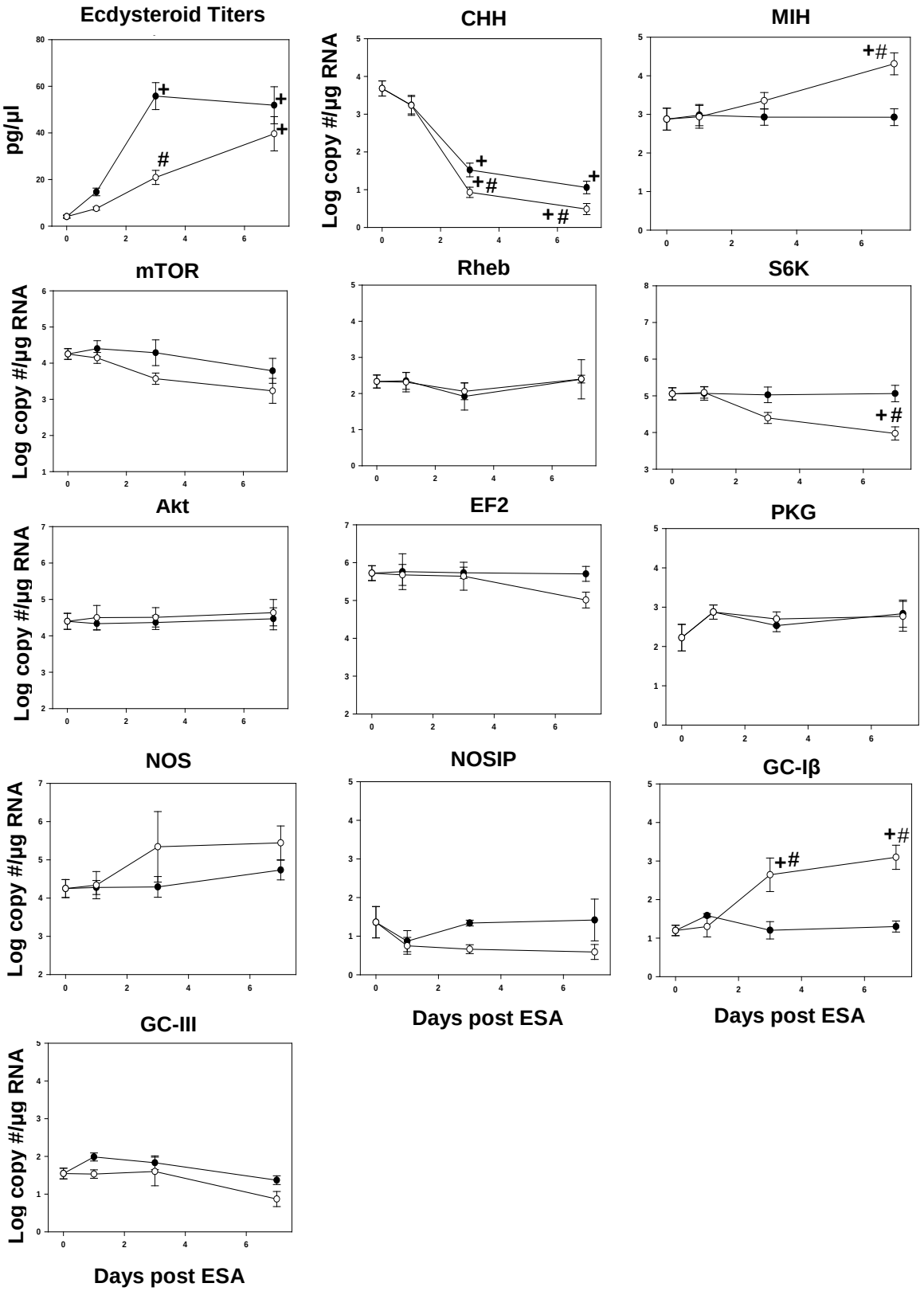
Ecdysteroid Titers
pg/µl
CHH
Log copy #/µg RNA
MIH
mTOR
Log copy #/µg RNA
Rheb
S6K
Akt
Log copy #/µg RNA
EF2
PKG
NOS
Log copy #/µg RNA
NOSIP
GC-Iβ
Days post ESA
Days post ESA
GC-III
Log copy #/µg RNA
Days post ESA

**5.5A**

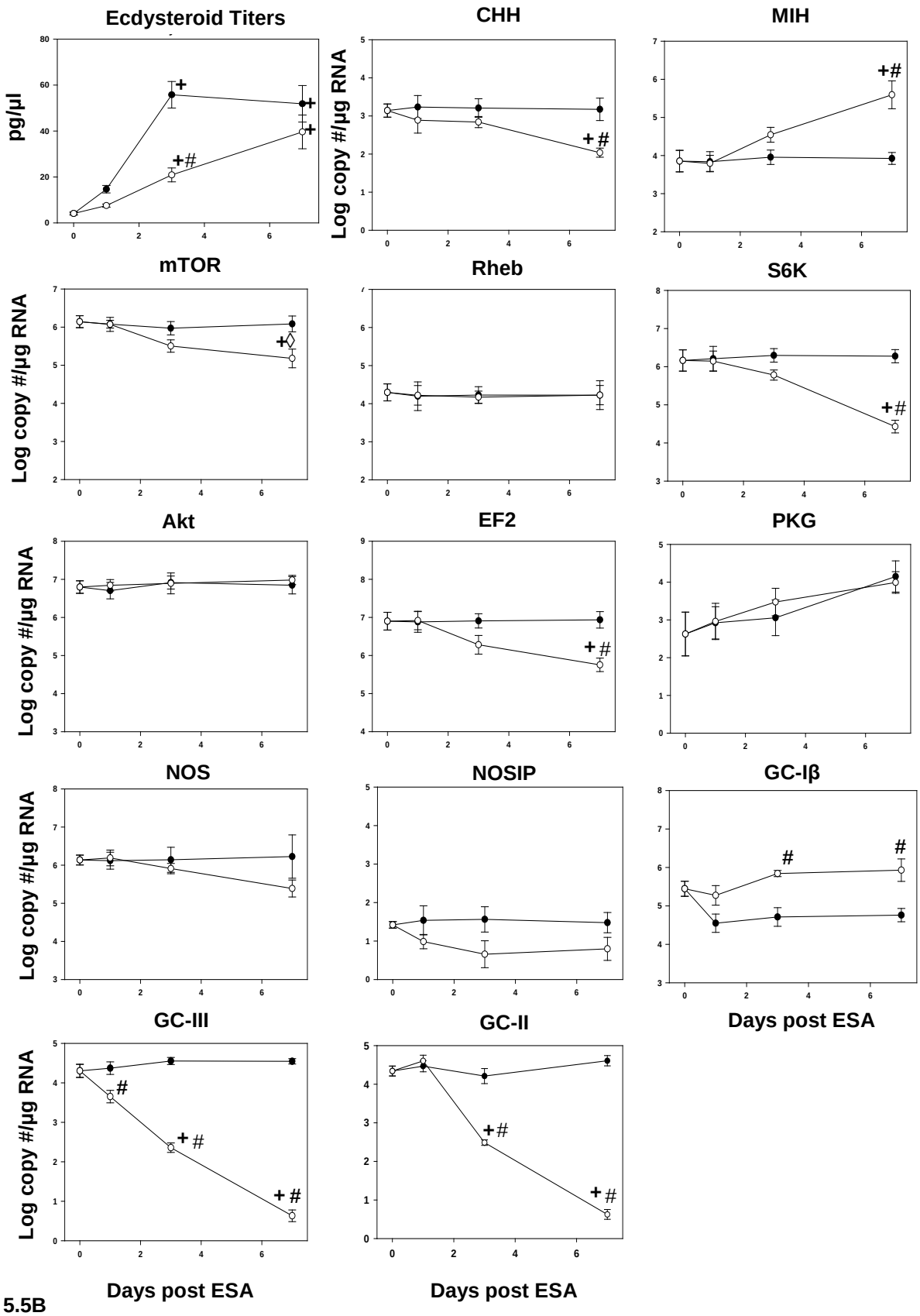
Ecdysteroid Titers
pg/µl
CHH
MIH
mTOR
Rheb
S6K
Akt
EF2
PKG
NOS
NOSIP
GC-Iβ
GC-III
GC-II
Log copy #/µg RNA
Days post ESA

**5.5B**

**Figure 5.5: Changes in gene expression in response to molt induction in two CNS tissues from rapamycin injected and control animals.** Data for rapamycin injected animals is represented by open circles and control by filled circles. Significant differences between control and injected animals at the same time point are indicated with a "#". Significant differences between D0 and D1, D3, or D7 for animals within the same group are indicated by a "+". Only significant differences of $p < 0.01$ are indicated on the graphs. Ecdysteroid titers were greater in control animals at D3. Titers at D3 and D7 were greater in both control and rapamycin when compared to D0; however, titers increased faster in control animals. A. Changes in gene expression in the Br. A significant effect of ESA in injected animals was observed in four genes; *Gl-CHH, Gl-MIH, Gl-S6K,* and *Gl-GC-Iβ*. *Gl-CHH* significantly decreased at D3 and D7 in injected and controls. *Gl-MIH* expression increased at D7 in injected and animals and *Gl-S6K* expression decreased. *Gl-GC-Iβ* was higher at D3 and D7 compared to D0 in injected animals. B. Changes in TG gene expression. At D7 genes expression in injected animals decreased and was significantly lower than controls for the following genes; *Gl-CHH, Gl-mTOR, Gl-S6K*, and *Gl-EF2.* A sharp reduction in expression of *Gl-GC-II* and *Gl-GC-III* occurred at both D3 and D7 in injected animals. Expression of *Gl-GC-II* and *Gl-GC-III* in controls was unaffected by ESA. *Gl-MIH* expression in rapamycin injected animals increased at D7 and is greater than controls. At D3 and D7 *Gl-GC-Iβ* had higher expression in injected animals compared to controls.

# REFERENCES


Abuhagr, A.M., Blindert, J.L., Nimitkul, S., Zander, I.A., LaBere, S.M., Chang, S.A., MacLea, K.S., Chang, E.S., Mykles, D.L., 2014a. Molt regulation in green and red color morphs of the crab *Carcinus maenas*: Gene expression of molt-inhibiting hormone signaling components. J. Exp. Biol. 217, 796-808.

Abuhagr, A.M., MacLea, K.S., Chang, E.S., Mykles, D.L., 2014b. Mechanistic target of rapamycin (mTOR) signaling genes in decapod crustaceans: Cloning and tissue expression of mTOR, Akt, Rheb, and p70 S6 kinase in the green crab, *Carcinus maenas*, and blackback land crab, *Gecarcinus lateralis*. Comp. Biochem. Physiol. 168, 25-39.

Chang, E.S., Mykles, D.L., 2011. Regulation of crustacean molting: A review and our perspectives. Gen. Comp. Endocrinol. 172, 323-330.

Covi, J.A., Bader, B.D., Chang, E.S., Mykles, D.L., 2010. Molt cycle regulation of protein synthesis in skeletal muscle of the blackback land crab, *Gecarcinus lateralis*, and the differential expression of a myostatin-like factor during atrophy induced by molting or unweighting. J. Exp. Biol. 213, 172-183.

Covi, J.A., Chang, E.S., Mykles, D.L., 2009. Conserved role of cyclic nucleotides in the regulation of ecdysteroidogenesis by the crustacean molting gland. Comp. Biochem. Physiol. 152, 470-477.

Covi, J.A., Chang, E.S., Mykles, D.L., 2012. Neuropeptide signaling mechanisms in crustacean and insect molting glands. Invert. Reprod. Dev. 56, 33-49.

Dell, S., Sedlmeier, D., Böcking, D., Dauphin-Villemant, C., 1999. Ecdysteroid biosynthesis in crayfish Y-organs: Feedback regulation by circulating ecdysteroids. Arch. Insect Biochem. Physiol. 41, 148-155.

Gu, P.L., Chan, S.M., 1998. The shrimp hyperglycemic hormone-like neuropeptide is encoded by multiple copies of genes arranged in a cluster. FEBS Lett. 441, 397-403.

Gu, S.H., Yeh, W.L., Young, S.C., Lin, P.L., Li, S., 2012. TOR signaling is involved in PTTH-stimulated ecdysteroidogenesis by prothoracic glands in the silkworm, *Bombyx mori*. Insect Biochem. Molec. Biol. 42, 296-303.

Hopkins, P.M., 2012. The eyes have it: A brief history of crustacean neuroendocrinology. Gen. Comp. Endocrinol. 175, 357-366.

Kemirembe, K., Liebmann, K., Bootes, A., Smith, W.A., Suzuki, Y., 2012. Amino acids and TOR signaling promote prothoracic gland growth and the initiation of larval molts in the tobacco hornworm *Manduca sexta*. Plos One 7.

Kingan, T.G., 1989. A competitive enzyme-linked immunosorbent assay: Application in the assasy of peptides, steroids, and cyclic nucleotides. Anal. Biochem. 183, 283-289.

Lachaise, F., Leroux, A., Hubert, M., Lafont, R., 1993. The molting gland of crustaceans; Localization, activity, and endocrine control (a review). . J. Crustacean Biol. 13, 198-234.

Lee, K.J., Kim, H.W., Gomez, A.M., Chang, E.S., Covi, J.A., Mykles, D.L., 2007a. Molt-inhibiting hormone from the tropical land crab, *Gecarcinus lateralis*: Cloning, tissue expression, and expression of biologically active recombinant peptide in yeast. Gen. Comp. Endocrinol. 150, 505-513.

Lee, S.G., Kim, H.W., Mykles, D.L., 2007b. Guanylyl cyclases in the tropical land crab, *Gecarcinus lateralis*: Cloning of soluble (NO-sensitive and -insensitive) and membrane receptor forms. Comp. Biochem. Physiol. 2D, 332-344.

MacLea, K.S., Abuhagr, A.M., Pitts, N.L., Covi, J.A., Bader, B.D., Chang, E.S., Mykles, D.L., 2012. Rheb, an activator of target of rapamycin, in the blackback land crab, *Gecarcinus lateralis*: cloning and effects of molting and unweighting on expression in skeletal muscle. J. Exp. Biol. 215, 590-604.

Mykles, D.L., 2011. Ecdysteroid metabolism in crustaceans. J. Steroid Biochem. Mol. Biol. 127, 196-203.

Nakatsuji, T., Sonobe, H., 2004. Regulation of ecdysteroid secretion from the Y-organ by molt-inhibiting hormone in the American crayfish, *Procambarus clarkii*. Gen. Comp. Endocrinol. 135, 358-364.

Skinner, D.M., 1985. Molting and regeneration, in: D.E. Bliss, L.H. Mantel (Eds.), The Biology of Crustacea. Academic Press, New York, 44-146.

Skinner, D.M., Graham, D.E., 1972. Loss of limbs as a stimulus to ecdysis in Brachyura (true crabs). Biol. Bull. 143, 222-233.

Stewart, M.J., Stewart, P., Sroyraya, M., Soonklang, N., Cummins, S.F., Hanna, P.J., Duan, W., Sobhon, P., 2013. Cloning of the crustacean hyperglycemic hormone and evidence for molt-inhibiting hormone within the central nervous system of the blue crab *Portunus pelagicus*. Comp. Biochem. Physiol. 164A, 276-290.

Stuenkel, E.L., 1985. Simultaneous monitoring of electrical and secretory activity in peptidergic neurosecretory terminals of the crab. J. Physiol. Lond. 359, 163-187.

Tiebe, M., Lutz, M., De La Garza, A., Buechling, T., Boutros, M., Teleman, A.A., 2015. REPTOR and REPTOR-BP regulate organismal metabolism and transcription downstream of TORC1. Dev. Cell 33, 272-284.

Tiu, S.H.K., Chan, S.M., 2007. The use of recombinant protein and RNA interference approaches to study the reproductive functions of a gonad-stimulating hormone from the shrimp *Metapenaeus ensis*. FEBS J. 274, 4385-4395.

Webster, S.G., Dircksen, H., 1991. Putative molt-inhibiting hormone in larvae of the shore crab *Carcinus maenas*: An immunocytochemical approach. Biol. Bull. 180, 65-71.

Yu, X.L., Chang, E.S., Mykles, D.L., 2002. Characterization of limb autotomy factor-proecdysis ($LAF_{pro}$), isolated from limb regenerates, that suspends molting in the land crab *Gecarcinus lateralis*. Biol. Bull. 202, 204-212.

Zeleny, C., 1905. Compensatory regulation. J. Exp. Zool. 2, 347-369.

Zhu, D.F., Hu, Z.H., Shen, J.M., 2011. Moult-inhibiting hormone from the swimming crab, *Portunus trituberulatus* (Miers, 1876); PCR cloning, tissue distribution, and expression of recombinant protein in *Escherichia coli* (Migula, 1895). Crustaceana 84, 1481-1496.

# CHAPTER SIX

## SUMMARY AND FUTURE DIRECTIONS

Molt-inhibiting hormone (MIH) is a peptide hormone that regulates molting in decapod crustaceans. MIH is synthesized in the X-organ (XO) and secreted from the sinus gland (SG) in the eyestalk ganglia (ESG). MIH inhibits production of the molting hormones (ecdysteroids) from the Y-organ (YO). Most research dedicated to understanding the molecular regulation of molting in decapod crustaceans has focused on ecdysteroid production in the YO. This dissertation explores molting from a novel perspective by examining the importance of MIH synthesis and secretion from the XO/SG.

Chapter two of this dissertation investigates the effects of molt induction by multiple limb autotomy (MLA) and molt suspension by limb bud autotomy (LBA) on transcript abundance in the ESG of *G. lateralis*. The expression of MIH is expected to decrease as an animal progress through molt. However, the data shows that *Gl-MIH* is elevated during early, mid, late, and post molt compared to intermolt in MLA animals. Given that MIH titers in the hemolymph fluctuate during the molt cycle, MIH release from the SG must be dependent on a post transcriptional mechanism. A similar trend is observed in the expression of *Gl-EF2*, *Gl-GC-Iβ* and mTOR signaling pathway genes *Gl-mTOR*, *Gl-S6K*, and *Gl-Rheb*. The up-regulation in transcription of multiple genes from different signaling pathways in animals induced to molt via MLA may be a potential mechanism for maintaining overall homoeostasis during the taxing process of molting. Molt suspension via LBA was unsuccessful. Changes in gene expression in LBA animals was nearly identical to MLA animals indicating that LBA had no effect on molt cycle progression.

Chapter two also explores how transcript levels in ESG of naturally molting *C. maenas* change throughout the molt cycle. Similar to *G. lateralis*, *Cm-MIH* is elevated during pre and post molt compared to intermolt, suggesting that fluctuations in MIH hemolymph titers is regulated post transcriptionally. With the exception of a decrease in *Cm-EF2* in post molt animals, transcript abundance was constant throughout the molt cycle in all genes examined. This is in agreement with previously published data and supports the hypothesis that molting in *C. maenas* is regulated post transcriptionally.

The next step in understanding the molecular mechanisms regulating molt cycle progression is to examine how protein levels are effected during this process. Sequencing of an ESG proteome throughout the molt cycle would be the simplest way to address this question. However, ultimately the sequencing of an entire decapod crustacean genome will be necessary to fully appreciate the systemic changes that occur during molting.

An important and novel discovery is made in chapter three of this dissertation. An unidentified nitric oxide (NO) binding protein is found in the SG of *C. maenas.* This protein is not a heme or copper binding protein and its identity remains unknown. This protein allows for the sequestration of NO in the SG for an extended period of time. NO is a gaseous neurotransmitter that is hypothesized to inhibit neuropeptide secretion from the SG. An NO binding protein permits the continuous presence of NO and therefore rapid inhibition of MIH secretion.

Chapter three also identifies a novel technique for imaging NO *in vitro*. Using a copper fluorescent ligand (CuFL) in conjunction with NO scavengers, donors, and NOS inhibitors, NO based fluorescence was quantified in the SG of *C. maenas*. To our knowledge this is the first time NO has been imaged in a crustacean tissue. Additionally, CuFL was found to be a powerful NO scavenger and will be beneficial in future *in vitro* experiments examining NO/cGMP signaling.

Since the identity of the NO binding protein remains unknown, an important next step will be to identify this protein and establish its function. A mass spectrometry analysis of SG homogenate would provide a platform for formulating a list of candidate proteins. In order to determine if MIH secretion from the SG is NO-dependent, MIH concentrations in the presence of NO scavengers, donors, NOS inhibitors, and GC-Iβ activators will need to be quantified *in vitro*. Experiments addressing this question are in their infancy and use a time resolved-fluoroimmunoassay (see appendix for preliminary results).

The development of a Gl-MIH antibody in chapter four is also an important contribution to the field of crustacean endocrinology. This antibody allows for the use of numerous techniques to image, localize, and quantify MIH in multiple decapod crustacean species. Using this antibody MIH was localized to the SG, thoracic ganglia (TG), and brain (Br) of three crustacean species. These results are in line with previously published data indicating that the ESG is not the only source of MIH. Using this antibody in conjunction with a universal nitric oxide synthase (NOS) antibody, NOS and MIH were co-localized in the

SG and TG of two decapod species. Given that NO is a gaseous signaling molecule, in the absence of a binding protein it would have to be produced in close proximity to MIH filled synaptic vesicles to regulate secretion. The co-localization of MIH and NOS in the SG and TG supports the hypothesis that NO regulates synaptic vesicle release and suggests that these two CNS tissue share a similar mechanism for MIH secretion. Future experiments based on data from this chapter are the same as in chapter three and are discussed above.

Chapter five addresses a long standing observation that some *G. lateralis* are unresponsive to molt-induction techniques. These animals are identified as "blocked" and do not initiate premolt 12 weeks post MLA. In an attempt to understand the cause of this phenomenon, YO, TG, and Br were harvested from blocked animals at 1, 3, and 7 days after they underwent a second molt induction technique, eyestalk ablation (ESA). Changes in transcript levels of two neuropeptides, *Gl-MIH* and *Gl-CHH* as well as mTOR signaling pathway genes *Gl-mTOR, Gl-S6K, Gl-Rheb*, and *Gl-Akt* and MIH signaling pathway genes *Gl-CaN, Gl-CaM, Gl-NOS, Gl-GC-Iβ, Gl-PKG, Gl-PKA*, and *Gl-AC* were examined in all three tissues. With the exception of an increase in both neuropeptides in response to ESA, there was no effect of ESA in the TG and Br of blocked animals. However, in the YO five components from the predicted MIH signaling pathway, *Gl-NOS, Gl-GC-Iβ, Gl-PKG, Gl-PKA*, and *Gl-AC*, were up-regulated in blocked animals. This indicates that MIH signaling pathway in blocked animals is constitutively active, inhibiting ecdysteroid production and molt progression.

Chapter five also identifies an NOS inhibitory protein (NOSIP) in the YO of crustaceans. This protein binds and regulates endothelial NOS in mammalian tissues. To date only one NOS isoform has been identified in crustaceans. The crustacean NOS isoform is homologous to mammalian neuronal NOS. Therefore the presence of an endothelial NOS binding protein indicates that more than one NOS isoform is present in crustaceans. This is also supported by the absence of NOS localization in the brain in chapter 4. NOS is detected in the brain via qPCR but the universal NOS antibody fails to recognize NOS in the brain of all three species examined. Previous studies localized NADPH, a byproduct of NO production, in the brain of several crustacean species. Taken together this data suggests that more than one NOS isoform is expressed in crustaceans.

In order to explore the blocked phenomenon further, *in vitro* experiments examining the effects of MIH on ecdysteroid production in the YO of blocked animals should be conducted. These experiments will help to uncover whether the YO's in these animals are refractory to MIH or if another mechanism is responsible for maintaining their blocked state. Also, examining changes in protein expression of MIH signaling pathway genes will be critical for fully uncovering if this pathway is constitutively active. Finally, once a crustacean genome has been sequenced it will be possible to develop this pathway completely by manipulating the expression of various pathway components.

This project addresses two questions: 1) How is MIH secretion from the SG regulated during the molt cycle? 2) Why are some animals' refractory to molt induction techniques? The first question focuses on the role NO plays in the regulation of MIH secretion from the SG. Very little research has been dedicated to understanding the role of MIH secretion in molt regulation. With the development of a technique to quantify NO production and an MIH antibody, future work can be directed toward establishing a relationship between NO and MIH release. The second question focuses on the MIH signaling pathway in the YO and its activity in blocked animals. Data indicating that this pathway is constitutively active in blocked animals provides a novel hypothesis for this poorly understood phenomenon.

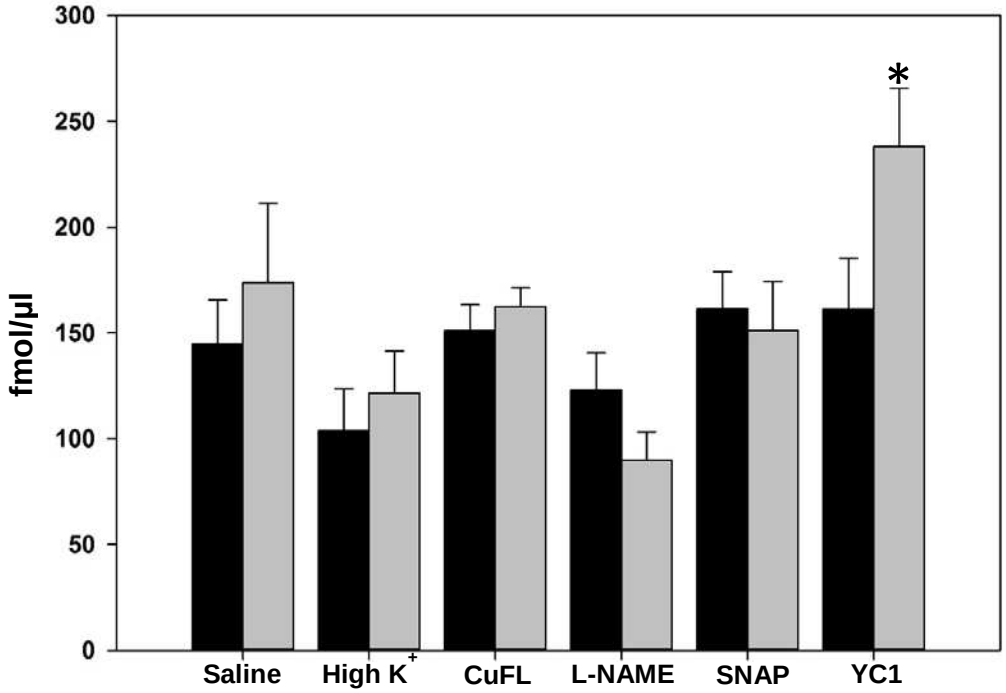


**Appendix IA. *In vitro* quantification of MIH secretion from the ESG of *Carcinus maenas.*** Eyestalk ganglia (ESG) were dissected from *C. maenas* and incubated *in virto* for 6 h. One ESG was used as a control and was incubated in saline (black bars) the second ESG was incubated in one of the following compounds in crab saline: high $K^+$ (35 mM), CuFL (0.05 uM), L-NAME (1 mM), SNAP (1 mM), or YC1 (1 mM) (gray bars). At the end of the 6 hr period the media was collected and flash frozen in liquid nitrogen. MIH concentrations were measured using time resolved-fluoroimmunoassay (TR-FIA). MIH secretion from ESG incubated in YC1 was significantly higher than controls ($p < 0.05$).

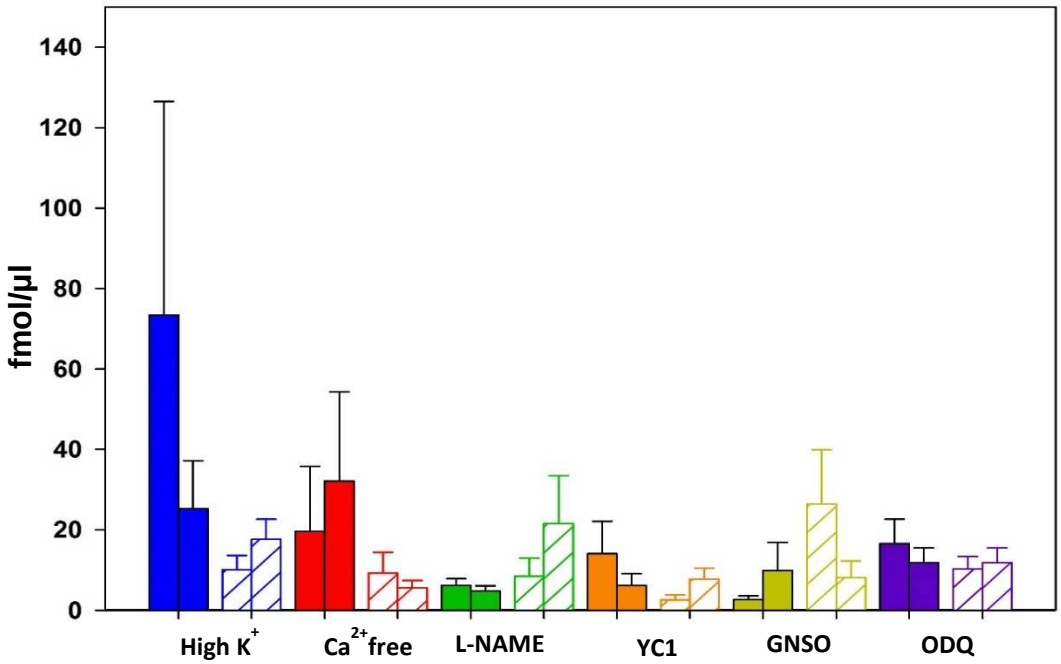


**Appendix IB. *In vitro* quantification of MIH secretion from the ESG of *Carcinus maenas.*** Eyestalk ganglia (ESG) were dissected from *C. maenas* and allowed to equilibrate in crab saline for 15 min. One ESG was used as a control and was incubated in saline (striped bars) the second ESG was incubated in the indicated compound (solid bars). Fifteen minutes post dissection the saline was removed and 200 µl of fresh saline was added to each ESG. Fifteen minutes later the saline was removed and flash frozen as a baseline measurement (first bar from each pair). In controls fresh saline was applied and in experimental one of the following compounds in crab saline was added: high $K^+$ (35 mM; purple), $Ca^{2+}$ free (red), L-NAME (1 mM; green), YC-1 (1 mM; orange), GNSO (1 mM; yellow), and ODQ (1 mM; ODQ). Media was collected 15 minutes after the compound was added and flash frozen. MIH concentrations were measured using time resolved-fluoroimmunoassay (TR-FIA).